**UNIVERSITY OF SOUTHAMPTON**

FACULTY OF PHYSICAL AND APPLIED SCIENCES

# The second-order gravitational self-force

by

**Jeremy Miller**

Thesis for the degree of Doctor of Philosophy

October 2017

UNIVERSITY OF SOUTHAMPTON

ABSTRACT

FACULTY OF PHYSICAL AND APPLIED SCIENCES

Doctor of Philosophy

THE SECOND-ORDER GRAVITATIONAL SELF-FORCE

by Jeremy Miller

This project makes progress towards a first calculation of the second-order gravitational self-force in extreme-mass-ratio binaries. This is an important component in the modeling of these key astrophysical sources of gravitational waves. Computing the second-order self-force requires the second-order metric perturbation, which can be calculated by solving the Einstein field equations through second order in the mass ratio. Here we have developed, for the first time, a practical scheme for solving the second-order equations. The main ingredient is a certain "puncture" field, which describes the local metric perturbation near the small member of the binary, and for which we obtain a useful covariant-form expression. We apply this method to the case of a quasicircular binary of nonrotating black holes. As a first test we numerically solve the first-order field equations and compute the first-order self-force, finding good agreement with previous results obtained using a different method. The calculation of the second-order metric perturbation brings about two additional technical difficulties: the need for a certain regularization at infinity and on the event horizon of the large black hole, and the strong divergence of the second-order source of the field equations near the small object. We show how these issues can be resolved, first in a simple scalar-field toy model, and then in the second-order gravitational problem. We finally apply our method in full in order to numerically solve the second-order perturbation equations in the quasicircular case, focusing on the monopole piece of the perturbation as a first example.

# Contents

# List of Figures

# List of Tables

## Declaration of Authorship

I, Jeremy Miller , declare that the thesis entitled *The second-order gravitational self-force* and the work presented in the thesis are both my own, and have been generated by me as the result of my own original research. I confirm that:

- this work was done wholly or mainly while in candidature for a research degree at this University;
- where any part of this thesis has previously been submitted for a degree or any other qualification at this University or any other institution, this has been clearly stated;
- where I have consulted the published work of others, this is always clearly attributed;
- where I have quoted from the work of others, the source is always given. With the exception of such quotations, this thesis is entirely my own work;
- I have acknowledged all main sources of help;
- where the thesis is based on work done by myself jointly with others, I have made clear exactly what was done by others and what I have contributed myself;
- parts of this work have been published as: [1] and [2]

Signed:.......................................................................................................

July 10th 2017
Date:..........................................................................................................

# Acknowledgements

Many thanks go to my supervisors Leor Barack and Adam Pound. I would like to thank Adam Pound for many fruitful discussions, with whom it has been a pleasure to collaborate. Thank you to Leor Barack for welcoming me to the Self Force research group and funding my Ph.D. I would also like to thank my colleagues Niels Warburton and Barry Wardell for fruitful discussions. With the oversight of my main supervisor, editorial advice has been sought. No changes of intellectual content were made as a result of this advice.

# Chapter 1

# Introduction

## 1.1 Gravitational-wave astronomy and the binary inspiral problem

In 1915 Einstein published [3] the theory of General Relativity (GR). The theory came as a radical generalisation of Newton's law of gravity and describes gravity in terms of a geometrical curvature of spacetime. In 1916 Einstein found that the linearized weak-field equations possessed wave solutions, which spurred the prediction of the existence of gravitational waves (GWs), tiny ripples in the fabric of spacetime that propagate at the speed of light. Almost 100 years later, on September 14, 2015, GWs were detected for the first time [4] at the Laser Interferometer Gravitational-Wave Observatory (LIGO). The GWs in this observation originated from a binary black-hole system merging into one black hole. Less than a year later LIGO detected GWs from another black-hole binary [5]. These landmark observations verify that GWs exist, and stand as an important test of the validity of GR [6]. They also directly prove the existence of black holes in nature, and demonstrate that black holes can occur in binaries and merge. LIGO's observations mark the dawn of a new age in astronomical research: the age of *Gravitational Wave Astronomy*.

### 1.1.1 Brief history of gravitational waves

GWs are a relativistic phenomenon manifest in spacetimes with a large time-varying quadrupole moment, or higher multipole moments. An example is the spacetime geometry of a binary system of two compact bodies, such as neutron stars or black holes (BHs). The gravitational field of such a system contains propagating GWs.

The very existence of GWs has historically been marked by controversy. Poincaré first postulated the existence of GWs in 1905 [7], suggesting that by analogy with the electromagnetic waves emanating from an accelerated electric charge, so too an accelerated mass in a relativistic field theory should emit GWs. Following this Einstein investigated whether the field equations predicted the existence of GWs, and under certain assumptions attempted to simplify and cast them into a format analogous to the Maxwell equations of electromagnetism. Einstein vacillated on the question of their existence, because people thought the waves were ripples in coordinates, not ripples in the spacetime geometry. But finally, in 1936 Einstein and Rosen submitted a paper to the Physical Review claiming that GWs *could not* exist because any such solution of the field equations would have a singularity. The paper was reviewed by Robertson who reported that the singularities in question were simply the harmless coordinate singularities of the cylindrical coordinates used [8]. Initially Einstein angrily withdrew the manuscript, but was later convinced by Infeld that the criticism was in fact correct [9], and the paper was rewritten with the position that GWs do in fact exist, and published in a different journal [10]. Afterwards the question of whether GWs transmit energy was addressed at the first GR conference at Chapel Hill in 1957. Richard Feynman answered the question based on the "sticky bead argument" [11], convincingly demonstrating that GWs do in fact transmit energy. This was later explained by Bondi in detail in Ref. [12].

The first experimental evidence of GWs came following the discovery of the binary pulsar PSRB1913+16 by Hulse and Taylor in 1974 [13]. The gradual decay of its orbital period, observed over many years, precisely agreed with the loss of energy and angular momentum due to GW radiation as predicted by GR [14].

The binary pulsar provided indirect evidence of GWs. A more direct method for detecting GWs was proposed by Joseph Weber in the early 1960s, using resonant bars. Weber's bar detectors consisted of solid aluminum cylinders, about two meters long and one meter in diameter, suspended on steel wires. A passing GW would set one of these cylinders vibrating at its resonant frequency (about 1660 Hz), and piezoelectric crystals firmly attached around the cylinder's waist would convert that vibration into an electrical signal. Weber published his results in 1968 in [15], claiming that he had detected GWs. However, his experiment was repeated by others, none of whom detected anything but random noise. By the late 1970s, everyone but Weber agreed that his claimed detections were spurious.

The main technology used today for detecting GWs is based on the idea of Michaelson-type laser interferometry. This method was first proposed by Gertsenshtein and Pustovoit in 1962, only a year after Weber's proposal [16]. After the pioneering development of the GEO600 detector in Germany during the 1990s, the search for GWs using laser interferometry began in earnest in 2002, when the Laser Interferometer Gravitational-wave Observatory (LIGO) began its initial phase of operation. The LIGO experiment consists of two detectors: one in Hanford, Washington, and another in Livingston, Louisiana, 3002 km away. These two widely separated detectors operate in unison, to help rule

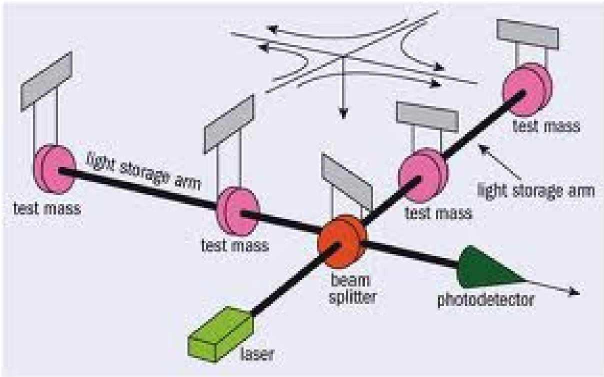


Figure 1.1: Schematic diagram of LIGO, taken from Fig. 2 in Ref. [17]. The laser emits a light beam, which is split by the beam splitter into two beams that travel repeatedly between two sets of mirrors. The system is calibrated so that, in the absence of incident GWs, the interference between the two beams directs all of the light back toward the laser. If there is any difference between the lengths of the two arms due to a passing GW, some light will travel to where it can be recorded by a photo-detector

out false signals from local disturbances. Figure 1.1 illustrates the operation principle of each of the two LIGO interferometers.

Currently there are several more ground-based detectors being constructed that will complement LIGO's existing efforts. The Kamioka Gravitational Wave Detector (KAGRA), Advanced Virgo and LIGO-India detectors will all become operational within the next decade. There is also a strong motivation for having detectors in space, since this will open up the possibility of detecting GWs in the mHz band, not accessible from Earth due to noise from seismic gravity-gradient perturbations. To this end, plans are underway for the Laser Interferometer Space Antenna (LISA). LISA will be comprised of three satellites in a triangular formation that follows behind Earth's orbit around the Sun. The satellites are separated by a distance of the order of one million km, and that distance is continuously measured via laser interferometry. There is also a proposal for the space-based Deci-Hertz Interferometer Gravitational-Wave Observatory (DECIGO) [18, 19], designed to be sensitive in the frequency band between 0.1 and 10 Hz, filling in the gap between the sensitivity bands of LIGO and LISA.

### 1.1.2 Inspiralling binaries as sources of gravitational waves

The first directly detected signal [4], GW150914, came from the merger of two BHs of mass $36^{+5}_{-4}M_\odot$ and $29^{+4}_{-4}M_\odot$, into a single BH of mass $62^{+4}_{-4}M_\odot$, 410 mega-parsecs from Earth. The second signal, GW151226, detected on December 26 2015 [5], came from the coalescence of two BHs of mass $14.2^{+8.3}_{-3.7}M_\odot$ and $7.5^{+2.3}_{-2.3}M_\odot$, into one BH of mass $20.8^{+6.1}_{-1.7}M_\odot$, 440 mega-parsecs from Earth. Both signals were confidently detected, despite having a gravitational wave-strain as small as $1.0 \times 10^{-21}$.

Binaries of this kind, comprising two closely bound, very dense objects such as BHs or neutron stars, are intrinsically strong emitters of GWs. As they radiate, they continuously lose energy. Consequently, the two bodies spiral in towards each other and eventually merge.

Such binaries are characterised by the mass-ratio $M/\mu$, $M$ being the mass of the larger object and $\mu$ the mass of the smaller object (see Fig. 1.2). They come in three categories: *comparable-mass* inspirals have $M/\mu$ values between 1 and a few; *extreme mass-ratio* inspirals (EMRIs) have $\mu \ll M$ ($10^4 \lesssim M/\mu \lesssim 10^7$ for astrophysically relevant sources); and *intermediate mass-ratio* inspirals (IMRIs) span the intermediate range of mass ratios ($M/\mu$ from a few tens to a few thousand for astrophysically relevant sources). The GW frequency of inspiralling binaries in the final stage of the inspiral is roughly inversely proportional to the total mass of the system. A merging binary of two stellar-size masses emits in the LIGO/Virgo band, while a binary of two massive BHs (MBHs) emits in the LISA band. Examples of IMRIs include the inspiral of a neutron star or a stellar-mass BH into an intermediate-mass BH (one of mass between a few tens and a few thousands); and the inspiral of an intermediate-mass BH into an MBH. The former are potential sources for LISA, while the latter emit in the LIGO/Virgo band.

This work focuses on EMRIs. EMRIs are binary systems comprised of a stellar-mass compact object (a white dwarf, neutron star or stellar-mass BH) spiraling into an MBH. EMRIs emit GWs with frequencies within the bandwidth of LISA. A typical EMRI spends the last few years of inspiral in a tight orbit around the MBH, emitting $\sim M/\mu$ GW cycles over that period, while the small object is in close proximity to the event horizon of the BH. This scenario will be discussed in more detail in Sec. 1.1.4.

### 1.1.3 Models of binary systems

A number of methods are available for modeling binary systems. Different methods apply in different regimes, depending on the mass ratio and orbital separation. A diagram showing which methods are relevant for which types of binaries can be found in Fig. 1.2. At large orbital separations post-Newtonian (PN) theory applies. Numerical relativity (NR), which solves the full non-linear Einstein equations, is in principle valid across the entire parameter space depicted in Fig. 1.2. However, in practice, computational burdens restrict its use to comparable mass inspirals with small orbital separations. Effective-one-body (EOB) theory is a phenomenological model that is also theoretically valid across the entire parameter space. It models the binary system as a test particle moving in an effective external metric, taken to be a deformed Schwarzschild metric with extra free functions and parameters. NR-calibrated EOB waveforms had an important role in enabling the exact interpretation of both LIGO's first [4] and second [5] signal.

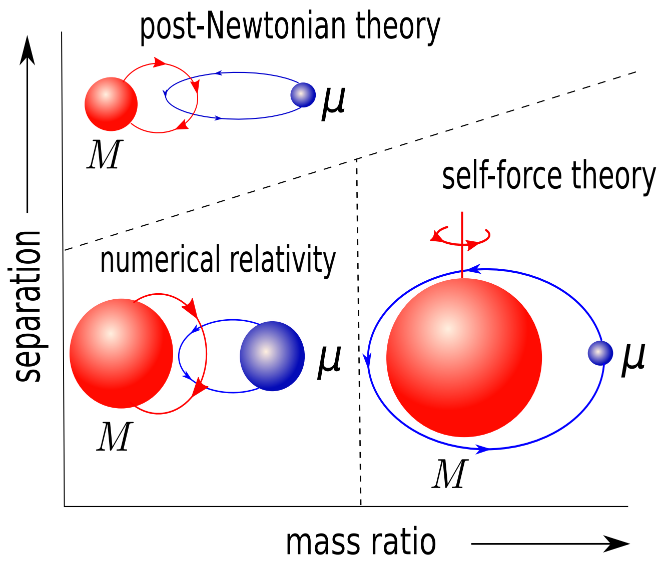


Figure 1.2: The two-dimensional space of the essential parameters of a binary system, which consists of two compact objects or black holes of masses $M$ and $\mu$. The horizontal axis shows the mass ratio $(M/\mu)$ and the vertical axis shows the orbital separation. The diagram schematically illustrates the parameter regions where post-Newtonian theory, self-force theory and numerical relativity apply.

In the case of IMRIs and EMRIs, where $\mu$ is significantly smaller than $M$, there are currently no accurate models available. In the case of EMRIs, PN theory is inaccurate because the system is highly relativistic, and NR cannot accommodate the two very different length scales and large number of orbits in the inspiral. The natural method for providing an accurate description of EMRIs is the gravitational self-force (GSF) model, which (roughly speaking) is an expansion of the binary's metric in powers of the mass ratio $\mu/M$. In this expansion, the smaller object's gravitational field represents a small perturbation of the field of the larger object, and it exerts a "self-force" back on the smaller object.

A detailed overview of SF physics and its history is given in Sec. 1.2 of this introduction. Not only is the SF model directly relevant to the EMRI problem, but also GSF results have an important application further afield in improving models of binaries in other regimes of the problem. At first order, numerical SF data has been fruitfully used to fix higher-order terms and otherwise-free parameters in PN [20–23] and EOB [24–27] models. In addition, SF data set benchmarks in the extreme-mass-ratio limit of NR.

### 1.1.4 Extreme mass ratio inspirals

Many types of GW sources offer strong observational tests of GR. However, EMRIs are particularly powerful in that regard. EMRIs have a long inspiral time and they generate many tens of thousands of GW cycles in the strong-field regime, as the small object orbits very close to the MBH. As such, they trace out a detailed map of the curved spacetime around the MBH, and the emitted radiation carries precise information about its physical parameters. For example, the mass of the MBH can be measured to within an accuracy of 0.1 %, as well as the spin and quadrupole moment to within a similar accuracy [28, 29]. The GWs also encode information about the orbital dynamics. Typically, EMRI orbits can be eccentric, inclined and rapidly precessing, offering a rich set of relativistic phenomena to study. For example, the precession rate of the orbit can be extracted from GW signals.

While EMRI GWs transmit information on the physical parameters of the MBH, the "no-hair" theorem restricts the amount of information that exists. The "no-hair" theorem states that all stationary vacuum BH solutions of the Einstein equations are completely characterized by three parameters: mass, spin and electric charge. For astrophysical objects the electric charge is typically zero since any net electric charge will have been neutralized. Thus, the Kerr geometry is believed to represent the unique final state of any collapsing star [30]. The Kerr metric depends on two parameters, the mass ($M$) and spin ($aM$) of the BH. All higher mass and spin multipole moments of the spacetime are uniquely determined by $M$ and $a$.

Information carried by EMRI GWs can be used to directly probe the spacetime in the region close to the MBH and provide a detailed picture of its curved geometry. In particular this will tell us whether or not the surrounding spacetime differs from Kerr spacetime, and hence whether the no-hair theorem is valid. We can also determine if there is an event horizon present, simply from the sudden truncation of the signal [31].

In order to extract this detailed information, detailed models are needed so that we can filter out the GW data from instrumental and foreground noises. EMRI signals are expected to be relatively weak and typically buried deep within the noise. We can dig them out using the matched filtering technique. An explanation of matched filtering can be found in the introduction of Ref. [32]. One important reason we need matched filtering is that GW detectors (unlike optical telescopes) cannot be "pointed" to a source; they hear all sources mixed together at the same time. To filter out irrelevant sources we need at our disposal theoretical templates of the waveforms. Inspirals are driven by the gravitational SF. Therefore, knowledge of the gravitational SF is a prerequisite for modeling the waveforms.

## 1.2 The self-force

### 1.2.1 Historical overview

The history of SF research began with the study of the electromagnetic (EM) radiation-reaction force. The EM radiation-reaction force acts on an accelerating charged particle and is caused by the particle emitting EM radiation. The emission of radiation removes energy and angular momentum from the particle, which leads to a damping of its acceleration. It was first studied by Abraham and Lorentz [33] prior to the publication of Special Relativity, and named the Abraham-Lorentz force. Later on, Dirac [34] in 1938 derived its special-relativistic extension.

In 1960 DeWitt and Brehme generalised Dirac's result to curved spacetime [35]. In their result, the equation of motion has the same form as Dirac's, but with an additional "tail" term. This tail term is the integral of the retarded EM Green's function along the past worldline of the particle. The origin of this term, which lies in the scattering of waves off spacetime curvature, will be explained in Sec. 1.2.3. In flat space the tail integral vanishes and the equation of motion reduces to Dirac's equation. In curved space, the particle deviates from geodesic motion even in the absence of any external EM forces, due to the tail effect. Hobbs corrected DeWitt and Brehme's result [36] some years later, finding the addition of an explicit Ricci-tensor term in the equation of motion.

The field progressed from EM to linearized gravity in 1997, when Mino, Sasaki and Tanaka derived the GSF to first order in $\mu$ [37], using an approach called matched asymptotic expansions, to be discussed in Chapter 2. Soon after, the same result was derived [38] by Quinn and Wald using an axiomatic approach. The equation of motion they derived, now referred to as the MiSaTaQuWa equation, represents the first subleading correction to the geodesic, test-particle approximation. Like the EM SF, the GSF was found to arise from tail effects.

Since then, GSF theory has been given a rigorous mathematical foundation [39,40], extended to arbitrary perturbative order in $\mu$ [41], and even developed in the fully nonlinear context [42]. Explicit equations of motion have been derived through second order in $\mu$ by Gralla [43], Pound [44] and Rosenthal [45]. The formulation of Pound will provide the basis for the work in this thesis.

### 1.2.2 The electromagnetic self-force in flat space

In this and in the following sections, we give an overview of the physics underlying SF theory and some of its main results. Our description closely follows the review article by Poisson, Pound and Vega [46]. We begin with the Dirac radiation-reaction force [34] acting on a charged particle in flat space. An electric charge moving in flat spacetime produces a vector potential $A^\alpha$ that satisfies the wave equation

$$\Box A^\alpha = -4\pi j^\alpha, \tag{1.1}$$

where $j^\alpha$ is the particle's current density, and the Lorenz gauge condition

$$\partial_\alpha A^\alpha = 0. \tag{1.2}$$

The charge current $j^\alpha$ is infinite on the particle's worldline, and so too is $A^\alpha$ based on Eq. (1.1). Because the field is infinite, it is unclear what force it exerts on the charge, or whether there even exists a sensible force. To gain some insight into the nature of the force, consider the case of a negatively charged particle orbiting a much heavier, positively charged particle. Neglecting quantum effects, the negative charge will emit EM radiation, lose energy and eventually spiral into the positive charge. This inspiral must be driven by a dissipative, time-asymmetric radiation-reaction force in the particle's equation of motion. Based on that fact, the form of the radiation-reaction force can be derived by the following heuristic argument. We first note that in the retarded solution to Eq. (1.1), $A^\alpha_{\rm ret}$, radiation propagates outwards, breaking the time-reversal invariance of Maxwell's theory. Choosing the advanced solution $A^\alpha_{\rm adv}$ instead, radiation would propagate inwards. The linear combination[1]

$$A^\alpha_{\rm S} = \frac{1}{2}\left(A^\alpha_{\rm ret} + A^\alpha_{\rm adv}\right) \tag{1.3}$$

is a solution that restores time-reversal invariance. It corresponds to an equal amount of radiation propagating outwards and inwards. Hence, no radiation reaction occurs, rather the particle's energy remains constant. Ergo, $A^\alpha_{\rm S}$ has no contribution to the radiation-reaction force.

The remaining, time-asymmetric piece of $A^\alpha$ must therefore be entirely responsible for the radiation-reaction force. Inasmuch as the radiation-reaction force is defined on the particle, the piece of $A^\alpha$ that generates it must be non-singular on the worldline. But $A^\alpha_{\rm S}$ is just as singular on the worldline as the retarded potential, since $A^\alpha_{\rm ret}$, $A^\alpha_{\rm adv}$ and $A^\alpha_{\rm S}$ all satisfy Eq. (1.1). Hence, the singular behaviour of $A^\alpha_{\rm ret}$ can be removed by subtracting $A^\alpha_{\rm S}$, leaving a well-behaved, regular-on-the-worldline potential $A^\alpha_{\rm R}$, where[2]

$$A^\alpha_{\rm R} = A^\alpha_{\rm ret} - A^\alpha_{\rm S} = \frac{1}{2}\left(A^\alpha_{\rm ret} - A^\alpha_{\rm adv}\right). \tag{1.4}$$

With this in mind, we can reasonably suppose that $A^\alpha_{\rm R}$ generates an ordinary Lorentz force, as

$$\mu a_\mu = f^{\rm ext}_\mu + eF^{\rm R}_{\mu\nu}u^\nu, \tag{1.5}$$

[1]The subscript "S" refers to its symmetric time-dependence, or the fact that it is singular on the worldline, as we will see below.

[2] The subscript "R" stands for "regular", because $A^\alpha_{\rm R}$ is nonsingular on the worldline, or "radiation" since this field gives rise to the radiation-reaction force.

where $\mu$ is the mass of the charge, $F^{\rm R}_{\mu\nu} = \partial_\mu A^{\rm R}_\nu - \partial_\nu A^{\rm R}_\mu$ and $f^{\rm ext}_\mu$ is any external force acting on the charge. Dirac arrived at Eq. (1.5) by considering stress-energy conservation in a small tube around the particle's worldline [34]. It can be most rigorously derived from stress-energy conservation of an extended charge distribution in the limit of zero mass, charge, and size [47]. Explicitly evaluating $A^\alpha_{\rm R}$ leads to the more concrete expression

$$\mu a_\mu = f^{\rm ext}_\mu + \frac{2e^2}{3m}\left(\delta^\mu_\nu + u^\mu u_\nu\right)\frac{df^\nu_{\rm ext}}{d\tau}. \tag{1.6}$$

The second term is the radiation-reaction force. It is orthogonal to the four-velocity, proportional to $e^2$ and depends on the rate of change of the external force.

To prepare the ground for our discussion of the SF in curved spacetime, it is worthwhile to examine the properties of $A^\alpha_{\rm S}$ and $A^\alpha_{\rm R}$ in the language of Green's functions. In analogy with Eqs. (1.3) and (1.4), we may define singular and regular Green's functions

$$G_{{\rm S}}{}^{\alpha}{}_{\beta'}(x,x') = \frac{1}{2}\Big[G_{+}{}^{\alpha}{}_{\beta'}(x,x') + G_{-}{}^{\alpha}{}_{\beta'}(x,x')\Big], \tag{1.7}$$

$$G_{{\rm R}}{}^{\alpha}{}_{\beta'}(x,x') = \frac{1}{2}\Big[G_{+}{}^{\alpha}{}_{\beta'}(x,x') - G_{-}{}^{\alpha}{}_{\beta'}(x,x')\Big], \tag{1.8}$$

where a subscript '+' denotes the retarded Green's function, and a subscript '$-$' the advanced Green's function. Then the potential

$$A^\alpha_{\rm S}(x) = \int G_{{\rm S}}{}^{\alpha}{}_{\beta'}(x,x') j^{\beta'}(x')\, d^4x' \tag{1.9}$$

satisfies the flat-space wave equation of Eq. (1.1) and is singular on the worldline, while

$$A^\alpha_{\rm R}(x) = \int G_{{\rm R}}{}^{\alpha}{}_{\beta'}(x,x') j^{\beta'}(x')\, d^4x' \tag{1.10}$$

satisfies the flat-space homogeneous equation $\Box A^\alpha = 0$ and is smooth on the worldline.

In flat space, the Green's functions can be written explicitly as

$$G_{\pm}{}^{\alpha}{}_{\beta'}(x,x') = \delta^\alpha_{\beta'}\delta(t - t' \mp |\boldsymbol{x} - \boldsymbol{x'}|)/|\boldsymbol{x} - \boldsymbol{x'}|. \tag{1.11}$$

Eq. (1.11) suggests that the retarded potential, $A^\alpha_{\rm ret}$ at $x$, is sourced at the point where the worldline and $x$'s past light cone intersect, as depicted in Fig. 1.3. EM radiation propagates from the point $x'$ on the past worldline to the field point $x$, along null curves. Similarly, the advanced potential, $A^\alpha_{\rm adv}$, is sourced at the intersection of the worldline and the future light cone of the field point $x$, also shown in Fig. 1.3. Away from the worldline, $A^\alpha_{\rm R}$ inherits this noncausal dependence from $A^\alpha_{\rm adv}$. However, when evaluated at a point on the worldline, $A^\alpha_{\rm R}$ depends only on the state of the particle at that point.


Figure 1.3: In flat spacetime, the retarded potential at $x$ depends on the particle's state of motion at the retarded point $x'$ , where the worldline intersects the past light cone of $x$. The advanced potential depends on the state of motion at the advanced point $x'$, where the worldline intersects the future light cone of $x$.

### 1.2.3 The electromagnetic self-force in curved space

In a curved spacetime with metric $g_{\alpha\beta}$, the field $A^\alpha$ obeys

$$\Box A^\alpha - R^\alpha{}_\beta A^\beta = -4\pi j^\alpha, \tag{1.12}$$

where $\Box = g^{\alpha\beta}\nabla_\alpha\nabla_\beta$ is the covariant wave operator, $\nabla_\alpha$ denotes covariant differentiation consistent with $g_{\alpha\beta}$ and $R_{\alpha\beta}$ is the spacetime's Ricci tensor. The Lorenz gauge condition (1.2) in curved space becomes

$$\nabla_\alpha A^\alpha = 0. \tag{1.13}$$

The retarded/advanced solutions are given in terms of the corresponding Green's functions as

$$A^\alpha_{\mathrm{ret/adv}}(x) = \int G_{\pm}{}^{\alpha}{}_{\beta'}(x, x') j^{\beta'}(x') \sqrt{-\mathrm{g}}\, d^4x', \tag{1.14}$$

where g is the determinant of the metric, $G_{\pm}{}^{\alpha}{}_{\beta'}(x, x')$ is the Green's function for Eq. (1.12), $x$ is an arbitrary field point and $x'$ is a source point on the worldline. Tensors at $x$ are identified with unprimed indices, while primed indices refer to tensors at $x'$.

In curved spacetime the Green's functions take a more complicated form than in flat space. $G^\alpha_{\pm\beta'}(x, x')$ has support not only when $x$ is on the past or future light cone of $x'$, but within that light cone. This failure of Huygens' principle can be interpreted as a consequence of EM waves scattering off spacetime curvature, effectively causing them to propagate at all speeds smaller than or equal to the speed of light. Formally speaking, $G_{+}{}^{\alpha}{}_{\beta'}(x, x')$ is nonzero for all $x \in J^+(x')$, the entire *causal future* of $x'$, and $G_{-}{}^{\alpha}{}_{\beta'}(x, x')$ is nonzero for all $x \in J^-(x')$, the entire *causal past* of $x'$. Here we define $J^+(x')$ as the set of events that can be reached by a future directed *causal curve*, i.e. a curve whose tangent vector is timelike or null, starting from $x'$. An analogous definition holds for $J^-(x')$. This follows the convention that can be found on p.190 in Ref. [48]. Fig. 1.4 describes the retarded and advanced solutions if the source is a point charge.

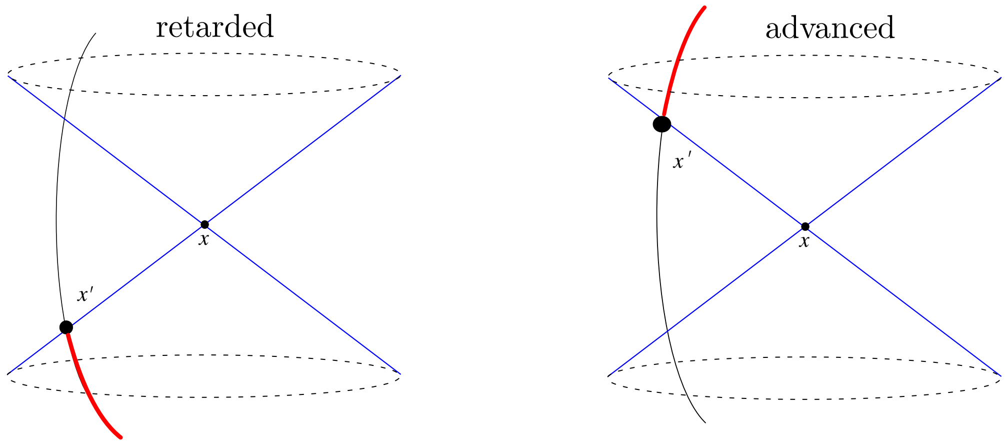


Figure 1.4: In curved spacetime, the retarded potential at $x$ depends on the past history of the worldline, which lies inside the past light cone of $x$. The advanced potential at $x$ depends on the future history of the worldline, which lies inside the future light cone of $x$.

On the grounds that the curved-space advanced Green's function has support on the entire causal future, $G^{\beta'}_{\mathrm{R}\alpha}$ as defined in (1.8) would lead to an unphysical SF in curved space. True, the resulting potential $A^{\alpha}_{\mathrm{R}}$ would satisfy the homogeneous equation, and be regular on the worldline, but it would also depend on the particle's entire future history. A SF constructed from this potential would be non-causal, so an alternative definition for $G^{\alpha}_{\mathrm{R}\beta'}$ is needed.

The correct singular and regular Green's functions were eventually derived by Detweiler and Whiting (DW) [49]. They introduced the Green's functions

$$G_{\mathrm{S}}{}^{\alpha}_{\beta'}(x,x') = \frac{1}{2}\Big[G_{+}{}^{\alpha}_{\beta'}(x,x') + G_{-}{}^{\alpha}_{\beta'}(x,x') - H^{\alpha}_{\beta'}(x,x')\Big], \tag{1.15}$$

$$\begin{aligned} G_{\mathrm{R}}{}^{\alpha}_{\beta'}(x,x') &= G_{+}{}^{\alpha}_{\beta'}(x,x') - G_{\mathrm{S}}{}^{\alpha}_{\beta'}(x,x') \\ &= \frac{1}{2}\Big[G_{+}{}^{\alpha}_{\beta'}(x,x') - G_{-}{}^{\alpha}_{\beta'}(x,x') + H^{\alpha}_{\beta'}(x,x')\Big]. \end{aligned} \tag{1.16}$$

The two-point function $H^{\alpha}_{\beta'}(x,x')$ is a homogeneous solution to the wave equation (1.12). Its introduction in Eqs. (1.15) and (1.16) is designed to yield a SF that is causal, through the following imposed conditions. Firstly,

$$H^{\alpha}_{\beta'}(x,x') = G_{-}{}^{\alpha}_{\beta'}(x,x') \;\text{ when }\; x \in I^{-}(x'), \tag{1.17}$$

where $I^{\pm}(x')$ is the chronological future (past) of the point $x'$. Here we define $I^{+}(x')$ as the set of events that can be reached by a future directed *chronological curve*, i.e. a curve whose tangent vector is timelike, starting from $x'$. An analogous definition holds for $I^{-}(x')$, where we follow the convention on p.190 in Ref. [48]. Since $G_{+}{}^{\alpha}_{\beta'}(x,x') = 0$ when $x \in I^{-}(x')$, (1.17) guarantees that $G_{\mathrm{S}}{}^{\alpha}_{\beta'}(x,x')$ vanishes when $x$ is in the chronological past of $x'$. The retarded and advanced Green's function satisfy the reciprocal property

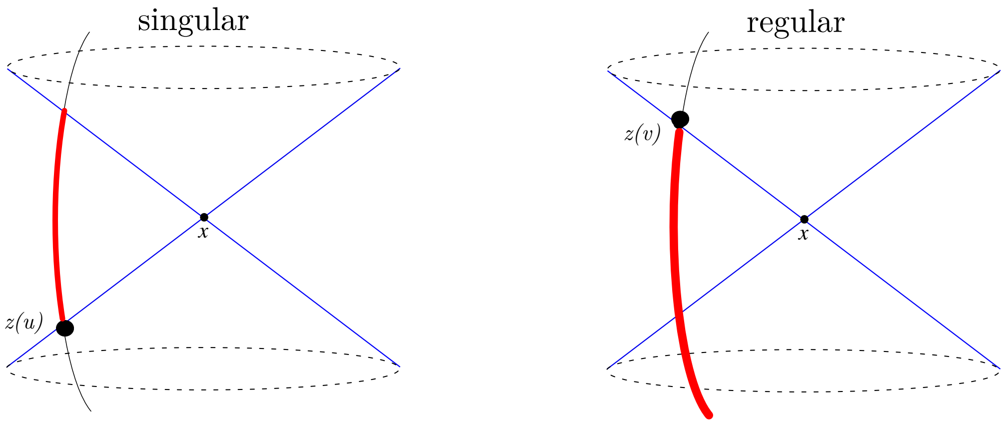


Figure 1.5: In curved spacetime, the singular potential at $x$ depends on the particle's history during the interval $u \leq \tau \leq v$, where $(v, u)$ are the advanced and retarded time coordinates associated with the point $x$. The regular potential at $x$ depends on the particle's history during the interval $-\infty < \tau \leq v$.

$G^{+}_{\alpha\beta'}(x, x') = G^{-}_{\beta'\alpha}(x', x)$, which implies straight from (1.17) that

$$H^{\alpha}{}_{\beta'}(x, x') = G_{+}{}^{\alpha}{}_{\beta'}(x, x') \quad \text{when} \quad x \in I^{+}(x'). \tag{1.18}$$

Then, because $G_{-}{}^{\alpha}{}_{\beta'}(x, x') = 0$ when $x \in I^{+}(x')$, (1.18) ensures that $G_{\mathrm{S}}{}^{\alpha}{}_{\beta'}(x, x')$ also vanishes when $x$ is in the chronological future of $x'$.

Accordingly, the dependence of $A^{\alpha}_{\mathrm{S}}(x)$ is limited to the worldline segment between times $u \leq \tau \leq v$, where $(v, u)$ are the advanced and retarded time coordinates associated with the point $x$, as shown in Fig. 1.5. This potential satisfies Eq. (1.12), and thus $A^{\alpha}_{\mathrm{S}}(x)$ is just as singular as the retarded potential close to the worldline.

Similarly, the Detweiler-Whiting regular two-point function (1.16) ensures that the regular potential has the desired properties. On the right-hand side of (1.16) there is $G_{\mathrm{S}}{}^{\alpha}{}_{\beta'}(x, x')$, which has support only for spatially separated $x$ and $x'$, and $G_{+}{}^{\alpha}{}_{\beta'}(x, x')$, which has support on and within the past light cone of $x$. Hence, the potential $A^{\alpha}_{\mathrm{R}}(x)$ constructed from $G_{\mathrm{R}}{}^{\alpha}{}_{\beta'}(x, x')$ depends on the worldline segment highlighted in Fig. 1.5, at all times $\tau$ prior to the advanced time $v$. Even though $A^{\alpha}_{\mathrm{R}}(x)$ is non-causal when evaluated away from the worldline, on the worldline it *is* causal, depending only on the past history. Furthermore, like its flat-spacetime analogue, it satisfies the homogeneous wave equation and is smooth on the worldline.

As in the flat-space case, one can show that the self-force is simply the Lorentz force exerted by the regular field, $eF^{\mathrm{R}}_{\mu\nu}u^{\nu}$, where $F^{\mathrm{R}}_{\mu\nu} = \nabla_{\alpha}A^{\mathrm{R}}_{\beta} - \nabla_{\beta}A^{\mathrm{R}}_{\alpha}$. Hence, the curved-spacetime generalization of the equation of motion (1.5) is

$$\mu a_{\mu} = f^{\mathrm{ext}}_{\mu} + eF^{\mathrm{R}}_{\mu\nu}u^{\nu}, \tag{1.19}$$

where $a^\mu = Du^\mu/d\tau$ is now the covariant acceleration and $f^{\rm ext}_\mu$ accounts for any external (non-gravitational) forces acting on the particle.

A detailed derivation of the explicit form of $F^{\rm R}_{\mu\nu}$ can be found in the review article [46]. Substituting it into (1.19) leads to a more concrete version of the equation of motion, which reads

$$\begin{aligned}\mu a^\mu =& f^\mu_{\rm ext} + e^2\big(\delta^\mu{}_\nu + u^\mu u_\nu\big)\left(\frac{2}{3}\frac{Df^\nu_{\rm ext}}{d\tau} + \frac{1}{3}R^\nu{}_\lambda u^\lambda\right) \\ &+ 2e^2 u_\nu \int_{-\infty}^{\tau^-} \nabla^{[\mu} G_{+}{}^{\nu]}{}_{\lambda'}\big(z(\tau), z(\tau')\big) u^{\lambda'}\, d\tau', \end{aligned} \tag{1.20}$$

where all terms in this expression are evaluated at $z(\tau)$ on the worldline. The integration range in the final term stops at $\tau' = \tau^- \equiv \tau - 0^+$, avoiding the singular behaviour of the retarded Green's function at coincidence.

As discussed in Sec. 1.2.1, the equation of motion (1.20) was first derived by DeWitt and Brehme [35] and later corrected by Hobbs [36]. They followed Dirac's method, but as in the flat-space case, the result has since been more rigorously derived by considering the point-particle limit of an asymptotically small but extended charge distribution [47]. The equation differs from the flat-space result (1.6) most prominently by the presence of a tail integral. This integral arises from the fact that the Green's function has support inside the past light cone, unlike in flat space. It represents radiation emitted earlier and coming back to the particle after interacting with the spacetime curvature.

### 1.2.4 The (linearized) gravitational self-force

In this section we review relevant results for the first-order GSF. A detailed derivation of these results will be given later, in Chapter 2. Consider a small body of mass $\mu$ moving in a smooth vacuum region of spacetime, described by a background metric $g_{\alpha\beta}$; although we are primarily interested in EMRIs, the discussion applies in any vacuum background. The small body generates a gravitational field described by a metric perturbation $h_{\alpha\beta}$. Fig. 1.6 illustrates this for the particular case of an EMRI. At leading order the small body moves along a geodesic of the background $g_{\alpha\beta}$, just like a test particle. But due to its finite mass and size there are corrections to this geodesic motion at each order of mass $\mu$. At first order in $\mu$, the field $h_{\alpha\beta}$ is a linear perturbation of the background $g_{\alpha\beta}$. The GSF arises due to the back reaction from this perturbation on the small body, as depicted in Fig. 1.7, accelerating it away from geodesic motion in the background spacetime.

Our description of the SF in linearized gravity closely parallels the description in EM. The geometry of the full spacetime is described by the metric $\mathrm{g}_{\alpha\beta}$, where $\mathrm{g}_{\alpha\beta} =$

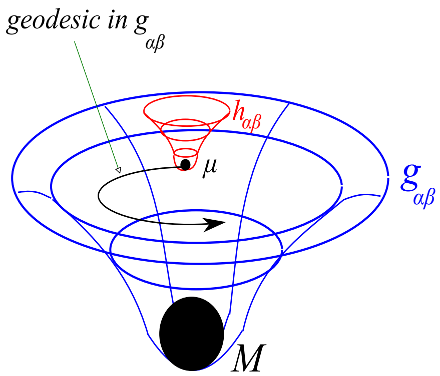


Figure 1.6: The small body of mass $\mu$ gives rise to a gravitational field $h_{\alpha\beta}$ shown in red, and the large black hole of mass $M$ is the source of the background spacetime $g_{\alpha\beta}$ shown in blue. At leading order, neglecting the interaction of the small body with its own field, the small body moves along a geodesic of the background $g_{\alpha\beta}$.

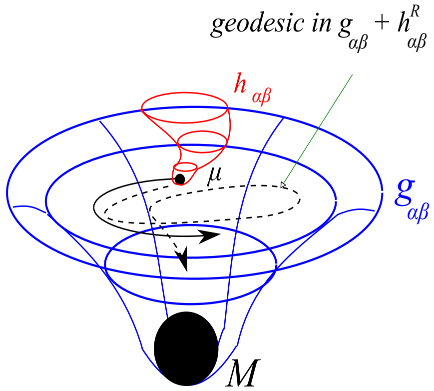


Figure 1.7: The gravitational field $h_{\alpha\beta}$ of the small body (red) induces a perturbation to the background spacetime $g_{\alpha\beta}$ (blue). The back reaction of $h_{\alpha\beta}$ on the small body accelerates it away from geodesic motion in the background spacetime (solid black line) to a geodesic in the spacetime described by the effective metric $g_{\alpha\beta} + h^{\mathrm{R}}_{\alpha\beta}$ (dotted line).

$g_{\alpha\beta} + h_{\alpha\beta}$. It satisfies the Einstein equation

$$G_{\alpha\beta}[\mathrm{g}] = 8\pi\mathcal{T}_{\alpha\beta}, \tag{1.21}$$

where $\mathcal{T}^{\alpha\beta}$ is the exact energy-momentum tensor of the small body. Here and throughout this thesis, standard geometrized units are used with $G = c = 1$. Retaining only linear terms in $h$ on the left-hand side, and defining the trace-reversed metric perturbation $\bar{h}_{\alpha\beta} \equiv h_{\alpha\beta} - \frac{1}{2}\left(g^{\gamma\delta}h_{\gamma\delta}\right)g_{\alpha\beta}$, leads to the linearized Einstein equation

$$\Box\bar{h}_{\alpha\beta} + 2R^{\gamma\ \,\delta}_{\ \alpha\ \,\beta}\bar{h}_{\gamma\delta} = -16\pi T^{1}_{\alpha\beta}, \tag{1.22}$$

where $R^{\gamma\ \,\delta}_{\ \alpha\ \,\beta}$ is the Riemann tensor of $g$, where indices are raised with the inverse of $g_{\alpha\beta}$, and $T^{1}_{\alpha\beta}$ is an approximate stress-energy tensor for the small body. As was shown by D'Eath [50] and later by Gralla and Wald [39], the extended body can be treated as a point mass at linear order. This is true even if the body is a black hole, when the exact stress-energy $\mathcal{T}^{\alpha\beta}$ vanishes; we will explain how this result is derived from the method of matched asymptotic expansions in Chapter 2. Therefore, $T^{1}_{\alpha\beta}$ is given by

$$T^{1}_{\alpha\beta} = \mu\int_{\gamma} d\tau\ u_{\alpha}u_{\beta}\frac{\delta^{4}\left(x - z\left(\tau\right)\right)}{\sqrt{-g}}, \tag{1.23}$$

where $z^{\mu}(\tau)$ are coordinates on the particle's worldline $\gamma$, $u^{\alpha} \equiv dz^{\alpha}/d\tau$ is the particle's four-velocity, and $\tau$ is proper time on $\gamma$ with respect to the background metric $g_{\alpha\beta}$. $\delta^{4}\left(x - z(\tau)\right) \equiv \delta\left(x_0 - z_0(\tau)\right)\delta\left(x_1 - z_1(\tau)\right)\delta\left(x_2 - z_2(\tau)\right)\delta\left(x_3 - z_3(\tau)\right)$, where $\delta\left(x - y\right)$

is the standard Dirac-delta function. Like in the EM case, we arrived at the wave equation (1.22) by making a particular choice of gauge. Specifically, we have imposed

$$\nabla_\beta \bar{h}^{\alpha\beta} = 0. \tag{1.24}$$

Eq. (1.24) is the Lorenz-gauge condition for the gravitational field $h_{\alpha\beta}$.

The retarded solution to (1.22) is

$$\bar{h}^{\alpha\beta}(x) = 4\mu \int_\gamma G_{+\ \mu\nu}^{\ \alpha\beta}(x, z(\tau)) u^\mu u^\nu \, d\tau + O(\mu^2), \tag{1.25}$$

where $G_{+\ \mu\nu}^{\ \alpha\beta}(x,z)$ is the retarded Green's function associated with Eq. (1.22). In exact analogy with the DW singular-regular split of the EM field described above, the retarded field can be written as the singular-regular decomposition [49]

$$h^{\text{ret}}_{\alpha\beta} = h^{\text{S}}_{\alpha\beta} + h^{\text{R}}_{\alpha\beta}. \tag{1.26}$$

$h^{\text{S}}_{\alpha\beta}$ is a certain singular piece of the retarded field defined from a Green's function analogous to (1.15), which is just as singular as the retarded field on the worldline, and has no effect on the particle's motion. It satisfies the wave equation (1.22). $h^{\text{R}}_{\alpha\beta}$ , defined from a two-point function analogous to (1.16), is regular on the worldline and is entirely responsible for the motion of the particle. It satisfies the homogeneous version of the wave equation (1.22).

Just as the point charge behaves as an ordinary test particle in the regular potential $A^{\text{R}}$, the point mass behaves as a test particle in the regular metric $g + h^{\text{R}}$. Its equation of motion is

$$a^\mu = -\frac{1}{2}\left(g^{\mu\nu} + u^\mu u^\nu\right)\left(2h^{\text{R}}_{\nu\lambda;\rho} - h^{\text{R}}_{\lambda\rho;\nu}\right) u^\lambda u^\rho + O(\mu^2), \tag{1.27}$$

where $a^\mu = Du^\mu/d\tau$ is the four-acceleration and ";" refers to covariant differentiation consistent with $g_{\mu\nu}$, with all terms on the right-hand side evaluated on $\gamma$. Eq. (1.27) is identical to the geodesic equation in $g + h^{\text{R}}$ (expanded to linear order in $h^{\text{R}}$). The right-hand side of (1.27) can be thought of as an effective gravitational force per unit mass. Explicitly evaluating it in terms of Green's functions leads to an expression for the GSF analogous to (1.20), involving a tail integral. As discussed in Sec. 1.2.1, it was that form of the equation of motion that was first derived by Mino, Sasaki, and Tanaka and Quinn and Wald. Like in the EM case, the result is most rigorously derived by considering an appropriate limiting process for a small body, which we will describe in Chapter 2.

### 1.2.5 Nonlinear gravitational self force

In the above discussion, we have only discussed the linear effects of the small object's perturbation. Over the last twenty years, since the MiSaTaQuWa equation was first derived, there has been an international effort to compute those effects in binary inspirals. Major progress has been made toward that end, which we review in the next section. However, the first-order GSF alone is insufficient for interpreting GW data coming from EMRIs because the contribution from the second-order GSF can be important, as the following argument [1] will demonstrate.

Let us denote the particle's energy as $E$ and let $\dot{E}$ refer to its rate of change. Note that $E$ decreases due to the dissipation of GWs. The inspiral will take place over a time-scale $\Delta t = E/\dot{E} \sim M^2/\mu$. Therefore, for a typical EMRI where $M/\mu \sim 10^6$, the inspiral time is very large (compared to the orbital period), and a sufficiently accurate model is needed that relates the waveforms to the motion over that large time-scale. To quantify how accurate, consider the acceleration $a^\mu$ of the smaller object due to the GSF, which will cause a shift $\delta z^\mu$ away from geodesic motion in the background. After the inspiral time $\Delta t$ this shift $\delta z^\mu$ will be of the order

$$\delta z^\mu \sim a^\mu \Delta t^2 = \left(\epsilon^0 a_0^\mu + \epsilon^1 a_1^\mu + \epsilon^2 a_2^\mu + O(\epsilon^3)\right) \Delta t^2, \tag{1.28}$$

where $a_0^\mu$, the leading order acceleration, is zero. The parameter $\epsilon \equiv 1$ simply counts powers of the mass $\mu$. $a_n^\mu$ is the $n$th-order-in-mass piece of the acceleration. Hence, Eq. (1.28) tells us that after an inspiral time, the second-order correction to the acceleration will lead to an accumulated shift of order $\epsilon^2 a_2^\mu \Delta t^2 \sim M$, which is large. Therefore, we cannot neglect second-order effects. Furthermore, if we include the second-order acceleration term, then the remnant error in Eq. (1.28) is only $\epsilon^3 a_3^\mu \Delta t^2 \sim \mu \ll M$, which we can safely neglect. In light of this, we can expect that second-order results will be both necessary and sufficient to model the waveform produced by an EMRI.

Motivated by this need, several researchers have developed second-order (and higher) extensions of the MiSaTaQuWa results. Rather than the linearized approximation (1.22), we must consider the Einstein equations through second order. The exact Einstein tensor can be expanded in orders of the metric perturbation $h_{\alpha\beta}$, as

$$G_{\alpha\beta}[\mathrm{g}] = G_{\alpha\beta}[g] + \delta G_{\alpha\beta}[h] + \delta^2 G_{\alpha\beta}[h] + O(h^3), \tag{1.29}$$

where the first term is the Einstein tensor associated with the background metric $g_{\alpha\beta}$, and

$$\delta^n G_{\alpha\beta}[h] \equiv \frac{1}{n!} \frac{d^n G_{\alpha\beta}[g+\lambda h]}{d\lambda^n}\bigg|_{\lambda=0}. \tag{1.30}$$

We then consider the full metric as a one-parameter family with parameter $\mu$, and expand it in terms of that parameter:

$$\mathrm{g}_{\alpha\beta} = \epsilon^0 g_{\alpha\beta} + \epsilon h^1_{\alpha\beta} + \epsilon^2 h^2_{\alpha\beta} + O(\epsilon^3). \tag{1.31}$$

After substituting this into Eq. (1.29), we seek equations for the perturbations $h^1_{\alpha\beta}$ and $h^2_{\alpha\beta}$. However, an obstacle arises in deriving the right-hand sides of those equations because at second order, the point-mass approximation breaks down. To understand why we can no longer model the body as a point mass, let us suppose that we could use a point-mass stress-energy tensor in the full equation (1.21). Staying with the same notation as Sec. 1.2.4, we shall refer to the worldline of this point mass as $\gamma$. Then substituting Eqs. (1.29) and (1.31) into Eq. (1.21) would lead to the Einstein equations at each order in $\mu$, through second order, as

$$\delta G_{\alpha\beta}[h^1] = 8\pi T^1_{\alpha\beta}, \tag{1.32}$$
$$\delta G_{\alpha\beta}[h^2] = -\delta^2 G_{\alpha\beta}[h^1, h^1] + 8\pi T^2_{\alpha\beta}, \tag{1.33}$$

where $T^1_{\alpha\beta}$ and $T^2_{\alpha\beta}$ are the first- and second-order in $\mu$ pieces of the stress-energy tensor for a point mass. The full stress-energy tensor for the point mass would read

$$\mathcal{T}_{\alpha\beta} = \mu \int_\gamma d\mathsf{t}\ \mathsf{u}_\alpha \mathsf{u}_\beta \frac{\delta^4\left(x - z\left(\mathsf{t}\right)\right)}{\sqrt{-\mathrm{g}}}, \tag{1.34}$$

where $\mathsf{u}^\alpha \equiv dz^\alpha/d\mathsf{t}$ and $\mathsf{t}$ is proper time on the worldline with respect to the metric of the full spacetime. $T^1_{\alpha\beta}$ would be the correct, well-defined point source in (1.23). But $T^2_{\alpha\beta}$ would contain terms of the form

$$\mu \int_\gamma d\tau\, u_\alpha u_\beta \left(-\frac{1}{2} g^{\mu\nu} h^1_{\mu\nu}\right) \frac{\delta^4(x - z(\tau))}{(-g)^{1/2}}. \tag{1.35}$$

This leads to difficulties, since the solution for $h^1_{\alpha\beta}$ diverges as $1/r$ on the worldline, where $r$ is a measure of distance to the particle. Consequently, $T^2_{\alpha\beta}$ diverges like $\delta(r)/r$ on the worldline, which is ill-defined and precludes Eq. (1.33) from having a solution. Even if we do not assume (1.34) but instead take $T^2_{\alpha\beta}$ to be some well-behaved point source, difficulties still arise from the term $\delta^2 G[h^1, h^1]$ in Eq. (1.33). Since it has the schematic form $\delta^2 G[h^1, h^1] = \left(\partial h^1\right)^2 + h^1 \partial^2 h^1$, it possesses a $1/r^4$ divergence. This divergence is not integrable and not a well-defined distribution.

Rather than seeking a distributional equation for the retarded field, we instead find a local solution for it outside the object, where we can safely solve vacuum field equations. Based on that solution, we then define field equations for a different variable, with a well-behaved source, near the worldline. This will be described in the next section.

Because we cannot write down a valid distributional source at second order, we also cannot define singular and regular fields in terms of Green's functions. However, we can define analogs to them based on the form of the local solution outside the object as

$$h^n_{\alpha\beta} = h^{\mathrm{S}n}_{\alpha\beta} + h^{\mathrm{R}n}_{\alpha\beta}. \tag{1.36}$$

$h^{\mathrm{S}n}$ and $h^{\mathrm{R}n}$ are the $n$th-order singular and regular fields, respectively, which are a generalisation of the first-order singular/regular split of Eq. (1.26). Their precise definition is very technical, and will be given in the next chapter. We mention a few of their key properties here, which are preserved from first order. The regular field $h^{\mathrm{R}n}_{\alpha\beta}$ is a smooth solution to the $n$th-order vacuum Einstein field equation and causal on the worldline of the small object. The singular field $h^{\mathrm{S}n}_{\alpha\beta}$ is, loosely speaking, the $n$th-order self-field of the small object, characterized by the multipole structure of the small object. $h^{\mathrm{S}}$ and $h^{\mathrm{R}}$ are identified using matched asymptotic expansions, as will be detailed in Chapter 2.

The equation of motion at second order is given by [41, 44]

$$\begin{aligned}\frac{D^2 z^\mu}{d\tau^2} &= -\frac{1}{2}\left(g^{\mu\nu} + u^\mu u^\nu\right)\left(g_\nu{}^\gamma - h^{\mathrm{R}}_\nu{}^{\gamma}\right)\left(2h^{\mathrm{R}}_{\beta\gamma;\alpha} - h^{\mathrm{R}}_{\alpha\beta;\gamma}\right)u^\alpha u^\beta + O(\epsilon^3)\\ &= \epsilon F^\mu_1 + \epsilon^2 F^\mu_2 + O(\epsilon^3)\,,\end{aligned} \tag{1.37}$$

where $F^\mu_n$ is the $n$th-order GSF per unit mass, and $h^{\mathrm{R}}_{\mu\nu} = \epsilon h^{\mathrm{R1}}_{\mu\nu} + \epsilon^2 h^{\mathrm{R2}}_{\mu\nu}$. Like Eq. (1.27), Eq. (1.37) is equivalent to the geodesic equation in the vacuum spacetime $g_{\mu\nu} + h^{\mathrm{R}}_{\mu\nu}$. Both results can be interpreted as a *generalised equivalence principle*. We will review the derivation of this result in Chapter 2.

## 1.3 Numerical implementations and state of the art

A number of physical effects have been calculated from the conservative part of the GSF, including the orbital precession in Schwarzschild [51] and in Kerr [52], the shift in frequency of the innermost stable circular orbit (ISCO) in Schwarzschild [23, 53, 54] and in Kerr [55], Detweiler's redshift variable (the ratio of proper time measured along the geodesic in the regular metric to the time measured by an inertial observer at infinity) [51, 56], spin precession [57] and tidal effects [58]. The most advanced GSF code can calculate the GSF along generic bound geodesic orbits in the equatorial plane of a Kerr BH [52, 59].

Generic inspiral orbits incorporating first-order GSF effects have been simulated in Schwarzschild [60]. Moreover, in Kerr, simulations of bound equatorial inspirals can in principle be simulated including first-order GSF effects, now that all the necessary input for the calculation is available [61]. However, these simulations are missing important second-order effects.

Several strategies are capable of calculating the first-order GSF in the time domain [62, 63] and in the frequency domain [64–66]. Of these strategies there are three main categories: The *mode-sum* approach, the *effective-source* approach and the *worldline convolution* approach.

The worldline convolution approach [67] computes the GSF by constructing a retarded Green's function and directly evaluating the tail integrals, like (1.20). It is historically the most obvious approach, since the MiSaTaQuWa equation, as well as the scalar and EM self-forces were first written in terms of tail integrals. The drawback of the method is that it is difficult to accurately compute the Green's function, and in principle one needs to compute it for all possible pairs of points. The merit is that once the Green's function is known, computing the GSF in any given scenario becomes a simple matter of evaluating an integral.

The mode-sum approach was introduced in Refs. [68, 69]. The GSF is calculated from the formula (1.27), as

$$F^\alpha_{\rm self} = \lim_{x\to z}\left[F^\alpha_{\rm ret}(x) - F^\alpha_{\rm S}(x)\right], \tag{1.38}$$

where $F^\alpha_{\rm ret}$ and $F^\alpha_{\rm S}$ are given by $\mu a^\alpha$ where $a^\alpha$ is given by Eq. (1.27), with $h^{\rm R}$ replaced with $h^{\rm ret}$ and $h^{\rm S}$, respectively, and $u^\alpha$ replaced with any smooth extension of the four-velocity off of $\gamma$. Here, $\lim_{x\to z}$ denotes the limit from a generic point $x$ off the wordline to the point $z$ on the worldline. While $F^\alpha_{\rm ret}(x)$ and $F^\alpha_{\rm S}(x)$ blow up on the particle, referring to a decomposition into spherical-harmonic modes, the $\ell$ modes $F^{\alpha\,\ell}_{\rm ret}(x)$ and $F^{\alpha\,\ell}_{\rm S}(x)$, are bounded there. $F^\alpha_{\rm self}$ is then obtained from the sum

$$F^\alpha_{\rm self} = \sum_{\ell=0}^{\infty}\lim_{x\to z}\left[F^{\alpha\ell}_{\rm ret}(x) - F^{\alpha\ell}_{\rm S}(x)\right]. \tag{1.39}$$

The key idea of mode-sum regularisation is to compute individual modes of $h^{\rm ret}$ by numerically solving Eq. (1.22), and then subtract off the modes of $h^{\rm S}$, which are found analytically from a local expansion of $h^{\rm S}$ near the worldline. It is the most easily implemented method and historically the most commonly used. Its basic idea can be applied to any quantity constructed from the regular field, and the vast majority of numerical computations, both in Schwarzschild and in Kerr, have been based on it.

At second order the worldline convolution method does not work because the source is not a well-defined distribution, preventing us from easily obtaining concrete expressions for the regular field in terms of integrals against Green's functions. Mode-sum regularization is also ruled out at second-order because the individual multipole modes of the second-order retarded field diverge at the particle, and again, we cannot directly solve for the retarded field because it does not have a distributional source. This only leaves the effective-source method at second order.

The effective-source method (also called a puncture scheme) was first used by [70, 71]. It was designed for situations in which the physical, retarded numerical variable would diverge at the worldline, as is the case when solving for the first-order metric perturbation in 2+1 or 3+1 dimensions. This made it ideal for solving the Lorenz-gauge field equations in Kerr, which are nonseparable. At second order it becomes a more crucial ingredient in the formalism.

In the effective-source method one defines a puncture field $h^{\mathcal{P}} \sim h^{\rm S}$ to be a truncation of the singular field at a certain order in an expansion in the distance to the particle. The residual field $h^{\mathcal{R}}$ is then defined as

$$h^{\mathcal{R}} \equiv h^{\rm ret} - h^{\mathcal{P}}. \tag{1.40}$$

We then rewrite the field equations as equations for $h^{\mathcal{R}}$. Having ascertained that we cannot write the second-order field equation in the point-particle form (1.33), we instead start with the vacuum equations outside the object,

$$\delta G_{\alpha\beta}[h^1] = 0, \tag{1.41}$$
$$\delta G_{\alpha\beta}[h^2] = -\delta^2 G_{\alpha\beta}[h^1, h^1]. \tag{1.42}$$

We then take the solutions to these equations and extend them down to all points $x \notin \gamma$. We write the punctured version of the equations by moving the punctures to the right-hand sides, which yields

$$\delta G_{\alpha\beta}[h^{1\mathcal{R}}] = -\delta G_{\alpha\beta}[\,h^{1\mathcal{P}}\,] \qquad \equiv S^{1\,\rm eff}_{\alpha\beta}, \tag{1.43}$$
$$\delta G_{\alpha\beta}[h^{2\mathcal{R}}] = -\delta G_{\alpha\beta}[h^{2\mathcal{P}}] - \delta^2 G_{\alpha\beta}[h^1, h^1] \qquad \equiv S^{2\,\rm eff}_{\alpha\beta}, \tag{1.44}$$

valid for all points $x \notin \gamma$. Provided that the expansions of $h^{1\mathcal{P}}$ and $h^{2\mathcal{P}}$ are sufficiently high order in powers of distance to $\gamma$, we may define the right-hand sides of (1.43) and (1.44) on $\gamma$ also, by taking the limit from off $\gamma$. Note that (1.43) is equivalent to Eq. (1.22) but for the absence of an explicit $T^1_{\alpha\beta}$ term. More traditionally, we could have written Eq. (1.43) as the distributional equation $\delta G_{\alpha\beta}[h^{1\mathcal{R}}] = 8\pi T^1_{\alpha\beta} - \delta G_{\alpha\beta}[h^{1\mathcal{P}}]$. In that case, $\delta G_{\alpha\beta}[\,h^{1\mathcal{P}}\,]$ is treated as a distribution, unlike in (1.43). It contains a delta function that cancels the one in $T^1_{\alpha\beta}$. After that cancellation, we are left with a remainder equivalent to (1.43). But we deliberately did not write the first-order equation like that, because we cannot write an equation in such a way at second order.

In this way, rather than first solving for the retarded field and then subtracting the singular field, we directly solve for a field that locally approximates the regular field. Hence, the effective-source method can be applied at second order because although we do not have a distributional equation for the retarded field, we can find a local approximation to it outside the small object. From that local approximation, we can construct a puncture, and from the puncture we can derive equations for a residual field.

All discussions and derivations of the second-order GSF [41, 43, 44, 72, 73] have put forward a puncture scheme as the most viable way of solving the second-order field equations. Although puncture schemes were initially designed for computations in 2+1D and 3+1D, they can work just as well, and more accurately, in the 1D frequency domain.

## 1.4 Outline of the thesis

The overall goal of this thesis is to develop the tools necessary for implementing a frequency-domain puncture scheme at second order, and to apply them in the simplest nontrivial scenario of quasicircular orbits in Schwarzschild spacetime.

In Chapter 2 we review the foundations of self-force theory, which are based on matched asymptotic expansions. Three things emerge from this: a useful definition of the second-order singular and regular fields, the equation of motion in terms of the regular field, and a local expansion of the singular field, which will be the starting point for the puncture scheme. This local expansion is valid in any background spacetime, but it is expressed in local coordinates centered on the object's worldline.

In Chapter 3 we describe the puncture scheme in more detail, in 4D, in an arbitrary background spacetime. The main goal of this chapter is to convert the local expansion of the singular field into a more practical, covariant form, utilizing the geometrical definitions of the local coordinates.

In Chapter 4 we begin to specialize to quasicircular orbits in Schwarzschild. Focusing on first order to illustrate the basic ideas, we decompose the puncture and the field equations into tensor spherical harmonics and frequency modes. In this chapter, we approximate the orbit as a fixed circular geodesic, a restriction to be lifted in later chapters. We present a new version of the frequency-domain puncture scheme, complementary to the one used by Wardell and Warburton [74], and we present a successful numerical implementation of it.

In Chapters 5 and 6 we describe two difficulties that arise in applying the methods of Chapter 4 to second order. Using a simple scalar toy model, we illustrate the difficulties and how to overcome them. In Chapter 5, we show how computing the source near the worldline becomes numerically difficult in the context of a mode decomposition. Closer and closer to the particle, an arbitrarily large number of modes of the first-order field are needed to calculate a single mode of the second-order source. We overcome this problem by expressing the most singular piece of the source in terms of the first-order 4D puncture field, instead of as a sum over pairs of first-order modes.

In Chapter 6, we review key results from [75], which showed why incorporating the inspiral of the orbit is difficult. We introduce a two-timescale expansion of the field equations, in which the inspiral of the orbit is encoded in the dependence on a slow-time variable. But this approximation turns out to fail at large distances, and the retarded integral over the source develops an infrared divergence. In the context of the scalar model, this problem can be overcome by introducing a second expansion at large distances.

In Chapter 7, taking the lessons of the toy model, we lay out a computational framework for the second-order puncture scheme, specialized to quasicircular orbits in Schwarzschild. The scheme is based on a two-timescale expansion of the Einstein equations, combined with additional expansions near infinity and the horizon. The two-timescale equations can be solved using the methods of Chapter 4, with boundary conditions provided by the additional two expansions.

In Chapter 8, as a first test of Chapter 7's framework, we numerically implement the puncture scheme for the $\ell = 0$ mode at second order. We perform a variety of consistency checks.

In Chapter 9 we summarize our results and draw conclusions from them. We discuss ways in which the research of this work can be continued.

This thesis contains a number of appendices. In Appendix A we give explicit formulas for the first- and second-order metric perturbations. In Appendix B we summarise how to construct Fermi-Walker (FW) coordinates and give explicit formulas for the metric and Christoffel symbols in terms of them. In Appendix C we outline the derivation of the first- and second-order-in-mass punctures, for a point-particle in a Schwarzschild background. In Appendix D we give formulas for the mixing matrices in the mode-decomposed field equations, which appear in Chapter 4. In Appendix E we give explicit formulas, which describe a certain coordinate transformation between two sets of polar coordinates, needed for the discussion in Chapter 5. In Appendix F we detail the steps in the evaluation of a certain integral, which is required for the discussion in Chapter 6. Finally, in Appendix G we derive a number of analytical properties and relations of the monopole piece of the second-order Ricci tensor.

This thesis uses the following conventions. A "mostly positive" metric signature, $(-,+,+,+)$, is used for the spacetime metric, the Christoffel symbols are defined by $\Gamma^{\mu}_{\alpha\beta} = \frac{1}{2}g^{\mu\nu}\left(g_{\nu\beta,\alpha} + g_{\nu\alpha,\beta} - g_{\alpha\beta,\nu}\right)$, the Riemann tensor is $R^{\mu}{}_{\nu\alpha\beta} = \Gamma^{\mu}_{\nu\beta,\alpha} - \Gamma^{\mu}_{\nu\alpha,\beta} + \Gamma^{\mu}_{\sigma\beta}\Gamma^{\sigma}_{\nu\alpha} - \Gamma^{\mu}_{\sigma\alpha}\Gamma^{\sigma}_{\nu\beta}$, the Ricci tensor and scalar are $R_{\alpha\beta} = R^{\mu}{}_{\alpha\mu\beta}$ and $R = R_{\mu}{}^{\mu}$, and the Einstein equations are $G_{\alpha\beta} = R_{\alpha\beta} - \frac{1}{2}g_{\alpha\beta}R = 8\pi T_{\alpha\beta}$. Greek indices are used for four-dimensional spacetime components and lower-case Latin letters are used for spatial components. Capital Latin letters are used for indices on the two-sphere.

# Chapter 2

# Gravitational self-force formalism

This chapter is a review of previous work done by other authors. A local analysis of the metric in a small region around the object is given. Two things come out of the analysis: (i) the equation of motion and (ii) local solutions for the first- and second-order fields, which will be the starting point for the construction of the puncture. Full details of the derivation through first order can be found in [46], and through second order in [44]. We will begin by reviewing the perturbed Einstein field equations and show how to solve them for the first- and second-order fields of the small body.

To begin with, in Sec. 2.1 we introduce the method of matched asymptotic expansions, which will be used later in Sec. 2.3 to derive the first- and second-order metric perturbations in the local region. Next, in Sec. 2.2, starting with the full Einstein equations, we show how to write the perturbed Einstein equations in a form suitable for our problem. In Sec. 2.3 we go through the steps of deriving the first- and second-order fields by solving the perturbed field equations, using the method of matched asymptotic expansions introduced in Sec. 2.1. In Sec. 2.4 we give a precise definition of the singular-regular split of the metric perturbation, according to the definition of Pound [1]. We give a brief synopsis of how the equation of motion at first order is derived in Sec. 2.5, and at second order in Sec. 2.6.

## 2.1 Matched asymptotic expansions

Matched asymptotic expansions is a standard method used for solving problems with two different scales. In our case of a binary inspiral, we have a spacetime with two disparate lengthscales, associated with the dimensions (or masses) of the two objects. The spacetime geometry close to the small body is predominantly influenced by the small body's gravity, whereas far away from the small body the spacetime geometry is dominated by the gravity of the large black hole. This sets up two distinct regions of spacetime with different geometries, although they blend into each other in a smooth transition. In the above two regions the metric of the spacetime can be expanded in two different ways. The field of the small body is derived by demanding that the two expansions agree in a certain buffer region.

Let us now describe how to apply this method in more detail. We will denote by $g_{\alpha\beta}$ the metric of the background spacetime associated with the large black hole. But note that this derivation applies in any vacuum background. Let $\mathrm{g}_{\alpha\beta}(x, \epsilon)$, the metric of the full spacetime (small compact object + black hole), be an exact solution of the Einstein equations. We introduce the parameter $\epsilon$ in order to count powers of the mass $\mu$, where $\mu/M \ll 1$ for EMRIs. $\epsilon$ is a formal expansion parameter which is set equal to 1 after expanding the metric perturbation. Let $r$ be a measure of radial distance from the small body and let $\mathcal{R} \gg \mu$ be the radius of curvature of the background spacetime, which serves to represent the external length scale.

Let us define the two separate regions mentioned above in terms of these two quantities. The outer region is defined as $r \gtrsim \mathcal{R} \gg \mu$. In this region the mass $\mu$ can be treated as the source of a small perturbation $h_{\alpha\beta}(x, \epsilon)$ to the background metric. The first of three assumptions we make is that in the outer region, the full metric can be expanded in powers of $\epsilon$ as

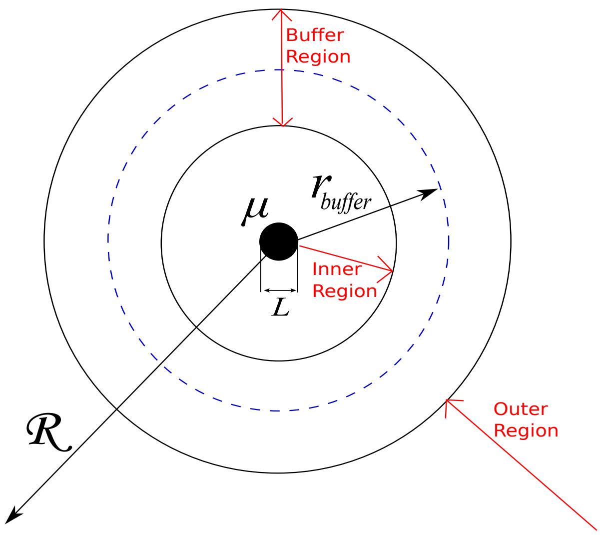


Figure 2.1: A schematic representation of the buffer region in which we apply matched asymptotic expansions. The black blob in the center of the diagram depicts the small compact body of mass $\mu$ in the binary inspiral. $L$ loosely refers to the size of the small body, where $L \sim \mu$ since the small body is compact. $\mathcal{R}$ refers to the radius of curvature of the external spacetime due to the large black hole, which is used to quantify the scale of the external spacetime. The outer region depicted here is the region where the radial distance $r$ from the small body $\sim \mathcal{R}$. The inner region shown is the region where $r \sim \mu$. $r_{buffer}$ refers to the radial distance from the small body in the buffer region, where $\mu \ll r_{buffer} \ll \mathcal{R}$.

$$\mathrm{g}_{\alpha\beta}(x^\mu, \epsilon) = g_{\alpha\beta}(x) + h_{\alpha\beta}(x, \epsilon)\,, \tag{2.1}$$
$$h_{\alpha\beta}(x, \epsilon) = \epsilon h^1_{\alpha\beta}(x;\gamma) + \epsilon^2 h^2_{\alpha\beta}(x;\gamma) + O(\epsilon^3), \tag{2.2}$$

on a manifold $\mathcal{M}_E$. We call this the outer expansion. In this setup, $(g_{\alpha\beta}, \mathcal{M}_E)$ defines an external background spacetime with no small body in it, and $h_{\alpha\beta}(x, \epsilon)$ describes perturbations due to the small body. The perturbation fields $h^n_{\alpha\beta}$ depend on the motion of the small body itself. We will encode that motion in a representative, $\epsilon$-dependent worldline $\gamma \in \mathcal{M}_E$, and we write $h^n_{\alpha\beta} = h^n_{\alpha\beta}(x;\gamma)$. Allowing $h^n_{\alpha\beta}$ to depend on $\gamma$ in this way is called the self-consistent approach [40].

The inner region is defined by $r \sim \epsilon\mathcal{R} \ll \mathcal{R}$, very near to the small body. We take the $\epsilon \to 0$ limit in this region by using re-scaled coordinates, where the radial coordinate gets re-scaled as $\tilde{r} \equiv r/\epsilon$. We fix $\tilde{r}$ when we take the $\epsilon \to 0$ limit, which ensures that we remain close to the small body. Our second assumption is that in the inner region, the metric can be expanded as

$$\mathrm{g}_{\alpha\beta}(x, \epsilon) = g^{\text{body}}_{\alpha\beta}(t, \tilde{r}, \theta^A) + H_{\alpha\beta}(t, \tilde{r}, \theta^A)\,, \tag{2.3}$$
$$H_{\alpha\beta}(t, \tilde{r}, \theta^A) = \sum_{n\geq 1} \epsilon^n H^n_{\alpha\beta}(t, \tilde{r}, \theta^A), \tag{2.4}$$

on a manifold $\mathcal{M}_I$. We call this the inner expansion. In this setup, $(g^{\text{body}}_{\alpha\beta}, \mathcal{M}_I)$ is the internal background metric, which describes the geometry of the spacetime around the small body, were it isolated. $H^n_{\alpha\beta}$ are perturbations to the field of the small body due to interactions with the external spacetime of the black hole.

We define the buffer region to be the region where $\mu \ll r \ll \mathcal{R}$, which lies between the outer region and the inner region, as depicted in Fig. 2.1. Our third assumption is that the outer and inner expansions are sufficiently well behaved, such that the overlap condition holds, namely their domains of validity can be extended into the buffer region and overlap with one another. This implies that an order-by-order matching condition holds. To perform the expansion we impose that the inner- and outer-expansions are both in the Lorenz-gauge and in Fermi-Walker (FW) coordinates $(t, r, \theta^A)$ centered on $\gamma$, as described in Sec. 2.3. As such, when the outer expansion (2.1) is re-expanded for small $r$ at fixed $\epsilon$, and the inner expansion (2.3) is re-expanded for small $\epsilon$ (after replacing $\tilde{r}$ with $r/\epsilon$) at fixed $r$, the two expansions must agree order by order in $r$ and $\epsilon$, because they are expansions of the same exact metric $\mathrm{g}_{\alpha\beta}$.

Practically speaking, this means that we take the terms in the outer expansion (2.2), valid in the outer region $r \gg \epsilon$, and expand them for $r \ll \mathcal{R}$ as

$$\epsilon^n h^n_{\alpha\beta}(x) = \epsilon^n \sum_{p\geq -n} h^{n,p}_{\alpha\beta}(t, \theta^A) r^p, \tag{2.5}$$

where $\theta^A = (\theta, \varphi)$ are the usual angular coordinates defined from $x^a$. The expansion (2.5) starts with the leading-order term of order $\epsilon^n r^{-n}$, such that

$$\epsilon^n h^n_{\alpha\beta}(x) = \frac{\epsilon^n}{r^n} h^{n,-n}_{\alpha\beta}(t, \theta^A) + O(\epsilon^n r^{-n+1}). \tag{2.6}$$

The reason for this is that we allow no negative powers of $\epsilon$ in the inner expansion (2.3)-(2.4), meaning $\epsilon^n h^n_{\mu\nu}$ must have no negative powers of $\epsilon$ when written as a function of $\tilde{r} = r/\epsilon$. This follows from our third assumption, that it has to match (2.3) in the buffer region.

Next we re-expand the terms in the inner-expansion (2.3) for the case where $r \gg \epsilon$, as

$$\begin{aligned} g^{\text{body}}_{\alpha\beta}(t, \tilde{r}, \theta^A) &= \eta_{\alpha\beta} + \sum_{p\geq 1} \frac{1}{\tilde{r}^p} g^{p\,\text{body}}_{\alpha\beta}(t, \theta^A) \\ &= \eta_{\alpha\beta} + \sum_{p\geq 1} \left(\frac{\epsilon}{r}\right)^p g^{p\,\text{body}}_{\alpha\beta}(t, \theta^A), \end{aligned} \tag{2.7}$$

$$\begin{aligned} \epsilon^n H^n_{\alpha\beta}(t, \tilde{r}, \theta^A) &= \epsilon^n \sum_{p\geq -n} \frac{1}{\tilde{r}^p} H^{n,p}_{\alpha\beta}\left(t, \theta^A\right) \\ &= \epsilon^n \sum_{p\geq -n} \frac{\epsilon^p}{r^p} H^{n,p}_{\alpha\beta}\left(t, \theta^A\right) \\ &= r^n H^{n,-n}_{\alpha\beta}\left(t, \theta^A\right) + O\left(\epsilon r^{n-1}\right), \end{aligned} \tag{2.8}$$

where $\eta = \text{diag}\,(-1, 1, 1, 1)$ is the flat-space Minkowski metric. The summation limit in Eq. (2.8) follows from the matching condition: there can be no negative powers of $\epsilon$ in the re-expansion of $H$ at fixed $r$, because there are no negative powers of $\epsilon$ in the outer expansion in Eq. (2.5).

The matched asymptotic expansions method stipulates that the outer expansion (2.6) and the inner expansion (2.7) have to match order by order. Hence, the most singular term in the $n$th-order perturbation $h^n_{\alpha\beta}$ (the $1/r^n$ term) is equal to the $1/r^n$ contribution to the $n$th-order piece of the metric of the small body $g^{n\,\text{body}}_{\alpha\beta}$:

$$h^{n,-n}_{\alpha\beta}(t, \theta^A) = g^{n\,\text{body}}_{\alpha\beta}(t, \theta^A). \tag{2.9}$$

Eq. (2.9) states that at each order in $\epsilon$, the most singular piece of the perturbation $h^n_{\alpha\beta}$ in the buffer region is equal to the $r \gg \mu$ asymptotic behaviour of the unperturbed metric of the small body $g^{\text{body}}_{\alpha\beta}$. It follows from the fact that when the outer expansion is written in terms of $\tilde{r}$, $\epsilon^n h^{n,-n}/r^n = h^{n,-n}/\tilde{r}^n$ is the only term that's independent of $\epsilon$. This tells us that it must match to something in the zeroth-order metric of the inner expansion, and the behaviour with $\tilde{r}$ then tells us that $g^{n\,\text{body}}/\tilde{r}^n$ is the particular term it must match.

Because $g^{\text{body}}_{\alpha\beta}$ varies slowly with time (when compared to its spatial variation), it has standard, well-defined multipole moments, which we can think of as the moments of the body itself. Each coefficient $g^{n\,\text{body}}_{\alpha\beta}$ in its large-$\tilde{r}$ expansion is fully characterized by those moments. Therefore, based on the statement in Eq. (2.9), we find that the leading-order contribution to the $n$th-order field $h^n_{\alpha\beta}$ is determined from the multipole structure of the small body. This important result will be key to deriving the first- and second-order fields of the small body.

## 2.2 The perturbed Einstein field equations

In this section we will introduce the perturbed Einstein equations for the binary inspiral, which we began to describe in Sec. 1.2.5 of the introduction. The vacuum Einstein field equations of the full spacetime read

$$G_{\alpha\beta}[\,\mathrm{g}\,] = 0, \tag{2.10}$$

where $G_{\alpha\beta}\,[\,\mathrm{g}\,] = R_{\alpha\beta}\,[\,\mathrm{g}\,] - \frac{1}{2}\mathrm{g}_{\alpha\beta}R\,[\,\mathrm{g}\,]$ is the Einstein tensor. Eq. (2.10) applies in the vacuum region of spacetime outside the small body. Taking the trace of both sides implies that $R\,[\,\mathrm{g}\,] = 0$, so Eq. (2.10) can be re-cast in the equivalent format

$$R_{\alpha\beta}[\,\mathrm{g}\,] = 0. \tag{2.11}$$

Let $R_{\alpha\beta}\,[\,\mathrm{g}\,] = R_{\alpha\beta}\,[\,g + h\,]$ be written as an expansion in orders of the metric perturbation $h$ as

$$R_{\alpha\beta}[\,\mathrm{g}\,] = R_{\alpha\beta}\,[\,g\,] + \delta R_{\alpha\beta}\,[\,h\,] + \delta^2 R_{\alpha\beta}\,[\,h\,] + O(h^3) = 0, \tag{2.12}$$

where $\delta^n R_{\alpha\beta}\,[\,h\,]$ is the piece of $R_{\alpha\beta}\,[\,g + h\,]$ which is $n$th-order in $h$, given by

$$\delta^n R_{\alpha\beta}[h] \equiv \frac{1}{n!}\frac{d^n R_{\alpha\beta}[g + \lambda h]}{d\lambda^n}\bigg|_{\lambda=0}. \tag{2.13}$$

The expression for $\delta R_{\alpha\beta}\,[\,h\,]$ is given by [46]

$$\delta R_{\alpha\beta}\,[\,h\,] = -\frac{1}{2}\left(E_{\alpha\beta}[\,h\,] - B_{\alpha\beta}[\,h\,] + g_{\alpha\beta}\nabla_\nu Z^\nu[\,h\,]\right) \tag{2.14}$$

where

$$E_{\alpha\beta}\,[\,h\,] \equiv \nabla^\mu\nabla_\mu\, h_{\alpha\beta} + 2R^{\mu}{}_{\alpha}{}^{\nu}{}_{\beta} h_{\mu\nu}\,, \tag{2.15}$$

$$B_{\alpha\beta}[\,h\,] \equiv g_{\alpha\beta}\nabla_\nu Z^\nu[\,h\,] - \nabla_\alpha Z_\beta[\,h\,] - \nabla_\beta Z_\alpha[\,h\,], \tag{2.16}$$

$$Z_\alpha[\,h\,] \equiv \nabla^\beta \bar{h}_{\alpha\beta}. \tag{2.17}$$

We will refer to $E_{\alpha\beta}[\,h\,]$ as the wave operator. The covariant derivatives are compatible with the background $g$ and indices are raised and lowered with $g$. The formula for the second-order variation of the Ricci-tensor $\delta^2 R_{\alpha\beta}$ is

$$\begin{aligned}
\delta^2 R_{\alpha\beta}\,[\,h\,] =& \frac{1}{2}\nabla_\mu \bar{h}^{\mu\nu}\left(2\nabla_{(\alpha}h_{\beta)\nu} - \nabla_\nu h_{\alpha\beta}\right) \\
&+ \frac{1}{4}\nabla_\alpha h^{\mu\nu}\nabla_\beta h_{\mu\nu} + \frac{1}{2}\nabla^\nu h^\mu_\beta \nabla_\nu h_{\mu\alpha} - \frac{1}{2}\nabla^\nu h^\mu_\beta \nabla_\mu h_{\nu\alpha} \\
&- \frac{1}{2}h^{\mu\nu}\left(2\nabla_\mu\nabla_{(\alpha}h_{\beta)\nu} - \nabla_\mu\nabla_\nu h_{\alpha\beta} - \nabla_\alpha\nabla_\beta h_{\mu\nu}\right). \qquad (2.18)
\end{aligned}$$

A derivation can be found in Ref. [37].

The perturbations $h^n_{\alpha\beta}$ depend on $\epsilon$ through their dependence on $\gamma$. Hence, we cannot just solve Eq. (2.12) order by order in $\epsilon$. Instead, we impose the Lorenz gauge condition on the full perturbation. The Lorenz gauge condition reads

$$Z_\alpha[\,h\,] = 0. \qquad (2.19)$$

By imposing the gauge condition on $h_{\alpha\beta}$, we split Eq. (2.12) into two equations, one being a weakly non-linear wave equation for the perturbation fields, and the other being the gauge condition, which constrains the matter degrees of freedom, in particular the equation of motion for $\gamma$ and evolution equations for the multipole moments of the small body. Unlike Eq. (2.12), the wave equation can be split up into a sequence of equations for each subsequent $h^n_{\alpha\beta}$, even if $\gamma$ depends on $\epsilon$, as

$$\begin{aligned}
O(\epsilon^0):& \qquad R_{\alpha\beta}[\,g\,] = 0, & (2.20)\\
O(\epsilon^1):& \qquad E_{\alpha\beta}[\,h^1\,] = 0, & (2.21)\\
O(\epsilon^2):& \qquad E_{\alpha\beta}[\,h^2\,] = 2\delta^2 R_{\alpha\beta}[\,h^1, h^1\,], & (2.22)\\
\vdots& & \\
O(\epsilon^n):& \qquad E_{\alpha\beta}[\,h^n\,] = \mathcal{S}^n_{\alpha\beta}[\,h^1, \ldots, h^{n-1}\,], & (2.23)
\end{aligned}$$

where the source term, $\mathcal{S}^n_{\alpha\beta}$, consists of nonlinear terms in the expansion of the Ricci tensor. Here we define $h^n_{\alpha\beta}$ as a functional of $\gamma$ to be the retarded solution to the $n$th-order equation in the sequence, for arbitrary $\gamma$. Our goal is to solve Eqs. (2.21) and (2.22), such that the solution preserves the correct motion of the worldline and agrees with the inner expansion in the buffer region. The latter requirement acts as a free boundary value.

We impose the gauge condition in order to determine $\gamma$. The gauge condition splits up into a set of equations, which can be solved exactly for the acceleration of $\gamma$, in the following way. Let $z^\mu(\tau)$ refer to coordinates on $\gamma$ and $\tau$ be proper time on $\gamma$. Proper time is defined with respect to the background metric $g$. The acceleration of $\gamma$ is defined as $a^\mu(\tau) \equiv Du^\mu(\tau)/d\tau$, where $D/d\tau$ denotes covariant differentiation and $u^\mu(\tau) \equiv Dz^\mu(\tau)/d\tau$ is the worldline's four-velocity. We assume that $a^\mu(\tau)$ can be expanded in powers of $\epsilon$ as

$$a^\mu(\tau) = a_0^\mu(\tau) + \epsilon a_1^\mu(\tau;\gamma) + \epsilon^2 a_2^\mu(\tau;\gamma) + O(\epsilon^3)\,. \tag{2.24}$$

The fields $h^n_{\alpha\beta}$ will depend on the acceleration, such that when substituted into the gauge condition (2.19), we recover a set of gauge conditions at each order of $\epsilon$, as

$$O(\epsilon^1): \qquad Z^0_\alpha[\,h^1\,] = 0, \tag{2.25}$$

$$O(\epsilon^2): \qquad Z^1_\alpha[\,h^1\,] = -Z^0_\alpha[\,h^2\,], \tag{2.26}$$

$$\vdots$$

$$O(\epsilon^{n+1}): \qquad Z^n_\alpha[\,h^1\,] = -\sum_{m=1}^{n} Z^{n-m}_\alpha[\,h^{m+1}\,], \tag{2.27}$$

where $Z^0_\mu[\,h\,]$ is the Lorenz-gauge operator acting on $h_{\alpha\beta}$ evaluated with $a^\mu = a^\mu_0$, and $Z^n_\mu[\,h\,]$ is the piece of $Z_\mu[\,h\,]$ linear in terms like $a_n$, $a_1 a_{n-1}$, $a_1 a_1 a_{n-2}$, etc. Imposing this set of gauge conditions on the solutions to the wave equations determines the acceleration of the worldline, order by order. In this way, the equation of motion can be derived.

## 2.3 The first and second-order fields

In this section we will outline the approach used to derive the first- and second-order fields. The full formulas for the first- and second-order fields through $O(r)$ are given in Appendix A. By constraining the solutions to satisfy the Lorenz gauge condition, the equation of motion through first order is obtained.

Rather than $\gamma$ being the worldline of the center of mass of the small object, as one might expect, in this section $\gamma$ is a worldline that is allowed to be displaced from the center of mass. We will ultimately choose $\gamma$ to be the center-of-mass worldline when presenting an equation of motion for the body, but it will be useful to have intermediate results that allow for a slightly different $\gamma$. These results will be essential in Chapters 7 and 8, in which we will need to expand the center-of-mass worldline around a different, nearby worldline.

We begin by introducing new notation. $(t, x^a)$ denotes FW coordinates centered on a given worldline $\gamma$. $r = \sqrt{\delta_{ab}x^a x^b}$ is the radial distance from $\gamma$ and $(\theta, \varphi)$ are the usual angular coordinates defined from $x^a$. Lowercase Latin indices are raised and lowered with $\delta_{ab}$. For a more comprehensive overview of FW coordinates see Appendix B. The quantity

$$n^a = \frac{x^a}{r} \tag{2.28}$$

denotes the radial outward pointing unit vector, such that $n_a n^a = 1$. The upper-case letter $L$ when it appears as an index refers to a multi-index, e.g.

$$n^L = n^{i_1} n^{i_2} n^{i_3} \dots n^{i_\ell}. \tag{2.29}$$

Tensors with indices between angular brackets $\langle \dots \rangle$ refer to symmetric trace-free (STF) tensors with respect to the flat three-dimensional metric $\delta_{ab}$, i.e. $\delta^{ab} A_{\langle abc \rangle} = 0$, $A_{\langle abc \rangle} = A_{\langle cab \rangle} = A_{\langle bca \rangle}$. Tensors with a hat on top indicate that the tensor is STF, e.g.

$$\hat{n}^L = n^{\langle i_1} n^{i_2} \dots n^{i_\ell \rangle}. \tag{2.30}$$

We use the following notation for background tidal quantities:

$$\mathcal{E}_{ab} \equiv R_{0a0b}, \tag{2.31a}$$
$$\mathcal{B}_{ab} \equiv \frac{1}{2} \varepsilon^{pq}{}_{(a} R_{b)0pq}, \tag{2.31b}$$
$$\mathcal{E}_{abc} \equiv \underset{abc}{\mathrm{STF}}\, R_{0a0b|c}, \tag{2.31c}$$
$$\mathcal{B}_{abc} \equiv \frac{3}{8} \underset{abc}{\mathrm{STF}}\, \varepsilon^{pq}{}_a R_{b0pq|c}, \tag{2.31d}$$

where 'STF' denotes the STF combination of the indicated indices. $\mathcal{E}_{ab}$ and $\mathcal{B}_{ab}$ are the even- and odd-parity tidal quadrupole moments of the background spacetime in the neighbourhood of $\gamma$, and $\mathcal{E}_{abc}$ and $\mathcal{B}_{abc}$ are the even- and odd-parity tidal octupole moments. $\mathcal{E}_{ab}$ is symmetric, and trace-free if the Ricci tensor vanishes. Similarly $\mathcal{B}_{ab}$ is symmetric, but trace-free by virtue of the Bianchi identity, regardless of whether the Ricci tensor vanishes. Note that $\mathcal{E}_{ab}$ is transverse in the sense that $\mathcal{E}_{ab} u^b = 0$. In this notation, the Riemann tensor's spatial components can be expressed as

$$R_{abcd} = \delta_{ac} \mathcal{E}_{bd} + \delta_{bd} \mathcal{E}_{ac} - \delta_{ad} \mathcal{E}_{bc} - \delta_{bc} \mathcal{E}_{ad}\,, \tag{2.32a}$$
$$R_{0bcd} = -\varepsilon_{cdi} \mathcal{B}^i_b. \tag{2.32b}$$

Note the following contraction identities:

$$\delta^{ab} \mathcal{E}_{ab} = 0\,, \qquad \delta^{cd} R_{acbd} = \mathcal{E}_{ab}\,, \qquad \delta^{ac} R_{0abc} = 0\,. \tag{2.33}$$

The first- and second-order wave equations (2.21) and (2.22) are given explicitly as

$$\nabla^\mu \nabla_\mu h^1_{\alpha\beta} + 2 R^{\mu}{}_{\alpha}{}^{\nu}{}_{\beta} h^1_{\mu\nu} = 0\,, \tag{2.34}$$
$$\nabla^\mu \nabla_\mu h^2_{\alpha\beta} + 2 R^{\mu}{}_{\alpha}{}^{\nu}{}_{\beta} h^2_{\mu\nu} = 2\delta^2 R_{\alpha\beta}\,[\,h^1\,,\,h^1\,]\,. \tag{2.35}$$

The covariant derivative and the Riemann-tensor terms in Eqs. (2.34), (2.35) are associated with the background metric $g$, which we write in terms of FW coordinates. Explicit expressions for the background metric and Christoffel symbols in terms of FW coordinates are given in Eqs. (B.29)-(B.31). It turns out that in these coordinates the covariant derivative has the form $\nabla_\alpha = x^a_\alpha \partial_a + O(r^0)$, such that $\Box \equiv g^{\alpha\beta}\nabla_\alpha\nabla_\beta = \partial^a\partial_a + O(1/r)$, $\partial^a\partial_a$ being just the flat-space Laplacian. Hence, the wave operator $E_{\alpha\beta}$ consists of a flat-space Laplacian plus corrections of order $1/r$.

In these coordinates, Eq. (2.5) has the explicit form

$$h^1_{\alpha\beta}(x) = \frac{1}{r}h^{1,-1}_{\alpha\beta} + h^{1,0}_{\alpha\beta} + rh^{1,1}_{\alpha\beta} + r^2 h^{1,2}_{\alpha\beta} + O(r^3), \tag{2.36}$$

$$h^2_{\alpha\beta}(x) = \frac{1}{r^2}h^{2,-2}_{\alpha\beta} + \frac{1}{r}h^{2,-1}_{\alpha\beta} + h^{2,0}_{\alpha\beta} + \ln r h^{2,0,\ln}_{\alpha\beta} + rh^{2,1}_{\alpha\beta} + O(r^2), \tag{2.37}$$

where the $h^{n,m}_{\alpha\beta}$ are functions of $(t,\theta,\varphi)$ and also have an implicit functional dependence on $\gamma$. To obtain a general solution to the Einstein equation we write each $h^{n,m}_{\alpha\beta}$ as an expansion in terms of irreducible STF pieces as (see p.146 in Ref. [46])

$$h^{n,m}_{tt} = \sum_{\ell\geq 0} \hat{A}^{(n,m)}_L \hat{n}^L, \tag{2.38a}$$

$$h^{n,m}_{ta} = \sum_{\ell\geq 0} \hat{B}^{(n,m)}_L \hat{n}_a{}^L + \sum_{\ell\geq 1}\left[\hat{C}^{(n,m)}_{aL-1}\hat{n}^{L-1} + \epsilon_{ab}{}^c \hat{D}^{(n,m)}_{cL-1}\hat{n}^{bL-1}\right], \tag{2.38b}$$

$$\begin{aligned} h^{n,m}_{ab} &= \delta_{ab}\sum_{\ell\geq 0}\hat{K}^{(n,m)}_L\hat{n}^L + \sum_{\ell\geq 0}\hat{E}^{(n,m)}_L\hat{n}_{ab}{}^L \\ &\quad + \sum_{\ell\geq 1}\left[\hat{F}^{(n,m)}_{L-1\langle a}\hat{n}_{b\rangle}{}^{L-1} + \epsilon^{cd}{}_{(a}\hat{n}_{b)c}{}^{L-1}\hat{G}^{(n,m)}_{dL-1}\right] \\ &\quad + \sum_{\ell\geq 2}\left[\hat{H}^{(n,m)}_{abL-2}\hat{n}^{L-2} + \epsilon^{cd}{}_{(a}\hat{I}^{(n,m)}_{b)dL-2}\hat{n}_c{}^{L-2}\right]. \end{aligned} \tag{2.38c}$$

Note that in the above STF decomposition, the coefficients $\hat{A}^{(n,m)}_L$, $\hat{B}^{(n,m)}_L$, etc. in front of the $\hat{n}^L$'s are functions of $t$, while the $\hat{n}^L$ depend only on the angular coordinates $(\theta,\varphi)$. From the definitions of Eqs. (2.28) and (2.29) stem the useful relations $\partial_a r = n_a$ and $n^a\partial_a\hat{n}^L = 0$. The eigenvalue equation

$$r^2\partial^a\partial_a\hat{n}^L = -\ell(\ell+1)\hat{n}^L \tag{2.39}$$

makes this expansion particularly useful.

The first-order field is derived by substituting the expansions (2.36) and (2.38) into Eq. (2.34) and solving order by order in $r$. To solve the second-order equation, we take the solution to Eq. (2.34) for $h^1$ and substitute it into the RHS of (2.35), as well as substituting the expansions (2.37) and (2.38) into the LHS of Eq. (2.35). We then solve Eq. (2.35) order by order in $r$ to obtain the second-order field.

The bulk of the calculation consists of determining the unknown coefficients $\hat{A}^{(n,m)}$, $\hat{B}^{(n,m)}$, and so on. Some of these coefficients can be determined from the matching condition (2.9) together with the gauge conditions (2.25) and (2.26). Some of the coefficients remain undetermined, and these terms go into the unknown, regular piece of $h^1$ and $h^2$, whose precise definition will be given below.

To see how the matching condition (2.9) is used, consider its explicit form for $n = 1$. It tells us that the most singular ($1/r$) piece of the first-order field, $h^{1,-1}_{\alpha\beta}$, is equal to the first-order piece of the metric of the small body $g^{1\,\text{body}}_{\alpha\beta}$. We identify $\mu$ with the ADM mass of the internal background spacetime of the small body. The matching formula (2.9) allows us to replace $g^{1\,\text{body}}$ with $h^{1,-1}$ in the formula for the ADM mass (see Chap. 4 of [76]). Doing so, and writing $h^{1,-1}$ using the STF decomposition (2.38) leads to the result

$$\hat{A}^{(1,-1)} = 2\mu\,. \tag{2.40}$$

Hence, we have recovered $h^1_{\alpha\beta} \propto 2\mu/r + O(r^0)$, where the leading-order term is just the Newtonian-like potential, as expected.

Likewise at second-order, from Eq. (2.9) the leading-order ($1/r^2$) piece of the second-order external metric, $h^{2,-2}_{\alpha\beta}$, and the second-order piece of the small body's metric, $g^{2\,\text{body}}_{\alpha\beta}$, are equal. The formulas for the mass dipole moment, $M_i$, and spin dipole moment, $S_i$, are given in terms of $g^{2\,\text{body}}_{\alpha\beta}$. $M_i = \mu\delta z_i$, where $\delta z_i$ is the coordinate displacement of $g^{\text{body}}_{\mu\nu}$'s center of mass relative to the origin of the coordinates. $S_i$ is equal to the ADM angular momentum of $g^{\text{body}}_{\mu\nu}$. By replacing $g^{2\,\text{body}}_{\alpha\beta}$ with $h^{2,-2}_{\alpha\beta}$ in these formulas, and writing $h^{2,-2}_{\alpha\beta}$ as the STF decomposition (2.38), we find that

$$\hat{A}^{(2,-2)}_i = 2M_i, \qquad \hat{D}^{(2,-2)}_i = 2S_i. \tag{2.41}$$

## 2.4 The singular-regular split of the metric perturbation.

In the introduction we described the singular-regular split of the metric perturbation at first order. We now give a concrete definition of the singular and regular pieces at $n$th order. We use the choice of $h^{\text{R}}_{\alpha\beta}$ and $h^{\text{S}}_{\alpha\beta}$ defined by Pound [44]. This definition agrees locally with the Detweiler-Whiting definition [49] at first order, but unlike the Detweiler-Whiting definition, applies at all orders.

The metric perturbation in Fermi-Walker coordinates has a local expansion [41]

$$h^n_{\mu\nu} = \sum_{p\geq -n}\sum_{q,\ell} r^p (\ln r)^q h^{(npq\ell)}_{\mu\nu L}(t)\hat{n}^L, \tag{2.42}$$

where we have generalized Eq. (2.5) to allow for logarithms and combined the various hatted tensors in Eq. (2.38) into the coefficients $h^{(npq\ell)}_{\mu\nu L}$. The $n$th-order singular-regular split of this field is defined in terms of the coefficients $h^{(npq\ell)}_{\mu\nu L}$, which we will now describe.

Substituting Eq. (2.42) into the wave equations (2.21) and (2.22) transforms them into a sequence of Poisson equations of the form

$$\partial^a\partial_a\left[r^p(\ln r)^q h^{(npq\ell)}_{\mu\nu L}(t)\hat{n}^L\right] = P_{\mu\nu L}[h^{(n'<n,p'<p,q',L')}]\hat{n}^L, \tag{2.43}$$

which can be solved order by order in $r$. As indicated, the source on the right-hand side depends on modes with lower $n$ and $p$. Since we begin with no source at the very lowest order ($n=1,\ p=-1$), it follows that when solving order by order in $r$, every mode $h^{(npq\ell)}_{\mu\nu L}$ will be written as a linear or nonlinear combination of the modes satisfying the homogeneous equation

$$\partial^a\partial_a\left[r^p h^{(np0\ell)}_{\mu\nu L}(t)\hat{n}^L\right] = 0. \tag{2.44}$$

These special modes come in the forms

$$\frac{1}{r^{\ell+1}}h^{(n,-\ell-1,0,\ell)}_{\mu\nu L}\hat{n}^L \quad \text{for modes with } p<0, \tag{2.45}$$

$$r^\ell h^{(n,\ell,0,\ell)}_{\mu\nu L}\hat{n}^L \quad \text{for modes with } p\geq 0. \tag{2.46}$$

The functions $h^{(n,-\ell-1,0,\ell)}_{\mu\nu L}(t)$ and $h^{(n,\ell,0,\ell)}_{\mu\nu L}(t)$ are determined by (i) the multipole moments of the spacetime $g^{\rm body}_{\mu\nu}$, (ii) the gauge condition, and (iii) global boundary conditions. Factor (i) relates the modes $h^{(n,-\ell-1,0,\ell)}_{\mu\nu L}$ to multipole moments of $g^{\rm body}_{\mu\nu}$ or corrections to them. Eqs (2.40) and (2.41) are two such examples. Factor (ii) provides evolution equations for the multipole moments and relationships between the various modes. Our choice of singular-regular split is made in a way that is independent of global boundary conditions. Specifically, we define the regular field to be the piece of Eq. (2.42) containing no linear or nonlinear combinations of the modes $h^{(n,-\ell-1,0,\ell)}_{\mu\nu L}$; in other words, prior to imposing any global boundary conditions, it does not involve the object's multipole moments and is made up of freely specifiable functions. We define the singular field to be everything else in Eq. (2.42), meaning $h^{{\rm S}n}_{\mu\nu} = h^n_{\mu\nu} - h^{{\rm R}n}_{\mu\nu}$.

With these definitions, the regular field $h^{\rm R}_{\mu\nu} = \sum_n \epsilon^n h^{{\rm R}n}_{\mu\nu}$ possesses several nice properties [41, 44, 77]:

- It is $C^\infty$ at $r=0$.
- It is a solution to the vacuum Einstein equation; through second order that means $R_{\mu\nu}[g+h^{\rm R}] = O(\epsilon^3)$, including at $r=0$.
- Through second order, the equation of motion is found to be equivalent to geodesic motion in the effective metric $g_{\mu\nu} + \epsilon h^{\rm R1}_{\mu\nu} + \epsilon^2 h^{\rm R2}_{\mu\nu}$ (assuming the object's leading-order spin and quadrupole moments are negligible).

The singular field $h^{\rm S}_{\mu\nu} = \sum_n \epsilon^n h^{{\rm S}n}_{\mu\nu}$ satisfies the following properties:

- In any domain that excludes $r=0$, its first- and second-order terms are solutions to the equations $\delta R_{\mu\nu}[h^{\rm S1}]=0$ and $E_{\mu\nu}[h^{\rm S2}]=2\delta^2 R_{\mu\nu}[h^1,h^1]-2\delta^2 R_{\mu\nu}[h^{\rm R1},h^{\rm R1}]$. If there exist boundary conditions for which $h^{\rm R1}_{\mu\nu}\equiv 0$, then with those boundary conditions and for $r\neq 0$, $h^{\rm S}_{\mu\nu}$ satisfies the vacuum equation $R_{\mu\nu}[g+h^{\rm S}]=O(\epsilon^3)$.

- In a domain including $r=0$, $h^{\rm S1}_{\mu\nu}$ is a solution to the wave equation with a point-mass source, $E_{\mu\nu}[h^{\rm S1}]=-8\pi m\delta_{\mu\nu}\delta^3(x^i)$, while $h^{\rm S2}_{\mu\nu}$ is not known to satisfy any distributionally well-defined equation.

- Unlike the regular field, it carries local information about the object's structure; it is made up entirely of terms that explicitly depend on the object's multipole moments or corrections to them.

This list of properties does not uniquely define the singular and regular fields. Neither is the regular field defined to be the piece of the full field responsible for the GSF. Alternative choices exist that satisfy all of the above properties. For example, we could split one of the functions $h^{(1,\ell,0,\ell)}_{\mu\nu L}$ with $\ell\geq 2$ into two pieces, $h^{(1,\ell,0,\ell)}_{(1)\mu\nu L}$ and $h^{(1,\ell,0,\ell)}_{(2)\mu\nu L}$, and all terms in the solution (2.42) that are proportional to $h^{(1,\ell,0,\ell)}_{(2)\mu\nu L}$ could then be moved from the regular field to the singular field. The Pound choice of definitions is convenient, because before making reference to any global boundary conditions, all the terms that involve the object's multipole moments go into the singular field, and all the terms made up entirely of unknown functions go into the regular field. At least through order $r^2$, the singular and regular fields $h^{\rm S1}_{\mu\nu}$ and $h^{\rm R1}_{\mu\nu}$ defined in this way coincide with those defined by Detweiler and Whiting [49]. This can be seen concretely in the results displayed in Chapter 3 below.

The full formulas for the first- and second-order fields through order $O(r)$ can be found in Appendix A. We briefly describe here their form. The first-order singular field near $\gamma$ has the schematic form

$$h^{\rm S1}_{\alpha\beta}=\frac{2\mu}{r}\delta_{\alpha\beta}+\mu\tilde{h}^{\rm S1}_{\alpha\beta}(r,a^i,\mathcal{E}_{ab},\mathcal{B}^a_b)\,. \tag{2.47}$$

The leading-order term in (2.47) is the Newtonian-like potential and $\tilde{h}^{\rm S1}_{\alpha\beta}$ contains the $O(r^0)$ corrections to $h^{\rm S1}_{\alpha\beta}$, which are functions of tidal quantities and of the acceleration of $\gamma$. The first-order singular field describes the self-field of the small body through first order. It diverges on the worldline at $r=0$. For $r\neq 0$ it is a homogeneous solution of the first-order wave equation, $E_{\alpha\beta}[\,h^{\rm S1}\,]=0$, and on the domain $r\geq 0$ it is a solution to the point-particle equation $E_{\alpha\beta}[h^{\rm S1}]=16\pi\bar{T}^1_{\alpha\beta}$, where $\bar{T}^1_{\alpha\beta}$ is the trace-reversed first-order point-particle energy-momentum tensor give in Eq. (1.23). On the other hand, $h^{\rm R1}_{\alpha\beta}$ is a solution everywhere to the homogeneous equation $E_{\alpha\beta}[h^{\rm R1}]=0$, even at $r=0$. $h^{\rm R1}_{\alpha\beta}$ remains unknown analytically and can only be calculated after imposing global boundary conditions.

At second order, the singular field $h^{\rm S2}_{\alpha\beta}$ can be expressed in the form

$$h^{\rm S2}_{\alpha\beta} = h^{\rm SS}_{\alpha\beta} + h^{\rm SR}_{\alpha\beta} + h^{\delta m}_{\alpha\beta} + h^{\rm spin}_{\alpha\beta} + h^{\delta z}_{\alpha\beta}. \tag{2.48}$$

The first piece, $h^{\rm SS}_{\alpha\beta}$, can be written schematically as

$$h^{\rm SS}_{\alpha\beta} \sim \frac{\mu^2}{r^2} + \mu^2 \tilde{h}^{\rm SS}_{\alpha\beta}(r, a^i, \mathcal{E}_{ab}, \mathcal{B}^a_b), \tag{2.49}$$

where $\tilde{h}^{\rm SS}_{\alpha\beta}(r, a^i, \mathcal{E}_{ab}, \mathcal{B}^a_b)$ begins at order $1/r$ and depends on tidal quantities of the background. The $h^{\rm SS}$ piece is a solution to $E_{\alpha\beta}[h^{\rm SS}] = 2\delta^2 R_{\alpha\beta}[\, h^{\rm S1}\,,\, h^{\rm S1}\,]$ away from the worldline (i.e., $r \neq 0$). The second piece, $h^{\rm SR}$, is given by

$$h^{\rm SR}_{tt} = -\frac{\mu h^{\rm R1}_{ab}\hat{n}^{ab}}{r} + O(r^0), \tag{2.50a}$$

$$h^{\rm SR}_{ta} = -\frac{\mu h^{\rm R1}_{tb}\hat{n}_a{}^b}{r} + O(r^0), \tag{2.50b}$$

$$h^{\rm SR}_{ab} = \frac{\mu}{r}\Big[2h^{\rm R1}_{c(a}\hat{n}_{b)}{}^c - \delta_{ab}h^{\rm R1}_{cd}\hat{n}^{cd} - \left(h^{\rm R1}_{ij}\delta^{ij} + h^{\rm R1}_{tt}\right)\hat{n}_{ab}\Big] + O(r^0). \tag{2.50c}$$

It is a solution to $E_{\alpha\beta}[\, h^{\rm SR}\,] = 2\delta^2 R_{\alpha\beta}[\, h^{\rm S1}\,, h^{\rm R1}\,] + 2\delta^2 R_{\alpha\beta}[\, h^{\rm R1}\,, h^{\rm S1}\,]$. The term $h^{\delta m}$ is given by

$$h^{\delta m}_{tt} = \frac{\delta m_{tt}}{r} + O(r^0), \tag{2.51a}$$

$$h^{\delta m}_{ta} = \frac{\delta m_{ta}}{r} + O(r^0), \tag{2.51b}$$

$$h^{\delta m}_{ab} = \frac{\delta m_{ab}}{r} + O(r^0). \tag{2.51c}$$

It is a solution to the homogeneous wave equation $E_{\alpha\beta}[\, h^{\delta m}\,] = 0$ at $r \neq 0$. In a domain that includes $r = 0$, it is a solution to the sourced wave equation $E_{\alpha\beta}[\, h^{\delta m}\,] = -4\pi\delta m_{\alpha\beta}(t)\delta^3(x^i)$. As such, as far as the wave equation is concerned, each component $\delta m_{\alpha\beta}$ is an arbitrary of function of time, but the gauge condition (2.26) at order $O(1/r)$ constrains its components to have the form given explicitly in Eqs. (A.9). $\delta m_{\alpha\beta}$ is a correction to the monopole moment of the small object, that enters into the second-order field. The term $h^{\rm spin}$ is given by

$$h^{\rm spin}_{tt} = O(1/r), \tag{2.52a}$$

$$h^{\rm spin}_{ta} = \frac{2S^i\varepsilon_{aij}n^j}{r^2} + O(1/r), \tag{2.52b}$$

$$h^{\rm spin}_{ab} = O(1/r), \tag{2.52c}$$

where $\varepsilon_{aij}$ is the totally antisymmetric, three-dimensional Levi-Civita tensor.

The final piece, $h^{\delta z}$, is given by

$$h^{\delta z}_{tt} = \frac{2\mu\delta z_a n^a}{r^2} + O(r^0), \tag{2.53a}$$

$$h^{\delta z}_{ta} = O(r^0), \tag{2.53b}$$

$$h^{\delta z}_{ab} = \frac{2\mu\delta z_c n^c\delta_{ab}}{r^2} + O(r^0), \tag{2.53c}$$

where $\delta z^\alpha$ is the deviation of the small object from the reference worldline that lies at the center of our FW coordinates. $h^{\delta z}_{\alpha\beta}$ is a solution to the homogeneous wave equation $E_{\alpha\beta}[\,h^{\delta z}\,] = 0$ off $r = 0$. In a domain including $r = 0$, it is a solution to the wave equation with a source equivalent to that created by the displacement of a point mass,

$$E_{\alpha\beta}[\,h^{\delta z}\,] = 8\pi\mu\delta_{\alpha\beta}\delta z^a\partial_a\delta^3(x^i). \tag{2.54}$$

In later sections of this chapter, $h^{\delta z}_{\alpha\beta}$ will be set to zero to ensure that $\gamma$ represents the center of mass, but it will be utilized in later chapters.

The second-order regular field $h^{\rm R2}_{\alpha\beta}$ satisfies the second-order vacuum equation $E_{\alpha\beta}[h^{\rm R2}] = 2\delta^2 R_{\alpha\beta}[h^{\rm R1}, h^{\rm R1}]$. Like $h^{\rm R1}$, it remains unknown analytically and can only be calculated after imposing global boundary conditions.

The regular field $h^{\rm R}_{\alpha\beta} \equiv \epsilon h^{\rm R1}_{\alpha\beta} + \epsilon^2 h^{\rm R2}_{\alpha\beta}$ is responsible for the self-force through second order, and the small body moves on a geodesic in the effective spacetime $g + h^{\rm R}$. This is shown by the equation of motion through second order, which we will discuss in Secs. 2.5 and 2.6.

## 2.5 The first-order equation of motion

The equation of motion through first order is derived by imposing the gauge conditions (2.25) and (2.26) on the first- and second-order fields. The $O(\epsilon)$ gauge condition (2.25) yields

$$\partial_t\mu = 0\,, \qquad a_0 = 0\,. \tag{2.55}$$

This tells us that the small body has constant mass and the zeroth-order acceleration vanishes. Hence, at leading order the small body behaves as a test particle and $\gamma$ is a geodesic of the background spacetime.

The first-order equation of motion falls out from the second-order gauge condition (2.26). Solving (2.26) at each order of $r$ yields the conditions

$$\partial_t S_a = 0, \tag{2.56}$$

$$\partial_t^2 M_a + \mathcal{E}_{ab}M^b = -\mu a^1_a + \frac{\mu}{2}\partial_a h^{\rm R1}_{tt} - \mu\partial_t h^{\rm R1}_{ta} - S_i\mathcal{B}^i_a, \tag{2.57}$$

where all quantities are evaluated on $\gamma$. Eq. (2.56) tells us that the small body's spin is constant at leading order. Eq. (2.57) gives the first-order acceleration of $\gamma$. In covariant form it can be written as

$$\frac{D^2M^\mu}{d\tau^2} - R^\mu{}_{\alpha\nu\beta}u^\alpha u^\nu M^\beta = -\mu a_1^\mu + \frac{1}{2}R^\mu{}_{\alpha\nu\beta}u^\alpha S^{\beta\nu} - \frac{\mu}{2}\left(g^{\mu\nu}+u^\mu u^\nu\right)\left(2h^{\rm R1}_{\beta\nu;\alpha} - h^{\rm R1}_{\alpha\beta;\nu}\right)u^\alpha u^\beta. \tag{2.58}$$

Eq. (2.58) is the equation of motion of the centre-of-mass of the small body relative to $\gamma$, where $M^\alpha \equiv M^i x_i^\alpha$, $u^\mu$ is the four-velocity along $\gamma$, $a_1^\alpha$ is the first-order acceleration of $\gamma$, and $S^{\mu\nu} = g^{\mu a}g^{\nu b}S_{ab}$, $S_{ab} = \varepsilon_{abi}S^i$ is the spin written in covariant form. The second term on the LHS represents the fact that the background curvature will cause the small body to accelerate relative to $\gamma$, if the body is displaced from $\gamma$. If we set $\gamma$ to be the worldline of the small body, then $M^\alpha = 0$ and $a_1^\alpha$ becomes the acceleration of the small body itself. If we further specialise to a non-spinning object, Eq. (2.58) simplifies to

$$\frac{D^2z^\mu}{d\tau^2} = -\frac{1}{2}\left(g^{\mu\nu}+u^\mu u^\nu\right)\left(2h^{\rm R1}_{\beta\nu;\alpha} - h^{\rm R1}_{\alpha\beta;\nu}\right)u^\alpha u^\beta + O(\epsilon^2)\,. \tag{2.59}$$

Eq. (2.59) is the first-order equation of motion of the small body. The right-hand side equals the self-force per unit mass. As Eq. (2.59) shows, the self-force arises due to the interaction of the small body with its own regular field $h^{\rm R1}$, whereas the singular field $h^{\rm S1}$ does not contribute to the self-force at all.

After some algebra, Eq. (2.59) can be re-arranged to yield

$$\tilde{u}^\alpha\tilde{\nabla}_\alpha\tilde{u}^\beta = O(\epsilon^2), \tag{2.60}$$

where $\tilde{\nabla}$ is the covariant derivative associated with the metric $g + h^{\rm R1}$, and $\tilde{u}^\alpha$ is the four-velocity normalized in the effective spacetime as $(g_{\alpha\beta} + h^{\rm R1}_{\alpha\beta})\tilde{u}^\alpha\tilde{u}^\beta = -1$. Hence, an important implication of Eq. (2.59) is that the small body moves along a geodesic of the effective spacetime $g_{\alpha\beta} + h^{\rm R}_{\alpha\beta}$ through first order.

## 2.6 The second-order equation of motion

Now we turn to describing the derivation of the equation of motion at second order. We closely follow the strategy detailed in [44, 78], where full details can be found. Note that the first-order equation of motion was derived from the gauge condition on the second-order field. Analogously, the second-order equation of motion would be derived from the third-order field. Rather than tackling the arduous task of directly solving the third-order field equations in the outer expansion, we instead make greater use of the inner expansion. We specialize to a small body which is spherical and non-spinning. Since the equation of motion will be derived in the buffer region, where the metric is dictated by the multipole structure of the small body, we can look at an inner expansion for any such small body which is both spherical and non-spinning. A convenient example of such a metric that we have at our disposal is that of a tidally-perturbed, non-rotating black hole $\mathrm{g}_{\alpha\beta}^{\text{tidal BH}}$ of mass $\mu$, derived by Poisson in [79] through third order in $\epsilon$.

The tidal distortion of the spacetime of the small black hole is caused by the curvature of the external spacetime, as well as by interactions between the external spacetime and the small object's own field. The small black hole metric in [79] is given in light-cone coordinates $\left(v, R, \theta^A\right)$, centered on the worldline of the small black hole. Because we will write this metric as an inner-expansion, we use $R$ for the radial coordinate, so as not to conflict with $r$ used for the radial coordinate in the outer expansion in Sec. 2.1. In the buffer region, these coordinates differ from those in the preceding sections by a small amount, and the matching conditions in Sec. 2.1 is imposed only after applying a small coordinate transformation, as discussed later in this section. The metric is written in a certain gauge (not the Lorenz gauge), where mass-dipole terms and acceleration terms do not appear in the metric, telling us that the black hole is mass-centered on the worldline and also at rest on it. The way that we will extract the second order acceleration is to find a gauge transformation that will take us from this gauge to the Lorenz gauge, while preserving the location of the worldline on which the black hole is centered.

Let us write this metric in the form of the inner expansion (2.3). We take the metric of the tidally perturbed black hole in [79], and rewrite it in terms of scaled coordinates $\tilde{R} = R/\epsilon$. This, as we explained in Sec. 2.1, re-scales the coordinates and keeps us in a region close to the small body, which in our case is the tidally perturbed black hole. This gives us an inner expansion of the form

$$\begin{aligned}\mathrm{g}_{\alpha\beta}^{\text{tidal BH}}(v,\tilde{R},\theta^A) =& \epsilon^0 g_{\alpha\beta}^{\text{BH}}(v,\tilde{R},\theta^A) + \epsilon^1 H^1_{\alpha\beta}(v,\tilde{R},\theta^A) + \epsilon^2 H^2_{\alpha\beta}(v,\tilde{R},\theta^A)\\ &+ \epsilon^3 H^3_{\alpha\beta}(v,\tilde{R},\theta^A) + O(\epsilon^4)\,. \end{aligned}\tag{2.61}$$

The first term on the right hand side, $g_{\alpha\beta}^{\text{tidal BH}}$, is the metric of the unperturbed black hole,

$$g_{vv}^{\text{BH}} = -\left(1 - 2\mu/\tilde{R}\right), \tag{2.62a}$$

$$g_{vr}^{\text{BH}} = 1, \tag{2.62b}$$

$$g_{vA}^{\text{BH}} = 0, \tag{2.62c}$$

$$\frac{1}{R^2} g_{AB}^{\text{BH}} = \Omega_{AB}, \tag{2.62d}$$

Here, $\Omega_{AB}$ is the metric on the two-sphere, with $\Omega_{AB} \equiv \left(1, \sin^2\theta\right)$. $H^n_{\alpha\beta}$ are tidal perturbations, which are functions of $\mathcal{E}_{ab}$ and $\mathcal{B}_{ab}$ and their derivatives, where $\mathcal{E}_{ab} = \mathcal{E}^0_{ab} + \epsilon\delta\mathcal{E}_{ab} + O(\epsilon^2)$, $\mathcal{B}_{ab} = \mathcal{B}^0_{ab} + \epsilon\delta\mathcal{B}_{ab} + O(\epsilon^2)$. The zeroth order fields $\mathcal{E}^0_{ab}$, $\mathcal{B}^0_{ab}$ will be identified with the tidal fields of the external background. The self-tides $\delta\mathcal{E}_{ab}$ and

$\delta\mathcal{B}_{ab}$, are corrections to the tidal fields due to the field of the small black hole interacting with the background. The $H^n_{\alpha\beta}$ are given below explicitly, in Tables 2.1-2.3. Symbols in Table 2.2 are defined in terms of the unit vectors $\Omega^a = (\sin\theta\cos\varphi, \sin\theta\sin\varphi, \cos\theta)$, which are related to $n^a$ by a small transformation. The tidal perturbations are given in a light-cone gauge, in which $H_{\alpha R} = 0$ for all $\alpha$. This gauge preserves the geometrical meaning of the Eddington-Finkelstein coordinates in the perturbed spacetime: $v$ remains a label on ingoing lightcones, and $R$ remains an affine parameter on ingoing null rays.

Table 2.1: Tidal perturbation terms $H^n_{\alpha\beta}$ that appear in the inner expansion of the tidally perturbed black hole metric (2.61). Definitions of the irreducible tidal fields, $\mathcal{E}^{\mathsf{q}}$, $\mathcal{B}^{\mathsf{q}}$ and so on, can be found in Table 2.2. The explicit form of the radial functions $e_n = e_n(r)$ and $b_n = b_n(r)$ can be found in Table 2.3. A dot on top of a term denotes a time derivative.

$$
\begin{aligned}
H^1_{\alpha\beta} &= 0 \\
H^2_{vv} &= -\tilde{R}^2 e_1 \mathcal{E}^{\mathsf{q}} \\
H^3_{vv} &= -\tfrac{1}{3}\tilde{R}^3 e_2 \dot{\mathcal{E}}^{\mathsf{q}} - \tfrac{1}{3}\tilde{R}^3 e_3 \mathcal{E}^{\mathsf{o}} - \tilde{R}^2 e_1 \delta\mathcal{E}^{\mathsf{q}} \\
R^{-1}H^2_{vA} &= -\tfrac{2}{3}\tilde{R}^2\left(e_4\mathcal{E}^{\mathsf{q}}_A - b_4\mathcal{B}^{\mathsf{q}}_A\right) \\
R^{-1}H^3_{vA} &= \tfrac{1}{3}\tilde{R}^3\left(e_5\dot{\mathcal{E}}^{\mathsf{q}}_A - b_5\dot{\mathcal{B}}^{\mathsf{q}}_A\right) - \tfrac{1}{4}\tilde{R}^3\left(e_6\mathcal{E}^{\mathsf{o}}_A - b_6\mathcal{B}^{\mathsf{o}}_A\right) \\
&\quad -\tfrac{2}{3}\tilde{R}^2\left(e_4\delta\mathcal{E}^{\mathsf{q}}_A - b_4\delta\mathcal{B}^{\mathsf{q}}_A\right) \\
R^{-2}H^2_{AB} &= -\tfrac{1}{3}\tilde{R}^2\left(e_7\mathcal{E}^{\mathsf{q}}_{AB} - b_7\mathcal{B}^{\mathsf{q}}_{AB}\right) \\
R^{-2}H^3_{AB} &= \tfrac{5}{18}\tilde{R}^3\left(e_8\dot{\mathcal{E}}^{\mathsf{q}}_{AB} - b_8\dot{\mathcal{B}}^{\mathsf{q}}_{AB}\right) - \tfrac{1}{6}\tilde{R}^3\left(e_9\mathcal{E}^{\mathsf{o}}_{AB} - b_9\delta\mathcal{B}^{\mathsf{o}}_{AB}\right) \\
&\quad -\tfrac{1}{3}\tilde{R}^2\left(e_7\delta\mathcal{E}^{\mathsf{q}}_{AB} - b_7\delta\mathcal{B}^{\mathsf{q}}_{AB}\right)
\end{aligned}
$$

Currently, the inner metric (2.61) is in a mass-centered rest gauge [44]. Our goal is to derive an equation of motion, through second order, for the small body in the Lorenz gauge. Let us refer to the worldline in the mass-centered rest-gauge as $\tilde{\gamma}$, and the worldline in the Lorenz gauge as $\gamma$. Since $\tilde{\gamma}$ is a good representative of the black hole's center-of-mass position, we impose $\gamma = \tilde{\gamma}$. We will derive the equation of motion by performing a gauge transformation $x^\mu \to x'^\mu = x^\mu - \xi^\mu$ from the mass-centered rest-gauge to the Lorenz gauge. The gauge-vector $\xi^\mu$ shall be determined by the matching of the inner expansion, Eq. (2.61), with the outer expansion that we have already derived in Sec. 2.5. We further demand that the smooth part of $\xi^\alpha$ vanishes at the origin of our coordinate system. This condition, which will be stated more explicitly below, preserves the location of the worldline at the coordinate origin. Otherwise the gauge-transformation would cause a shift in the coordinates' origin, leading to an arbitrary relationship between these two coordinates, and an arbitrary relationship between $\gamma$ and $\tilde{\gamma}$.

The calculation proceeds as follows. Take the inner expansion (2.61) and perform an outer expansion, which means replacing $\tilde{R}$ with $R/\epsilon$ and then re-expanding in powers of $\epsilon$. This is tantamount to expanding in powers of the mass $\mu$ of the small black hole.

Table 2.2: tidal fields, taken from [79], that appear in Table 2.1. Each field is identified with a sans-serif superscript that specifies its multipole content. A field labeled with a "q" is a quadrupole field, and one labeled with an "o" is an octupole field. The tidal fields appearing in Table 2.1 are related to the ones listed here by the coordinate transformations $\mathcal{E}^{\mathsf{q}}_A = \mathcal{E}^{\mathsf{q}}_a \Omega^a_A$, $\mathcal{E}^{\mathsf{q}}_{AB} = \mathcal{E}^{\mathsf{q}}_{ab}\Omega^a_A\Omega^b_B$, and so on, where $\Omega^a_A = \partial\Omega^a/\partial\theta^A$.

$$
\begin{aligned}
\mathcal{E}^{\mathsf{q}} &= \mathcal{E}^0_{ab}\Omega^a\Omega^b \\
\mathcal{E}^{\mathsf{q}}_a &= (\delta_a{}^c - \Omega_a\Omega^c)\mathcal{E}^0_{cd}\Omega^d \\
\mathcal{E}^{\mathsf{q}}_{ab} &= 2(\delta_a{}^c - \Omega_a\Omega^c)(\delta_b{}^d - \Omega_b\Omega^d)\mathcal{E}^0_{cd} + (\delta_{ab} - \Omega_a\Omega_b)\mathcal{E}^{\mathsf{q}} \\
\mathcal{B}^{\mathsf{q}}_a &= \varepsilon_{abc}\Omega^b\mathcal{B}^{0\,c}{}_d\Omega^d \\
\mathcal{B}^{\mathsf{q}}_{ab} &= \varepsilon_{acd}\Omega^c\mathcal{B}^{0\,d}{}_e(\delta^e{}_b - \Omega^e\Omega_b) + (a \leftrightarrow b) \\
\mathcal{E}^{\mathsf{o}} &= \mathcal{E}^0_{abc}\Omega^a\Omega^b\Omega^c \\
\mathcal{E}^{\mathsf{o}}_a &= (\delta_a{}^b - \Omega_a\Omega^b)\mathcal{E}^0_{bcd}\Omega^c\Omega^d \\
\mathcal{E}^{\mathsf{o}}_{ab} &= 2(\delta_a{}^c - \Omega_a\Omega^c)(\delta_b{}^d - \Omega_b\Omega^d)\mathcal{E}^0_{cde}\Omega^e + (\delta_{ab} - \Omega_a\Omega_b)\mathcal{E}^{\mathsf{o}} \\
\mathcal{B}^{\mathsf{o}}_a &= \tfrac{4}{3}\varepsilon_{acd}\Omega^c\mathcal{B}^{0\,d}{}_{ef}\Omega^e\Omega^f \\
\mathcal{B}^{\mathsf{o}}_{ab} &= \tfrac{4}{3}\varepsilon_{acd}\Omega^c\mathcal{B}^{0\,d}{}_{ef}(\delta^e{}_b - \Omega^e\Omega_b)\Omega^f + (a \leftrightarrow b)
\end{aligned}
$$

The first step is to transform to pseudo-Cartesian coordinates $X^a = R\Omega^a$, with $\Omega^a$ defined in Table 2.2. We will end up with an expansion that looks like

$$
\begin{aligned}
\mathrm{g}_{\alpha\beta}(v, X^a; \epsilon) = g_{\alpha\beta}(v, X^a) + \epsilon h'^1_{\alpha\beta}(v, X^a) + \epsilon^2 h'^2_{\alpha\beta}(v, X^a) + \epsilon^3 h'^3_{\alpha\beta}(v, X^a) \\
+ O(\epsilon^4). \qquad (2.63)
\end{aligned}
$$

There are some subtleties related to the ordering of terms, which we will not go into but which are discussed in [78]. We note that (2.63) is valid not only for a black hole, but for any non-spinning compact object with no quadrupole moments.

The next thing we want to do is perform a coordinate transformation from light-cone to FW coordinates, so that the outer expansion (2.63) is in the same coordinates as the outer expansion we derived in Sec. 2.5. Take the light-cone coordinates $(v, X^a)$ and write them in terms of ordinary FW normal coordinates $(t, x^a)$ centered on the worldline as the expansions

$$
v = t - R + \sum_{p,\ell,k} R^p \ln R^k \delta v_L \hat{n}^L\,, \qquad X^i = x^i + \sum_{p,\ell,k} R^p \ln R^k \delta X^i_L \hat{n}^L\,, \qquad (2.64)
$$

where the $\delta v_L$, $\delta X^i_L$ are functions of $t$. In what follows, a bar above indices refers to components in light-cone coordinates, and indices with no bar are components in ordinary FW coordinates. Aided by these expansions, take the background metric $g_{\bar{\alpha}\bar{\beta}}(v, X^a)$,

Table 2.3: Radial functions that appear in the metrics of Table 2.3, expressed in terms of $x \equiv \tilde{R}/(2\mu)$ and $\tilde{f} \equiv 1 - 2\mu/\tilde{R}$. At $\tilde{R} = 2\mu$ we have $e_7 = \frac{1}{2}$, $e_9 = \frac{1}{10}$, $b_7 = -\frac{1}{2}$, and $b_9 = -\frac{1}{10}$, with all other functions vanishing.

$$
\begin{aligned}
e_1 &= \tilde{f}^2 \\
e_2 &= \tilde{f}\left(\frac{3}{4x^4} + \frac{7}{4x^3} - \frac{3}{4x^2}(4\log x + 9) + \frac{1}{4x}(12\log x + 5) + 1\right) \\
e_3 &= \tilde{f}^2\left(1 - \frac{1}{2x}\right) \\
e_4 &= \tilde{f} \\
e_5 &= \tilde{f}\left(-\frac{1}{2x^4} - \frac{3}{2x^3} - \frac{5}{2x^2} + \frac{1}{6x}(12\log x + 13) + 1\right) \\
e_6 &= \tilde{f}\left(1 - \frac{2}{3x}\right) \\
e_7 &= 1 - \frac{1}{2x^2} \\
e_8 &= \frac{3}{5x^4} - \frac{1}{5x^3}(3\log x + 7) - \frac{9}{5x^2} + \frac{2}{5x}(3\log x + 4) + 1 \\
e_9 &= \tilde{f} + \frac{1}{10x^3} \\
b_4 &= \tilde{f} \\
b_5 &= \tilde{f}\left(-\frac{1}{6x^4} - \frac{1}{2x^3} - \frac{3}{2x^2} + \frac{1}{6x}(12\log x + 7) + 1\right) \\
b_6 &= \tilde{f}\left(1 - \frac{2}{3x}\right) \\
b_7 &= 1 - \frac{3}{2x^2} \\
b_8 &= \frac{1}{5x^4} - \frac{1}{5x^3}(3\log x + 2) - \frac{9}{5x^2} + \frac{6\log x + 5}{5x} + 1 \\
b_9 &= \tilde{f} - \frac{1}{10x^3}
\end{aligned}
$$

and the $h'^{n}_{\bar{\alpha}\bar{\beta}}(v, X^a)$ in light-cone coordinates and transform them to FW coordinates, as

$$g_{\alpha\beta}(t, x^i) = \frac{\partial x^{\bar{\alpha}}}{\partial x^{\alpha}}\frac{\partial x^{\bar{\beta}}}{\partial x^{\beta}} g_{\bar{\alpha}\bar{\beta}}(v, X^i)\,, \tag{2.65}$$

$$h'^{n}_{\alpha\beta}(t, x^a) = \frac{\partial x^{\bar{\alpha}}}{\partial x^{\alpha}}\frac{\partial x^{\bar{\beta}}}{\partial x^{\beta}} h'^{n}_{\bar{\alpha}\bar{\beta}}(v, X^a). \tag{2.66}$$

In this format $g_{\alpha\beta}(t, x^i)$ is the background metric of the large black hole in FW coordinates, derived in Eq. (B.29). The numerical coefficients in (2.64) are determined from Eq. (2.65).

Now inserting (2.64) into (2.65) and (2.66) puts the outer expansion in the same coordinates as (2.2), except (2.64) is in the rest gauge and (2.2) is in the Lorenz gauge. We need a gauge transformation that brings (2.64) into the form of (2.2), so that we can match them to determine what the form of the gauge transformation should be. To match the two expansions at orders $\epsilon$ and $\epsilon^2$, we require a unique gauge transformation $x^\mu \to x^\mu - \epsilon\,\xi_1^\mu - \epsilon^2\,\left(\xi_2^\mu - \frac{1}{2}\xi_1^\nu \partial_\nu \xi_1^\mu\right) + O(\epsilon^3)$. We have

$$h'^1_{\alpha\beta}(t,x^i) = h^1_{\alpha\beta}(t,x^i) + \mathcal{L}_{\xi_1} g_{\alpha\beta}(t,x^i)\,, \tag{2.67}$$

$$h'^2_{\alpha\beta}(t,x^i) = h^2_{\alpha\beta}(t,x^i) + \mathcal{L}_{\xi_2} g_{\alpha\beta}(t,x^i) + \frac{1}{2}\mathcal{L}^2_{\xi_1} g_{\alpha\beta}(t,x^i) + \mathcal{L}_{\xi_1} h^1_{\alpha\beta}(t,x^i)\,, \tag{2.68}$$

where $h'^1_{\alpha\beta}(t,x^i)$ are the metric perturbations in the mass-centered rest gauge, and $h^1_{\alpha\beta}(t,x^i)$ are the metric perturbations in the Lorenz gauge. Note that all of the terms in Eqs. (2.67) and (2.68) are expressed in FW coordinates. As such the $h^n_{\alpha\beta}$ are the same metric perturbations whose expressions were derived in the previous section. $\mathcal{L}_X$ represents the Lie derivative with respect to the vector $X^\alpha$, and $\xi_1$ and $\xi_2$ are the first-order and second-order contributions to the gauge vector.

The final step in our derivation is to insert the expansion of the gauge vector, $\xi_n^\alpha = \sum_{p,\ell} r^p \xi^\alpha_{(n,p,\ell),L}\hat{n}^L$, and insert the local expressions for $h^1_{\alpha\beta}$ and $h^2_{\alpha\beta}$ derived in Sec. 2.5 into Eq. (2.67) and Eq. (2.68). We demand that the specific piece $\xi^a_{(n,0,0)}$, which corresponds to a translation of the origin, vanishes. This ensures that the worldline remains at the origin of our coordinates, as discussed above. We find that if $\xi^a_{(n,0,0)} = 0$, then Eqs. (2.67) and (2.68) can only be satisfied if the acceleration terms $a^i_n$ satisfy certain equations. Fixing all the coefficients in the gauge vector ensures that this result is unique; all the freedom in the transformation is exhausted, so it cannot be used to change the result.

Matching the metric perturbations uniquely determines the result of Eq. (2.59) for the first-order acceleration $\epsilon\,a_1^\mu$. Matching order-$\epsilon r^2$ terms in the metric determines the $\delta\mathcal{E}_{ab}$ and $\delta\mathcal{B}_{\alpha\beta}$ as a function of $h^1_{\alpha\beta}$. The order $\epsilon^2$ transformation up to order $r$ uniquely determines the second-order acceleration $\epsilon^2\,a_2^\mu$. Adding the first-order and second-order accelerations, $a^\mu = \epsilon a_1^\mu + \epsilon^2\,a_2^\mu$, leads to the final expression for the self-force through second order,

$$a^\mu = -\frac{1}{2}\left(g^{\mu\nu} + u^\mu u^\nu\right)\left(g_\nu{}^\gamma - h^{\mathrm{R}\ \gamma}_\nu\right)\left(2h^{\mathrm{R}}_{\beta\gamma;\alpha} - h^{\mathrm{R}}_{\alpha\beta;\gamma}\right)u^\alpha u^\beta\,, \tag{2.69}$$

where $h^{\mathrm{R}}_{\alpha\beta} = \epsilon h^{\mathrm{R1}}_{\alpha\beta} + \epsilon^2 h^{\mathrm{R2}}_{\alpha\beta}$ . Eq. (2.69) confirms that at second-order the worldline of the small body is a geodesic of the effective spacetime $g_{\alpha\beta} + \epsilon h^{\mathrm{R1}}_{\alpha\beta} + \epsilon^2\,h^{\mathrm{R2}}_{\alpha\beta}$. We can write an equation analogous to Eq. (2.60) as

$$\tilde{u}^\alpha \tilde{\nabla}_\alpha \tilde{u}^\beta = O(\epsilon^3). \tag{2.70}$$

where $\tilde{\nabla}$ is the covariant derivative associated with the metric $g + h^{\mathrm{R}}$, and $\tilde{u}^\alpha$ is the four-velocity normalized in the effective spacetime as $(g_{\alpha\beta} + h^{\mathrm{R1}}_{\alpha\beta} + h^{\mathrm{R2}}_{\alpha\beta})\tilde{u}^\alpha\tilde{u}^\beta = -1$.

# Chapter 3

# The puncture scheme

In this chapter we begin to develop the puncture scheme that we will use to solve the field equations (2.21) and (2.22) globally. We recall, as described in the introduction, that at second order, the source $\delta^2 R_{\alpha\beta}$ is not integrable in any region covering the worldline, meaning we cannot easily solve for the full field. The puncture scheme gets around this problem by rewriting Eqs. (2.21) and (2.22) as equations for "residual" fields that locally approximate $h^{\mathrm{R}1}$ and $h^{\mathrm{R}2}$. This scheme ensures that our total metric perturbation (puncture plus residual field) agrees with the metric outside a small compact object, as derived in the previous chapter. As a convenient numerical output, it also directly yields a field that can be used in the equation of motion (2.69).

There have been a collection of previous implementations of a puncture scheme. Barack and Golbourn [70] implemented such a scheme for a scalar charge in Schwarzschild spacetime. A similar calculation was performed by Vega and Detweiler [71]. Whereas Barack and Golbourn utilized an azimuthal-mode decomposition, with the intention of later capitalizing on the azimuthal symmetry of Kerr, Vega and Detweiller solved the scalar wave equation directly in 3+1 dimensions. Later implementations of the puncture method include the calculation of the scalar-field self-force for circular orbits in Schwarzschild by Barack and Dolan [80], and in Kerr by Barack, Dolan and Wardell [81]. This calculation was generalised to computing the gravitational self-force at first order for circular orbits in Schwarzschild [63] and in Kerr [82]. Diener *et al.* calculated the self-consistent orbital evolution of a (scalar) particle [83] in Schwarzschild in 3+1 dimensions, and Thornburg and Wardell computed the scalar self-force for highly eccentric orbits in Kerr in 2+1 dimensions [84]. I in collaboration with Pound [1] have constructed generic covariant formulas for the first- and second-order punctures, which may be applied to any spacetime, in any chosen coordinate system. This calculation is detailed in this chapter. With the eventual aim of numerically implementing our second-order punctures in a 1D, frequency-domain scheme, Warburton and Wardell have performed frequency-domain puncture-scheme computations for a scalar field [85] and for the first-order gravitational field [74].

This chapter is organised in the following way. In Sec. 3.1 we will show how to construct the puncture-scheme system of equations, which allows us to solve the field equations for the residual field. Next in Sec. 3.2 we give an overview of our derivation of a practical, covariant expression for the puncture field. Finally, in Sec 3.3 we show how to write the puncture in a specified coordinate system.

## 3.1 The basic idea of the puncture field

We start by restating the vacuum field equations that we are trying to solve, at first- and second-order as given in Eqs. (2.21) and (2.22). We take these vacuum equations, valid in a region outside the small object, and extend them down to all points $r > 0$, as

$$E_{\alpha\beta}[\,h^1\,] = 0 \qquad r > 0, \tag{3.1}$$

$$E_{\alpha\beta}[\,h^2\,] = 2\delta^2 R_{\alpha\beta}[\,h^1, h^1\,] \qquad r > 0. \tag{3.2}$$

The goal is then to solve these equations, and to find the corresponding regular fields, subject to the condition that near $r = 0$, the solutions must agree with the locally determined ones in Chapter 2. Based on that condition, as discussed below Eq. (2.47), we can also write (3.1) in the more familiar form

$$E_{\alpha\beta}[\,h^1\,] = -16\pi T^1_{\alpha\beta}. \tag{3.3}$$

The basic idea of the puncture method is to subtract a puncture field from the full field of the small body and then solve for the residual remainder. Given a particular choice of singular and regular fields, we define a puncture field, $h^{\mathcal{P}n}_{\alpha\beta}$, as a truncation of a local expansion of the $n$th-order singular field, $h^{\mathrm{S}n}_{\alpha\beta}$, in powers of spatial distance from the worldline of the small object, $\gamma$, at a certain order. The puncture contains all the divergent terms of the field on the worldline, at $r = 0$. We then define the residual field

$$h^{\mathcal{R}n}_{\alpha\beta} \equiv h^n_{\alpha\beta} - h^{\mathcal{P}n}_{\alpha\beta}. \tag{3.4}$$

We then write field equations for $h^{\mathcal{R}n}_{\alpha\beta}$ instead of the $n$th-order retarded field, $h^n_{\alpha\beta}$. Removing the puncture field allows us to work in global coordinates everywhere, even in the region including $\gamma$. The better $h^{\mathcal{P}n}_{\alpha\beta}$ represents $h^{\mathrm{S}n}_{\alpha\beta}$, the better $h^{\mathcal{R}n}_{\alpha\beta}$ represents $h^R_{\alpha\beta}$. For example, if

$$\lim_{x\to\gamma}[h^{\mathcal{P}n}_{\alpha\beta}(x) - h^{\mathrm{S}n}_{\alpha\beta}(x)] = 0, \tag{3.5}$$

then

$$\lim_{x\to\gamma}[h^{\mathcal{R}n}_{\alpha\beta}(x) - h^{\mathrm{R}n}_{\alpha\beta}(x)] = 0, \tag{3.6}$$

that is, the residual field agrees with the regular field on the worldline. Throughout the discussion in this chapter, we will use the dimensionless parameter $\lambda(= 1)$ to count powers of distance from the worldline. If $h^{\mathcal{P}n}_{\alpha\beta}$ is one order more accurate, meaning $h^{\mathcal{P}n}_{\alpha\beta} - h^{\mathrm{S}n}_{\alpha\beta} = O(\lambda)$, then

$$\lim_{x\to\gamma} \nabla_\rho h^{\mathcal{R}n}_{\alpha\beta} = \lim_{x\to\gamma} \nabla_\rho h^{\mathrm{R}n}_{\alpha\beta}. \tag{3.7}$$

Because the self-force is constructed from first derivatives of $h^{\mathrm{R}n}_{\alpha\beta}$, as in Eq. (2.69), this condition guarantees that the self-force can be calculated from $h^{\mathcal{R}n}_{\alpha\beta}$. That is, we may calculate the self-force by replacing $h^{\mathrm{R}n}_{\alpha\beta}$ with $h^{\mathcal{R}n}_{\alpha\beta}$ in Eq. (2.69), with $h^{\mathcal{R}}_{\alpha\beta} \equiv \epsilon h^{\mathcal{R}1}_{\alpha\beta} + \epsilon^2 h^{\mathcal{R}2}_{\alpha\beta}$, as

$$\frac{D^2 z^\alpha}{d\tau^2} = -\frac{1}{2}\left(g^{\mu\nu} + u^\mu u^\nu\right)\left(g_\nu{}^\gamma - h^{\mathcal{R}\gamma}_\nu\right)\left(2h^{\mathcal{R}}_{\beta\gamma;\alpha} - h^{\mathcal{R}}_{\alpha\beta;\gamma}\right) u^\alpha u^\beta\,. \tag{3.8}$$

In some circumstances, we require less of the puncture, and in the calculations in later chapters, we will use a lower-order truncation than needed for Eq. (3.7).

We are going to calculate the residual fields using the worldtube method [70]. In this approach, the worldline $\gamma$ is surrounded by a worldtube $\Gamma$. Outside $\Gamma$, we solve the wave equations for the retarded fields $h^1_{\alpha\beta}$ and $h^2_{\alpha\beta}$. Inside $\Gamma$, we solve the wave equations for the residual fields $h^{\mathcal{R}1}_{\alpha\beta}$ and $h^{\mathcal{R}2}_{\alpha\beta}$. The puncture scheme is then summarized by the coupled set of equations

$$E_{\alpha\beta}[\,h^{\mathcal{R}1}\,] = -E_{\alpha\beta}[\,h^{\mathcal{P}1}\,] \equiv S^{\mathrm{eff}1}_{\mu\nu} \qquad \text{inside } \Gamma, \tag{3.9a}$$

$$E_{\alpha\beta}[\,h^1\,] = 0 \qquad \text{outside } \Gamma, \tag{3.9b}$$

$$E_{\alpha\beta}[\,h^{\mathcal{R}2}\,] = 2\delta^2 R_{\alpha\beta}[\,h^1, h^1\,] - E_{\alpha\beta}[\,h^{\mathcal{P}2}\,] \equiv S^{\mathrm{eff}2}_{\mu\nu} \qquad \text{inside } \Gamma, \tag{3.9c}$$

$$E_{\alpha\beta}[\,h^2\,] = 2\delta^2 R_{\alpha\beta}[\,h^1, h^1\,] \qquad \text{outside } \Gamma, \tag{3.9d}$$

and the equation of motion (3.8). In the self-consistent approach, the puncture diverges on the worldline $z^\mu$ determined by (3.8). Solving Eqs. (3.9) for $h^{\mathcal{R}1}_{\alpha\beta}$ and $h^{\mathcal{R}2}_{\alpha\beta}$, the motion of the worldline is calculated by feeding the result into the equation of motion (3.8).

The source terms in Eqs. (3.9a) and (3.9c) are initially only defined for points $x \notin \gamma$, but we can include $\gamma$ in our domain as follows. In Eq. (3.9a), we evaluate $-E[\,h^{1\mathcal{P}}\,]$ as a field on the domain $x \notin \gamma$; unless we have $h^{1\,\mathcal{P}} = h^{\,1\mathrm{S}}$ exactly, the result will then exhibit some nonremovable nonsmoothness at $\gamma$, but it will be integrable and hence be a valid source on the whole domain $\Gamma$. (As per the discussion in Sec. 1.3, this treatment differs slightly from the one in which we write the source as $-16\pi T^1 - E[\,h^{1\mathcal{P}}\,]$, but the two sources are ultimately the same.) Similarly, in (3.9c), we evaluate $2\delta^2 R[\,h^1, h^1\,] - E[\,h^{2\,\mathcal{P}}\,]$ as a field on the domain $x \notin \gamma$ , canceling the nonintegrable singularities, and then take the resulting integrable function as our effective source on the whole of $\Gamma$. If the expansions of $h^{1\mathcal{P}}$ and $h^{2\mathcal{P}}$ in powers of distance from $\gamma$ (powers of $\lambda$) are of sufficiently high order, then the effective sources can be defined on $\gamma$ by taking the limit from off $\gamma$; however, continuity of the effective source is not necessary, and in this thesis our $h^{2\mathcal{P}}$ will not be of such a high order in $\lambda$.

Now we need a practical way of calculating the puncture field. This will be the goal of the next section.

## 3.2 A practical covariant puncture

Having formulated a way of solving the field equations using the puncture scheme, we now need practical covariant formulas for the puncture field through second order. Such expressions give us the freedom to write the puncture field in any coordinates we desire. We follow a two-step procedure, whereby we first obtain the puncture in a tensorial form, and then write it as a coordinate expansion. In the next chapter, when we come to solve for the first-order field for circular orbits in Schwarzschild, we will write the puncture field as a coordinate expansion in Schwarzschild coordinates, suitable for that scenario.

Throughout the discussion in this chapter we will refer to a generic timelike worldline as $\gamma$, and we will allow $\gamma$ to differ slightly from the worldline of the center of mass of the small object, by a small distance of order $\epsilon$. The reasoning behind this set up is that we will eventually use the two timescale expansion mentioned in the introduction, in which we expand the center-of-mass worldline of the small object around a slowly evolving, leading-order worldline. We note however that this slowly evolving, leading-order worldline is not a geodesic of the background.

### 3.2.1 Outline of conversion strategy

Currently we have expressions for the singular field components, $h^{\mathrm{S}1}_{\alpha\beta}$ and $h^{\mathrm{S}2}_{\alpha\beta}$, given in Appendix A in terms of local Fermi-Walker coordinates. These expressions were derived, using matched asymptotic expansions, as described in Chapter 2. The basic idea is to take the singular fields and write them in a tensorial form, as

$$h^{\mathrm{S}} = h^{\mathrm{S}}_{tt} dt\otimes dt + h^{\mathrm{S}}_{ta}(dt\otimes dx^a + dx^a\otimes dt) + h^{\mathrm{S}}_{ab} dx^a\otimes dx^b\,. \tag{3.10}$$

Here, $h^{\mathrm{S}}$ is used as a short-form that refers to the first- or second-order singular fields. Using geometrical definitions of the Fermi-Walker coordinates, we will express each of the components and one-forms in Eq. (3.10) in terms of covariant quantities. In this approach Eq. (3.10) will become a covariant expression which no longer depends on Fermi-Walker coordinates, or indeed on any other coordinate system. From the expression (3.10), we are free to pick whatever coordinate system suits us and truncate the resulting expression at the desired order of distance.

Firstly let us introduce Synge's world function. Here we follow the formalism that can be found on p.42 of Ref. [46]. Consider two points $\bar{x}$ and $x$, and a geodesic, $\beta$ that

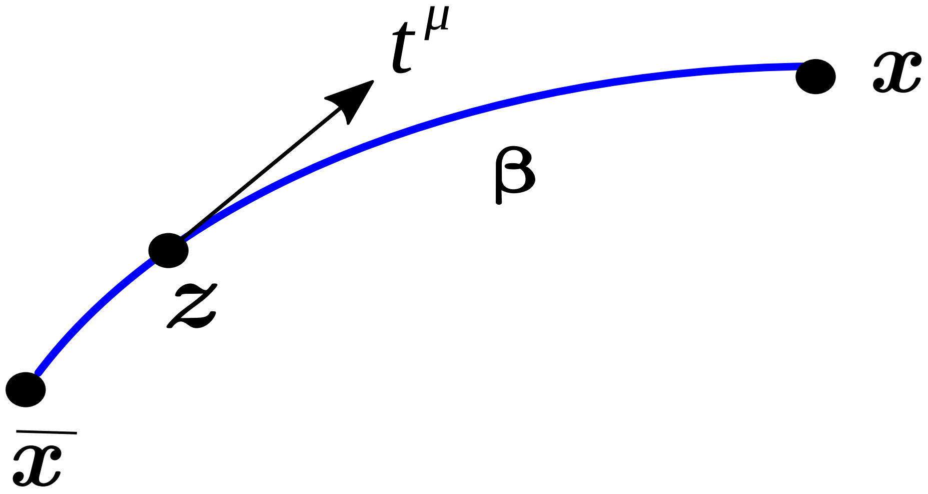


Figure 3.1: The base point $\bar{x}$, the field point $x$, and the geodesic segment $\beta$ that links them. The geodesic is described by parametric relations $z^\mu(\xi)$ and $t^\mu = dz^\mu/d\xi$ is its tangent vector.

connects them described by parametric relations $z^\mu(\xi)$, as illustrated in Fig. 3.1. Let $\xi$ be an affine parameter along $\beta$, with $\xi_0$, $\xi_1$ being the values of $\xi$ at $x$ and $\bar{x}$, respectively. In terms of $\xi$ we define the tangent vector $t^\mu$ at coordinate points $z^\mu(\xi)$ along $\beta$, as $t^\mu \equiv dz^\mu/d\xi$. Synge's world function is a scalar function of the source point $\bar{x}$ and the field point $x$, defined by

$$\sigma(x, \bar{x}) = \frac{1}{2}(\xi - \xi_0) \int_{\xi_0}^{\xi_1} g_{\mu\nu}(z) t^\mu t^\nu \, d\xi, \tag{3.11}$$

where $g_{\mu\nu}$ is the metric of the background spacetime and the integral is evaluated on the geodesic $\beta$ that links $x$ to $\bar{x}$. But we note that the geodesic equation implies that $\zeta \equiv g_{\mu\nu} t^\mu t^\nu$ is constant along $\beta$. Hence,

$$\sigma(x, \bar{x}) = \frac{1}{2}\zeta(\xi_1 - \xi_0)^2. \tag{3.12}$$

If the geodesic is timelike, we may set $\xi$ equal to the proper time $\tau$, which implies $\zeta = -1$. If the geodesic is spacelike, then $\xi$ can be set equal to the proper distance $s$, which implies that $\zeta = 1$. If the geodesic is null, then $\sigma(x, \bar{x})$ vanishes. Therefore,

$$\sigma(x, \bar{x}) = \begin{cases} -\frac{1}{2}(\Delta\tau)^2 & \beta \text{ timelike,} \\ \frac{1}{2}(\Delta s)^2 & \beta \text{ spacelike,} \\ 0 & \beta \text{ null,} \end{cases} \tag{3.13}$$

that is, in general, $\sigma(x, \bar{x})$ is half the squared geodesic distance between the points $\bar{x}$ and $x$, assuming that $\bar{x}$ lies within a normal convex neighbourhood of $x$. In flat spacetime, the geodesic linking $x$ to $\bar{x}$ is a straight line, and $\sigma(x, \bar{x}) = \frac{1}{2}\eta_{\alpha\beta}(x - \bar{x})^\alpha (x - \bar{x})^\beta$ in Lorentzian coordinates.

Covariant derivatives are written as $\sigma_\alpha(x, \bar{x}) \equiv \nabla_\alpha \sigma(x, \bar{x})$, $\sigma_{\bar{\alpha}}(x, \bar{x}) \equiv \nabla_{\bar{\alpha}} \sigma(x, \bar{x})$, where barred (unbarred) indices indicate that the derivative is evaluated at the point $\bar{x}$ ($x$). $\sigma_\alpha(x, \bar{x})$ is a vector that is tangent to $\beta$ at the point $x$ and $\sigma_{\bar{\alpha}}(x, \bar{x})$ is a vector that is tangent to $\beta$ at the point $\bar{x}$.

Fermi-Walker coordinates $(t, x^a)$ are constructed from a tetrad $(u^{\bar{\alpha}}, e^{\bar{\alpha}}_a)$ established along $\gamma$. The spatial triad is Fermi-Walker transported along the worldline according to

$$\frac{De^{\bar{\alpha}}_a}{d\tau} = a_a u^{\bar{\alpha}}, \tag{3.14}$$

where $a_a \equiv a_\mu e^\mu_a$ is a spatial component of $\gamma$'s acceleration, $a^\mu$. At each instant $\bar{\tau}$ of proper time, spatial geodesics are sent out orthogonally from the point $\bar{x} = z(\bar{\tau})$ on $\gamma$. These geodesics generate a spatial hypersurface $\Sigma_{\bar{\tau}}$, and on that hypersurface, coordinates $x^a$ are defined as

$$x^a = -e^a_{\bar{\alpha}} \sigma^{\bar{\alpha}}. \tag{3.15}$$

The geodesic distance from $\bar{x}$ to $x$ is given by $r \equiv \sqrt{\delta_{ab} x^a x^b}$. $\sigma^{\bar{\alpha}}$ is tangent to a generator of $\Sigma_{\bar{\tau}}$, satisfying

$$\sigma_{\bar{\alpha}} u^{\bar{\alpha}} = 0. \tag{3.16}$$

Each of the hypersurfaces is labeled with time $t = \bar{\tau}$, defining the coordinates $(t, x^a)$ at each point in the convex normal neighbourhood of $\gamma$.

We will frequently write tensor components contracted with members of the tetrad as, for example

$$R_{\bar{u}\,\bar{a}\,\bar{b}\,\bar{c}\,|\,\bar{d}} \equiv R_{\bar{\alpha}\,\bar{\mu}\,\bar{\beta}\,\bar{\nu}\,;\,\bar{\gamma}} u^{\bar{\alpha}} e^{\bar{\mu}}_a e^{\bar{\beta}}_b e^{\bar{\nu}}_c e^{\bar{\gamma}}_d. \tag{3.17}$$

We will use the metric in Fermi-Walker coordinates to raise and lower indices, given through order $r^3$ in Eqs. (B.29).

Now let us move on to describe how we obtain the covariant puncture. The singular-field components $h^{\mathrm{S1}}_{\alpha\beta}$ and $h^{\mathrm{S2}}_{\alpha\beta}$ are currently written as functions of Fermi-Walker coordinates $(t, r, n^a)$, as in Eqs. (A.2) and (A.4). We will replace the dependence on $t$ with a dependence on $\bar{x}$, and we will replace $r$ and $n^a$ through the relations

$$r = \sqrt{2\bar{\sigma}}\,, \tag{3.18}$$

$$n^a = -\frac{e^a_{\bar{\alpha}}\sigma^{\bar{\alpha}}}{\sqrt{2\bar{\sigma}}}. \tag{3.19}$$

The notation

$$\bar{\sigma} \equiv \sigma(x, \bar{x}) \tag{3.20}$$

is adopted to refer to the world function $\sigma(x, \bar{x})$.

The other ingredients required to construct the covariant puncture, as in (3.10), are expressions for the one-forms $dt$ and $dx^a$. We can derive identities for these one-forms in Fermi-Walker coordinates, by taking total derivatives of Eqs. (3.15) and (3.16) [46]. This derivation is given in Appendix B, while just the final result is stated here:

$$dt = B\sigma_{\bar{\alpha}\alpha}u^{\bar{\alpha}}dx^\alpha\,, \qquad dx^a = -e^a_{\bar{\alpha}}\left(\sigma^{\bar{\alpha}}_{\alpha} + \mu\sigma^{\bar{\alpha}}_{\bar{\beta}}\sigma_{\alpha\bar{\gamma}}u^{\bar{\beta}}u^{\bar{\gamma}}\right)dy^\alpha\,. \tag{3.21}$$

Here, $y^\alpha$ are an arbitrary set of coordinates, and

$$B = -\left(\sigma_{\bar{\alpha}\bar{\beta}}u^{\bar{\alpha}}u^{\bar{\beta}} + \sigma_{\bar{\alpha}}a^{\bar{\alpha}}\right)^{-1}\,. \tag{3.22}$$

The next step is to re-write these expansions in terms of $x'$, an arbitrarily chosen point on the worldline within a convex normal neighbourhood of $x$. We do this because expressing the field at $x$ in terms of quantities at $\bar{x}$ is not ideal. $\bar{x}$ is always connected to $x$ by a geodesic that intersects $\gamma$ orthogonally, and if we wished to implement a puncture scheme in a particular coordinate system, we would have to express the coordinates at $\bar{x}$ in terms of the coordinates at $x$, which would create unnecessary complications. So rather than leaving our results in terms of $\bar{x}$, we expand the dependence on $\bar{x}$ about a nearby point $x'$ on $\gamma$. $x'$ is spatially related to $x$, but it is otherwise arbitrary. The general relationship between $x$, $\bar{x}$, and $x'$ is illustrated in Fig. 3.2; since $x'$ is arbitrary, its specific relationship to $x$ can be chosen to maximize convenience. For example, $x$ and $x'$ can be made to have the same coordinate time in the coordinates one uses in one's numerics. In Chapter 4 we will choose $x'$ to have the same Schwarzschild time as $x$. We will use the notation

$$\sigma = \sigma(x, x') \tag{3.23}$$

for Synge's world function for the points $x, x'$, not to be confused with $\bar{\sigma}$. Primed indices, as in $\sigma_{\alpha'}, \sigma_{\alpha'\beta'}$, shall refer to derivatives evaluated at the point $x'$.

The worldline $\gamma$ is described by the parametric functions $z^\mu(\tau)$. Hence, to express our quantities in terms of $x'$, we may write $\bar{x} = z(\bar{\tau})$ and $x' = z(\tau')$, and we expand in powers of

$$\Delta\tau \equiv \bar{\tau} - \tau'. \tag{3.24}$$

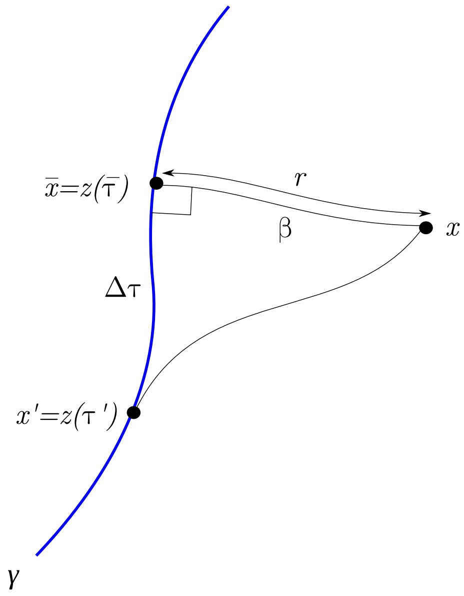


Figure 3.2: Illustration of the relationship between the points $\bar{x}$ and $x'$ on the worldline $\gamma$ of the small body, depicted by the thick blue line, and the field point $x$. The field point $x$ and the point $\bar{x}$ are connected by a unique geodesic $\beta$ of spatial length $r$, which intersects the worldline $\gamma$ orthogonally at $\bar{x}$. A different point $x'$ on $\gamma$ that lies in the convex normal neighbourhood of $x$, is also connected to $x$ by a unique geodesic. The two points are separated on the worldline by the proper-time distance $\Delta\tau$.

This procedure is made straightforward by the fact that each of the quantities $h^{\rm S}_{tt}$, $h^{\rm S}_{ta}$, $h^{\rm S}_{ab}$, $dt$, and $dx^a$ is a scalar at $\bar{x}$, meaning each can be expanded in an ordinary power series. So, for example,

$$h^{\rm S}_{tt} = h^{\rm S}_{tt}(x, z(\bar{\tau})) = h^{\rm S}_{tt}(x, x') + \frac{dh^{\rm S}_{tt}}{d\tau'}(x, x')\Delta\tau + O(\Delta\tau^2). \tag{3.25}$$

In the end, we wish our result to be in the form of a near-coincidence expansion in powers of $\sigma^{\alpha'}$. To achieve that, we will require the standard near-coincidence expansions [86]

$$\sigma_{\alpha\beta'} = -g^{\alpha'}_{\alpha}\Big[g_{\alpha'\beta'} + \tfrac{1}{6}\lambda^2 R_{\alpha'\gamma'\beta'\zeta'}\sigma^{\gamma'}\sigma^{\zeta'} - \tfrac{1}{12}\lambda^3 R_{\alpha'\gamma'\beta'\zeta';\iota'}\sigma^{\gamma'}\sigma^{\zeta'}\sigma^{\iota'} + O(\lambda^4)\Big], \tag{3.26a}$$

$$\sigma_{\alpha'\beta'} = g_{\alpha'\beta'} - \tfrac{1}{3}\lambda^2 R_{\alpha'\gamma'\beta'\zeta'}\sigma^{\gamma'}\sigma^{\zeta'} + \tfrac{1}{12}\lambda^3 R_{\alpha'\gamma'\beta'\zeta';\iota'}\sigma^{\gamma'}\sigma^{\zeta'}\sigma^{\iota'} + O(\lambda^4), \tag{3.26b}$$

$$g^{\alpha'}_{\mu;\mu'} = g^{\beta'}_{\mu}\Big[-\tfrac{1}{2}\lambda R^{\alpha'}{}_{\beta'\mu'\gamma'}\sigma^{\gamma'} + \tfrac{1}{6}\lambda^2 R^{\alpha'}{}_{\beta'\mu'\gamma';\zeta'}\sigma^{\gamma'}\sigma^{\zeta'} + O(\lambda^3)\Big]. \tag{3.26c}$$

Here, $g^{\mu'}_{\mu}$ is a parallel propagator. It takes a vector at $x'$ and parallel-transports it to $x$ along the unique geodesic that links these points.

After expanding the components $h^{\rm S}_{tt}$, $h^{\rm S}_{ta}$, $h^{\rm S}_{ab}$ around $x'$, expanding the one-forms $dt$ and $dx^a$ around $x'$, and combining the results, we obtain the right-hand side of Eq. (3.10) in the form

$$h^{\mathrm{S}}_{\alpha\beta}dy^\alpha dy^\beta = \left[h^{\mathrm{S}}_{tt}\frac{\partial t}{\partial y^\alpha}\frac{\partial t}{\partial y^\beta} + 2h^{\mathrm{S}}_{ta}\frac{\partial t}{\partial y^{(\alpha}}\frac{\partial x^a}{\partial y^{\beta)}} + h^{\mathrm{S}}_{ab}\frac{\partial x^a}{\partial y^\alpha}\frac{\partial x^b}{\partial y^\beta}\right] dy^\alpha dy^\beta, \tag{3.27}$$

with the quantity in square brackets written entirely in terms of tensors containing no remnant of Fermi-Walker coordinates. We will eliminate the dependence on the triad legs in this expression using the identity

$$e^\alpha_a e^{a\beta} = P^{\alpha\beta} \tag{3.28}$$

where

$$P_{\mu\nu} \equiv g_{\mu\nu} + u_\mu u_\nu \tag{3.29}$$

projects onto a plane orthogonal to $\gamma$. We will then be left with a tensorial expression for $h^{\mathrm{S}}_{\alpha\beta}$ .

To simplify expressions, we define the distances

$$\mathsf{r} \equiv u_{\mu'}\sigma^{\mu'}, \tag{3.30}$$

which, in a rough sense, describes the proper time between $x'$ and $x$, and

$$\mathsf{s} \equiv \sqrt{P_{\mu'\nu'}\sigma^{\mu'}\sigma^{\nu'}}, \tag{3.31}$$

which roughly describes the spatial distance between $x'$ and $x$. Both bits of notation are taken from Ref. [87] by way of Ref. [88]. In terms of these distances, we have the relation

$$\sigma^{\mu'}\sigma_{\mu'} = 2\sigma(x,x') = \mathsf{s}^2 - \mathsf{r}^2. \tag{3.32}$$

As stated in the previous section, we do not always require a puncture of sufficiently high order in $\lambda$ to ensure that Eq. (3.7) is satisfied. However, for generality, we will carry all our expansions to that order. Since $h^{\mathrm{S2}}_{\mu\nu}$ begins at order $1/\lambda^2$, and Eq. (3.7) demands that we include all terms through order $\lambda$, we must include four total orders in our expansions. This is precisely the number of orders included in the FW results in Chapter 2. For brevity, we truncate some of the explicit expressions at a lower order in $\lambda$, but our full results can be found in Ref. [1].

### 3.2.2 Expansion of $\Delta\tau$

Rather than moving directly to the components of the singular field, we first obtain expansions for various quantities that go into the expressions for the singular field. Since our strategy requires expanding the metric components and the one-forms around the point $x'$, we first derive an expansion of $\Delta\tau$, the time interval in (3.24), in terms of

$\sigma$. We define the function

$$p(\tau') \equiv \sigma_{\alpha'}(x, z(\tau'))u^{\alpha'}, \tag{3.33}$$

and expand $p(\bar{\tau})$ around $p(\tau')$. Note that from Eq. (3.16), $p(\bar{\tau}) = 0$. Hence $0 = p(\bar{\tau}) = p(\tau' + \Delta\tau)$, which we may expand as

$$\begin{aligned} p(\tau' + \Delta\tau) =& p(\tau') + p'(\tau')\Delta\tau + \frac{1}{2!}p''(\tau')\Delta\tau^2 + \frac{1}{3!}p'''(\tau')\Delta\tau^3 + \dots \\ =& \sigma_{\alpha'}u^{\alpha'} + \left(\sigma_{\alpha'\beta'}u^{\alpha'}u^{\beta'} + \sigma_{\alpha'}u^{\alpha'}\right)\Delta\tau \\ &+ \frac{1}{2}\left(\sigma_{\alpha'\beta'\gamma'}u^{\alpha'}u^{\beta'}u^{\gamma'} + 3\sigma_{\alpha'\beta'}u^{\alpha'}u^{\beta'} + \sigma_{\alpha'}\dot{a}^{\alpha'}\right)\Delta\tau^2 \\ &+ \frac{1}{3!}\frac{D^3\sigma_{\alpha'}u^{\alpha'}}{d\tau'^3}\Delta\tau^3 + \frac{1}{4!}\frac{D^4\sigma_{\alpha'}u^{\alpha'}}{d\tau'^4}\Delta\tau^4 + O(\Delta\tau^5), \end{aligned} \tag{3.34}$$

where in Eq. (3.34), we have used $D/d\tau' = u^{\alpha'}\nabla_{\alpha'}$, and similar identities for higher derivatives.

The next step is to insert the near-coincidence expansions (3.26b) for $\sigma_{\alpha'\beta'\dots}$; third and higher derivatives of $\sigma$ are obtained from (3.26b) recursively. To solve Eq. (3.34) for $\Delta\tau$, we expand $\Delta\tau$ itself in powers of $\lambda$ as

$$\Delta\tau = \lambda\Delta_1\tau + \lambda^2\Delta_2\tau + \lambda^3\Delta_3\tau + \lambda^4\Delta_4\tau + O(\lambda^5). \tag{3.35}$$

We then insert (3.35) into (3.34), and solve order by order in $\lambda$. The results are

$$\Delta_1\tau = \mathsf{r}, \tag{3.36a}$$

$$\Delta_2\tau = -\mathsf{r}a_\sigma, \tag{3.36b}$$

$$\Delta_3\tau = -\frac{1}{6}\mathsf{r}^3a_{\alpha'}a^{\alpha'} + \frac{1}{2}\mathsf{r}^2\dot{a}^\sigma + \mathsf{r}(a^\sigma)^2 - \frac{1}{3}\mathsf{r}R_{u\sigma u\sigma}, \tag{3.36c}$$

$$\begin{aligned} \Delta_4\tau =& -\frac{5}{24}\mathsf{r}^4a^{\alpha'}\dot{a}_{\alpha'} + \frac{1}{6}\mathsf{r}^3\ddot{a}^\sigma - \frac{2}{3}\mathsf{r}^3a_{\alpha'}a^{\alpha'}a^\sigma + \frac{3}{2}\mathsf{r}^2a^\sigma\dot{a}^\sigma \\ &+ \mathsf{r}(a^\sigma)^3 - \frac{1}{6}\mathsf{r}^3a^{\alpha'}R_{\alpha'uu\sigma} - \frac{1}{2}\mathsf{r}^2a^{\alpha'}R_{\alpha'\sigma u\sigma} - \frac{2}{3}\mathsf{r}a^\sigma R_{u\sigma u\sigma} \\ &- \frac{1}{8}\mathsf{r}^2\dot{R}_{u\sigma u\sigma} + \frac{1}{12}\mathsf{r}R_{u\sigma u\sigma|\sigma}, \end{aligned} \tag{3.36d}$$

where, e.g., $R_{u\sigma u\sigma} \equiv R_{\alpha'\beta'\gamma'\delta'}u^{\alpha'}\sigma^{\beta'}u^{\gamma'}\sigma^{\delta'}$.

### 3.2.3 Expansion of $\sigma(x, \bar{x})$

Continuing to assemble useful ingredients, we next turn to $\sigma$ itself. Since the components $h^{\mathrm{S}}_{tt}$, $h^{\mathrm{S}}_{ta}$, and $h^{\mathrm{S}}_{ab}$ involve $r = \sqrt{2\bar{\sigma}}$, it will be convenient to obtain an expansion of $\sigma(x, \bar{x})$

around $\sigma(x, x')$. We expand $\sigma(x, \bar{x})$ in the interval of proper time $\Delta\tau$, as

$$\sigma(x, z(\bar{\tau})) = \sigma(x, z(\tau')) + \frac{d\sigma}{d\tau'}\Delta\tau + \frac{1}{2!}\frac{d^2\sigma}{d\tau'^2}\Delta\tau^2 + \frac{1}{3!}\frac{d^3\sigma}{d\tau'^3}\Delta\tau^3 + \frac{1}{4!}\frac{d^4\sigma}{d\tau'^4}\Delta\tau^4 + \frac{1}{5!}\frac{d^5\sigma}{d\tau'^5}\Delta\tau^5 + O(\lambda^6), \tag{3.37}$$

and afterwards insert the expansion (3.35) and the near-coincidence expansions (3.26b). The outcome is

$$\sigma(x, z(\bar{\tau})) = \lambda^2\sigma_2(x, x') + \lambda^3\sigma_3(x, x') + \lambda^4\sigma_4(x, x') + \lambda^5\sigma_5(x, x') + O(\lambda^6), \tag{3.38}$$

where

$$\sigma_2 = \frac{1}{2}\mathsf{s}^2, \tag{3.39a}$$

$$\sigma_3 = -\frac{1}{2}\mathsf{r}^2 a_\sigma, \tag{3.39b}$$

$$\sigma_4 = \frac{1}{6}\mathsf{r}^3\dot{a}_\sigma - \frac{1}{24}\mathsf{r}^4 a_{\alpha'}a^{\alpha'}_{\frac{1}{2}}\mathsf{r}^2(a_\sigma)^2 - \frac{1}{6}\mathsf{r}^2 R_{u\sigma u\sigma}, \tag{3.39c}$$

$$\sigma_5 = -\frac{1}{24}\mathsf{r}^5 a^{\alpha'}\dot{a}_{\alpha'} + \frac{1}{24}\mathsf{r}^4\ddot{a}_\sigma - \frac{1}{6}\mathsf{r}^4 a_{\alpha'}a^{\alpha'}a_\sigma + \frac{1}{2}\mathsf{r}^3 a_\sigma\dot{a}_\sigma + \frac{1}{2}\mathsf{r}^2(a_\sigma)^3 - \frac{1}{24}\mathsf{r}^4 a^{\alpha'}R_{\alpha' u u\sigma} - \frac{1}{6}\mathsf{r}^3 a^{\alpha'}R_{\alpha'\sigma u\sigma} - \frac{1}{3}\mathsf{r}^2 a^\sigma R_{u\sigma u\sigma} - \frac{1}{24}\mathsf{r}^3\dot{R}_{u\sigma u\sigma} + \frac{1}{24}\mathsf{r}^2 R_{u\sigma u\sigma|\sigma}. \tag{3.39d}$$

### 3.2.4 Expansions of $dt$ and $dx^a$

The expansion of the one-forms $dt$ and $dx^a$ follows the same procedure as the expansion of $\sigma(x, \bar{x})$: first expand in powers of $\Delta\tau$, then substitute Eq. (3.35) and the near-coincidence expansion of derivatives of Synge's world function. In the case of $dx^a$, we will also have to make use of Eq. (3.14) for the derivative of $e^a_\alpha$ along the worldline.

It is helpful to first expand $B$ near coincidence; recall this quantity's appearance in Eqs. (3.21). The result of that expansion is

$$B = 1 + \lambda a_{\bar{\sigma}} + \lambda^2\left[(a_{\bar{\sigma}})^2 - \tfrac{1}{3}R_{\bar{u}\bar{\sigma}\bar{u}\bar{\sigma}}\right] + \lambda^3\left[(a_{\bar{\sigma}})^3 - \tfrac{2}{3}a_{\bar{\sigma}}R_{\bar{u}\bar{\sigma}\bar{u}\bar{\sigma}} + \tfrac{1}{12}R_{\bar{u}\bar{\sigma}\bar{u}\bar{\sigma}|\bar{\sigma}}\right] + O(\lambda^4), \tag{3.40}$$

where, e.g., $R_{\bar{u}\bar{\sigma}\bar{u}\bar{\sigma}} \equiv R_{\bar{\alpha}\bar{\beta}\bar{\gamma}\bar{\delta}}u^{\bar{\alpha}}\sigma^{\bar{\beta}}u^{\bar{\gamma}}\sigma^{\bar{\delta}}$. We place a bar over the subscripted $\sigma$'s and $u$'s to distinguish contracted quantities at $\bar{x}$ from those we defined at $x'$ as, e.g., $R_{u\sigma u\sigma} \equiv R_{\alpha'\beta'\gamma'\delta'}u^{\alpha'}\sigma^{\beta'}u^{\gamma'}\sigma^{\delta'}$.

Following the procedure in the case of $dt$, beginning from Eq. (3.21), we arrive at

$$dt = \left(t_{0\mu} + \lambda t_{1\mu} + \lambda^2 t_{2\mu} + \lambda^3 t_{3\mu} + O(\lambda^4)\right) dx^\mu\,, \tag{3.41}$$

where

$$t_{0\mu} = -\, g_\mu^{\alpha'} u_{\alpha'}, \tag{3.42a}$$

$$t_{1\mu} = -\, g_\mu^{\alpha'} \left(\mathsf{r} a_{\alpha'} + a_\sigma u_{\alpha'}\right), \tag{3.42b}$$

$$\begin{aligned} t_{2\mu} =& g_\mu^{\alpha'}\Bigg(\frac{1}{2}\mathsf{r}^2 a_{\mu'}a^{\mu'}u_{\alpha'} - \mathsf{r}\dot{a}_\sigma u_{\alpha'} - (a_\sigma)^2 u_{\alpha'} - \frac{1}{2}\mathsf{r}^2\dot{a}_{\alpha'} - 2\mathsf{r}a_{\alpha'}a_\sigma \\ &- \frac{2}{3}\mathsf{r}R_{\alpha' u u\sigma} - \frac{1}{6}R_{\alpha'\sigma u\sigma} + \frac{1}{3}u_{\alpha'}R_{u\sigma u\sigma}\Bigg), \end{aligned} \tag{3.42c}$$

$$\begin{aligned} t_{3\mu} =& g_\mu^{\alpha'}\Big[\tfrac{2}{3}\mathsf{r}^3 a_{\mu'}a^{\mu'}a_{\alpha'} - \tfrac{3}{2}\mathsf{r}^2 a_\sigma\dot{a}_{\alpha'} + 2\mathsf{r}^2 a_{\mu'}a^{\mu'}a_\sigma u_{\alpha'} - 3\mathsf{r}a_\sigma\dot{a}_\sigma u_{\alpha'} \\ &- (a_\sigma)^3 u_{\alpha'} - \tfrac{1}{6}\mathsf{r}^3\ddot{a}_{\alpha'} - \tfrac{3}{2}\mathsf{r}^2 a_{\alpha'}\dot{a}_\sigma - 3\mathsf{r}a_{\alpha'}(a_\sigma)^2 + \tfrac{2}{3}\mathsf{r}a_{\alpha'}R_{u\sigma u\sigma} \\ &+ \tfrac{5}{6}\mathsf{r}^3 a^{\mu'}\dot{a}_{\mu'}u_{\alpha'} - \tfrac{1}{6}\mathsf{r}^3 a^{\mu'}R_{\alpha' u\mu' u} - \tfrac{1}{2}\mathsf{r}^2\ddot{a}_\sigma u_{\alpha'} \\ &+ \tfrac{7}{12}\mathsf{r}^2 a^{\mu'}R_{\mu'\alpha' u\sigma} - \tfrac{1}{12}\mathsf{r}^2 a^{\mu'}R_{\mu' u\alpha'\sigma} - \tfrac{5}{12}\mathsf{r}^2 a^{\mu'}R_{\mu'\sigma\alpha' u} \\ &- \tfrac{1}{6}a^{\mu'}\mathsf{r}R_{\mu'\sigma\alpha'\sigma} + \tfrac{1}{2}a^{\mu'}\mathsf{r}^2 u_{\alpha'}R_{\mu' u u\sigma} - \tfrac{4}{3}\mathsf{r}a_\sigma R_{\alpha' u u\sigma} + a^{\mu'}\mathsf{r}u_{\alpha'}R_{\mu'\sigma u\sigma} \\ &- \tfrac{1}{6}a_\sigma R_{\alpha'\sigma u\sigma} + \tfrac{2}{3}a_\sigma u_{\alpha'}R_{u\sigma u\sigma} - \tfrac{1}{4}\mathsf{r}^2\dot{R}_{\alpha' u u\sigma} - \tfrac{1}{12}\mathsf{r}\dot{R}_{\alpha'\sigma u\sigma} \\ &+ \tfrac{1}{4}\mathsf{r}R_{\alpha' u u\sigma|\sigma} + \tfrac{1}{12}R_{\alpha'\sigma u\sigma|\sigma} + \tfrac{1}{4}\mathsf{r}u_{\alpha'}\dot{R}_{u\sigma u\sigma} - \tfrac{1}{12}u_{\alpha'}R_{u\sigma u\sigma|\sigma}\Big]. \end{aligned} \tag{3.42d}$$

Following the procedure in the case of $dx^a$, beginning from Eq. (3.21), we arrive at

$$dx^a = \left(x^a_{0\mu} + \lambda x^a_{1\mu} + \lambda^2 x^a_{2\mu} + \lambda^3 x^a_{3\mu} + O(\lambda^4)\right) dx^\mu\,, \tag{3.43}$$

where

$$x^a_{0\mu} = g_\mu^{\beta'} a^a_{\beta'}, \tag{3.44a}$$

$$x^a_{1\mu} = g_\mu^{\beta'} e^{a\alpha'}\mathsf{r}u_{\beta'}a_{\alpha'}, \tag{3.44b}$$

$$\begin{aligned} x^a_{2\mu} =& g_\mu^{\beta'} e^{a\alpha'}\Bigg(\frac{1}{2}\mathsf{r}^2 a_{\alpha'}a_{\beta'} + \mathsf{r}a_{\alpha'}a_\sigma u_{\beta'} + \frac{1}{2}\mathsf{r}^2\dot{a}_{\alpha'}u_{\beta'} + \frac{1}{6}\mathsf{r}^2 R_{\alpha' u\beta' u} \\ &- \frac{1}{2}\mathsf{r}R_{\alpha'\beta' u\sigma} - \frac{1}{3}\mathsf{r}R_{\sigma(\alpha'\beta')u} + \frac{1}{6}R_{\alpha'\sigma\beta'\sigma} - \frac{1}{3}\mathsf{r}u_{\beta'}R_{\alpha' u u\sigma} - \frac{1}{3}u_{\beta'}R_{\alpha'\sigma u\sigma}\Bigg), \end{aligned} \tag{3.44c}$$

$$x^a_{3\mu} = g_\mu^{\beta'} e^{a\alpha'}\Big[\mathsf{r}a_{\alpha'}(a_\sigma)^2 u_{\beta'} + \tfrac{1}{3}\mathsf{r}^3 a_{\beta'}\dot{a}_{\alpha'} + \tfrac{1}{6}\mathsf{r}^3 a_{\alpha'}\dot{a}_{\beta'} + \mathsf{r}^2 a_{\alpha'}a_{\beta'}a_\sigma - \tfrac{1}{3}\mathsf{r}^2 a_{\beta'}R_{\alpha' u u\sigma}$$

$$
\begin{aligned}
&- \tfrac{1}{3}\mathsf{r} a_{\beta'} R_{\alpha'\sigma u\sigma} - \tfrac{1}{3}\mathsf{r}^3 a_{\alpha'} a_{\mu'} a^{\mu'} u_{\beta'} + \tfrac{1}{6}\mathsf{r}^3 a^{\mu'} R_{\alpha'[\mu'\beta']u} - \tfrac{1}{6}\mathsf{r}^3 a^{\mu'} u_{\beta'} R_{\alpha' u\mu' u} \\
&+ \tfrac{1}{12}\mathsf{r}^3 a^{\mu'} R_{\alpha' u\beta'\mu'} + \mathsf{r}^2 a_\sigma \dot{a}_{\alpha'} u_{\beta'} + \tfrac{1}{2}\mathsf{r}^2 a_{\alpha'} \dot{a}_\sigma u_{\beta'} + \tfrac{1}{3}\mathsf{r}^2 a_\sigma R_{\alpha' u\beta' u} \\
&- \tfrac{1}{6}\mathsf{r}^2 a^{\mu'} R_{\mu'(\alpha'\beta')\sigma} - \tfrac{1}{4}\mathsf{r}^2 a^{\mu'} R_{\alpha'\beta'\mu'\sigma} + \tfrac{1}{3}\mathsf{r}^2 a^{\mu'} u_{\beta'} R_{\alpha'[\mu'\sigma]u} - \tfrac{1}{3}\mathsf{r}^2 a^{\mu'} u_{\beta'} R_{\alpha' u\mu'\sigma} \\
&- \tfrac{1}{2}\mathsf{r} a_\sigma R_{\alpha'\beta' u\sigma} - \tfrac{1}{3}\mathsf{r} a_\sigma R_{u(\alpha'\beta')\sigma} - \tfrac{1}{3}\mathsf{r} a^{\mu'} u_{\beta'} R_{\alpha'\sigma\mu'\sigma} - \tfrac{2}{3}\mathsf{r} a_\sigma u_{\beta'} R_{\alpha' uu\sigma} \\
&- \tfrac{1}{3} a_\sigma u_{\beta'} R_{\alpha'\sigma u\sigma} + \tfrac{1}{6}\mathsf{r}^3 \ddot{a}_{\alpha'} u_{\beta'} + \tfrac{2}{3}\mathsf{r}^2 a_{\alpha'} R_{\beta' uu\sigma} + \tfrac{1}{6}\mathsf{r} a_{\alpha'} R_{\beta'\sigma u\sigma} \\
&+ \tfrac{1}{12}\mathsf{r}^3 \dot{R}_{\alpha' u\beta' u} + \tfrac{1}{12}\mathsf{r}^3 \dot{R}_{\alpha' u\beta' u} - \tfrac{1}{6}\mathsf{r}^2 \dot{R}_{\alpha'\beta' u\sigma} - \tfrac{1}{6}\mathsf{r}^2 \dot{R}_{\sigma(\beta'\alpha')u} \\
&+ \tfrac{1}{12}\mathsf{r} \dot{R}_{\alpha'\sigma\beta'\sigma} + \tfrac{1}{6}\mathsf{r} R_{\alpha'\beta' u\sigma|\sigma} - \tfrac{1}{12}\mathsf{r}^2 R_{\alpha' u\beta' u|\sigma} + \tfrac{1}{6}\mathsf{r} R_{\sigma(\beta'\alpha')u|\sigma} \\
&- \tfrac{1}{12} R_{\alpha'\sigma\beta'\sigma|\sigma} - \tfrac{2}{3}\mathsf{r} a_{\alpha'} u_{\beta'} R_{u\sigma u\sigma} - \tfrac{1}{4}\mathsf{r}^2 u_{\beta'} \dot{R}_{\alpha' uu\sigma} - \tfrac{1}{4}\mathsf{r} u_{\beta'} \dot{R}_{\alpha'\sigma u\sigma} \\
&+ \tfrac{1}{12}\mathsf{r} u_{\beta'} R_{\alpha' uu\sigma|\sigma} + \tfrac{1}{12} u_{\beta'} R_{\alpha'\sigma u\sigma|\sigma}\Big].
\end{aligned} \tag{3.44d}
$$

### 3.2.5 Components of $h^{\mathrm{S}}_{\alpha\beta}$ in terms of covariant quantities

We now move onto the components of the singular field. Our first step is to express the components $h^{\mathrm{S}}_{tt}$, $h^{\mathrm{S}}_{ta}$, and $h^{\mathrm{S}}_{ab}$ in terms of covariant quantities. We will replace the dependence on $t$ with a dependence on $\bar{x}$, and we will replace $r$ with $n^a$ through the relations (3.18) and (3.19). In this way, we can re-cast all of the terms in (A.2) and (A.4) in terms of the Synge world-function $\bar{\sigma}$. For example,

$$
a_i n^i = \frac{a_i \tilde{e}^i_{\bar{\alpha}} \sigma^{\bar{\alpha}}}{\sqrt{2\bar{\sigma}}} = \frac{a_{\bar{\alpha}} \sigma^{\bar{\alpha}}}{\sqrt{2\bar{\sigma}}} = \frac{a_{\bar{\sigma}}}{\sqrt{2\bar{\sigma}}}\,, \tag{3.45}
$$

$$
\mathcal{E}_{ab}\hat{n}^{ab} = R_{a0b0}\left(n^a n^b - \frac{1}{3}\delta^{ab}\right) = R_{\bar{\alpha}\bar{\mu}\bar{\beta}\bar{\nu}} e^{\bar{\alpha}}_a e^{\bar{\beta}}_b u^{\bar{\mu}} u^{\bar{\nu}}\ \frac{\tilde{e}^a_{\bar{\gamma}} \tilde{e}^b_{\bar{\delta}} \sigma^{\bar{\gamma}} \sigma^{\bar{\delta}}}{2\bar{\sigma}} = \frac{R_{\bar{\alpha}\bar{u}\bar{\beta}\bar{u}} \sigma^{\bar{\alpha}} \sigma^{\bar{\beta}}}{2\bar{\sigma}}, \tag{3.46}
$$

where in the second identity the completeness relation (B.5) was invoked and we have introduced the definitions

$$
R_{\bar{\alpha}\bar{u}\bar{\beta}\bar{u}} \equiv R_{\bar{\alpha}\bar{\mu}\bar{\beta}\bar{\nu}} u^{\bar{\mu}} u^{\bar{\nu}}\,, \qquad\qquad a_{\bar{\sigma}} \equiv a_{\bar{\alpha}} \sigma^{\bar{\alpha}}. \tag{3.47}
$$

Using the identities given in Table 3.1, the singular-field components $h^{\mathrm{S}1}_{\alpha\beta}$ in Eq. (A.2) may be written in terms of $\bar{\sigma}$ as

$$
h^{\mathrm{S}1}_{tt} = \frac{2\mu}{\sqrt{2\bar{\sigma}}}\left(2\lambda^{-1} - 3\lambda^0 a_{\bar{\sigma}} + \frac{5}{3}\lambda R_{\bar{u}\bar{\sigma}\bar{u}\bar{\sigma}} - \frac{7}{12}\lambda^2 R_{\bar{\sigma}\bar{u}\bar{\sigma}\bar{u}|\bar{\sigma}}\right) + O(\lambda a^2, \lambda^2 a, \lambda^3)\,, \tag{3.48a}
$$

$$
\begin{aligned}
h^{\mathrm{S}1}_{ta} = {}& \frac{\mu e^{\bar{\alpha}}_a}{\sqrt{2\bar{\sigma}}}\left(\lambda\frac{2}{3}R_{\bar{\alpha}\bar{\sigma}\bar{\sigma}\bar{u}} - 4\bar{\sigma}\dot{a}_{\bar{\alpha}}\right) + \lambda^2\left(\frac{4}{3}\bar{\sigma}\dot{R}_{\bar{\alpha}\bar{u}\bar{\sigma}\bar{u}} - \frac{1}{6}R_{\bar{\alpha}\bar{\sigma}\bar{\sigma}\bar{u}|\bar{\sigma}}\right) \\
&+ O(\lambda a^2, \lambda^2 a, \lambda^3)\,,
\end{aligned} \tag{3.48b}
$$

Table 3.1: Conversion of tidal quantities in Fermi-Walker coordinates to covariant format. $\bar\sigma \equiv \sigma(x,\bar x)$, $a^2 \equiv a_i a^i$, $a_{\bar\sigma} \equiv a_{\bar\alpha}\sigma^{\bar\alpha}$, $R_{\bar u\bar\alpha\bar u\bar\beta} \equiv R_{\bar\mu\bar\alpha\bar\beta\bar\nu}u^{\bar\mu}u^{\bar\nu}$.

$$
\begin{aligned}
\mathcal{E}_{ab}\hat n^{ab} &= \frac{R_{\bar u\bar\sigma\bar u\bar\sigma}}{2\bar\sigma} \\
\mathcal{E}_{ab}a^a\hat n^b &= -\frac{a^{\bar\alpha}R_{\bar u\bar\alpha\bar u\bar\sigma}}{\sqrt{2\bar\sigma}} \\
2\hat n_{(a}\mathcal{E}_{b)c}\hat n^c &= \left(R_{\bar u\bar\alpha\bar u\bar\beta} + \frac{g_{\bar\alpha\bar\beta}R_{\bar u\bar\sigma\bar u\bar\sigma}}{2\bar\sigma} - \frac{R_{\bar\alpha\bar\sigma\bar\beta\bar\sigma}}{2\bar\sigma}\right) e^{\bar\alpha}_a e^{\bar\beta}_b \\
\mathcal{E}_{abc}\hat n^{abc} &= -\frac{R_{\bar u\bar\sigma\bar u\bar\sigma|\bar\sigma}}{(2\bar\sigma)^{3/2}} \\
\mathcal{E}_{(a}{}^{cd}\hat n_{b)cd} &= \left(-\frac{R_{\bar u\bar\sigma\bar u\bar\sigma|\bar\alpha}\sigma_{\bar\beta}}{3(2\bar\sigma)^{3/2}} - \frac{2R_{\bar u\bar\sigma\bar u\bar\alpha|\bar\sigma}\sigma_{\bar\beta}}{3(2\bar\sigma)^{3/2}} + \frac{2R_{\bar u\bar\alpha\bar u\bar\beta|\bar\sigma}}{15(2\bar\sigma)^{3/2}} + \frac{4R_{\bar u\bar\alpha\bar u\bar\sigma|\bar\beta}}{15(2\bar\sigma)^{3/2}}\right) e^{\bar\alpha}_{(a}e^{\bar\beta}_{b)} \\
\mathcal{E}^d_{(a}a^c\hat n_{b)cd} &= \left(-\frac{a_{\bar\sigma}R_{\bar u\bar\sigma\bar u\bar\alpha}\sigma_{\bar\beta}}{(2\bar\sigma)^{3/2}} + \frac{a^{\bar\gamma}R_{u\bar\gamma u\bar\alpha}\sigma_{\bar\beta}}{5\sqrt{2\bar\sigma}} + \frac{R_{u\sigma u\bar\alpha}a_{\bar\beta}}{5\sqrt{2\bar\sigma}} + \frac{R_{\bar u\bar\alpha\bar u\bar\beta}a_{\bar\sigma}}{5\sqrt{2\bar\sigma}}\right) e^{\bar\alpha}_{(a}e^{\bar\beta}_{b)} \\
\mathcal{E}_{cd}\hat n^{cd}_{ab} &= \left(\frac{R_{\bar u\bar\sigma\bar u\bar\sigma}}{2\bar\sigma}\left(\frac{\bar\sigma_{\bar\alpha}\bar\sigma_{\bar\beta}}{2\bar\sigma} - \frac{1}{7}g_{\bar\alpha\bar\beta}\right) - \frac{4R_{\bar u\bar\sigma\bar u(\bar\alpha}\sigma_{\bar\beta)}}{7\bar\sigma} + \frac{2R_{\bar u\bar\alpha\bar u\bar\beta}}{35}\right) e^{\bar\alpha}_a e^{\bar\beta}_b \\
\mathcal{B}^{bc}\varepsilon_{acd}\hat n^d_b &= -\frac{R_{\bar u\bar\sigma\bar\alpha\bar\sigma}\sigma_{\bar\beta}e^{\bar\alpha}_a e^{\bar\beta}_b}{(2\bar\sigma)^{3/2}} + \frac{R_{\bar u\bar\beta\bar\alpha\bar\sigma}e^{\bar\alpha}_a e^{\bar\beta}_b}{5\sqrt{2\bar\sigma}} + \frac{R_{\bar u\bar\sigma\bar\alpha\bar\beta}e^{\bar\alpha}_a e^{\bar\beta}_b}{5\sqrt{2\bar\sigma}} \\
\mathcal{B}_{bcd}\hat n^{cdi}\varepsilon_{ia}{}^b &= \left(\frac{3R_{\bar u\bar\sigma\bar\alpha\bar\sigma|\bar\sigma}}{4(2\bar\sigma)^{3/2}} - \frac{\dot R_{\bar u\bar\sigma\bar u\bar\sigma}\sigma_{\bar\alpha}}{(2\bar\sigma)^{3/2}} + \frac{2\dot R_{\bar u\bar\sigma\bar u\bar\alpha}}{5\sqrt{2\bar\sigma}}\right) e^{\bar\alpha}_a
\end{aligned}
$$

$$
\begin{aligned}
h^{\rm S1}_{ab} = \frac{\mu e^{\bar\alpha}_a e^{\bar\beta}_b}{\sqrt{2\bar\sigma}} &\left(2\lambda^{-1}g_{\bar\alpha\bar\beta} + \lambda^0 g_{\bar\alpha\bar\beta}a_{\bar\sigma} - \lambda\left[\frac{2}{3}R_{\bar\alpha\bar\sigma\bar\beta\bar\sigma} + \frac{1}{3}g_{\bar\alpha\bar\beta}R_{\bar u\bar\sigma\bar u\bar\sigma} + 8\bar\sigma R_{\bar\alpha\bar u\bar\beta\bar u}\right]\right) \\
&+ \lambda^2\left(\frac{1}{12}g_{\bar\alpha\bar\beta}R_{\bar u\bar\sigma\bar u\bar\sigma|\bar\sigma} + \frac{1}{3}R_{\bar\alpha\bar\sigma\bar\beta\bar\sigma|\bar\sigma} + 4\bar\sigma R_{\bar\alpha\bar u\bar\beta\bar u|\bar\sigma}\right) + O(\lambda a^2, \lambda^2 a, \lambda^3)\,. \qquad (3.48c)
\end{aligned}
$$

The components of $h^{\rm S2} = h^{\rm SS} + h^{\rm SR} + h^{\delta m} + h^{\delta z}$ given in (A.4)-(A.10) may be written in terms of $\bar\sigma$ as

$$
h^{\rm SS}_{tt} = -\frac{\mu^2}{\lambda^2\bar\sigma} - \lambda^0\frac{7\mu^2 R_{\bar u\bar\sigma\bar u\bar\sigma}}{6\bar\sigma} + O(\lambda, a)\,, \qquad (3.49a)
$$

$$
h^{\rm SS}_{ta} = \lambda^0\mu^2\frac{5e^{\bar\alpha}_a}{3\bar\sigma}R_{\bar\alpha\bar\sigma\bar\sigma\bar u} + O(\lambda, a)\,, \qquad (3.49b)
$$

$$
\begin{aligned}
h^{\rm SS}_{ab} = \frac{\mu^2 e^{\bar\alpha}_a e^{\bar\beta}_b}{4\bar\sigma^2}&\Bigg[\lambda^{-2}\left(10\bar\sigma g_{\bar\alpha\bar\beta} - 7\sigma_{\bar\alpha}\sigma_{\bar\beta}\right) \\
&+ \lambda^0\left(\frac{2}{15}g_{\bar\alpha\bar\beta}\bar\sigma R_{\bar u\bar\sigma\bar u\bar\sigma} - \frac{16}{5}\bar\sigma R_{\bar\alpha\bar\sigma\bar\beta\bar\sigma} + \frac{104}{75}\bar\sigma^2 R_{\bar\alpha\bar u\bar\beta\bar u} + \frac{7}{5}\sigma_{\bar\alpha}\sigma_{\bar\beta}R_{\bar u\bar\sigma\bar u\bar\sigma}\right) \\
&- \frac{64}{15}\bar\sigma^2\ln(\lambda\sqrt{2\bar\sigma})R_{\bar u\bar\alpha\bar u\bar\beta}\Bigg] + O(\lambda\ln\lambda, a)\,, \qquad (3.49c)
\end{aligned}
$$

$$h^{\rm SR}_{tt} = -\frac{\mu h^{\rm R1}_{\bar\alpha\bar\beta}}{\sqrt{2\bar\sigma}}\left(\frac{\sigma^{\bar\alpha}\sigma^{\bar\beta}}{2\bar\sigma} - \frac{P^{\bar\alpha\bar\beta}}{3}\right) + O(\lambda^0)\,, \tag{3.50a}$$

$$h^{\rm SR}_{ta} = -\frac{\mu h^{\rm R1}_{\bar\gamma\bar\beta}u^{\bar\gamma}e^{\bar\alpha}_a}{\sqrt{2\bar\sigma}}\left(\frac{\sigma^{\bar\beta}\sigma_{\bar\alpha}}{2\bar\sigma} - \frac{P^{\bar\beta}_{\bar\alpha}}{3}\right) + O(\lambda^0)\,, \tag{3.50b}$$

$$\begin{aligned} h^{\rm SR}_{ab} = \frac{\mu e^{\bar\alpha}_a e^{\bar\beta}_b}{\sqrt{2\bar\sigma}}\Bigg\{&\frac{h^{\rm R1}_{\bar\gamma(\bar\alpha}\sigma_{\bar\beta)}\bar\sigma^{\bar\gamma}}{\bar\sigma} - \frac{2}{3}h^{\rm R1}_{\bar\alpha\bar\beta} + P_{\bar\alpha\bar\beta}h^{\rm R1}_{\bar\mu\bar\nu}\left(\frac{2}{3}P^{\bar\mu\bar\nu} + \frac{1}{3}u^{\bar\mu}u^{\bar\nu} - \frac{\sigma^{\bar\mu}\sigma^{\bar\nu}}{2\bar\sigma}\right) \\ &-\frac{\sigma_{\bar\alpha}\sigma_{\bar\beta}}{2\bar\sigma}h^{\rm R1}_{\bar\mu\bar\nu}\left(P^{\bar\mu\bar\nu} + u^{\bar\mu}u^{\bar\nu}\right)\Bigg\} + O(\lambda^0)\,, \end{aligned} \tag{3.50c}$$

where $P^{\bar\alpha\bar\beta} \equiv g^{\bar\alpha\bar\beta} + u^{\bar\alpha}u^{\bar\beta}$,

$$h^{\delta m}_{tt} = \frac{\delta m_{\bar\alpha\bar\beta}u^{\bar\alpha}u^{\bar\beta}}{\sqrt{2\bar\sigma}} + O(\lambda^0)\,, \tag{3.51a}$$

$$h^{\delta m}_{ta} = \frac{\delta m_{\bar\alpha\bar\beta}u^{\bar\alpha}e^{\bar\beta}_a}{\sqrt{2\bar\sigma}} + O(\lambda^0)\,, \tag{3.51b}$$

$$h^{\delta m}_{ab} = \frac{\delta m_{\bar\alpha\bar\beta}e^{\bar\alpha}_a e^{\bar\beta}_b}{\sqrt{2\bar\sigma}} + O(\lambda^0)\,, \tag{3.51c}$$

with

$$\begin{aligned} \frac{\delta m_{\bar\alpha\bar\beta}}{\mu} &= \frac{1}{3}\left(2h^{\rm R1}_{\bar\alpha\bar\beta} + g_{\bar\alpha\bar\beta}h^{\rm R1}\right) + \left(g_{\bar\alpha\bar\beta} + 2u_{\bar\alpha}u_{\bar\beta}\right)u^{\bar\mu}u^{\bar\nu}h^{\rm R1}_{\bar\mu\bar\nu} \\ &+ 4u_{(\bar\alpha}\left(h^{\rm R1}_{\bar\beta)\bar\mu}u^{\bar\mu} + 2\delta\dot z_{\bar\beta)}\right)\,, \end{aligned} \tag{3.52}$$

and

$$h^{\delta z}_{tt} = -\frac{2\mu\delta z_{\bar\alpha}\sigma^{\bar\alpha}}{(2\bar\sigma)^{3/2}} + O(\lambda^0), \tag{3.53a}$$

$$h^{\delta z}_{ta} = O(\lambda^0), \tag{3.53b}$$

$$h^{\delta z}_{ab} = -\frac{2\mu\delta z_{\bar\alpha}\sigma^{\bar\alpha}\delta_{ab}}{(2\bar\sigma)^{3/2}} + O(\lambda^0). \tag{3.53c}$$

### 3.2.6 Expansion of $h^{\rm S}_{tt}$, $h^{\rm S}_{ta}$ and $h^{\rm S}_{ab}$

The next step in the calculation is to convert the expressions (3.48)–(3.53) in terms of $\bar x$, to expressions in terms of the point $x'$ on $\gamma$. Inserting Eq. (3.38) into Eqs. (3.48) yields

$$\begin{aligned} h^{\rm S1}_{tt} = &\frac{2\mu}{\lambda \mathsf{s}} - \frac{\mu\lambda^0}{\mathsf{s}^3}(\mathsf{r}^2 + 3\mathsf{s}^2)a_\sigma + \frac{\mu\lambda}{3\mathsf{s}^3}\left(\left(\mathsf{r}^2 + 5\mathsf{s}^2\right)R_{u\sigma u\sigma} - \left(\mathsf{r}^3 + 9\mathsf{r}\mathsf{s}^2\right)\dot a_\sigma\right) \\ &- \frac{\mu\lambda^2}{12\mathsf{s}^5}\left(\mathsf{r}^2\mathsf{s}^2 R_{u\sigma u\sigma|\sigma} - \mathsf{r}^3\mathsf{s}^2\dot R_{u\sigma u\sigma} + 7\mathsf{s}^4 R_{u\sigma u\sigma|\sigma} - 13\mathsf{r}\mathsf{s}^4\dot R_{u\sigma u\sigma}\right) \end{aligned}$$

$$+O(\lambda a^2,\lambda^2 a,\lambda^3), \tag{3.54a}$$

$$\begin{aligned}h^{\rm S1}_{ta} &= -\mu e^{\alpha'}_a\left\{\frac{2\lambda}{3\mathsf{s}}\left(R_{\alpha'\sigma u\sigma}-\mathsf{r}R_{\alpha' u\sigma u}+3\mathsf{s}^2\dot a_{\alpha'}\right)\right.\\&\left.+\frac{\mu\lambda^2}{18\mathsf{s}^3}\left(9\mathsf{r}\mathsf{s}^2\dot R_{\alpha'\sigma u\sigma}-3\mathsf{s}^2R_{\alpha'\sigma u\sigma|\sigma}+3\mathsf{r}\mathsf{s}^2R_{\alpha' u\sigma u|\sigma}-(9\mathsf{r}^2\mathsf{s}^2+12\mathsf{s}^4)\dot R_{\alpha' u\sigma u}\right)\right\}\\&+O(\lambda a^2,\lambda^2 a,\lambda^3),\end{aligned} \tag{3.54b}$$

$$\begin{aligned}h^{\rm S1}_{ab} &= \mu e^{\alpha'}_{(a}e^{\beta'}_{b)}\left[\frac{2g_{\alpha'\beta'}}{\lambda\mathsf{s}}+\frac{\lambda^0}{\mathsf{s}^3}g_{\alpha'\beta'}a_\sigma(\mathsf{s}^2-\mathsf{r}^2)+\frac{\lambda}{3\mathsf{s}^2}\left(4\mathsf{r}\mathsf{s}^2R_{u(\alpha'\beta')\sigma}-2\mathsf{s}^2R_{\alpha'\sigma\beta'\sigma}\right.\right.\\&\left.\left.-12\mathsf{s}^4R_{\alpha' u\beta' u}+g_{\alpha'\beta'}(\mathsf{r}^2-\mathsf{s}^2)R_{u\sigma u\sigma}-g_{\alpha'\beta'}\mathsf{r}(\mathsf{r}^2-3\mathsf{s}^2)\dot a_\sigma\right)\right]\\&+\frac{\lambda^2}{12\mathsf{s}^3}\left[g_{\alpha'\beta'}(\mathsf{r}^3-3\mathsf{r}\mathsf{s}^2)\dot R_{u\sigma u\sigma}+4\mathsf{s}^2R_{\alpha'\sigma\beta'\sigma|\sigma}+g_{\alpha'\beta'}(\mathsf{s}^2-\mathsf{r}^2)R_{u\sigma u\sigma|\sigma}\right.\\&-4\mathsf{r}\mathsf{s}^2\dot R_{\alpha'\sigma\beta'\sigma|\sigma}+8\mathsf{r}\mathsf{s}^2R_{u(\alpha'\beta')\sigma|\sigma}+8\mathsf{r}^2\mathsf{s}^2\dot R_{u(\alpha'\beta')\sigma}\\&\left.+4\mathsf{s}^2(\mathsf{r}^2+6\mathsf{s}^2)\left(R_{\alpha' u\beta' u|\sigma}-\mathsf{r}\dot R_{\alpha' u\beta' u}\right)\right]+O(\lambda a^2,\lambda^2 a,\lambda^3).\end{aligned} \tag{3.54c}$$

Inserting Eq. (3.38) into Eqs. (3.49)–(3.53) yields the second-order singular field components in terms of $x'$, as

$$h^{\rm SS}_{tt} = -\frac{2\mu^2}{\lambda^2\mathsf{s}^2}-\frac{\mu^2\lambda^0}{3\mathsf{s}^4}(2\mathsf{r}^2+7\mathsf{s}^2)R_{u\sigma u\sigma}+O(\lambda a), \tag{3.55a}$$

$$h^{\rm SS}_{ta} = -\frac{10\mu^2\lambda^0 e^{\alpha'}_a}{3\mathsf{s}^2}\left(R_{\alpha'\sigma u\sigma}-\mathsf{r}R_{\alpha' u\sigma u}\right)+O(\lambda a), \tag{3.55b}$$

$$\begin{aligned}h^{\rm SS}_{ab} &= \mu^2 e^{\alpha'}_a e^{\beta'}_b\left\{\frac{1}{\lambda^2\mathsf{s}^4}\left(5\mathsf{s}^2g_{\alpha'\beta'}-7\sigma_{\alpha'}\sigma_{\beta'}\right)\right.\\&+\frac{\lambda^0}{\mathsf{s}^4}\left[g_{\alpha'\beta'}\left(\frac{5}{3}\mathsf{r}^2+\frac{1}{15}\mathsf{s}^2\right)R_{u\sigma u\sigma}+\frac{26}{75}\mathsf{s}^4R_{\alpha' u\beta' u}+\frac{16}{5}\mathsf{r}\mathsf{s}^2R_{u(\alpha'\beta')\sigma}\right.\\&-\frac{8}{5}\mathsf{r}^2\mathsf{s}^2R_{\alpha' u\beta' u}-\frac{8}{5}\mathsf{s}^2R_{\alpha'\sigma\beta'\sigma}+\frac{14}{3}\mathsf{r}\sigma_{(\alpha'}R_{\beta')\sigma u\sigma}-\frac{7}{3}\mathsf{r}^2\sigma_{(\alpha'}R_{\beta')u\sigma u}\\&\left.\left.+\left(\frac{7}{5}-\frac{14\mathsf{r}^2}{3\mathsf{s}^2}\right)R_{u\sigma u\sigma}\sigma_{\alpha'}\sigma_{\beta'}\right]-\frac{16}{15}\ln(\lambda\mathsf{s})R_{\alpha' u\beta' u}\right\}+O(\lambda\ln\lambda,a),\end{aligned} \tag{3.55c}$$

$$h^{\rm SR}_{tt} = \frac{\mu}{\mathsf{s}^3}\left[h^{\rm R1}_{\sigma\sigma}+2\mathsf{r}h^{\rm R1}_{u\sigma}+\mathsf{r}^2h^{\rm R1}_{uu}-\frac{1}{3}\mathsf{s}^2\left(h^{\rm R1}+h^{\rm R1}_{uu}\right)\right]+O(\lambda^0), \tag{3.56a}$$

$$h^{\rm SR}_{ta} = -\frac{\mu e^{\alpha'}_a}{\mathsf{s}^3}\left[\left(h^{\rm R1}_{u\sigma}+\mathsf{r}h^{\rm R1}_{uu}\right)\sigma_{\alpha'}-\frac{1}{3}\mathsf{s}^2h^{\rm R1}_{u\alpha'}\right]+O(\lambda^0), \tag{3.56b}$$

$$\begin{aligned}
h^{\rm SR}_{ab} = \frac{\mu^2 e^{\alpha'}_a e^{\beta'}_b}{\mathsf{s}^3}\Bigg[& 2h^{\rm R1}_{\sigma(\alpha'}\sigma_{\beta')} + 2\mathsf{r} h^{\rm R1}_{u(\alpha'}\sigma_{\beta')} - \frac{2}{3}\mathsf{s}^2 h^{\rm R1}_{\alpha'\beta'} \\
&+ g_{\alpha'\beta'}\left(\frac{2}{3}\mathsf{s}^2 h^{\rm R1} + \mathsf{s}^2 h^{\rm R1}_{uu} - h^{\rm R1}_{\sigma\sigma} - 2\mathsf{r} h^{\rm R1}_{u\sigma} - \mathsf{r}^2 h^{\rm R1}_{uu}\right) \\
&- \sigma_{\alpha'}\sigma_{\beta'}\left(h^{\rm R1} + 2h^{\rm R1}_{uu}\right)\Bigg] + O(\lambda^0),
\end{aligned} \tag{3.56c}$$

where $h^{\rm R1} \equiv g^{\mu'\nu'} h^{\rm R1}_{\mu'\nu'}$,

$$h^{\delta m}_{tt} = \frac{\delta m_{tt}(\tau')}{\mathsf{s}} + O(\lambda^0), \tag{3.57a}$$

$$h^{\delta m}_{ta} = \frac{\delta m_{ta}(\tau')}{\mathsf{s}} + O(\lambda^0), \tag{3.57b}$$

$$h^{\delta m}_{ab} = \frac{\delta m_{ab}(\tau')}{\mathsf{s}} + O(\lambda^0), \tag{3.57c}$$

and

$$h^{\delta z}_{tt} = 2\mu\left[\frac{1}{\lambda^2}\left(\frac{\delta z_\sigma + \delta z_u \mathsf{r}}{\mathsf{s}^3}\right) + \frac{1}{\lambda}\left(\frac{\delta z_u \mathsf{r} a_\sigma}{\mathsf{s}^3} - \frac{3\mathsf{r}^2 a_\sigma \delta z_\sigma}{2\mathsf{s}^5}\right)\right] + O(\lambda^0), \tag{3.58a}$$

$$h^{\delta z}_{ta} = O(\lambda^0), \tag{3.58b}$$

$$h^{\delta z}_{ab} = 2\mu\delta_{ab}\left[\frac{1}{\lambda^2}\left(\frac{\delta z_\sigma + \delta z_u \mathsf{r}}{\mathsf{s}^3}\right) + \frac{1}{\lambda}\left(\frac{\delta z_u \mathsf{r} a_\sigma}{\mathsf{s}^3} - \frac{3\mathsf{r}^2 a_\sigma \delta z_\sigma}{2\mathsf{s}^5}\right)\right] + O(\lambda^0), \tag{3.58c}$$

with $\delta z_\sigma \equiv \delta z_{\alpha'}\sigma^{\alpha'}$ and $\delta z_u \equiv \delta z_{\alpha'} u^{\alpha'}$.

### 3.2.7 Covariant form of the singular fields

The final step in the calculation is to combine the covariant expansions of the components $h^{\rm S}_{tt}$, $h^{\rm S}_{ta}$, and $h^{\rm S}_{ab}$ with the expansions (3.30) and (3.31) of the one-forms $dt$ and $dx^a$, yielding a concrete expression in the form of (3.27). The triad legs are eliminated using identity (3.28).

The explicit formula for the first-order singular field takes the form

$$h^{\rm S1}_{\alpha\beta} = h^{\rm S1\cancel{a}}_{\alpha\beta} + h^{\rm S1a}_{\alpha\beta}, \tag{3.59}$$

where $h^{\rm S1\cancel{a}}_{\alpha\beta}$ is the acceleration-independent part, and $h^{\rm S1a}_{\alpha\beta}$ is the acceleration-dependent part. The former is given by

$$\begin{aligned}
h^{\rm S1\cancel{a}}_{\mu\nu} = {}& \frac{2\mu}{\lambda\mathsf{s}} g^{\alpha'}_{\mu} g^{\beta'}_{\nu}\left(g_{\alpha'\beta'} + 2u_{\alpha'}u_{\beta'}\right) \\
&+ \lambda\frac{\mu g^{\alpha'}_{\mu} g^{\beta'}_{\nu}}{3\mathsf{s}^3}\Big[\left(\mathsf{r}^2 - \mathsf{s}^2\right)\left(g_{\alpha'\beta'} + 2u_{\alpha'}u_{\beta'}\right) R_{u\sigma u\sigma} \\
&- 12\mathsf{s}^4 R_{\alpha' u\beta' u} - 12\mathsf{r}\mathsf{s}^2 u_{(\alpha'}R_{\beta')u\sigma u}\Big] + \lambda^2\frac{\mu g^{\alpha'}_{\mu} g^{\beta'}_{\nu}}{12\mathsf{s}^3}\Big\{16\mathsf{r}\mathsf{s}^2 u_{(\alpha'}R_{\beta')u\sigma u|\sigma}
\end{aligned}$$

$$- 16\mathsf{s}^2\left(\mathsf{r}^2+\mathsf{s}^2\right)u_{(\alpha'}\dot{R}_{\beta')u\sigma u} + (g_{\alpha'\beta'}+2u_{\alpha'}u_{\beta'})\big[\mathsf{r}(\mathsf{r}^2-3\mathsf{s}^2)\dot{R}_{u\sigma u\sigma}$$

$$+ (\mathsf{s}^2-\mathsf{r}^2)R_{u\sigma u\sigma|\sigma}\big] + 24\mathsf{s}^4\left(R_{\alpha' u\beta' u|\sigma} - \mathsf{r}\dot{R}_{\alpha' u\beta' u}\right)\Bigg\} + O(\lambda^3), \tag{3.60}$$

and the acceleration-dependent terms are given by

$$\begin{aligned} h^{\mathrm{S1}\,\mathsf{a}}_{\mu\nu} &= \frac{\mu\lambda^0}{\mathsf{s}^3} g^{\alpha'}_{\mu} g^{\beta'}_{\nu}\left\{\left(\mathsf{s}^2-\mathsf{r}^2\right)a_\sigma(g_{\alpha'\beta'}+2u_{\alpha'}u_{\beta'}) + 8\mathsf{r}\mathsf{s}^2 a_{(\alpha'}u_{\beta')}\right\} \\ &+ \frac{\mu\lambda}{3\mathsf{s}^2} g^{\alpha'}_{\alpha} g^{\beta'}_{\beta}\left\{12\mathsf{s}^2(\mathsf{r}^2+\mathsf{s}^2)\dot{a}_{(\alpha')}u_{\beta')} + \mathsf{r}(3\mathsf{s}^2-\mathsf{r}^2)\dot{a}_\sigma(g_{\alpha'\beta'}+2u_{\alpha'}u_{\beta'})\right\} \\ &+ O(\lambda a^2, \lambda^2 a, \lambda^3)\,. \end{aligned} \tag{3.61}$$

The explicit form for the second-order singular field is

$$h^{\mathrm{S2}}_{\mu\nu} = h^{\mathrm{SS}}_{\mu\nu} + h^{\mathrm{SR}}_{\mu\nu} + h^{\delta m}_{\mu\nu} + h^{\delta z}_{\mu\nu}. \tag{3.62}$$

The covariant forms of $h^{\mathrm{SS}}_{\mu\nu}$, $h^{\mathrm{SR}}_{\mu\nu}$ and $h^{\delta m}_{\mu\nu}$ are given by

$$\begin{aligned} h^{\mathrm{SS}}_{\mu\nu} &= \lambda^{-2}\frac{\mu^2}{\mathsf{s}^4} g^{\alpha'}_{\mu} g^{\beta'}_{\nu}\left(5\mathsf{s}^2 g_{\alpha'\beta'} - 7\sigma_{\alpha'}\sigma_{\beta'} - 14\mathsf{r}u_{(\alpha'}\sigma_{\beta')} - \left(7\mathsf{r}^2-3\mathsf{s}^2\right)u_{\alpha'}u_{\beta'}\right) \\ &- \frac{16}{15}\mu^2 g^{\alpha'}_{\mu} g^{\beta'}_{\nu}\ln(\lambda\mathsf{s})R_{\alpha' u\beta' u} + \lambda^0\frac{\mu^2}{150\mathsf{s}^6} g^{\alpha'}_{\mu} g^{\beta'}_{\nu}\Bigg(10\mathsf{s}^2 g_{\alpha'\beta'}\left(25\mathsf{r}^2+\mathsf{s}^2\right) \\ &+ 20\mathsf{r}\mathsf{s}^2\left(35\mathsf{r}\sigma_{(\alpha'}R_{\beta')u\sigma u} + (35\mathsf{r}^2-31\mathsf{s}^2)u_{(\alpha'}R_{\beta')u\sigma u} - \mathsf{s}^2 R_{\sigma(\alpha'\beta')u}\right) \\ &+ 10\mathsf{s}^4 R_{\alpha'\sigma\beta'\sigma} - 350\mathsf{r}\mathsf{s}^2\sigma_{(\alpha'}R_{\beta')\sigma u\sigma} - 10\mathsf{s}^2(35\mathsf{r}^2-17\mathsf{s}^2)u_{(\alpha'}R_{\beta')\sigma u\sigma} \\ &+ 2\mathsf{s}^4(5\mathsf{r}^2+26\mathsf{s}^2)R_{\alpha' u\beta' u} - 70\Bigg[\left(10\mathsf{r}^2-3\mathsf{s}^2\right)\sigma_{\alpha'}\sigma_{\beta'} \\ &+ 4\mathsf{r}\left(5\mathsf{r}^2-4\mathsf{s}^2\right)u_{(\alpha'}\sigma_{\beta')}\Bigg]R_{u\sigma u\sigma} - 20\left(35\mathsf{r}^4-53\mathsf{r}^2\mathsf{s}^2-\mathsf{s}^4\right)u_{\alpha'}u_{\beta'}R_{u\sigma u\sigma}\Bigg), \end{aligned} \tag{3.63}$$

$$\begin{aligned} h^{\mathrm{SR}}_{\mu\nu} &= -\lambda^{-1}\frac{\mu g^{\alpha'}_{\mu} g^{\beta'}_{\nu}}{\mathsf{s}^3}\Bigg(g_{\alpha'\beta'}\left(\frac{2}{3}\mathsf{s}^2 h^{\mathrm{R1}} + (\mathsf{s}^2-\mathsf{r}^2)h^{\mathrm{R1}}_{uu} - h^{\mathrm{R1}}_{\sigma\sigma} - 2\mathsf{r}h^{\mathrm{R1}}_{u\sigma}\right) \\ &- \frac{2}{3}\mathsf{s}^2 h^{\mathrm{R1}}_{\alpha'\beta'} + 2h^{\mathrm{R1}}_{\sigma(\alpha'}\sigma_{\beta')} + 2h^{\mathrm{R1}}_{\sigma(\alpha'}u_{\beta')} \\ &- 2h^{\mathrm{R1}}_{\sigma\sigma}u_{\alpha'}u_{\beta'} - h^{\mathrm{R1}}\left(\sigma_{\alpha'}\sigma_{\beta'} - 2\mathsf{r}u_{(\alpha'}\sigma_{\beta')} + \left(\mathsf{r}^2-\mathsf{s}^2\right)u_{\alpha'}u_{\beta'}\right) \\ &+ 2\mathsf{r}h^{\mathrm{R1}}_{u(\alpha'}\sigma_{\beta')} + 2(\mathsf{r}^2-\mathsf{s}^2) + 2(\mathsf{r}^2-\mathsf{s}^2)h^{\mathrm{R1}}_{u(\alpha'}u_{\beta')} \\ &+ 4\mathsf{r}h^{\mathrm{R1}}_{u\sigma}u_{(\alpha'}\sigma_{\beta')} - 2h^{\mathrm{R1}}_{uu}\sigma_{\alpha'}\sigma_{\beta'}\Bigg) + O(\lambda^0), \end{aligned} \tag{3.64}$$

$$h^{\delta m}_{\mu\nu} = -\lambda^{-1}\frac{\mu g^{\alpha'}_{\mu} g^{\beta'}_{\nu}\,\delta m_{\alpha'\beta'}}{\mathsf{s}} + O(\lambda^0), \tag{3.65}$$

where

$$\delta m_{\alpha\beta} = \mu \left[ \frac{1}{3} \left( 2h^{\rm R1}_{\alpha\beta} + g_{\alpha\beta} h^{\rm R1} \right) + 4u_{(\alpha} h^{\rm R1}_{\beta)\mu} u^\mu + \left( g_{\alpha\beta} + 2u_\alpha u_\beta \right) u^\mu u^\nu h^{\rm R1}_{\mu\nu} \right], \tag{3.66}$$

and

$$h^{\delta z}_{\mu\nu} = -\frac{2\mu g^{\alpha'}_{\mu} g^{\beta'}_{\nu} \left( g_{\alpha'\beta'} + 2u_{\alpha'} u_{\beta'} \right)}{\lambda^2 \mathsf{s}^3} \left( \delta z^{\rho'} + \lambda \mathsf{r} \delta \dot{z}^{\rho'} \right) \sigma_{\rho'} + O\left(\lambda^0\right). \tag{3.67}$$

We are free to cast these formulas into any coordinate system we choose.

## 3.3 Puncture as a coordinate expansion

To solve Eqs. (3.9) numerically, we will require the puncture field in a specific set of coordinates. With covariant expressions for the singular field it is straightforward to construct the puncture field as an expansion in coordinate differences $\Delta x^{\alpha'} \equiv x^\alpha - x^{\alpha'}$, and truncate at some order of $\Delta x^{\alpha'}$ to obtain the puncture field. The only ingredients needed are the coordinate expansions of the covariant quantities $\sigma^{\alpha'}$ in powers of $\Delta x^{\alpha'}$. Following [88], the expansion of $\sigma_{\alpha'}$ is found by writing

$$\begin{aligned} \sigma(x,x') = {} & \frac{1}{2} g_{\alpha'\beta'}(x') \Delta x^{\alpha'} \Delta x^{\beta'} + A_{\alpha'\beta'\gamma'}(x') \Delta x^{\alpha'} \Delta x^{\beta'} \Delta x^{\gamma'} \\ & + B_{\alpha'\beta'\gamma'\delta'}(x') \Delta x^{\alpha'} \Delta x^{\beta'} \Delta x^{\gamma'} \Delta x^{\delta'} + \dots, \end{aligned} \tag{3.68}$$

then acting with partial derivatives on (3.68) to determine the coefficients $A_{\alpha'\beta'\gamma'}$, $B_{\alpha'\beta'\gamma'\delta'}$ etc. using $\sigma^{\alpha'}\sigma_{\alpha'} = 2\sigma(x,x')$. Similarly, the expansion of $g^{\alpha'}_{\beta}$ can be found by writing the expansion

$$g^{\alpha'}_{\beta} = \delta^{\alpha'}_{\beta'} + G^{\alpha'}{}_{\beta'\gamma'}(x') \Delta x^{\gamma'} + G^{\alpha'}{}_{\beta'\gamma'\delta'}(x') \Delta x^{\gamma'} \Delta x^{\delta'} + \dots, \tag{3.69}$$

acting with partial derivatives, and then determining the coefficients using the identity $\sigma^{\gamma'} g^{\alpha'}_{\beta;\gamma'} = g^{\alpha'}_{\beta,\gamma'} \sigma^{\gamma'} + \Gamma^{\alpha'}_{\gamma'\delta'} g^{\delta'}_{\beta} \sigma^{\gamma'} = 0$. The end result is an expansion of the form

$$h^{\mathcal{P}1}_{\alpha\beta}(x,x') = \frac{1}{\lambda} \frac{\mathcal{P}^{(0)}_{\alpha'\beta'}}{\rho} + \lambda^0 \frac{\mathcal{P}^{(3)}_{\alpha'\beta'}}{\rho^3} + \lambda \frac{\mathcal{P}^{(6)}_{\alpha'\beta'}}{\rho^5} + \lambda^2 \frac{\mathcal{P}^{(9)}_{\alpha'\beta'}}{\rho^7} + O(\lambda^3), \tag{3.70}$$

$$h^{\mathcal{P}2}_{\alpha\beta}(x,x') = \frac{1}{\lambda^2} \frac{\mathcal{P}^{(2)}_{\alpha'\beta'}}{\rho^4} + \lambda \frac{\mathcal{P}^{(5)}_{\alpha'\beta'}}{\rho^6} + \lambda^0 \frac{\mathcal{P}^{(8)}_{\alpha'\beta'}}{\rho^8} + \lambda \frac{\mathcal{P}^{(11)}_{\alpha'\beta'}}{\rho^{10}} + O(\lambda^2), \tag{3.71}$$

where $\rho \equiv \left( P_{\mu'\nu'} \Delta x^{\mu'} \Delta x^{\nu'} \right)^{1/2}$. The $\mathcal{P}^{(n)}_{\alpha'\beta'}$ are polynomials in $\Delta x^{\mu'}$ of homogeneous order $n$. Each polynomial is of the form

$$\mathcal{P}^{(n)}_{\alpha'\beta'}(x,x') = \widetilde{\mathcal{P}}^{(n)}_{\alpha'\beta'\mu'_1 \dots \mu'_n}(x') \Delta x^{\mu'_1} \dots \Delta x^{\mu'_n}. \tag{3.72}$$

We are now in a position to use Eqs. (3.9) to solve for the first- and second-order residual field. In the next chapter we will show how to implement Eqs. (3.9) numerically for the first-order field, using the puncture field specialised to the case of circular orbits in Schwarzschild.

# Chapter 4

# Frequency-domain application of the puncture scheme at first order.

We have now formulated a practical way of solving the first- and second-order field equations, by means of the puncture scheme. Even more, we have constructed a covariant expression for the puncture field that we can write in any set of coordinates. Now we want to take this formalism and implement it to solve the field equations, for quasicircular orbits in Schwarzschild. In this chapter we will describe a frequency-domain formulation of the puncture scheme, and we will present results of a concrete numerical implementation at first order. Similar results have been obtained by numerous authors using slightly different methods, but our results serve as validation of both our method and our code. In subsequent chapters, we will discuss and resolve the difficulties that arise in implementing our formulation at second order. Here, and for the rest of this thesis, we will refer to standard Schwarzschild coordinates as $(t, r, \theta, \varphi)$.

## 4.1 Quasicircular orbits in Schwarzschild

We consider the simplest nontrivial scenario: quasicircular orbits in Schwarzschild spacetime. These trajectories are approximately circular on the timescale of a few orbits, but they gradually lose energy due to the dissipative piece of the self-force. For simplicity, in this section we neglect the self-force and treat the orbit as a circular geodesic. This is justified by the fact that on the short timescale of a few orbits, the cumulative effect of the self-force is small, and the orbit remains within a distance $\sim \epsilon$ of a circular geodesic. So, in calculating the first-order metric perturbation on the orbital timescale, we may consistently treat the orbit as that circular geodesic. In later chapters, when proceeding to second order, we will generalize the discussion to account for the orbit's dissipative evolution.

We begin by revisiting some familiar details of Schwarzschild spacetime. The metric of Schwarzschild spacetime, in Schwarzschild coordinates, is given by

$$g_{\alpha\beta}dx^\alpha dx^\beta = -f dt^2 + f^{-1}dr^2 + r^2 d\theta^2 + r^2 \sin^2\theta d\varphi^2\,, \tag{4.1}$$
$$f \equiv 1 - \frac{2M}{r}\,. \tag{4.2}$$

The event horizon is the hypersurface $r = 2M$. Consider a timelike geodesic with tangent four-velocity $u^\alpha$. The spherical symmetry of the background spacetime implies that angular momentum is conserved, which, in turn, means that orbits are planar. Without loss of generality, then, let our orbit be confined to the equatorial plane, $\theta = \pi/2$, so that $u^\theta$ is identically zero. Since $\xi^\alpha_{(t)} = \delta^\alpha_t$ and $\xi^\alpha_{(\varphi)} = \delta^\alpha_\varphi$ are Killing vectors, the quantities

$$\mathscr{E} \equiv -\xi^\alpha_{(t)} u_\alpha\,, \qquad \mathscr{L} \equiv \xi^\alpha_{(\varphi)} u_\alpha \tag{4.3}$$

are constants of the motion, representing the (specific) energy and angular momentum of the orbit, respectively.

The normalisation of the four-velocity, $u^\alpha u_\alpha = -1$, together with Eq. (4.3), imply the following equation of motion for geodesic trajectories in Schwarzschild spacetime:

$$\left(\frac{dr}{d\tau}\right)^2 = \mathscr{E}^2 - V(r)\,, \qquad V(r) \equiv f\left(1 + \frac{\mathscr{L}^2}{r^2}\right), \tag{4.4}$$

where $V(r)$ is the effective potential and $\tau$ is proper-time along the geodesic. Differentiating the first equation with respect to $\tau$ yields

$$\frac{d^2 r}{d\tau^2} = -\frac{1}{2}\frac{dV(r)}{dr}\,. \tag{4.5}$$

For circular orbits, the radius $r$ of the orbit is a constant, which we will denote as $r_0$. Setting $d^2r/d\tau^2 = 0$ in Eq. (4.5), and solving for $r$, we obtain

$$r_0 = \frac{\mathscr{L}^2}{2M}\left[1 \pm \left(1 - \frac{12M^2}{\mathscr{L}^2}\right)^{1/2}\right]. \tag{4.6}$$

Eq. (4.6) informs us that circular orbits exist, provided $\mathscr{L}^2 \geq 12M^2$. For a given $\mathscr{L}$ that satisfies $\mathscr{L}^2 > 12M^2$, there are two circular-orbit solutions: a stable one ['+' in Eq. (4.6)] and an unstable one ['-' in Eq. (4.6)]. For the case $\mathscr{L}^2 = 12M^2$ there is a point of inflection in the effective potential where these two radii converge. This is the radius of the "innermost stable circular orbit" (ISCO), given by

$$r_{\rm ISCO} = 6M. \tag{4.7}$$

From Eq. (4.6) it follows that any circular geodesic orbit at radius $r_0$ has specific angular momentum

$$\mathscr{L}_0^2 = \frac{Mr_0}{1-3M/r_0}\,, \tag{4.8}$$

and since $\mathscr{E}^2 = V(r)$ for circular orbits, it has specific energy

$$\mathscr{E}_0^2 = \frac{f_0^2}{1-3M/r_0}\,, \tag{4.9}$$

where $f_0 \equiv 1-2M/r_0$. Referring to the four-velocity for circular orbits with the notation $u_0^\alpha$, Eqs. (4.3) tell us that $u_0^t$ and $u_0^\varphi$ are given by

$$u_0^t = \frac{1}{(1-3M/r_0)^{1/2}}\,, \qquad\qquad u_0^\varphi = \left(\frac{M/r_0^3}{1-3M/r_0}\right)^{1/2}. \tag{4.10}$$

The angular-frequency, $\Omega \equiv d\varphi/dt$, is easily derived from Eqs. (4.10) using $\Omega = u_0^t/u_0^\varphi$ and $\Omega \equiv d\varphi/dt = u_0^t/u_0^\varphi$, which yields

$$\Omega = \sqrt{\frac{M}{r_0^3}}\,. \tag{4.11}$$

The first-order stress-energy tensor for a point mass moving along a generic world-line was given in (1.23). Specialising to a circular equatorial orbit in Schwarzschild, it is given by

$$T^1_{\alpha\beta} = \frac{\mu}{u_0^t r_0^2}\delta(r-r_0)\delta(\theta-\theta_0)\delta(\varphi-\Omega t)u_{0\alpha}u_{0\beta}. \tag{4.12}$$

Here we are taking $\varphi(t=0)=0$ without loss of generality.

## 4.2 Fourier-harmonic decomposition

We now focus our attention on how to solve the puncture-scheme Eqs. (3.9a) and (3.9b) for the first-order field. Rather than solving for the retarded field $h^1_{\alpha\beta}$ itself, we will instead solve for its trace reverse, $\bar{h}^1_{\alpha\beta}$. The incentive is that the gauge constraint (2.19), given in terms of $\bar{h}^1_{\alpha\beta}$, reduces the number of equations needed to be solved, as we will see in this section. To take advantage of this, we re-write Eqs. (3.9a) and (3.9b) as equations for $\bar{h}^1_{\alpha\beta}$, as

$$E_{\alpha\beta}[\,\bar{h}^{\mathcal{R}1}\,] = -E_{\alpha\beta}[\,\bar{h}^{\mathcal{P}1}\,] \qquad \text{inside } \Gamma, \tag{4.13a}$$

$$E_{\alpha\beta}[\,\bar{h}^{1}\,] = 0 \qquad \text{outside } \Gamma. \tag{4.13b}$$

Our goal now is to solve Eqs. (4.13), for the particular case of circular orbits in Schwarzschild.

The most economical way to do this is by decomposing the retarded field into Fourier-harmonic modes. The motive is that the resulting field equations separate, leading to ordinary differential equations whose derivatives are just with respect to $r$. These are much easier to solve numerically than the partial differential equations in four variables.

We write $\bar{h}^1_{\alpha\beta}$ as a sum over tensor, spherical-harmonic modes, as

$$\bar{h}^1_{\alpha\beta}(t,r,\theta,\varphi) = \frac{\mu}{r}\sum_{\ell=0}^{\infty}\sum_{m=-\ell}^{\ell}\sum_{i=1}^{10} a_{i\ell}\,\bar{h}_{i\ell m}(t,r)Y^{i\ell m}_{\alpha\beta}(\theta,\varphi,r). \tag{4.14}$$

The factor of $\mu/r$ serves to factor out the scaling with $\mu$ and the dominant behaviour at large $r$. Here we use the particular harmonics introduced by Barack and Lousto [89], as slightly modified by Barack and Sago [62]:

$$Y^{1\ell m}_{\alpha\beta} = \frac{1}{\sqrt{2}}\begin{pmatrix} 1 & 0 & 0 & 0 \\ 0 & f^{-2} & 0 & 0 \\ 0 & 0 & 0 & 0 \\ 0 & 0 & 0 & 0 \end{pmatrix} Y^{\ell m}, \tag{4.15a}$$

$$Y^{2\ell m}_{\alpha\beta} = \frac{f^{-1}}{\sqrt{2}}\begin{pmatrix} 0 & 1 & 0 & 0 \\ 1 & 0 & 0 & 0 \\ 0 & 0 & 0 & 0 \\ 0 & 0 & 0 & 0 \end{pmatrix} Y^{\ell m}, \tag{4.15b}$$

$$Y^{3\ell m}_{\alpha\beta} = \frac{f}{\sqrt{2}}\begin{pmatrix} 1 & 0 & 0 & 0 \\ 0 & -f^{-2} & 0 & 0 \\ 0 & 0 & 0 & 0 \\ 0 & 0 & 0 & 0 \end{pmatrix} Y^{\ell m}, \tag{4.15c}$$

$$Y^{4\ell m}_{\alpha\beta} = \frac{r}{\sqrt{2\ell(\ell+1)}}\begin{pmatrix} 0 & 0 & \partial_\theta & \partial_\varphi \\ 0 & 0 & 0 & 0 \\ \partial_\theta & 0 & 0 & 0 \\ \partial_\varphi & 0 & 0 & 0 \end{pmatrix} Y^{\ell m}, \tag{4.15d}$$

$$Y^{5\ell m}_{\alpha\beta} = \frac{rf^{-1}}{\sqrt{2\ell(\ell+1)}}\begin{pmatrix} 0 & 0 & 0 & 0 \\ 0 & 0 & \partial_\theta & \partial_\varphi \\ 0 & \partial_\theta & 0 & 0 \\ 0 & \partial_\varphi & 0 & 0 \end{pmatrix} Y^{\ell m}, \tag{4.15e}$$

$$Y^{6\ell m}_{\alpha\beta} = \frac{r^2}{\sqrt{2}}\begin{pmatrix} 0 & 0 & 0 & 0 \\ 0 & 0 & 0 & 0 \\ 0 & 0 & 1 & 0 \\ 0 & 0 & 0 & s^2 \end{pmatrix} Y^{\ell m}, \tag{4.15f}$$

$$Y^{7\ell m}_{\alpha\beta} = \frac{r^2}{\sqrt{2\lambda\ell(\ell+1)}} \begin{pmatrix} 0 & 0 & 0 & 0 \\ 0 & 0 & 0 & 0 \\ 0 & 0 & D_2 & D_1 \\ 0 & 0 & D_1 & -s^2 D_2 \end{pmatrix} Y^{\ell m}, \tag{4.15g}$$

$$Y^{8\ell m}_{\alpha\beta} = \frac{r}{\sqrt{2\ell(\ell+1)}} \begin{pmatrix} 0 & 0 & s^{-1}\partial_\varphi & -s\,\partial_\theta \\ 0 & 0 & 0 & \\ s^{-1}\partial_\varphi & 0 & 0 & 0 \\ -s\,\partial_\theta & 0 & 0 & 0 \end{pmatrix} Y^{\ell m}, \tag{4.15h}$$

$$Y^{9\ell m}_{\alpha\beta} = \frac{r f^{-1}}{\sqrt{2\ell(\ell+1)}} \begin{pmatrix} 0 & 0 & 0 & 0 \\ 0 & 0 & s^{-1}\partial_\varphi & -s\,\partial_\theta \\ 0 & s^{-1}\partial_\varphi & 0 & 0 \\ 0 & -s\,\partial_\theta & 0 & 0 \end{pmatrix} Y^{\ell m}, \tag{4.15i}$$

$$Y^{10\ell m}_{\alpha\beta} = \frac{r^2}{\sqrt{2\lambda\ell(\ell+1)}} \begin{pmatrix} 0 & 0 & 0 & 0 \\ 0 & 0 & 0 & 0 \\ 0 & 0 & s^{-1}D_1 & -s\,D_2 \\ 0 & 0 & -s\,D_2 & -s\,D_1 \end{pmatrix} Y^{\ell m}. \tag{4.15j}$$

$s \equiv \sin\theta$, $\lambda \equiv (\ell-1)(\ell+2)$, $Y^{\ell m} \equiv Y^{\ell m}(\theta,\varphi)$ are the standard scalar spherical-harmonics, and

$$D_1 \equiv 2(\partial_\theta - \cot\theta)\partial_\varphi, \qquad D_2 \equiv \partial_{\theta\theta} - \cot\theta\,\partial_\theta - s^{-2}\partial_{\varphi\varphi}. \tag{4.16}$$

The radial factors involving $r$ and $f$ are introduced for dimensional balance and for settling the horizon behaviour.

This basis is orthogonal in the sense that

$$\int_0^{2\pi} d\varphi \int_0^{\pi} d\theta\, \sin\theta \eta^{\alpha\mu}\eta^{\beta\nu} Y^{i\ell m}_{\mu\nu} Y^{*j\ell' m'}_{\alpha\beta} = \kappa_i \delta_{ij}\delta_{\ell\ell'}\delta_{mm'}, \tag{4.17}$$

where $\eta^{\alpha\beta} = \mathrm{diag}\left(1, f^{-2}, r^{-2}, r^{-2}\sin^{-2}\theta\right)$, and [62]

$$\kappa_i = \begin{cases} f^2, & i = 3, \\ 1 & \text{otherwise.} \end{cases} \tag{4.18}$$

The coefficients $a_{i\ell}$ are introduced in (4.14) for the purpose of simplifying the form of Eqs. (4.25) below. They are defined to be

$$a_{i\ell} = \frac{1}{\sqrt{2}} \times \begin{cases} 1, & i = 1,2,3,6, \\ [\ell(\ell+1)]^{-1/2}, & i = 4,5,8,9, \\ [(\ell-1)\,\ell\,(\ell+1)\,(\ell+2)]^{-1/2}, & i = 7,10. \end{cases} \tag{4.19}$$

Let us introduce the parity transformation, $\theta \to \pi - \theta$, $\varphi \to \pi + \varphi$. The $i = 1, \ldots, 7$

tensor harmonics are *even* (i.e. do not change sign) under the parity transformation and the $i = 8, 9, 10$ tensor harmonics are *odd* (i.e. change sign) under the parity transformation [90]. We will refer to the $i = 1, \ldots, 7$ modes as even-parity modes, and the $i = 8, 9, 10$ modes as the odd-parity modes.

As the mode decomposition stands in Eqs. (4.14), the field equations (3.9) would separate into a set of two-dimensional partial differential equations in the time domain, with derivatives in both the $t$ and $r$ variables. We further decompose into frequency-domain modes as

$$\bar{h}_{i\ell m}(t, r) = \int_{-\infty}^{\infty} d\omega \, \bar{h}_{i\ell m\omega}(r) e^{-i\omega t} \,. \tag{4.20}$$

The range of frequencies of the first-order field may be determined from the following argument. In the same vein as (4.14), $T^1_{\alpha\beta}$ may be projected onto a basis of the same ten, tensor harmonics in the form

$$T^1_{\alpha\beta}(x) = \sum_{i=1}^{10} \sum_{\ell=0}^{\infty} \sum_{m=-\ell}^{\ell} \int_{-\infty}^{\infty} d\omega \, Y^{i\ell m}_{\alpha\beta} \, e^{-i\omega t} T_{i\ell m\omega}(r) \,, \tag{4.21}$$

and, from Eq. (4.17), we readily obtain the $i\ell m\omega$-modes

$$T_{i\ell m\omega}(r) = \frac{1}{2\pi\kappa_i} \int_{-\infty}^{\infty} dt \int_0^{2\pi} d\varphi \int_0^{\pi} d\theta \sin\theta \; \eta^{\alpha\mu}\eta^{\beta\nu} \, T^1_{\alpha\beta} \, Y^{*i\ell m}_{\mu\nu} \, e^{i\omega t}. \tag{4.22}$$

When we substitute $T^1_{\alpha\beta}$ from Eq. (4.12), recalling the factor $\delta(\varphi - \Omega t)$ in $T^1_{\alpha\beta}$, the $\exp(-im\varphi)$ factor from the spherical harmonic will integrate against $\exp(i\omega t)$ to yield $\delta(\omega - m\Omega)$. This tells us that for circular orbits, the frequency modes of the stress-energy tensor are integer multiples of the angular frequency, $\Omega$. In light of this, the retarded field naturally picks up the same range of frequencies, as do $h^{1\mathcal{P}}$ and $h^{1\mathcal{R}}$, and we may write the following ansatz for the spectrum of the first-order fields:

$$\omega = \omega_m \equiv m\Omega \,. \tag{4.23}$$

Based on this the mode-decompositions (4.14) with (4.20) may be re-cast as

$$\bar{h}^1_{\alpha\beta} = \frac{\mu}{r} \sum_{i=1}^{10} \sum_{\ell=0}^{\infty} \sum_{m=-\ell}^{\ell} a_{i\ell} \, Y^{i\ell m}_{\alpha\beta} \, e^{-im\Omega t} \, \bar{h}_{i\ell m}(r) \,, \tag{4.24}$$

where in Eq. (4.24) and for the rest of the thesis, we omit the $\omega$-dependence in the subscript of $\bar{h}_{i\ell m}(r)$.

After decomposing the field into tensor-harmonic modes, the partial differential equations (4.13) separate into a set of ten, coupled, ordinary differential equations for each $\ell m$-mode, which read

$$E_{i\ell m}[\,\bar{h}^{\mathcal{R}1}\,] = -E_{i\ell m}[\,\bar{h}^{\mathcal{P}1}\,] \equiv S^{1\mathrm{eff}}_{i\ell m} \qquad \text{inside } \Gamma, \tag{4.25a}$$

$$E_{i\ell m}[\,\bar{h}^{1}\,] = 0 \qquad \text{outside } \Gamma, \tag{4.25b}$$

with

$$E_{i\ell m}[\,\bar{h}\,] \equiv \Box^{2d}_{sc}\bar{h}_{i\ell m}(r) + \mathcal{M}^{ij}\bar{h}_{j\ell m}, \tag{4.26}$$

where $i,j = 1,\ldots,10$, $\Box^{2d}_{\mathrm{sc}}$ is the scalar-field wave operator, given by

$$\Box^{2d}_{sc} \equiv -\frac{1}{4}\left(f^2\partial_r^2 + \frac{2M}{r^2}f\partial_r + \omega_m^2\right) + V_\ell(r), \tag{4.27}$$

and

$$V_\ell(r) \equiv \frac{f}{4}\left(\frac{2M}{r^3} + \frac{\ell(\ell+1)}{r^2}\right). \tag{4.28}$$

The second term on the right-hand side of (4.26) is the vector formed by pre-multiplying the vector $\bar{h}_{j\ell m}(r)$ by the matrix $\mathcal{M}^{ij}$. These are first-order differential operators that couple between the various $\bar{h}_{j\ell m}$'s (with the same $\ell, m$). Explicit formulas for them are given in Appendix D. As expected, one finds that the seven equations for the even-parity modes $\bar{h}_{i\ell m}$ with $i = 1,\ldots,7$ decouple from the remaining three equations for the odd-parity modes $\bar{h}_{i\ell m}$ with $i = 8, 9, 10$: we have $\mathcal{M}^{ij} = 0$ for any $i = 1,\ldots,7$ with $j = 8, 9, 10$, and for any $i = 8, 9, 10$ with $j = 1,\ldots,7$.

Similarly, the four gauge equations, $\nabla^\alpha\bar{h}_{\alpha\beta} = 0$, separate into four gauge equations at each $(\ell, m)$-mode. Suppressing the $\ell, m$ mode numbers in the subscript, they read

$$i\omega_m\bar{h}_1 + f\left(i\omega_m\bar{h}_3 + \partial_r\bar{h}_2 + \frac{\bar{h}_2}{r} - \frac{\bar{h}_4}{r}\right) = 0, \tag{4.29a}$$

$$-\,i\omega_m\bar{h}_2 - f\partial_r\bar{h}_1 + f^2\partial_r\bar{h}_3 - \frac{f}{r}\left(\bar{h}_1 - \bar{h}_5 - f\bar{h}_3 - 2f\bar{h}_6\right) = 0, \tag{4.29b}$$

$$-\,i\omega_m\bar{h}_4 - \frac{f}{r}\left(r\partial_r\bar{h}_5 + 2\bar{h}_5 + \ell(\ell+1)\bar{h}_6 - \bar{h}_7\right) = 0, \tag{4.29c}$$

$$-\,i\omega_m\bar{h}_8 - \frac{f}{r}\left(r\partial_r\bar{h}_9 + 2\bar{h}_9 - \bar{h}_{10}\right) = 0. \tag{4.29d}$$

Eqs. (4.25) may be solved numerically for the modes of the residual fields, once formulas for the modes of the puncture have been provided. Wardell first obtained analytical formulas for the $i\ell m$ modes of the first-order punctures, for circular orbits in Schwarzschild [74]. I independently derived formulas for them and successfully checked my own results with those of Wardell. Expressions for the punctures and details of the derivation of their frequency-domain, harmonic modes are given in Appendix C. In the coming sections we detail the algorithm for how to solve Eqs. (4.25) numerically.

| Sector | Modes calculated from the field equations | Modes calculated from the gauge conditions | Vanishing modes |
|---|---|---|---|
| $\ell \geq 2,\ \ \ell+m$ - odd | $i=9,10$ | $i=8$ | $i=1-7$ |
| $\ell \geq 2,\ \ \ell+m$ - even | $i=1,3,5,6,7$ | $i=2,4$ | $i=8,9,10$ |
| $\ell=1,\ m=1$ | $i=1,3,5,6$ | $i=2,4$ | $i=7,8,9,10$ |
| $\ell \geq 2$ even , $m=0$ | $i=1,3,5$ | $i=6,7$ | $i=2,4,8,9,10$ |
| $\ell$ odd, $m=0$ - analytic | $i=8$ | none | $i \neq 8$ |
| $\ell=1, m=0$ - analytic | $i=8,9$ | none | $i \neq 8,9$ |
| $\ell=0, m=0$ - analytic | $i=1,3$ | 6 | $i=2,4,5,7,8,9,10$ |

Table 4.1: Summary of how the solutions for each mode are obtained. The first column displays the different sectors, into which the modes are divided. The second column lists the non-vanishing modes of the fields $\bar{h}_{i\ell m}$ that are calculated by directly solving the wave equations (4.25a) numerically. The third column lists the non-vanishing modes of the fields that can be calculated by solving the gauge conditions (4.29a)-(4.29d) algebraically. The odd-parity stationary modes ($m=0$ with odd $\ell$) and monopole mode ($\ell=0=m$) can be solved for analytically.

## 4.3 Hierarchical structure of the boundary value problem

In this section we will describe the hierarchical structure of the ten coupled equations, in (4.25a) and (4.25b). This structure significantly simplifies the task of numerically solving the equations. Focusing on the left-hand side of the equations, we observe that the odd-parity modes, $i=8,9,10$ are coupled, and the even-parity, $i=1,\ldots,7$ modes are coupled, but these two sets of modes do not mix. Focusing on the right-hand side of Eqs. (4.25), we find that the even-parity modes ($i=1,\ldots,7$) of the effective source, $S^{\text{eff1}}_{i\ell m}$ as defined in Eq. (4.25a), are non-vanishing for $\ell+m=$ even, and the odd-parity modes ($i=8,9,10$) are non-vanishing for $\ell+m=$ odd. We emphasise that this holds for orbits confined to the equatorial plane ($\theta=\pi/2$), but would not be true in general. There are also modes that vanish only when $m=0$. Overall, the non-vanishing modes of $S^{\text{eff1}}_{i\ell m}$ fall into the structure

$$\begin{cases} \ell=0, m=0, & i=1,3,6, \\ \ell \text{ odd}, m=0, & i=8, \\ \ell \text{ even}, m=0, & i=1,3,5,6,7, \\ \ell+m \text{ odd}, m>0, & i=8,9,10, \\ \ell=1, m=1, & i=1,\ldots,6 \\ \ell+m \text{ even}, m>0, & i=1,\ldots,7. \end{cases} \tag{4.30}$$

We impose regularity at the future horizon and future null infinity. Regularity at the horizon means that the components of the perturbation in coordinates that are regular on the horizon, like advanced Eddington-Finklestein (aEF) coordinates ($v=$

$t + r^*(R), R = r, \theta, \varphi)$, are smooth there. The aEF components, $\bar{h}^{(aEF)}_{\mu\nu}$, are related to the Schwarzschild components, $\bar{h}_{\mu\nu}$, of the metric perturbation via

$$\bar{h}^{(aEF)}_{vv} = \bar{h}_{tt}, \tag{4.31a}$$

$$\bar{h}^{(aEF)}_{vR} = \bar{h}_{tr} - f^{-1}\bar{h}_{tt}, \tag{4.31b}$$

$$\bar{h}^{(aEF)}_{RR} = \frac{\bar{h}_{tt}}{f^2} + \bar{h}_{rr} - \frac{2\bar{h}_{tr}}{f}, \tag{4.31c}$$

$$\bar{h}^{(aEF)}_{R\theta} = \bar{h}_{r\theta} - f^{-1}\bar{h}_{t\theta}, \tag{4.31d}$$

$$\bar{h}^{(aEF)}_{R\varphi} = \bar{h}_{r\varphi} - f^{-1}\bar{h}_{t\varphi}. \tag{4.31e}$$

and $\bar{h}^{(aEF)}_{\mu\nu} = \bar{h}_{\mu\nu}$ for all other components. Referring to the mode coefficients $\bar{h}_{i\ell m}(v, r)$ in Eq. (4.14), prior to the frequency decomposition, we have the relations

$$\bar{h}^{(aEF)}_{vv} = \frac{\mu}{\sqrt{2}r}\left[\bar{h}_{1\ell m}(v,r) + f\bar{h}_{3\ell m}(v,r)\right] Y^{\ell m}, \tag{4.32a}$$

$$\bar{h}^{(aEF)}_{vR} = \frac{\mu}{\sqrt{2}r}\left[\bar{h}_{2\ell m}(v,r) - \bar{h}_{1\ell m}(v,r) - f^{-1}\bar{h}_{3\ell m}(v,r)\right] Y^{\ell m}, \tag{4.32b}$$

$$\bar{h}^{(aEF)}_{RR} = \frac{\mu}{\sqrt{2}rf^2}\left[\bar{h}_{1\ell m}(v,r) - \bar{h}_{2\ell m}(v,r)\right] Y^{\ell m}, \tag{4.32c}$$

$$\begin{aligned}\bar{h}^{(aEF)}_{R\theta} =& -\frac{\mu}{\sqrt{2}rf\ell(\ell+1)}\left[\bar{h}_{4\ell m}(v,r) - \bar{h}_{5\ell m}(v,r)\right]\partial_\theta Y^{\ell m} \\ &+ \frac{\mu}{\sqrt{2}rf\ell(\ell+1)}\left[\bar{h}_{8\ell m}(v,r) - \bar{h}_{9\ell m}(v,r)\right]\csc\theta\partial_\varphi Y^{\ell m}.\end{aligned} \tag{4.32d}$$

From Eqs. (4.32), we see that for the components to be smooth at the horizon, the modes have to satisfy the following conditions:

$$\bar{h}_{ilm}(v,r) = \bar{h}_{i+1,lm}(v,r) + fB_{i\ell m}(v,r) \tag{4.33}$$

for $i = 4, 8$, where $B_{i\ell m}$ is $C^\infty$ at $r = 2M$,

$$\bar{h}_{2\ell m}(v,r) = \bar{h}_{1\ell m}(v,r) + f^2 B_{2\ell m}(v,r), \tag{4.34}$$

and $\bar{h}_{i\ell m}(v,r)$, $i = 1, 3, 5, 6, 7, 9, 10$ are $C^\infty$ at $r = 2M$.

Regularity at $r \to \infty$ means that the metric perturbation is asymptotically flat at future null infinity, i.e. its Cartesian components fall off at least as fast as $1/r$ at large $r$ (at fixed $u = t - r_*$), and its $r$-derivatives fall off faster than that.

For the nonzero-frequency modes, we further specify that the solutions behave as ingoing waves at the horizon, and outgoing waves at $r \to \infty$.

The non-vanishing modes of the effective source, given in (4.30), combined with the boundary conditions given above, specify the non-vanishing modes of the solution. The gauge conditions (4.29) allow us to solve for a subset of these modes algebraically, without the need to numerically solve ODEs for them. With this in mind, we may compute the modes using the hierarchical structure summarised in Table 4.1 [89].

## 4.4 Homogeneous solutions

In this section we describe how to solve the homogeneous wave equation $E_{i\ell m}[h] = 0$, whose solutions will be used to obtain the inhomogeneous solutions to Eqs. (4.25a) and (4.25b), in the manner to be explained in the following section. We will first quote the analytically known general homogeneous solutions for the monopole and odd-$\ell$, stationary sectors, and then proceed to describe the algorithm for solving for the remaining modes numerically. For each mode, we seek two separate sets of homogeneous solutions. For each non-stationary mode, one set are regular and behave as outgoing waves at infinity, and one set are regular and behave as ingoing waves at the horizon. For each stationary mode, there are no waves at either of the boundaries. Rather we seek two sets of homogeneous solutions, one set which is regular at infinity, and one which is regular at the horizon. We will use the notation $h^+_{i\ell m}(r)$ and $h^-_{i\ell m}(r)$ respectively, for the two different types.

To aid the coming discussion it will be useful to write down the homogeneous equation that we are solving, since we will refer to it frequently in this section. It reads

$$\Box^{2d}_{sc}\bar{h}_{i\ell m}(r) + \mathcal{M}^{ij}\bar{h}_{j\ell m} = 0. \tag{4.35}$$

### 4.4.1 Analytical solutions for the monopole ($\ell = 0, m = 0$) mode

For the monopole modes, only the $i = 1, 3, 6$ modes are non-zero. The $i = 1, 3$ monopole field equations can be further simplified using the gauge equation (4.29b) to decouple the $\bar{h}_{600}$ mode;

$$\bar{h}_{600} = -\frac{r}{2f}\partial_r\bar{h}_{100} - \frac{r}{2}\partial_r\bar{h}_{300} + \frac{1}{2f}\left(\bar{h}_{100} - f\bar{h}_{300}\right). \tag{4.36}$$

The remaining field equations for $\bar{h}_{100}$ and $\bar{h}_{300}$ are given by

$$\partial_r^2\bar{h}_{100} = -\frac{1}{r^2 f}\left[(r-4M)\,\partial_r\bar{h}_{100} - \bar{h}_{100} - f^2\left(r\partial_r\bar{h}_{300} - \bar{h}_{300}\right)\right], \tag{4.37a}$$

$$\partial_r^2\bar{h}_{300} = -\frac{1}{r^2}\left[r\partial_r\bar{h}_{300} - \bar{h}_{300} + \frac{1}{f^2}\left((4M-r)\,\partial_r\bar{h}_{100} + \bar{h}_{100}\right)\right]. \tag{4.37b}$$

Prior to stating the homogeneous solutions, we define

$$
\begin{aligned}
H &\equiv \frac{M}{\mu}\left\{\bar{h}_{tt}, \bar{h}_{rr}, \frac{1}{r^2}\bar{h}_{\theta\theta} = \frac{1}{r^2\sin^2\theta}\bar{h}_{\varphi\varphi}\right\} \\
&= \frac{M}{4\sqrt{\pi}r}\left\{\bar{h}_{100} + f\bar{h}_{300}, \frac{1}{f^2}\left(\bar{h}_{100} - f\bar{h}_{300}\right), \bar{h}_{600}\right\},
\end{aligned} \tag{4.38}
$$

The inverse relations are

$$
\bar{h}_{100} = 2\sqrt{\pi}\frac{r}{\mu}\left(\bar{h}_{tt} + f^2\bar{h}_{rr}\right), \tag{4.39}
$$

$$
\bar{h}_{300} = 2\sqrt{\pi}\frac{r}{\mu f}\left(\bar{h}_{tt} - f^2\bar{h}_{rr}\right). \tag{4.40}
$$

$$
\bar{h}_{600} = 4\sqrt{\pi}\frac{1}{\mu r}\bar{h}_{\theta\theta}, \tag{4.41}
$$

A complete basis of homogeneous solutions to the two coupled monopole field equations (4.37) is given by [65, 89]

$$
H_A = \left\{-f, f^{-1}, 1\right\}, \tag{4.42a}
$$

$$
H_B = \left\{-\frac{fM}{r^3}P(r), \frac{1}{fr^3}Q(r), \frac{f}{r^2}P(r)\right\}, \tag{4.42b}
$$

$$
H_C = \left\{-\frac{M^4}{r^4}, \frac{M^3}{r^4 f^2}\left(3M - 2r\right), \frac{M^3}{r^3}\right\}, \tag{4.42c}
$$

$$
\begin{aligned}
H_D = \Bigg\{ &\frac{M}{r^4}\left[W(r) + rP(r)f\ln f - 8M^3\ln(r/M)\right], \\
&\frac{1}{f^2r^4}\left[K(r) - rQ(r)f\ln f - 8M^3(2r-3M)\ln(r/M)\right], \\
&\frac{1}{r^3}\left[3r^3 - W(r) - rP(r)f\ln f + 8M^3\ln(r/M)\right]\Bigg\},
\end{aligned} \tag{4.42d}
$$

where

$$
P(r) = r^2 + 2rM + 4M^2, \tag{4.43a}
$$

$$
Q(r) = r^3 - r^2M - 2rM^2 + 12M^3, \tag{4.43b}
$$

$$
W(r) = 3r^3 - r^2M - 4rM^2 - \frac{28}{3}M^3, \tag{4.43c}
$$

$$
K(r) = r^3M - 5r^2M^2 - \frac{20}{3}rM^3 + 28M^4. \tag{4.43d}
$$

None of the four solutions are regular at both boundaries. Rather, $H_A$ and $H_B$ are regular at the horizon, but not regular at $r \to \infty$. $H_C$ and $H_D$ are regular at $r \to \infty$, but not regular at the horizon, according to the criteria set out in Sec. 4.3.

As is well known, homogeneous monopole perturbations of Schwarzschild spacetime are always perturbations toward another Schwarzschild solution. In our case, solution $H_A$ has a mass-energy of 1/2, $H_D$ has a mass-energy of 3/2, and $H_B$ and $H_C$ are pure gauge. These mass values can be found by, e.g., transforming the perturbations to a "Schwarzschild gauge" in which they take the form $\frac{\partial g_{\alpha\beta}}{\partial M}\delta M$ and then reading off $\delta M$.

### 4.4.2 Analytical solutions for the axially symmetric, odd-parity modes

Odd $\ell > 1, m = 0$ modes of the field are constructed, at each $\ell$, from the single function $\bar{h}_{8\,\ell m=0}(r)$. Denoting $\bar{h}_{8\,\ell m=0}(r) \equiv \phi_\ell(r)$, the homogeneous field equation for $\bar{h}_{8\,\ell m=0}$ [Eq. (4.35) with (D.1h)] takes the form

$$\partial_r^2\phi_\ell + V_\ell(r)\phi_\ell = 0. \tag{4.44}$$

The solution takes a different form for $\ell = 1$ and $\ell \geq 2$. We will discuss $\ell \geq 2$ first and then discuss the mode $\ell = 1$ separately below. For $\ell \geq 2$, solutions that are regular at the horizon and at infinity are, respectively [89],

$$\phi^+_{\ell\geq 2}(r) = \frac{x}{1+x}\sum_{n=0}^{\ell+1} a^\ell_n x^n, \tag{4.45}$$

$$\phi^-_{\ell\geq 2}(r) = \phi^+_{\ell\geq 2}(r)\ln f + \frac{1}{1+x}\sum_{n=0}^{\ell+1} b^\ell_n x^n, \tag{4.46}$$

where

$$x \equiv r/(2M) - 1, \tag{4.47}$$

and the coefficients read

$$a^\ell_n = \frac{\ell(\ell+1)(\ell+n-1)!}{(\ell-n+1)!(n+1)!n!}, \qquad b^\ell_n = \sum_{k=0}^{\ell-n+1}(-1)^k\frac{a^\ell_{n+k}}{k+1}. \tag{4.48}$$

These solutions have the following asymptotic behaviour at the horizon ($r \to 2M$, $x \to 0$, $f \to 0$) and at infinity ($r, x \to \infty$):

$$\phi^-_{\ell\geq 2}(r) \propto \begin{cases} f, & r \to 2M, \\ r^{\ell+1}, & r \to \infty, \end{cases} \tag{4.49}$$

$$\phi^+_{\ell\geq 2}(r) \propto \begin{cases} f\ln f, & r \to 2M, \\ r^{-\ell}, & r \to \infty. \end{cases} \tag{4.50}$$

The solution $\phi^-_{\ell\geq 2}(r)$ is regular (analytic) at the horizon but diverges at $r \to \infty$, whereas the solution $\phi^+_{\ell\geq 2}(r)$ is regular at $r \to \infty$ but irregular at the horizon (it vanishes there, but it is non-differentiable).

For $\ell = 1$, the function $\phi^+_\ell(r)$ of Eq. (4.45) fails to be a solution of the homogeneous part of Eq. (4.44) (although $\phi^-_{\ell=1}(r)$ still is a solution). Instead, the general homogeneous solution takes the simple form

$$\phi^{+}_{\ell=1}(r) \quad = 1/r, \tag{4.51}$$

$$\phi^{-}_{\ell=1}(r) \quad = r^2. \tag{4.52}$$

As stated above, the $i = 8$ mode is the only non-vanishing mode for odd $\ell \geq 3, m = 0$. But for $\ell = 1$, we find that a homogeneous solution

$$\bar{h}^{-}_{9,1,0} = \frac{4M^2 \bar{h}^{-}_{8,1,0}(r = 2M)}{r^2} \tag{4.53}$$

must be added to ensure regularity at the horizon. This stems from the second regularity condition below Eq. (4.32d).

### 4.4.3 Numerical solution for the higher modes

The remainder of the modes are obtained through solving (4.35) numerically, using retarded boundary conditions at the (future) event horizon and at (future) null infinity. For the purposes of this discussion it will be useful to sometimes refer to the boundaries in terms of the tortoise coordinate, $r_* \equiv r + 2M \ln[r/(2M) - 1]$. Spatial infinity is at $r_* \to \infty$, or equivalently $r \to \infty$, and the event horizon is at $r_* \to -\infty$, or equivalently $r \to 2M$.

Since we are interested in constructing the physical retarded solutions, non-stationary modes ($\omega_m \neq 0$) should represent purely outgoing waves $\propto e^{-i\omega_m(t-r_*)}$ at infinity, and purely ingoing waves $\propto e^{-i\omega_m(t+r_*)}$ at the horizon. From this we demand that the solutions exhibit the following asymptotic behaviour:

$$\bar{h}^{\pm}_{i\ell m}(r_* \to \pm\infty) \sim e^{\pm i\omega_m r_*} \tag{4.54}$$

When we construct boundary conditions, at $r \to \infty$ we assume a priori that the radial fields admit an asymptotic expansion in $1/r$ up to a factor of $\exp(i\omega r_*)$, and at $r - 2M$ we assume an asymptotic expansion in $r - 2M$, up to a factor of $\exp(-i\omega r_*)$. In the numerical implementation we obviously cannot use $r_* = \pm\infty$ for the location of the boundaries. Instead, we select finite values $r_{\text{out/in}}$ for the location of the boundaries at infinity/the horizon. These locations are chosen to be close enough to infinity/the horizon that any change bringing them closer does not affect the first 16 significant digits of the numerical solution.

With this in mind, for the radiative modes we use the following expansions for the boundary conditions:

$$\bar{h}^{+}_{i\ell m}(r_{\text{out}}) = e^{i\omega_m r^*_{\text{out}}} \sum_{k=0}^{k^+_{\text{max}}} \frac{a^i_k}{r^k_{\text{out}}}, \tag{4.55}$$

$$\bar{h}^{-}_{i\ell m}(r_{\text{in}}) = e^{-i\omega_m r^*_{\text{in}}} \sum_{k=0}^{k^-_{\text{max}}} b^i_k \left(r_{\text{in}} - 2M\right)^k, \tag{4.56}$$

where $r^*_{\text{in/out}} \equiv r_*(r_{\text{in/out}})$. The coefficients $a^i_k$ and $b^i_k$ depend on $\ell$, $m$, $\omega_m$. Since the equations are second order, we also require boundary conditions for the first derivatives of the fields, which may be taken from Eqs. (4.55) and (4.56). We numerically determine the $k^{\pm}_{\text{max}}$ for each of the sums at every $\ell m\omega_m$ mode, based on the requirement that the next term in the summation has relative magnitude less than $10^{-14}$, compared to the partial sum. The coefficients $a^i_k$ and $b^i_i$ are determined by substituting the ansatz (4.55) and (4.56) into the field equations themselves and generating recurrence relations between the $a^i_k$ and (separately) between the $b^i_k$. We omit these recurrence relations here, but the reader is directed to Appendix A of [91], where they can be found. For each $\ell m\omega_m$ there are $d$ freely specifiable parameters $a^i_k$, and $d$ more freely specifiable parameters $b^i_k$, where $d$ is the number of coupled equations to be solved according to the second column in Table 4.1. If we arrange these freely specifiable parameters in vector form as $\vec{a} = \{a_1, a_2, \ldots, a_d\}$ and $\vec{b} = \{b_1, b_2, \ldots, b_d\}$, then by choosing $d$ linearly independent vectors $\vec{a}$ ($\vec{b}$), we obtain a basis of $d$ linearly independent asymptotic homogeneous solutions $\bar{h}^{+k}_{i\ell m}$ ($\bar{h}^{-k}_{i\ell m}$), $k = 1, \ldots, d$, for each $\ell m$ mode. For example [74], for the odd-parity radiative modes we have $d = 2$, once the gauge condition (4.29d) has been imposed, i.e., one needs to solve for $\bar{h}_{9\ell m}$ and $\bar{h}_{10\ell m}$. For the outer homogeneous solutions the two elements of the basis are formed by setting $\left\{a^9_0, a^{10}_0\right\} = \{1, 0\}$ and $\left\{a^9_0, a^{10}_0\right\} = \{0, 1\}$. Similarly, we can repeat this with $\left\{b^9_0, b^{10}_0\right\}$ for the inner solutions.

For even-parity stationary modes ($\ell$ even, $m = 0$), there are no ingoing/outgoing waves at the boundaries. Instead, we impose numerical boundary conditions that are regular at the horizon/infinity as

$$\bar{h}^{+}_{i\ell m}(r_{\text{out}}) = \sum_{k=k^+_{\text{min}}}^{k^+_{\text{max}}} \frac{\left(a^i_k + \bar{a}^i_k \log r_{\text{out}}\right)}{r^k_{\text{out}}}, \tag{4.57}$$

$$\bar{h}^{-}_{i\ell m}(r_{\text{in}}) = \sum_{k=k^-_{\text{min}}}^{k^-_{\text{max}}} b^i_k \left(r_{\text{in}} - 2M\right)^k. \tag{4.58}$$

In contrast to Eqs. (4.55) and (4.56), for the static modes the sum in the ansatz starts at some $k^{\pm}_{\text{min}}$ that is not necessarily zero. How they are determined, and the form of the recurrence relations for the $a^i_k, \bar{a}^i_k, b^i_k$, is discussed in [91]. The extra $\log r_{\text{out}}$ term in

(4.57) is needed due to the fact that (4.55) does not produce the necessary number of freely specifiable parameters $a_k^i$ ($d = 3$ in this case - see Table 4.1).

With boundary conditions in place we solve the homogeneous equation (4.35) for each $i\ell m$ mode. The full computational algorithm is described below, in Sec. 4.6. After computing the homogeneous solutions, we may implement the puncture scheme equations (4.25a) and (4.25b) using the *worldtube method* described in the coming section.

## 4.5 Inhomogeneous solutions and the worldtube method

In this section we will describe the worldtube algorithm for solving the puncture scheme equations (4.25a) and (4.25b). The worldtube method for solving the first-order equations was developed in collaboration with Adam Pound and Leor Barack, but its implementation in the later sections of this chapter was entirely my work. Our method differs from the one used in a similar calculation in [74], where instead of a worldtube, a window function is used. In our method we construct a worldtube $\Gamma$ around the particle located at radius $r_0$, shown schematically in Fig. 4.1, and solve for the residual field modes, $\bar{h}^{\mathcal{R}}_{i\ell m}$, inside $\Gamma$ and for the retarded field modes, $\bar{h}_{i\ell m}$, outside $\Gamma$.

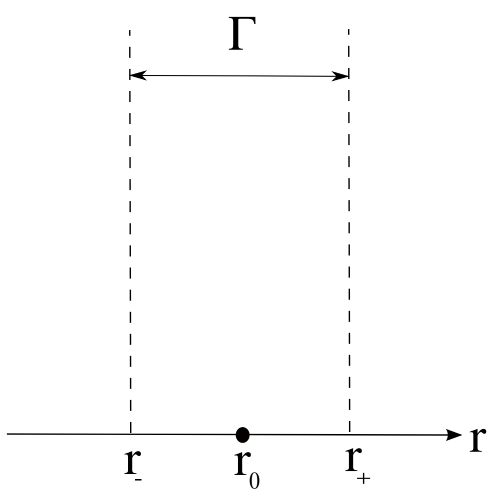


Figure 4.1: The worldtube $\Gamma : r \in [r_-, r_+]$ centered on the worldline, such that $r_0 = (r_+ - r_-)/2$ .

Let

$$\psi(r) = \begin{pmatrix} \bar{h}_1(r) \\ \bar{h}_3(r) \end{pmatrix} \qquad \text{for } \ell = 0,\ m = 0, \tag{4.59a}$$

$$\psi(r) = \begin{pmatrix} \bar{h}_8(r) \end{pmatrix} \qquad \text{for } \ell > 0,\ m = 0,\ \text{and } \ell \text{ odd}, \tag{4.59b}$$

$$\psi(r) = \begin{pmatrix} \bar{h}_1(r) \\ \bar{h}_3(r) \\ \bar{h}_5(r) \end{pmatrix} \qquad \text{for } \ell > 0,\ m = 0,\ \text{and } \ell \text{ even}, \tag{4.59c}$$

$$\psi(r) = \begin{pmatrix} \bar{h}_1(r) \\ \bar{h}_3(r) \\ \bar{h}_5(r) \\ \bar{h}_6(r) \end{pmatrix} \qquad \text{for } \ell = 1,\ m = 1, \tag{4.59d}$$

$$\psi(r) = \begin{pmatrix} \bar{h}_9(r) \\ \bar{h}_{10}(r) \end{pmatrix} \qquad \text{for } \ell > 0,\ m > 0,\ \text{and } \ell + m \text{ odd}, \tag{4.59e}$$

$$\psi(r) = \begin{pmatrix} \bar{h}_1(r) \\ \bar{h}_3(r) \\ \bar{h}_5(r) \\ \bar{h}_6(r) \\ \bar{h}_7(r) \end{pmatrix} \qquad \text{for } \ell > 0,\ m > 0,\ \text{and } \ell + m \text{ even}, \tag{4.59f}$$

with analogous definitions for $\psi^{\mathcal{R}}$ and $\psi^{\mathcal{P}}$ in terms of the modes of the residual field, $h^{\mathcal{R}}_{i\ell m}$, and the modes of the puncture field, $h^{\mathcal{P}}_{i\ell m}$, respectively. In this notation the first-order puncture-scheme equations (4.25) can be cast as

$$\frac{d^2\psi}{dr^2} + B\frac{d\psi}{dr} + A\psi = 0 \qquad \text{outside } \Gamma, \tag{4.60}$$

$$\frac{d^2\psi^{\mathcal{R}}}{dr^2} + B\frac{d\psi^{\mathcal{R}}}{dr} + A\psi^{\mathcal{R}} = J^{\text{eff}} \qquad \text{inside } \Gamma, \tag{4.61}$$

where $A$ and $B$ are $r$-dependent $d \times d$ matrices and the source $J^{\text{eff}}$ is a column vector with $d$ elements. It is comprised of modes of $S^{1\text{eff}}_{i\ell m}$ in the same format as Eqs. (4.59). The domain is $r \in (2M, \infty)$.

Now let $\hat{\psi} = \begin{pmatrix} \psi \\ \partial_r \psi \end{pmatrix}$ and $\hat{\psi}^{\mathcal{R}} = \begin{pmatrix} \psi^{\mathcal{R}} \\ \partial_r \psi^{\mathcal{R}} \end{pmatrix}$. Write the ordinary differential equations in first-order form, such that

$$\frac{d\hat{\psi}}{dr} + \hat{A}\hat{\psi} = \hat{0} \qquad \text{outside } \Gamma, \tag{4.62}$$

$$\frac{d\hat{\psi}^{\mathcal{R}}}{dr} + \hat{A}\hat{\psi}^{\mathcal{R}} = \hat{J}^{\text{eff}} \qquad \text{inside } \Gamma, \tag{4.63}$$

where $\hat{A} = \begin{pmatrix} \mathbf{0}_{d\times d} & -\mathbb{1}_{d\times d} \\ A & B \end{pmatrix}$ is a $2d \times 2d$ matrix and $\hat{J}^{\text{eff}} = \begin{pmatrix} \mathbf{0}_d \\ J^{\text{eff}} \end{pmatrix}$ has $2d$ elements. Then let $\Phi = \begin{pmatrix} \hat{\psi}_{[1]} & \cdots & \hat{\psi}_{[2d]} \end{pmatrix}$ be a $2d \times 2d$ matrix of independent homogeneous solutions $\hat{\psi}_{[k]} = \begin{pmatrix} \psi_{[k]} \\ \partial_r \psi_{[k]} \end{pmatrix}$. This implies $\Phi_{,r} + \hat{A}\Phi = 0$. The general solution to Eqs. (4.62) and

(4.63) is

$$\hat{\psi}^{-} = \Phi a^{-}, \qquad r < r_-, \tag{4.64}$$

$$\hat{\psi}^{+} = \Phi a^{+}, \qquad r > r_+, \tag{4.65}$$

$$\hat{\psi}^{\mathcal{R}} = \Phi\left(\int_{r^-}^{r} \Phi^{-1}\hat{\jmath}^{\text{eff}} dr' + a^{\mathcal{R}}\right), \qquad r_- \leq r \leq r_+, \tag{4.66}$$

where $a^{\pm}$ and $a^{\mathcal{R}}$ are arbitrary constant $2d$-vectors. Direct substitution of these expressions into Eqs. (4.62)–(4.63) verifies that these are general solutions.

To determine $a^{\pm}$ and $a^{\mathcal{R}}$, we impose the jump conditions

$$\hat{\psi}^{\mathcal{R}}(r^{\pm}) = \hat{\psi}^{\pm}(r^{\pm}) - \hat{\psi}^{\mathcal{P}}(r^{\pm}), \tag{4.67}$$

which yield

$$a^{\mathcal{R}} - a^{-} = -\Phi^{-1}(r_-)\hat{\psi}^{\mathcal{P}}(r_-), \tag{4.68}$$

$$a^{\mathcal{R}} - a^{+} = -\int_{r_-}^{r_+} \Phi^{-1}\hat{\jmath}^{\text{eff}} dr' - \Phi^{-1}(r_+)\hat{\psi}^{\mathcal{P}}(r_+). \tag{4.69}$$

Here we have two vector equations for the three unknown vectors $a_{\pm}$ and $a^{\mathcal{R}}$. To solve the equations, we impose retarded boundary conditions. We write $d$ independent homogeneous solutions that are regular/ingoing waves at the inner boundary and $d$ that are regular/outgoing waves at infinity, and we want an inhomogeneous solution that satisfies both those conditions. The matrix $\Phi$ can then be written as

$$\Phi = (\hat{\psi}_{[1-]}, \ldots, \hat{\psi}_{[d-]}, \hat{\psi}_{[1+]}, \ldots, \hat{\psi}_{[d+]}), \tag{4.70}$$

where $\hat{\psi}_{[k-]}$ is a homogeneous solution regular at $r = 2M$, and $\hat{\psi}_{[k+]}$ is a homogeneous solution regular at $\infty$. From Eqs. (4.64) and (4.65) and the boundary conditions, we have

$$a^{-} = (a_1^{-}, \ldots, a_d^{-}, 0, \ldots, 0)^T, \tag{4.71}$$

$$a^{+} = (0, \ldots, 0, a_1^{+}, \ldots, a_d^{+})^T, \tag{4.72}$$

for some constants $a_i^{\pm}$.

Writing $a^{\mathcal{R}} = (a^{\mathcal{R}}_{1-}, \ldots, a^{\mathcal{R}}_{k-}, a^{\mathcal{R}}_{1+}, \ldots, a^{\mathcal{R}}_{k+})^T$, we now have $4d$ scalar equations, namely Eqs. (4.68), (4.69), (4.71) and (4.72), for the $4d$ unknowns, $a^{\mathcal{R}}_{i\pm}$ and $a_i^{\pm}$. Subtracting Eqs. (4.69) from Eq. (4.68), we find

$$a = \int_{r_-}^{r_+} \Phi^{-1}\hat{\jmath}^{\text{eff}} dr + \Phi^{-1}(r_+)\hat{\psi}^{\mathcal{P}}(r_+) - \Phi^{-1}(r_-)\hat{\psi}^{\mathcal{P}}(r_-), \tag{4.73}$$

where

$$a \equiv (-a_1^-, \dots, -a_k^-, a_1^+, \dots, a_k^+)^T. \tag{4.74}$$

Substituting this back into Eq. (4.69) or (4.68), we find

$$a^{\mathcal{R}} = \begin{pmatrix} -\int_{r_-}^{r_+} \Phi_{\rm top}^{-1} \hat{J}^{\rm eff} dr - (\Phi_{\rm top}^{-1} \hat{\psi}^{\mathcal{P}})\big|_{r_+} \\ -(\Phi_{\rm bot}^{-1} \hat{\psi}^{\mathcal{P}})\big|_{r_-} \end{pmatrix}, \tag{4.75}$$

where $\Phi_{\rm top}^{-1}$ and $\Phi_{\rm bot}^{-1}$ are the top and bottom $d$ rows of $\Phi^{-1}$. The complete solution is then given by Eqs. (4.64)–(4.66) with Eqs. (4.73) and (4.75).

For the modes obtained from the gauge conditions (as listed in Table 4.1), the retarded field is calculated using Eqs. (4.29), and the residual field is recovered by subtracting the puncture directly from the retarded field. (Note that the modes of the residual field are not guaranteed to satisfy the gauge conditions.)

This completes our formulation of how to solve the puncture scheme equations (4.25a) and (4.25b). Having calculated $h^{\mathcal{R}}_{i\ell m}$, the full residual field components are found from the mode-sum $\bar{h}^{\mathcal{R}}_{\alpha\beta} = \mu/r \sum_{i\ell m} a_{i\ell} \bar{h}^{\mathcal{R}}_{i\ell m} Y^{i\ell m}_{\alpha\beta} e^{-i\omega_m t}$. In the next section we will describe how we implemented this at first order and present our results.

## 4.6 Implementation and results

### 4.6.1 Computational algorithm

For the purpose of this discussion we will refer to the the $\ell = 0$ mode and the odd $\ell$, $m = 0$ modes as analytical modes. We will refer to the $m \neq 0$ modes, and the even $\ell$ $m = 0$ modes that are listed in the second column of Table 4.1 as numerical modes. We will refer to all of the modes that are listed in the third column of Table 4.1 as gauge modes. The calculation of the modes of the first-order field proceeds as follows.

- Fix the radius $r_0$ of the orbit, and set the mass of the large black hole to be $M = 1$.
- For the analytical modes, the homogeneous solutions are obtained analytically as prescribed earlier in Secs. 4.4.1 and 4.4.2.
- For each numerical mode we construct retarded boundary conditions using the ansatz in Eqs. (4.55) - (4.58). By substituting the ansatz into the homogeneous equation (4.35), we obtain recurrence relations for the coefficients. We used *Mathematica* to aid this calculation. The recurrence relations can be found in full detail in [91]. We have constructed our own recurrence relations and checked our results numerically against the expressions in [91].

- For the numerical modes we feed the expressions for the boundary conditions into a numerical C++ code. The series in the ansatz for the boundary conditions truncates automatically at $k = k^{\pm}_{\rm max}$. We determine the cutoffs $k^{\pm}_{\rm max}$ for each $\ell, m, \omega$, such that the next term in the summation has a relative magnitude less than $10^{-14}$ compared to the partial sum.

- Then for the numerical modes we solve the homogeneous equations (4.35) using an 8th-order, Runge-Kutta Prince-Dormand routine (RKPD), which can be found in the Gnu Scientific Library (GSL) repositories [92]. This is an adaptive routine. In that routine we set the absolute accuracy goal ($\epsilon_{\rm abs}$) to $10^{-16}$ and the relative accuracy goal ($\epsilon_{\rm rel}$) to $10^{-14}$. $\epsilon_{\rm abs}$ and $\epsilon_{\rm rel}$ were determined such that reducing them made no difference to our numerical results up to the 16th significant figure. We solved using outer BCs from $r_{\rm out}$ to $r_-$, and using inner BCs from $r_{\rm in}$ to $r_+$, where $r_\pm$ are the boundaries of the worldtube $\Gamma$. We set $r_\pm = r_0 \pm M$. We set the outer boundary to be $r_{\rm out} = 10^4 M$ taking into account that moving the boundary further out did not change our results for the homogeneous solutions up to the 16th significant figure. Using similar considerations we set the inner boundary to be $r_{\rm in} = 2 + 10^{-8} M$.

- For all of the modes, we construct $\hat{J}^{\rm eff}$ from the modes of $h^{\mathcal{P}1}$ given in (C.25).

- We calculate the constant vectors $a^\pm$ and $a^{\mathcal{R}}$ for the numerical and the analytical modes according to Eqs. (4.73) and (4.75), using the following method. We invert the $\hat{\Phi}(r)$ matrix using the LU-decomposition method and compute $\hat{\Phi}^{-1}(r)\hat{J}^{\rm eff}(r)$ at every value of $r$, on a grid between $r_-$ and $r_+$. We found that we required a grid-separation of $10^{-3}$, in order to evaluate the integrals in (4.73) and (4.75) accurately. We found that reducing the grid-separation did not alter the result for these integrals up to machine precision. We calculate these integrals using a routine based on Simpson's rule.

- For the analytical and the numerical modes, we calculate the retarded field directly, in the regions to the left and right of $\Gamma$ using Eqs. (4.64) and (4.65), respectively. Inside $\Gamma$ we calculate the residual field using (4.66), evaluating the integral as described above, and adding the modes of the puncture to obtain the full retarded field.

- For the gauge modes, we calculate the retarded field in all regions from the gauge conditions (4.29). Whilst at every stage of this algorithm it sufficed to use double precision variables, when it came to computing the gauge modes we encountered siginificant numerical errors, in particular in the region close to $r_{\rm in}$. We established that this was due to subtracting one large number from another in the gauge conditions (4.29), for which more digits beyond double precision were required. We found that using long double variables to compute those modes resolved this issue and gave accurate results.

- We run a self-consistency check on our solutions by checking that the matching condition (4.67) holds at the tube boundaries.

The monopole mode requires some additional consideration. Physically, this spherically-symmetric mode describes the perturbation in the mass of the Schwarzschild background. More precisely, the perturbed geometry $g + h^{\text{monopole}}$ at $r < r_0$ is Schwarzschild with a certain mass $M + \delta M_<$, and the perturbed geometry at $r > r_0$ is again Schwarzschild, with a different mass $M + \delta M_>$. It can be shown that the mass difference is simply the geodesic energy of the particle: $\delta M_> - \delta M_< = \mu\mathscr{E}$.

Now, the Lorenz-gauge solution constructed as above, which is regular both at the horizon and at infinity (and anywhere else) was first derived by Berndtson in [93]. It can be shown (most easily by applying the Abbott-Deser conserved-integral formulation as explained in Ref. [65]) that, for Berndtson's solution,

$$\delta M_> = \frac{\mu\mathscr{E}\,(r_0 - 3M)}{(r_0 - 2M)}, \qquad r > r_0, \tag{4.76a}$$

$$\delta M_< = \mu\mathscr{E}\left[\frac{(r_0 - 3M)}{(r_0 - 2M)} - 1\right], \qquad r < r_0. \tag{4.76b}$$

Historically, a different monopole solution has typically been used, in which

$$\delta M_> = \mu\mathscr{E}, \qquad r > r_0, \tag{4.77a}$$

$$\delta M_< = 0, \qquad r < r_0. \tag{4.77b}$$

In this more commonly used solution, the only mass in the perturbation is the mass-energy of the particle. Unfortunately, the metric perturbation in this solution is not asymptotically flat, but rather one of its components tend to a constant. This choice of monopole leads to a poorly behaved, very slowly decaying second-order source. While most people use this solution, in this work we use the former, asymptotically flat solution, because otherwise the second-order source would behave badly at infinity.

We wish to highlight that the solution which contains mass inside the orbit remains a physical solution. We may interpret it as a re-definition of the mass of the background, $M$. Whereas in the solution satisfying Eq. (4.77), $M$ is identified with the central BH's mass, $M_{BH}$, we can redefine the background mass as $M = M_{BH} - \delta M_<$. This just corresponds to redistributing the total mass of the system between the background metric, $g$, and the perturbation metric, $h$. An alternative interpretation is that instead of looking at a specific binary with a fixed black-hole and perturbation mass, rather we are describing a family of binaries, each with a different black-hole and perturbation mass. As such, going from the solution satisfying (4.77), to the solution satisfying (4.76), corresponds to switching from a binary with masses $\mu$ and $M$ to a different binary with masses $\mu$ and $M + \delta M_<$.

### 4.6.2 Results

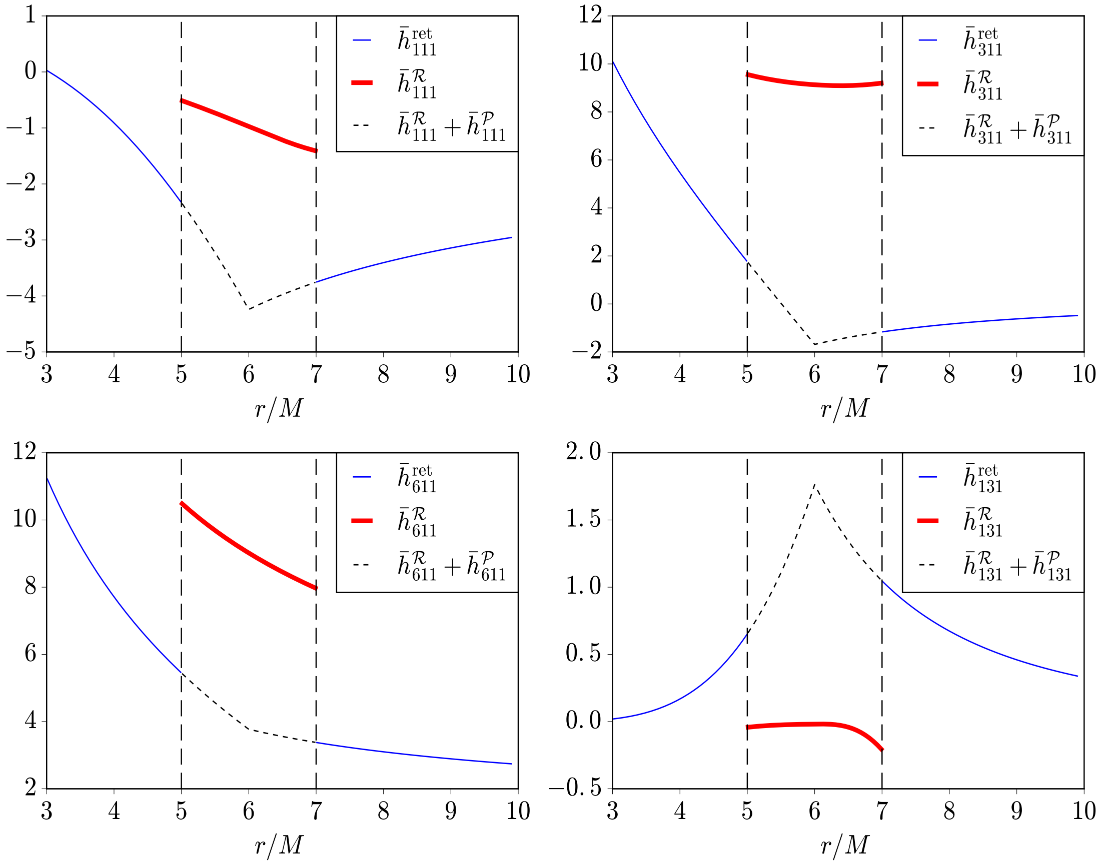


Figure 4.2: Modes of the first-order retarded and residual fields, for a particle in a circular orbit, with radius $r_0 = 6M$. At the boundaries of the worldtube, at $r_+ = r_0 + M$ and $r_- = r_0 - M$, the plots show that $\bar{h}^{\mathcal{R}}_{i\ell m} + \bar{h}^{\mathcal{P}}_{i\ell m} = \bar{h}^{\rm ret}_{i\ell m}$. At the particle, $\bar{h}^{\rm ret}_{i\ell m}$ is nondifferentiable whereas $\bar{h}^{\mathcal{R}}_{i\ell m}$ is smooth there.

We have performed numerous checks of our results. Fig. 4.2 shows the agreement between $\bar{h}^{\rm ret}_{i\ell m}$ and $\bar{h}^{\mathcal{R}}_{i\ell m} + \bar{h}^{\mathcal{P}}_{i\ell m}$ at the boundaries of the worldtube, at $r_\pm = r_0 \pm M$. The plots also show that while $\bar{h}^{\rm ret}_{i\ell m}$ is nondifferentiable at the particle, $\bar{h}^{\mathcal{R}}_{i\ell m}$ is differentiable everywhere within the worldtube.

Fig. 4.3 shows plots for a selection of modes for larger values of $r$. For the stationary $(m = 0)$ modes there are no oscillations, as to be expected, while the periodic behaviour of the $m \neq 0$ modes can be seen in the wave zone at large $r$. For the $i = 3$ non-stationary modes, we note a $1/r$ decay, unlike the other $i$ modes. This is a direct consequence of the gauge condition (4.29a). $\bar{h}_{3\ell m} = h_{6\ell m}$, which is proportional to $r^2\Omega^{AB}h_{AB}$ at large $r$. So we may interpret the $1/r$ decay of the $\bar{h}_{3\ell m}$ modes as indicating that the correction to the surface area of the two-sphere falls off relative quickly at large $r$, or in other words the background coordinate $r$ approaches the physical areal radius relatively quickly.

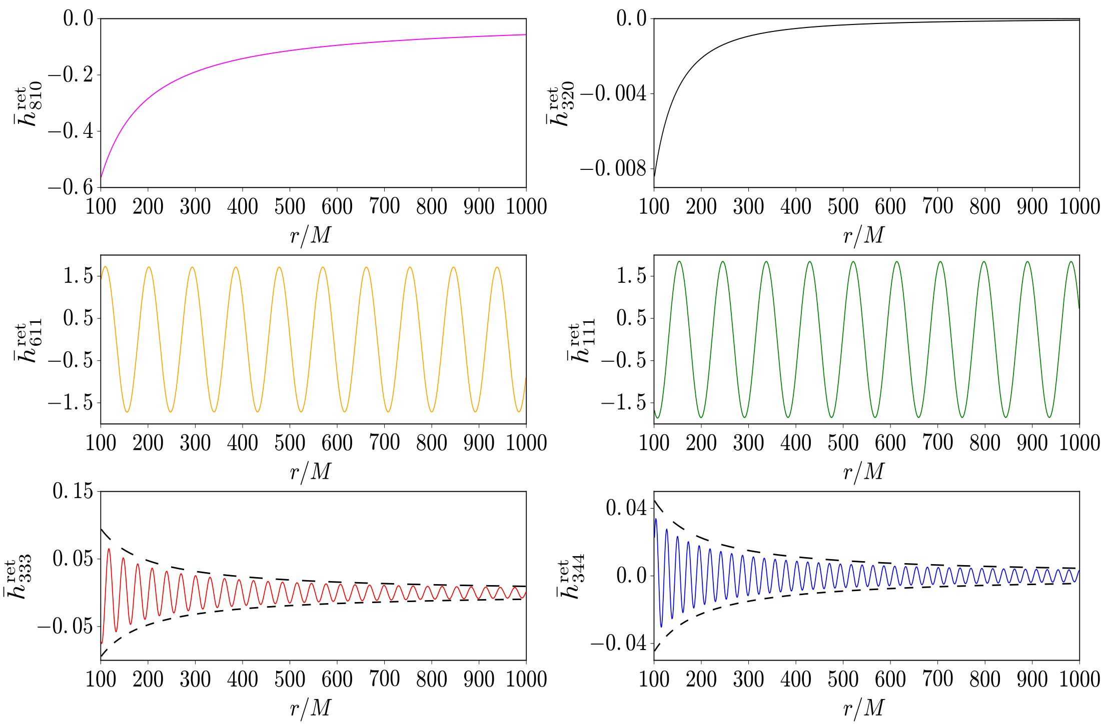


Figure 4.3: Sample of results for the modes of the first-order field, for $100M \leq r \leq 1000M$, using the same parameters as in Fig. 4.2. Our results show that stationary ($m = 0$) modes have no waves. Non-stationary modes exhibit wave behaviour at sufficiently large values of $r$, in line with the boundary conditions imposed at $r_{\rm out}$. The dashed line in the bottom two plots is const./$r$. For $i = 3$ the modes decay as $1/r$.

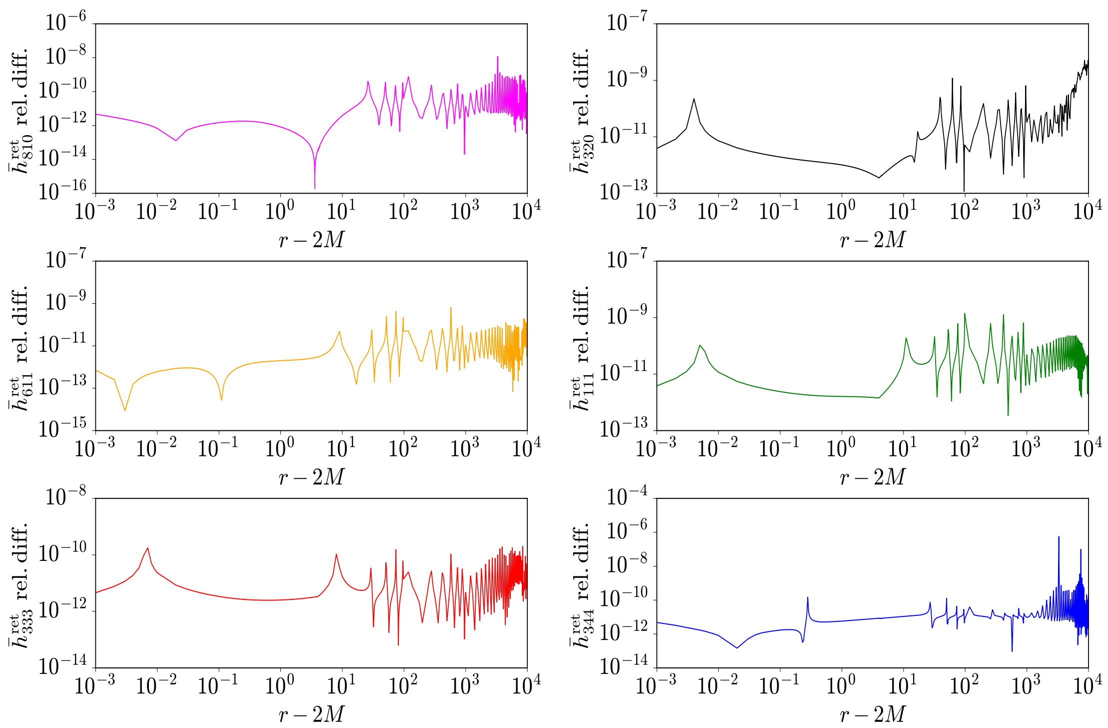


Figure 4.4: Relative difference between the retarded field modes computed in this work and data provided by Warburton, for a Schwarzschild circular orbit at radius $r_0 = 6M$.

We have compared our numerical results for the retarded-field with Warburton and Wardell [74], and found a relative difference of between $10^{-13}$ and $10^{-9}$, as shown in Figs. 4.4.

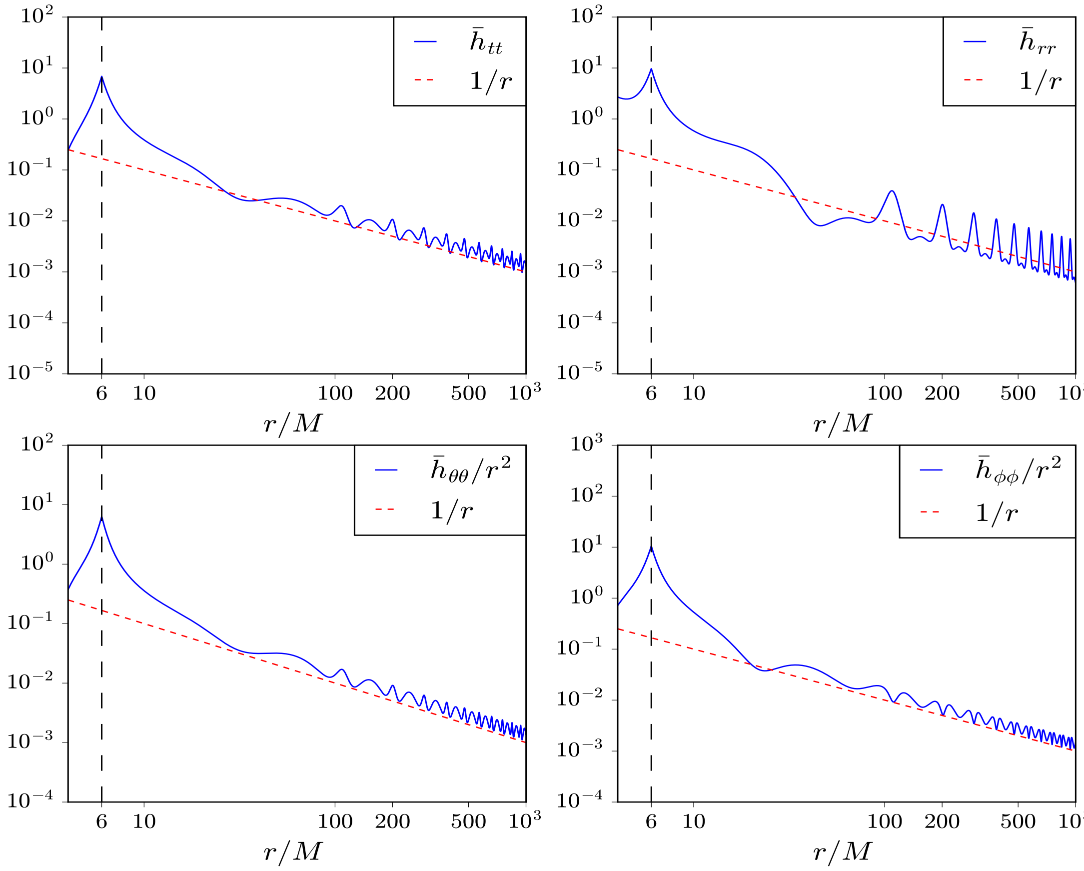


Figure 4.5: Plots of the full retarded field, according to the metric reconstruction formula (4.24), in the equatorial plane for a circular orbit of radius $r_0 = 6M$, on a log-log scale. The vertical, dashed line indicates the location of the radius of the orbit, at $r = r_0$. The field is evaluated at $\theta = \pi/2$ and $\varphi = \Omega t$.

Fig. 4.5 shows the diagonal components of $\bar{h}^{\rm ret}_{\mu\nu}$, as calculated using the metric reconstruction formula (4.24), for a circular orbit of radius $r_0 = 6M$. The field falls off as $1/r$ at large $r$, and oscillations can be seen for $r \gtrsim 100M$. Sufficiently far away from the particle, the mode sum in (4.24) converges fast enough to accurately approximate the components of the field. But moving closer to the particle, the field gets larger and the convergence becomes slower and slower. The mode sum approximates the field less accurately as we approach the particle and the divergence at the particle itself cannot be seen in Fig. 4.5, due to this arbitrarily slow convergence.

As a key test of our implementation, we have assessed the large-$\ell$ behaviour of the residual field on the worldline. The $\ell$ modes of $\bar{h}^{\mathcal{R}}_{\mu\nu}$ are given by

$$\bar{h}^{\mathcal{R}\ell}_{\mu\nu}(z) = \frac{\mu}{r_0} \sum_{m=-\ell}^{\ell} \sum_{i=1}^{10} a_{i\ell}\, Y^{i\ell m}_{\mu\nu}(\theta = \pi/2, \varphi = \Omega t, r_0)\; e^{-im\omega_m t}\, \bar{h}^{\mathcal{R}}_{i\ell m}(r_0). \tag{4.78}$$

| $r_0/M$ | this work | Berndston [93] | rel. diff. |
|---|---|---|---|
| 6 | $4.9685669(5) \times 10^{-2}$ | $4.9685669 \times 10^{-2}$ | $< 10^{-7}$ |
| 10 | $1.7454613(7) \times 10^{-2}$ | $1.7454613 \times 10^{-2}$ | $< 10^{-7}$ |

Table 4.2: Results for the radial component of the first-order self-force, for circular orbits in a Schwarzschild background. Our results were calculated with $\ell_{\max} = 50$, using the punctures that include terms through $O(\lambda^2)$ in powers of distance to the worldline. Numerals in parentheses show estimates for numerical error.

The more accurately the puncture approximates the singular field, the smoother the residual field becomes, and therefore the more quickly its mode sum converges. On the particle, the $\ell$ modes behave as [88]

$$\bar{h}^{\mathcal{R}\ell}_{\mu\nu}(z) \sim \ell^{-2\lfloor(k+1)/2\rfloor}, \tag{4.79}$$

where $k$ is the total number of orders of distance in the puncture, and $\lfloor s \rfloor$ denotes the largest integer less than or equal to $s$. Our puncture includes four of orders of distance, ranging from $O(1/\lambda)$ to $O(\lambda^2)$. Hence, $k = 4$, and we expect $\bar{h}^{\mathcal{R}\ell}_{\mu\nu}(z)$ to fall off at least as fast as $1/\ell^4$. With the residual field in hand, we can compute the self-force using Eq. (2.59), with $h^{1\mathrm{R}}$ replaced with $h^{1\mathcal{R}}$. We add the contribution from $\ell > \ell_{\max}$ by fitting a power-law tail $A/\ell^4 + B/\ell^6 + C/\ell^8 + D/\ell^{10}$ to the numerical data. In Table. 4.2 we give our results for the radial component of the self-force at a variety of orbital radii. We find agreement with the results of Berndtson [93] to a relative accuracy of $10^{-7}$. We found that our largest source of error was the value of $\ell_{\max}$, i.e. the number of modes included in the mode sum (4.78), and the number of terms in the formula for the tail. We found that for $\ell_{\max} \geq 30$ our final value did not change up to seven significant figures.

Fig. 4.6 shows plots of the $\ell$-modes of the non-vanishing components of $\bar{h}^{\mathcal{R}\ell}_{\mu\nu}(z)$, as given by Eq. (4.78). $\bar{h}^{\mathcal{R}\ell}_{tt}$, $\bar{h}^{\mathcal{R}\ell}_{rr}$, $\bar{h}^{\mathcal{R}\ell}_{\theta\theta}$, $\bar{h}^{\mathcal{R}\ell}_{t\varphi}$ and $\bar{h}^{\mathcal{R}\ell}_{\varphi\varphi}$ decay like $1/\ell^4$, whereas $\bar{h}^{\mathcal{R}\ell}_{tr}$ and $\bar{h}^{\mathcal{R}\ell}_{r\varphi}$ fall off exponentially with $\ell$. This exponential decay relates to the puncture either vanishing for these components, or being time-antisymmetric for these components.

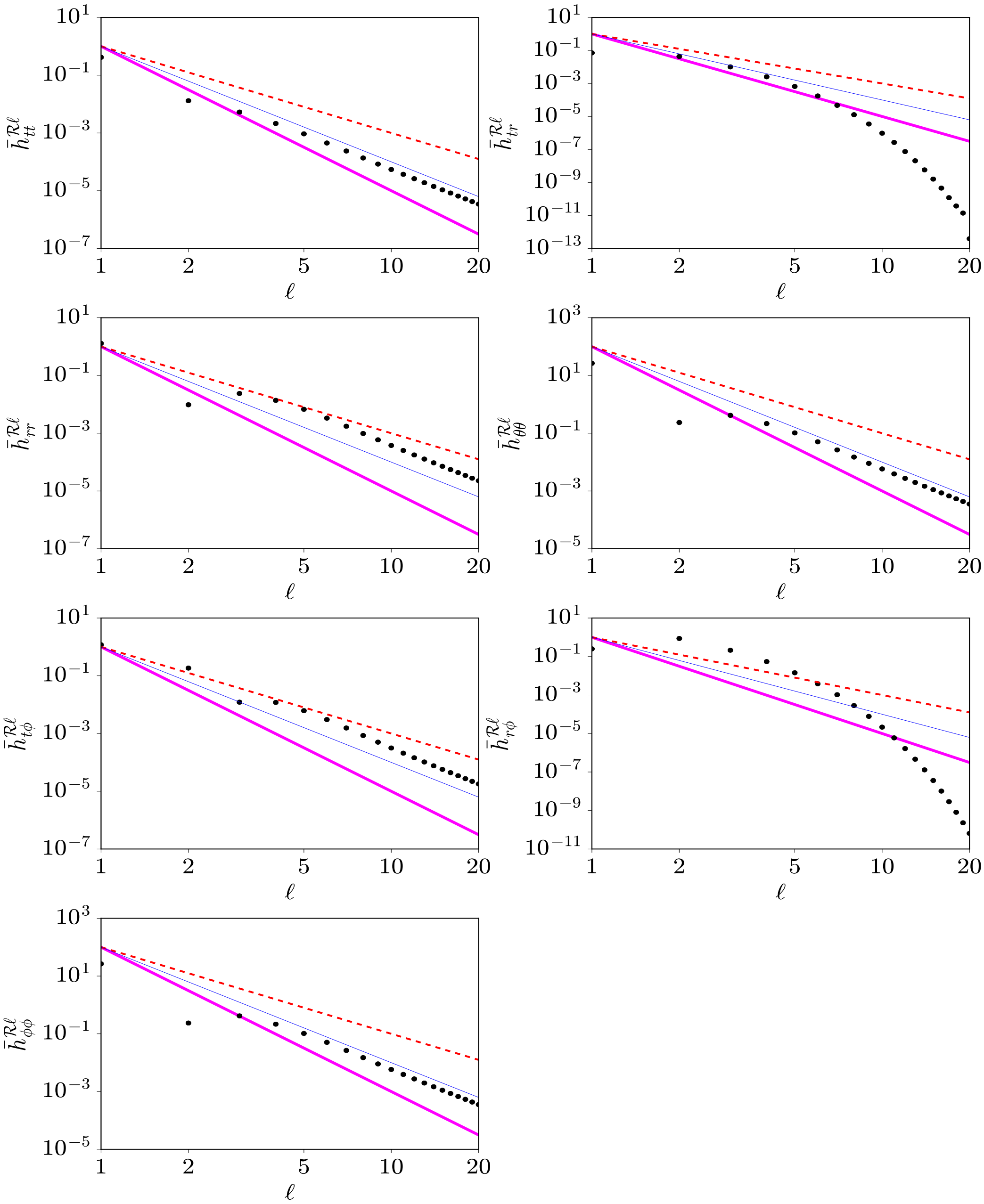


Figure 4.6: Plots of the non-vanishing components of $\bar{h}^{\mathcal{R}\ell}_{\mu\nu}(z)$ versus $\ell$, according to Eq. (4.78), for a circular orbit of radius $r_0 = 6M$, plotted on a log-log scale. The dots show $\bar{h}^{\mathcal{R}\ell}_{\mu\nu}(z)$ from $\ell = 1 - 20$, the dashed line is $1/\ell^3$, the solid (thin) line is $1/\ell^4$ and the solid (thick) line is $1/\ell^5$.

# Chapter 5

# Second-order perturbation theory in a scalar-field toy model: the problem of infinite mode coupling

While the first-order equation has been solved numerically without too much trouble, there are several obstacles standing in the way of us solving the second order equation. The first issue, which is addressed in this chapter, is that very near the worldline a large number of modes of the first-order field are required to accurately calculate a single mode of the second-order source. These findings are covered in our paper [2], together with a strategy for resolving the problem. The second issue is that the large-$r$ behaviour of the source prevents the retarded integral from converging. The following chapter gives a detailed overview of this issue and how it is resolved, based on the findings of Ref. [75].

To introduce the problem, we refer back to the Einstein equations through second order given in Eqs. (3.2) and (3.3). Following the approach described in Sec. 4.2, we reduce the 4D-field equations into a one-dimensional system by decomposing the fields into a basis of harmonics, as in Eq. (4.14). The field equations at each $i\ell m$-mode read

$$E_{i\ell m}[h^1] = 8\pi T^1_{i\ell m}, \tag{5.1}$$

$$E_{i\ell m}[h^2] = -\delta^2 R_{i\ell m}[h^1, h^1]. \tag{5.2}$$

For the purposes of this discussion, we can continue to neglect the inspiral of the orbit and work with the frequency spectrum of the circular geodesic. Now consider the source term $\delta^2 R_{i\ell m}$. Substituting the expansion (4.14) into $\delta^2 R_{\mu\nu}$ leads to a mode-coupling formula with the schematic form

$$\delta^2 R_{i\ell m} = \sum_{\substack{i_1\ell_1 m_1\\ i_2\ell_2 m_2}} \mathscr{D}^{i_1\ell_1 m_1 i_2\ell_2 m_2}_{i\ell m}[h^1_{i_1\ell_1 m_1}, h^1_{i_2\ell_2 m_2}], \tag{5.3}$$

where $\mathscr{D}^{i_1\ell_1m_1i_2\ell_2m_2}_{i\ell m}$ is a bilinear differential operator (given explicitly in Ref. [94]). A single mode $\delta^2 R_{i\ell m}$ is an infinite sum over first-order modes $h^1_{i\ell m}$. If $h^1_{i\ell m}$ falls off sufficiently rapidly with $\ell$, then the summation poses no problem. However, if $h^1_{i\ell m}$ falls off slowly with $\ell$, then the summation is potentially intractable. This is precisely the situation near the point-particle singularity in Eq. (5.1). $h^1_{\mu\nu}$ behaves approximately as a Coulomb field, blowing up as $\sim 1/\rho$, where $\rho$ is a spatial distance from the particle, as we saw in (2.47). The individual modes $h^1_{ilm}Y^{ilm}_{\mu\nu}$, after summing over $m$, then go as $\sim l^0$ on the particle [74, 95], not decaying at all; at points *near* the particle, the decay is arbitrarily slow.

This behaviour can be understood from the textbook example of a Coulomb field $\phi$ in flat space. For a static charged particle at radius $r_0$, the field's modes behave as $\phi_{\ell m}Y_{\ell m} \sim r^\ell_</r^{\ell+1}_>$, where $r_< \equiv \min(r_0, r)$ and $r_> \equiv \max(r_0, r)$. On the particle, where $r = r_0$, we have $\phi_{\ell m}Y_{\ell m} \sim \ell^0$. At any point $r \neq r_0$, we have exponential decay with $\ell$, but that decay is arbitrarily slow when $r \approx r_0$. Extrapolating this behaviour to the gravitational case (5.3), we can infer that unless the coupling operator $\mathscr{D}^{i_1\ell_1m_1i_2\ell_2m_2}_{i\ell m}$ introduces rapid decay (which it does not), we are faced with the following tenuous position: *to obtain a single mode of the second-order source near the particle, we must sum over an arbitrarily large number of first-order modes.*

In this chapter, we explicate this problem and present a robust, broadly applicable method of surmounting it. Rather than facing the full gravitational field equations (5.1)–(5.2) head-on, we use a simplified toy-model set of field equations introduced in Ref. [75], whose second-order source is designed to exhibit the same behaviour as the second-order gravitational source. The toy-model equations describe first- and second-order scalar fields, constructed in Minkowski spacetime as

$$\Box\phi^1 = -4\pi\varrho \equiv S^{(1)}, \tag{5.4}$$

$$\Box\phi^2 = t^{\alpha\beta}\partial_\alpha\phi^{(1)}\partial_\beta\phi^{(1)} \equiv S^{(2)}. \tag{5.5}$$

Here, in Cartesian coordinates $(t, x^i)$, $\Box = -\partial_t^2 + \partial^i\partial_i$ is the flat-space d'Alembertian,

$$\varrho \equiv \int_\gamma \frac{\delta^4(x - z(\tau))}{\sqrt{-g}} d\tau = \frac{\delta(x^i - x^i_p)}{dt/d\tau} \tag{5.6}$$

is a point charge distribution moving on a worldline $x^\mu_p(t) = (t, x^i(t))$ with proper time $\tau$, and $t^{\mu\nu} \equiv \mathrm{diag}(1, 1, 1, 1)$. With our chosen source terms, the first-order field $\phi^{(1)}$ mimics the behaviour of $h^1_{\mu\nu}$, and the second-order source $S^{(2)}$ mimics the behaviour of $\delta^2 R_{ilm}$.

Like Eq. (5.2), Eq. (5.5) is well defined only at points off the worldline. To solve it globally, one would have to rewrite it as

$$\Box\phi^{(2)\mathcal{R}} = S - \Box\phi^{(2)\mathcal{P}} = t^{\alpha\beta}\partial_\alpha\phi^{(1)}\partial_\beta\phi^{(1)} - \Box\phi^{(2)\mathcal{P}}, \tag{5.7}$$

where here, and for the rest of this chapter, we drop the superscript on $S^{(2)}$ and use $S$ instead to refer to the toy-model second-order source. $\phi^{(2)\mathcal{P}}$ is an analytically determined, singular "puncture" that guarantees the total field has the correct physical behaviour near the particle as described in Sec. 3.1, and $\phi^{(2)\mathcal{R}} \equiv \phi^{(2)} - \phi^{(2)\mathcal{P}}$is the regular "residual" difference between the total field and the puncture. However, here we only wish to address the preliminary question: *given the spherical harmonic modes of $\phi^{(1)}$, how can we accurately compute the modes of $S$?* Once that question is answered, the same method can be carried over directly to the gravitational case to compute the source $\delta^2 R_{i\ell m}$, and Eq. (5.2) can then be solved via a puncture scheme of the sort described in Secs. 3.1 and 4.5.

Before describing the technical details of our computations, we summarize the problem, our strategy for overcoming it, and our successful application of that strategy. For simplicity, we fix the particle on a circular orbit of radius $r_0$. The modes $\phi^{\rm ret}_{\ell m}$ of the first-order retarded field are then easily found; they are given by Eqs. (5.15) and (5.16). (To streamline the notation, we shall omit the subscript "(1)" on first-order fields.) From those modes, one can naively attempt to compute the modes $S_{\ell m}$ of the source using an analog of Eq. (5.3), given explicitly by Eq. (5.31) below. Figure 5.1 shows the failure of this direct computation in the case of the monopole mode $S_{00}$. Although the convergence is rapid at points far from the particle, it becomes arbitrarily slow near the particle's radial position $r_0$. In principle, this obstacle could be overcome with brute force, simply adding more modes until we achieve some desired accuracy at some desired nearest point to the particle. However, that relies on having all the modes of the retarded field at hand; in the first-order computation described in Chapter 4, the retarded field modes are found numerically, and the number of modes is limited by practical computational demands. Hence, we should rephrase the question from the previous paragraph: given the spherical harmonic modes of $\phi^{(1)}$ *up to some maximum* $\ell = \ell_{\max}$, how can we accurately compute the modes of $S$?

Our answer to this question is to utilize a 4D approximation to the point-particle singularity. As discussed in Sec. 2.3, the retarded field of a point particle can be split into two pieces as $\phi^{\rm ret} = \phi^{\rm S} + \phi^{\rm R}$, where $\phi^{\rm S}$ is the singular field, which is a particular solution to Eq. (5.4), and $\phi^{\rm R}$ is the corresponding regular field, which is a smooth solution to $\Box\phi^{\rm R} = 0$. The Detweiler-Whiting split [49] used here is the precise analog of the ones defined for the EM and gravity cases in the introduction. This is the same singular-regular split found in Eq. (1.36) of the metric perturbation, described in the introductory section 1.2.5. The slow falloff of $\phi^{\rm ret}_{\ell m}$ with $\ell$ is entirely isolated in the modes of the singular field, $\phi^{\rm S}_{\ell m}$; because $\phi^{\rm R}$ is smooth, its modes $\phi^{\rm R}_{\ell m}$ have a uniform exponential falloff with $\ell$. Generally, there is no way to obtain a closed-form expression for $\phi^{\rm S}$, but we *can* easily obtain a local expansion of $\phi^{\rm S}$ in powers of distance from the particle (i.e. powers of $\lambda$ using the notation introduced in Chapter 3). A truncation of that expansion at some finite order of $\lambda$ provides a puncture, which we denote by

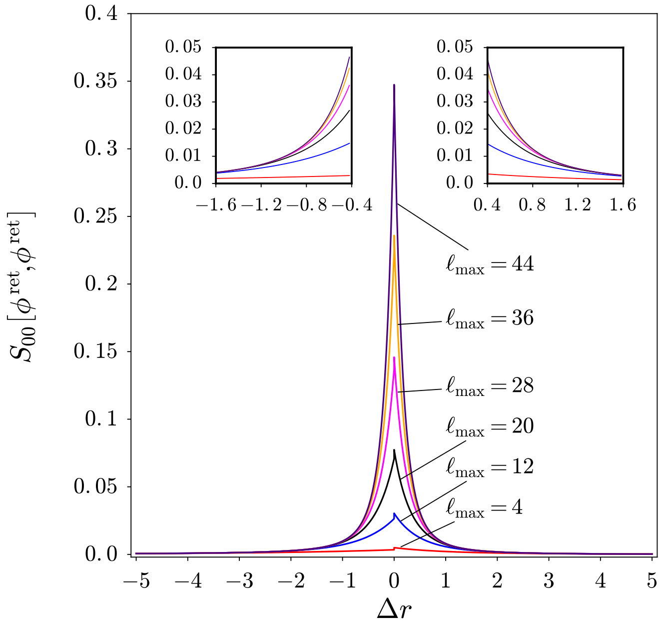


Figure 5.1: The source mode $S_{00}[\phi^{\rm ret},\phi^{\rm ret}]$ as a function of $\Delta r \equiv r - r_0$, with an orbital radius $r_0 = 10$, as computed from the mode-coupling formula (5.31). To assess the convergence of the sum in Eq. (5.31), we truncate the first-order field modes $\phi_{\ell m}$ at a maximum $\ell$ value $\ell_{\rm max}$, and we display the behaviour of $S_{00}$ for various values of $\ell_{\rm max}$. The insets show that far from the particle, the sum converges rapidly with $\ell_{\rm max}$. However, near the particle there is no evidence of numerical convergence.

$\phi^{\mathcal{P}}$; it is given explicitly by Eq. (5.22) below. It defines a residual field $\phi^{\mathcal{R}} \equiv \phi^{\rm ret} - \phi^{\mathcal{P}}$ that approximates $\phi^{\rm R}$. We make use of all this by writing the source in the suggestively quadratic form $S[\phi,\phi]$, and in some region near the particle, splitting the field into the two pieces $\phi^{\mathcal{P}} + \phi^{\mathcal{R}}$. An $\ell m$ mode of $S$ can then be written as

$$S_{\ell m} = S_{\ell m}[\phi^{\mathcal{R}},\phi^{\mathcal{R}}] + 2S_{\ell m}[\phi^{\mathcal{R}},\phi^{\mathcal{P}}] + S_{\ell m}[\phi^{\mathcal{P}},\phi^{\mathcal{P}}]. \tag{5.8}$$

The first two terms, $S_{\ell m}[\phi^{\mathcal{R}},\phi^{\mathcal{R}}]$ and $S_{\ell m}[\phi^{\mathcal{R}},\phi^{\mathcal{P}}]$, can be computed from the modes of $\phi^{\mathcal{R}}$ and $\phi^{\mathcal{P}}$ using Eq. (5.31); for sufficiently smooth $\phi^{\mathcal{R}}$, the convergence will be sufficiently rapid. The problem of slow convergence is then isolated in the third term, $S_{\ell m}[\phi^{\mathcal{P}},\phi^{\mathcal{P}}]$. This term cannot be accurately computed from the modes of $\phi^{\mathcal{P}}$. However, $S[\phi^{\mathcal{P}},\phi^{\mathcal{P}}]$ *can* be computed in 4D using the 4D expression for $\phi^{\mathcal{P}}$. Its modes $S_{\ell m}[\phi^{\mathcal{P}},\phi^{\mathcal{P}}]$ can then be computed directly, without utilizing the mode-coupling formula (5.31), simply by integrating the 4D expression against a scalar harmonic.

Our strategy is hence summarized as follows:

1. compute the modes $\phi^{\mathcal{P}}_{\ell m}$ by direct integration of the 4D expression (5.40). From the result, and Eqs. (5.15)–(5.16), compute the modes $\phi^{\mathcal{R}}_{\ell m} = \phi^{\rm ret}_{\ell m} - \phi^{\mathcal{P}}_{\ell m}$

2. evaluate $S_{\ell m}[\phi^{\mathcal{R}}, \phi^{\mathcal{R}}]$ and $S_{\ell m}[\phi^{\mathcal{R}}, \phi^{\mathcal{P}}]$ using the mode-coupling formula (5.31)

3. evaluate $S[\phi^{\mathcal{P}}, \phi^{\mathcal{P}}]$ in 4D, using Eq. (5.40), and obtain its modes $S_{\ell m}[\phi^{\mathcal{P}}, \phi^{\mathcal{P}}]$ by direct integration

4. combine these results in Eq. (5.8).

This strategy is to be applied in some region around $r = r_0$; outside that region, one may simply use the retarded modes in Eq. (5.31) without difficulty.

Figure 5.2 displays a successful implementation of this strategy. The true source mode $S_{00}$, as computed via our strategy, is shown in thick solid blue. The same mode $S_{00}$ as computed via mode coupling from $\phi^{\rm ret}_{\ell m}$, with a finite $\ell_{\max} = 20$, is shown in thin solid grey. As we can see, the two results agree far from the particle, where the source mode as computed via mode coupling has converged. But near the particle, the results differ by an arbitrarily large amount; the true source correctly diverges at $r = r_0$, due to the singularity in the first-order field, while the source computed via mode coupling remains finite due to the truncation at finite $\ell_{\max}$.

In the remaining sections of this chapter, we describe the technical details of our strategy, as well as the challenges that arise in implementing it. Section 5.1 summarizes the various relevant fields—retarded and advanced, singular and regular, puncture and residual. Section 5.2 derives the coupling formula that expresses a second-order source mode $S_{\ell m}$ as a sum over first-order field modes. Section 5.3 details the computation of $S_{\ell m}[\phi^{\mathcal{R}}, \phi^{\mathcal{R}}]$ and $S_{\ell m}[\phi^{\mathcal{R}}, \phi^{\mathcal{P}}]$; Sec. 5.4, the computation of $S_{\ell m}[\phi^{\mathcal{P}}, \phi^{\mathcal{P}}]$. In Sec. 5.5, we reiterate the outline of our strategy as it applies to the gravitational case; the successful application to gravity will be shown in Chapter 8.

To avoid repetition, we state in advance that all plots are for a particle at radius $r_0 = 10$.

## 5.1 First-order fields

### 5.1.1 Retarded and advanced solutions

To begin, we work in spherical polar coordinates $(t, r, \theta^A)$, where $\theta^A \equiv (\theta, \varphi)$. We place the particle on the equatorial circular orbit $x^\mu_p(t) = (t, r_0, \pi/2, \Omega t)$ with normalized four-velocity $u^\mu = (1-r_0^2\Omega^2)^{-1/2}(1, 0, 0, \Omega)$, and we adopt a Keplerian frequency $\Omega = \sqrt{1/r_0^3}$. The point source (5.6) can then be expanded in spherical and frequency harmonics by rewriting it as

$$\varrho = \frac{\delta(r - r_p)}{r^2 u^t} \sum_{\ell m} Y^*_{\ell m}(\theta^A_p) Y_{lm}(\theta^A) \tag{5.9}$$

and using $Y^*_{\ell m}(\theta^A_p) = e^{-im\Omega t} Y_{\ell m}(\pi/2, 0)$. Here $u^t = \frac{dt}{d\tau} = (1 - r_0^2\Omega^2)^{-1/2}$.

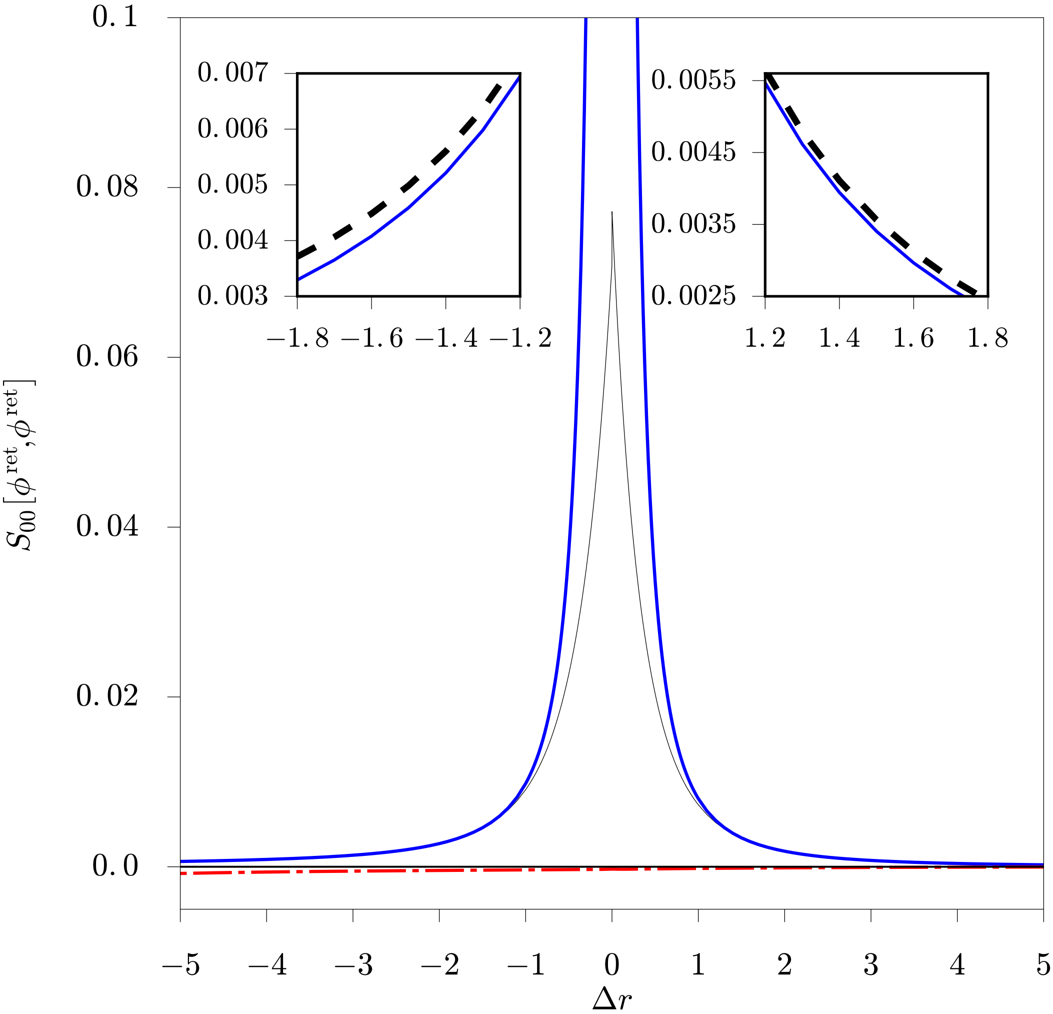


Figure 5.2: The source mode $S_{00}[\phi^{\rm ret}, \phi^{\rm ret}]$ as computed with the strategy outlined in the text. The dot-dashed red curve shows the contribution from $S_{00}[\phi^{\mathcal{R}}, \phi^{\mathcal{R}}] + 2S_{00}[\phi^{\mathcal{R}}, \phi^{\mathcal{P}}]$, the dashed black curve shows the contribution from $S_{00}[\phi^{\mathcal{P}}, \phi^{\mathcal{P}}]$, and the thick solid blue curve shows their sum $S_{00}[\phi^{\rm ret}, \phi^{\rm ret}]$, which diverges at $\Delta r = 0$. On the scale of the main plot, $S_{00}[\phi^{\mathcal{P}}, \phi^{\mathcal{P}}]$ is indistinguishable from $S_{00}[\phi^{\rm ret}, \phi^{\rm ret}]$; the insets show that they differ by a small, but distinguishable amount, which is made up by $S_{00}[\phi^{\mathcal{R}}, \phi^{\mathcal{R}}]+2S_{00}[\phi^{\mathcal{R}}, \phi^{\mathcal{P}}]$. For comparison, the thin grey curve displays the result for $S_{00}[\phi^{\rm ret}, \phi^{\rm ret}]$ as computed from the mode-coupling formula (5.31), which agrees with the correct result far from the particle but differs strongly from it near the particle. All curves were generated with $r_0 = 10$, all four orders in the puncture (5.22), and $\ell_{\rm max} = 20$.

Most of the fields we are interested in can be constructed by integrating this source against a Green's function. The retarded and advanced Green's functions satisfying $\Box G(x, x') = -4\pi\delta^4(x - x')$ are given by

$$G^{\rm ret/adv}(x, x') = \frac{\delta(t - t' \mp |\vec{x} - \vec{x}'|)}{|\vec{x} - \vec{x}'|}, \tag{5.10}$$

where $\vec{x}$ is a Cartesian three-vector. The Fourier transforms, $G_\omega^{\rm ret/adv} = \int e^{i\omega(t-t')}G^{\rm ret/adv}(x,x')dt$, are

$$G_\omega^{\rm ret/adv} = \frac{e^{\pm i\omega|\vec{x}-\vec{x}'|}}{|\vec{x}-\vec{x}'|}, \tag{5.11}$$

which can be expanded in spherical harmonics as

$$G_\omega^{\rm ret/adv} = \mp i \sum_{\ell m} \omega j_\ell(\omega r_<) h_\ell^{(1,2)}(\omega r_>) Y^*_{\ell m}(\theta^{A'}) Y_{\ell m}(\theta^A). \tag{5.12}$$

Here the upper sign and $h_\ell^{(1)}$ correspond to the retarded solution, and the lower sign and $h_\ell^{(2)}$ to the advanced. $h_\ell^{(1)}$ and $h_\ell^{(2)}$ are the spherical Hankel functions of the first and second kind, $j_\ell$ is the spherical Bessel function of the first kind, and when used in the Green's function, $r_\lessgtr \equiv \min/\max(r,r')$. In the static limit $\omega \to 0$, the retarded and advanced Green's functions both reduce to

$$G^{\rm ret/adv} = \frac{1}{|\vec{x}-\vec{x}'|} = \sum_{\ell m} \frac{1}{2\ell+1} \frac{r_<^\ell}{r_>^{\ell+1}} Y^*_{\ell m}(\theta^{A'}) Y_{\ell m}(\theta^A). \tag{5.13}$$

Integrating against these Green's functions, we find the retarded and advanced solutions

$$\phi^{\rm ret/adv} = \sum_{\ell m} \phi_{\ell m}^{\rm ret/adv}(r) e^{-im\Omega t} Y_{\ell m}(\theta^A), \tag{5.14}$$

where

$$\phi_{\ell m}^{\rm ret/adv} = \pm \frac{4\pi i}{u^t} N_{\ell m} m\Omega j_\ell(m\Omega r_<) h_\ell^{(1,2)}(m\Omega r_>) \tag{5.15}$$

for $m \neq 0$, and

$$\phi_{\ell 0}^{\rm ret/adv} = \frac{4\pi}{u^t} \frac{N_{l0}}{2\ell+1} \frac{r_<^\ell}{r_>^{\ell+1}} \tag{5.16}$$

for $m = 0$. Here

$$N_{\ell m} \equiv Y_{\ell m}(\pi/2, 0) \tag{5.17}$$

and we have reverted to the previous notation $r_\lessgtr \equiv \min/\max(r, r_0)$.

As discussed in the introduction to this chapter, the large-$\ell$ behaviour of these fields is the source of the infinite-coupling problem. Noting that $N_{\ell 0} \sim \ell^0$, we see that the stationary modes in Eq. (5.16) behave as $\phi_{\ell 0} \sim \frac{1}{\ell}\frac{r_<^\ell}{r_>^{\ell+1}}$. Hence, $\phi_{\ell 0}$ decays exponentially with $\ell$ at points far from $r = r_0$, still exponentially but more slowly at points close to $r = r_0$, and as $\ell^{-1}$ at $r = r_0$. The oscillatory, $m \neq 0$ modes exhibit similar behaviour, although it is not obvious from Eq. (5.15). After summing $\phi_{\ell m} Y_{\ell m}$ over $m$, the large-$\ell$ behaviour becomes $\sim \ell^0$ on the particle, with an exponential but arbitrarily weak suppression at points slightly off the particle. The quantitative consequences of this, already displayed in Fig. 5.1, will be spelled out in later sections.

### 5.1.2 Singular and regular fields

In flat space, the Detweiler-Whiting singular field is simply $\phi^{\rm S} \equiv \frac{1}{2}(\phi^{\rm ret} + \phi^{\rm adv})$. Its four-dimensional form can be written as

$$\phi^{\rm S} = \frac{1}{2}\int [G^{\rm ret}(x,x') + G^{\rm adv}(x,x')]\varrho(x')d^4x'. \tag{5.18}$$

Its modes are more easily found directly from Eqs. (5.15) and (5.16). For $m \neq 0$,

$$\phi^{\rm S}_{\ell m} = \frac{4\pi}{u^t} N_{\ell m} m\Omega j_\ell(m\Omega r_<) y_\ell(m\Omega r_>), \tag{5.19}$$

where $y_\ell$ is the spherical Bessel function of the second kind. For $m = 0$, $\phi^{\rm S}_{\ell 0} = \phi^{\rm ret/adv}_{\ell 0}$.

Correspondingly, in flat space the regular field is $\phi^{\rm R} = \phi^{\rm ret} - \phi^{\rm S} = \frac{1}{2}(\phi^{\rm ret} - \phi^{\rm adv})$. Its four-dimensional form can be written as an integral analogous to (5.18). Its modes can be found straightforwardly from Eqs. (5.15) and (5.16). For $m \neq 0$,

$$\phi^{\rm R}_{\ell m} = \frac{4\pi i}{u^t} N_{\ell m} m\Omega j_\ell(m\Omega r_<) j_\ell(m\Omega r_>), \tag{5.20}$$

and for $m = 0$, $\phi^{\rm R}_{\ell 0} = 0$.

### 5.1.3 Puncture and residual fields

The puncture field $\phi^{\mathcal{P}}$ is obtained in 4D by performing a local expansion of the integral representation (5.18) of the singular field. That procedure is common in the literature, and so we do not belabour it here; instead we refer the reader to, e.g., Ref. [88] for details, and give here only the main results. Letting $\lambda \equiv 1$ count powers of distance from the particle, the covariant expansion of the flat-space puncture to fourth-from-leading order in distance is

$$\begin{aligned}
\phi^{\rm S}(x,x') =& \frac{1}{\mathsf{s}} + \frac{\sigma_a\left(\mathsf{s}^2 - \mathsf{r}^2\right)}{2\mathsf{s}^3} \\
&+ \frac{a^2\mathsf{s}^2\left(\mathsf{r}^4 - 6\mathsf{r}^2\mathsf{s}^2 - 3\mathsf{s}^4\right) + 9\sigma_a^2\left(\mathsf{r}^2 - \mathsf{s}^2\right)^2 - 4\mathsf{r}\mathsf{s}^2\sigma_{\dot a}\left(\mathsf{r}^2 - 3\mathsf{s}^2\right)}{24\mathsf{s}^5} \\
&+ \frac{1}{48\mathsf{s}^7}\Big[2\mathsf{r}\mathsf{s}^4 a^\alpha \dot a_\alpha\left(\mathsf{r}^4 - 10\mathsf{r}^2\mathsf{s}^2 - 15\mathsf{s}^4\right) \\
&- 3a^2\mathsf{s}^2\sigma_a\left(\mathsf{r}^6 - 5\mathsf{r}^4\mathsf{s}^2 + 15\mathsf{r}^2\mathsf{s}^4 + 5\mathsf{s}^6\right) + 4\sigma_a\sigma_{\dot a}\mathsf{r}\mathsf{s}^2(3\mathsf{r}^4 - 10\mathsf{r}^2\mathsf{s}^2 + 15\mathsf{s}^4) \\
&- 15\sigma_a^3(\mathsf{r}^2 - \mathsf{s}^2)^3 - 2\sigma_{\ddot a}\mathsf{s}^4(\mathsf{r}^4 - 6\mathsf{r}^2\mathsf{s}^2 - 3\mathsf{s}^4)\Big] + O(\lambda^3).
\end{aligned} \tag{5.21}$$

where the terms are $O(\lambda^{-1})$, $O(\lambda^0)$, $O(\lambda^1)$ and $O(\lambda^2)$, respectively. Here we follow the notation of Chapter 3, in which $\sigma_X \equiv \sigma_{\alpha'}X^{\alpha'}$ for any vector $X^\alpha$; the bi-scalar $\sigma(x,x')$ is the Synge world function, equal to one half of the squared geodesic distance between $x$ and $x'$, and $\sigma_\alpha \equiv \frac{\partial\sigma}{\partial x^{\alpha'}}$; the vectors $a^\alpha \equiv u^\beta\nabla_\beta u^\alpha$, $\dot a^\alpha \equiv u^\beta\nabla_\beta a^\alpha$ and $\ddot a^\alpha \equiv u^\beta\nabla_\beta \dot a^\alpha$

are the acceleration and its first and second derivatives, respectively; and the quantities $\mathsf{r} \equiv \sigma_{\alpha'} u^{\alpha'}$ and $\mathsf{s} \equiv \sqrt{(g^{\alpha\beta} + u^{\alpha'} u^{\beta'})\sigma_{\alpha'}\sigma_{\beta'}}$ are projected components of the geodesic distance from the field point to the reference point $x'$ on the worldline. In our case, $g_{\alpha\beta}$ is the metric of flat spacetime and $\nabla_\alpha$ is the covariant derivative compatible with it.

To facilitate the computation of spherical harmonic modes, it is customary to express the field in a rotated coordinate system in which the particle is momentarily at the north pole. We refer back to Appendix. C, where we used these coordinates in the derivation of the modes of the first-order puncture. We label the angles in this system $\alpha^{A'} \equiv (\alpha, \beta)$, such that at a given instant $t$, the particle sits at $\alpha = 0$. More details can be found in Appendix E. As we describe there and in later sections of this chapter, in our calculations this rotation introduces new complications and loses some of its traditional advantages. Nevertheless, its benefits outweigh its drawbacks.

In terms of the rotated angles $\alpha^{A'}$, a puncture satisfying $\phi^{\mathcal{P}} = \phi^{\mathrm{S}} + O(\lambda^3)$ can be obtained from a coordinate expansion of Eq. (5.21). For the circular orbits we are interested in here, this is given explicitly by

$$\phi^{\mathcal{P}} = \lambda^{-1}\phi^{\mathcal{P}}_{(-1)} + \lambda^0\phi^{\mathcal{P}}_{(0)} + \lambda\phi^{\mathcal{P}}_{(1)} + \lambda^2\phi^{\mathcal{P}}_{(2)}, \tag{5.22}$$

where

$$\phi^{\mathcal{P}}_{(-1)} = \frac{1}{\rho}, \tag{5.23a}$$

$$\phi^{\mathcal{P}}_{(0)} = -\frac{\Delta r}{2r_0\rho\chi}(1 - 2v^2s^2) + \frac{\Delta r^3}{2r_0\chi_0\chi\rho^3}(1 - 2v^2s^2 + v^4s^2), \tag{5.23b}$$

$$\begin{aligned}\phi^{\mathcal{P}}_{(1)} = {}& \frac{3\Delta r^6}{8r_0^2\rho^5\chi_0^2\chi^2}\left(1 - 2v^2s^2 + v^4s^2\right)^2 + \frac{\rho v^2}{24r_0^2\chi_0^2\chi^2}[3v^6s^2 - 3(1+s^2) - 3v^2(2-7s^2) \\ &+ v^4(1 - 5s^2 - 8s^4)] + \frac{\Delta r^2}{24r_0^2\rho\chi_0^2\chi^2}[9 - 18v^2(1+s^2) - 6v^8s^2(1-4s^2) \\ &+ 3v^4(5 + 8s^2 + 8s^4) - 2v^6(1 + 4s^2 + 22s^4)] + \frac{\Delta r^4}{24r_0^2\rho^3\chi_0^2\chi^2}[-18 + 3v^8s^2(1-9s^2) \\ &+ 3v^2(7 + 19s^2) - 3v^4(1 + 21s^2 + 20s^4) + v^6(1 + s^2 + 88s^4)],\end{aligned} \tag{5.23c}$$

$$\begin{aligned}\phi^{\mathcal{P}}_{(2)} = {}& \frac{5\Delta r^9}{16r_0^3\rho^7\chi_0^3\chi^3}(1 - 2v^2s^2 + v^4s^2)^3 - \frac{\Delta r\rho v^2}{48r_0^3\chi_0^3\chi^3}[6v^{10}s^4 + 3(1+s^2) \\ &+ v^8s^2(7 - 8s^2 - 32s^4) + 3v^2(11 - 14s^2 + 2s^4) + v^4(13 - 62s^2 + 16s^4) \\ &- v^6(1 + 50s^2 - 124s^4 + 16s^6)] - \frac{\Delta r^7}{16r_0^3\rho^5\chi_0^3\chi^3}[15 - 3v^{12}s^4(1-7s^2) \\ &- 3v^2(6 + 25s^2) + 3v^4(1 + 33s^2 + 46s^4) - v^{10}s^2(1 - 8s^2 + 112s^4) \\ &+ v^8s^2(2 + 65s^2 + 188s^4) - v^6(1 + 22s^2 + 211s^4 + 96s^6)]\end{aligned}$$

$$
\begin{aligned}
&-\frac{\Delta r^3}{48r_0^3\rho\chi_0^3\chi^3}[15-3v^{12}s^4(7-16s^2)-3v^2(16+17s^2)-v^{10}s^2(17-13s^2+128s^4)\\
&+3v^4(11+61s^2+14s^4)-v^6(26+158s^2+125s^4+48s^6)\\
&+v^8(2+115s^2+19s^4+152s^6)]+\frac{\Delta r^5}{48r_0^3\rho^3\chi_0^3\chi^3}[45-6v^{12}s^4(4-15s^2)\\
&-3v^2(33+61s^2)-v^{10}s^2(13-47s^2+400s^4)+3v^4(23+131s^2+94s^4)\\
&-2v^6(5+134s^2+281s^4+108s^6)+v^8(1+53s^2+275s^4+520s^6)]. \qquad (5.23d)
\end{aligned}
$$

Here $v^2 \equiv r_0^2\Omega^2$, $s \equiv \sin\beta$, $\chi \equiv 1 - v^2s^2$, $\chi_0 \equiv 1 - v^2 = 1/(u^t)^2$, and

$$
\rho \equiv \left[\frac{2r_0^2\chi}{\chi_0}(\delta^2 + 1 - \cos\alpha)\right]^{1/2}, \qquad (5.24)
$$

with $\delta^2 \equiv \frac{\chi_0\Delta r^2}{2r_0^2\chi}$. Note that the only dependence of the singular field on $\alpha$ appears through $\rho$, while $\beta$ appears through $\rho$, $\chi$, and the explicit powers of $s$. Also note that the above expression for $\phi^{\mathcal{P}}(\alpha^{A'})$ is valid only at the instant when the particle is at the north pole of the rotated coordinate system.

Given this choice of puncture field, the residual field is defined implicitly by $\phi^{\mathcal{R}} \equiv \phi^{\rm ret} - \phi^{\mathcal{P}}$. Since we do not have a closed-form expression for $\phi^{\rm ret}$, we cannot write an exact result for $\phi^{\mathcal{R}}$ in 4D. However, we can compute its modes from those of $\phi^{\rm ret}$ and $\phi^{\mathcal{P}}$ using $\phi^{\mathcal{R}}_{\ell m} = \phi^{\rm ret}_{\ell m} - \phi^{\mathcal{P}}_{\ell m}$.

Before proceeding, note that in Eq. (5.22), we have kept the first four orders from the local expansion of $\phi^{\rm S}$. We refer to this as a fourth-order puncture; if in a particular calculation we include only the first three of them, we refer to it as a third-order puncture, and so on. The higher the order of the puncture, the smoother the residual field, and hence the more rapid the falloff of $\phi^{\mathcal{R}}_{\ell m}$ with $\ell$. In the following sections we will explore how our strategy of computing $S$ is impacted by this, and we shall find that the puncture must be of at least third order for our strategy to succeed.

## 5.2 Second-order source

We are now interested in how the modes of the fields are coupled in the source $S = t^{\mu\nu}\partial_\mu\phi_1\partial_\nu\phi_1$. For later use, we derive the mode-coupling formula in both $\theta^A$ and $\alpha^{A'}$ coordinates. The method of derivation, and the end result in $\theta^A$ coordinates, was previously presented in Ref. [75], and so we omit some details here.

### 5.2.1 In $\theta^A$ coordinates

Written as a bilinear functional, $S$ is given more explicitly by

$$S[\phi^{(1)}, \phi^{(2)}] = \partial_t\phi^{(1)}\partial_t\phi^{(2)} + \partial_r\phi^{(1)}\partial_r\phi^{(2)} + \frac{1}{r^2}\Omega^{AB}\partial_A\phi^{(1)}\partial_B\phi^{(2)}, \tag{5.25}$$

where $\phi^{(1)}$ and $\phi^{(2)}$ are any two differentiable fields, $\Omega_{AB} = \mathrm{diag}(1, \sin^2\theta)$ is the metric of the unit sphere and $\Omega^{AB}$ is its inverse. Substituting $\phi^{(n)} = \sum_{\ell m}\phi^{(n)}_{\ell m}(r)e^{-im\Omega t}Y_{\ell m}$, we get

$$\begin{aligned} S = \sum_{\substack{\ell_1 m_1\\ \ell_2 m_2}} e^{-i(m_1+m_2)\Omega t}\Big[&\big(\partial_r\phi^{(1)}_{\ell_1 m_1}\partial_r\phi^{(2)}_{\ell_2 m_2} - m_1 m_2\Omega^2\phi^{(1)}_{\ell_1 m_1}\phi^{(2)}_{\ell_2 m_2}\big)Y_{\ell_1 m_1}Y_{\ell_2 m_2} + \\ &\frac{1}{r^2}\phi^{(1)}_{\ell_1 m_1}\phi^{(2)}_{\ell_2 m_2}\partial^A Y_{\ell_1 m_1}\partial_A Y_{\ell_2 m_2}\Big], \end{aligned} \tag{5.26}$$

where indices are raised with $\Omega^{AB}$.

To obtain the spherical-harmonic coefficient of Eq. (5.26), we first rewrite $\partial_A Y_{\ell m}$ in terms of spin-weighted harmonics ${}_sY_{\ell m}$ (see Ref. [96] for an overview), as

$$\partial_A Y^{\ell m} = \frac{1}{2}\sqrt{\ell(\ell+1)}\left({}_{-1}Y^{\ell m}m_A - {}_1Y^{\ell m}m^*_A\right), \tag{5.27}$$

where $m^A \equiv \left(1, \frac{i}{\sin\theta}\right)$ and its complex conjugate $m^{*A}$ form a null basis on the unit sphere. This allows us to compute $S_{\ell m}$, which is an integral against $Y^*_{\ell m} = {}_0Y^*_{\ell m}$, by appealing to the general formula

$$\oint {}_sY^{\ell m *}\,{}_{s_1}Y^{\ell_1 m_1}\,{}_{s_2}Y^{\ell_2 m_2}d\Omega = C^{\ell m s}_{\ell_1 m_1 s_1 \ell_2 m_2 s_2}, \tag{5.28}$$

(see for example Sec. 30B of the text by Hecht [97]) where $d\Omega = \sin\theta\, d\theta\, d\phi$ and for $s = s_1 + s_2$,

$$\begin{aligned} &C^{\ell m s}_{\ell_1 m_1 s_1 \ell_2 m_2 s_2} = \\ &(-1)^{m+s}\sqrt{\frac{(2\ell+1)(2\ell_1+1)(2\ell_2+1)}{4\pi}}\begin{pmatrix}\ell & \ell_1 & \ell_2\\ s & -s_1 & -s_2\end{pmatrix}\begin{pmatrix}\ell & \ell_1 & \ell_2\\ -m & m_1 & m_2\end{pmatrix}. \end{aligned} \tag{5.29}$$

Here the arrays are $3j$ symbols, which enforce

$$m = m_1 + m_2, \tag{5.30a}$$

$$s = s_1 + s_2, \tag{5.30b}$$

$$|\ell_1 - \ell_2| \leq \ell \leq \ell_1 + \ell_2. \tag{5.30c}$$

We refer to (5.30c) as the triangle inequality. If $s = s_1 = s_2 = 0$, Eq. (5.28) reduces to the standard formula for the integral of three ordinary spherical harmonics. We refer the reader to Ref. [75] for more details.

After using Eq. (5.27), $m^A m_A = 0$, $m^A m^*_A = 2$, and Eq. (5.28), we find that Eq. (5.26) can be written as $S = \sum_{\ell m} S_{\ell m}(r) e^{-im\Omega t} Y_{\ell m}$, with modes given by

$$S_{\ell m}[\phi^{(1)}, \phi^{(2)}] = \sum_{\substack{\ell_1 m_1 \\ \ell_2 m_2}} \Bigg[ C^{\ell m 0}_{\ell_1 m_1 0 \ell_2 m_2 0} \left( \partial_r \phi^{(1)}_{\ell_1 m_1} \partial_r \phi^{(2)}_{\ell_2 m_2} - m_1 m_2 \Omega^2 \phi^{(1)}_{\ell_1 m_1} \phi^{(2)}_{\ell_2 m_2} \right)$$
$$- \frac{1}{2r^2} \sqrt{\ell_1(\ell_1+1)\ell_2(\ell_2+1)} C^{\ell m 0}_{\ell_1 m_1 -1 \ell_2 m_2 1} \left( \phi^{(1)}_{\ell_1 m_1} \phi^{(2)}_{\ell_2 m_2} + \phi^{(2)}_{\ell_1 m_1} \phi^{(1)}_{\ell_2 m_2} \right) \Bigg]. \tag{5.31}$$

We have used the freedom to relabel $\ell_1 m_1 \leftrightarrow \ell_2 m_2$ and the symmetry $C^{\ell m s}_{\ell_1 m_1 s_1 \ell_2 m_2 s_2} = C^{\ell m s}_{\ell_2 m_2 s_2 \ell_1 m_1 s_1}$ to slightly simplify this result. We note that the range of the sum is restricted by the $3j$ symbols in $C^{\ell m s}_{\ell_1 m_1 s_1 \ell_2 m_2 s_2}$, which enforce (5.30a) and (5.30c). The first of these restrictions has been used to replace $e^{-i(m_1+m_2)\Omega t}$ with $e^{-im\Omega t}$, and it can be further used to eliminate the sum over $m_2$.

In our toy model, Eq. (5.31) plays the role of Eq. (5.3) from the gravitational case. When we only have access to a finite number of modes $\phi^{(n)}_{\ell m}$ up to $\ell = \ell_{\max}$, then the sum is truncated: explicitly, it becomes the partial sum

$$S^{\ell_{\max}}_{\ell m} \equiv \sum_{\ell_1=0}^{\ell_{\max}} \sum_{\ell_2=0}^{\ell_{\max}} \sum_{m_1=-\ell_1}^{\ell_1} S^{\ell_1 m_1 \ell_2, m-m_1}_{\ell m}, \tag{5.32}$$

where we have eliminated the sum over $m_2$, and for brevity we have suppressed the functional arguments and defined $S^{\ell_1 m_1 \ell_2 m_2}_{\ell m}$ as the summand in Eq. (5.31). By appealing to the triangle inequality, we could write the second sum even more explicitly as $\sum_{\ell_2=|\ell-\ell_1|}^{\min(\ell_{\max}, \ell+l_1)}$.

The slow convergence of the limit $S^{\ell_{\max}}_{\ell m} \to S_{\ell m}$ was illustrated in Fig. 5.1. Its behaviour will be more carefully analyzed in the following sections.

### 5.2.2 In $\alpha^{A'}$ coordinates

Although Eq. (5.31) is the mode-coupling formula that we will utilize in explicit computations, we will also make use of the analogous formula in the rotated coordinates $\alpha^{A'}$. Deriving that result additionally provides an opportunity to introduce the 4D form of $S$ in these coordinates, which will be essential in Sec. 5.4.

Obtaining the source in the rotated coordinates involves a new subtlety: the 4D expression for $S$ involves $t$ derivatives, while our expression (5.22) for $\phi^{\mathcal{P}}(\alpha^{A'})$ is intended to only be instantaneously valid at the instant when the particle is at the north pole of the rotated coordinate system. We discuss this subtlety in Appendix E. In brief, we may treat the coordinates $\alpha^{A'}$ as themselves dependent on $t$, and appropriately account for that time dependence when acting with $t$ derivatives. The 4D expression for $S$ is then given by Eq. (E.4), which we reproduce here for convenience:

$$S[\phi^{(1)},\phi^{(2)}]=\dot{\alpha}^{A'}\partial_{A'}\phi^{(1)}\dot{\alpha}^{A'}\partial_{A'}\phi^{(2)}+\partial_r\phi^{(1)}\partial_r\phi^{(2)}+\frac{1}{r^2}\Omega^{A'B'}\partial_{A'}\phi^{(1)}\partial_{B'}\phi^{(1)}, \tag{5.33}$$

where $\Omega^{A'B'}=\mathrm{diag}(1,\csc^2\alpha)$ is the inverse metric on the unit sphere in the rotated coordinates, and the time derivatives in Eq. (5.25) now manifest in the quantity $\dot{\alpha}^{A'}=\Omega(-\cos\beta,\cot\alpha\sin\beta)$.

The modes of the source in the rotated coordinates are given by

$$S_{\ell m'}=\oint S(\alpha^{A'})Y^*_{\ell m'}(\alpha^{A'})d\Omega'. \tag{5.34}$$

We will consistently use $m'$ to denote the azimuthal number in the rotated coordinates; because $\ell$ is invariant under rotations, it is the same in both sets of coordinates.

In Sec. 5.4 we will evaluate the integral (5.34) for $S[\phi^{\mathcal{P}},\phi^{\mathcal{P}}]$ *without first decomposing $\phi^{\mathcal{P}}$ into modes*. But generically, if we expand each $\phi^{(n)}$ as $\sum_{\ell m'}\phi^{(n)}_{\ell m'}Y_{\ell m'}$, then we can evaluate the integral analytically in the same way as we did for $S_{\ell m}$. This is made possible by first writing $\dot{\alpha}^{A'}$ in terms of spin-weight $\pm1$ harmonics as

$$\dot{\alpha}^{A'}=\sqrt{\frac{\pi}{3}}\Omega\big[({}_{-1}Y_{11}+{}_{-1}Y_{1,-1})m^{A'}+({}_{1}Y_{11}+{}_{1}Y_{1,-1})m^{*A'}\big]. \tag{5.35}$$

Next, we use Eq. (5.27), which is covariant on the unit sphere and hence also applies in $\alpha^{A'}$ coordinates. Combining these results, invoking Eqs. (5.28)-(5.29), and using the properties of the $3j$ symbols to simplify, we find

$$\dot{\alpha}^{A'}\partial_{A'}\phi=\frac{\Omega}{2}\sum_{\ell m'}(\mu^-_{\ell m'}\phi_{\ell,m'+1}-\mu^+_{\ell m'}\phi_{\ell,m'-1})Y_{\ell m'}, \tag{5.36}$$

where $\mu^{\pm}_{\ell m'}\equiv\sqrt{(\ell\pm m')(\ell\mp m'+1)}$.

Substituting Eq. (5.36) into Eq. (5.33) and following the same procedure as in the previous section, we find

$$\begin{aligned}S_{\ell m'}=\sum_{\substack{\ell_1 m_1'\\ \ell_2 m_2'}}\Bigg\{&C^{\ell m'0}_{\ell_1 m_1'0\ell_2 m_2'0}\big[\partial_r\phi^{(1)}_{\ell_1 m_1'}\partial_r\phi^{(2)}_{\ell_2 m_2'}\\&+\tfrac{1}{4}\Omega^2(\mu_1^-\phi^{(1)}_{\ell_1,m_1'+1}-\mu_1^+\phi_{\ell_1,m_1'-1})(\mu_2^-\phi_{\ell_2,m_2'+1}-\mu_2^+\phi_{\ell_2,m_2'-1})\big]\\&-\frac{1}{2r^2}\sqrt{\ell_1(\ell_1+1)\ell_2(\ell_2+1)}C^{\ell m'0}_{\ell_1 m_1'-1\ell_2 m_2'1}\left(\phi^{(1)}_{\ell_1 m_1'}\phi^{(2)}_{\ell_2 m_2'}+\phi^{(2)}_{\ell_1 m_1'}\phi^{(1)}_{\ell_2 m_2'}\right)\Bigg\},\end{aligned} \tag{5.37}$$

where $\mu_i^{\pm}\equiv\mu^{\pm}_{l_i m_i'}$. Note that unlike Eq. (5.31), which gave the coefficient in $\sum_{\ell m}S_{\ell m}(r)e^{-im\Omega t}Y_{\ell m}(\theta^A)$, Eq. (5.37) gives the coefficient in $\sum_{\ell m}S_{\ell m'}(r)Y_{\ell m}(\alpha^{A'})$, with no phase factor; the time dependence is entirely contained in the $\alpha^{A'}$ dependence.

## 5.3 Computing $S_{\ell m}[\phi^{\mathcal{R}}, \phi^{\mathcal{R}}]$ and $S_{\ell m}[\phi^{\mathcal{R}}, \phi^{\mathcal{P}}]$

Following the strategy outlined in the introduction, we now compute $S_{\ell m}[\phi^{\mathcal{R}}, \phi^{\mathcal{R}}]$ and $S_{\ell m}[\phi^{\mathcal{R}}, \phi^{\mathcal{P}}]$ from the modes of $\phi^{\mathcal{R}}$ and $\phi^{\mathcal{P}}$ using the mode-coupling formula (5.31). In Sec. 5.4 we will then complete our calculation by computing $S_{\ell m}[\phi^{\mathcal{P}}, \phi^{\mathcal{P}}]$ from the 4D expression for $\phi^{\mathcal{P}}$.

### 5.3.1 Outline of the strategy

As input for $S_{\ell m}[\phi^{\mathcal{R}}, \phi^{\mathcal{R}}]$ and $S_{\ell m}[\phi^{\mathcal{R}}, \phi^{\mathcal{P}}]$ in Eq. (5.31), we require the modes $\phi^{\mathcal{P}}_{\ell m}$. We begin by computing the modes

$$\phi^{\mathcal{P}}_{\ell m'} = \oint \phi^{\mathcal{P}}(\alpha^{A'}) Y^*_{\ell m'}(\alpha^{A'}) d\Omega' \tag{5.38}$$

in the rotated coordinates $\alpha^{A'}$. The modes in the unrotated coordinates $\theta^A$ are then retrieved using

$$\phi^{\mathcal{P}}_{\ell m} = \sum_{m'} \phi^{\mathcal{P}}_{\ell m'} D^{\ell}_{mm'}(\pi, \pi/2, \pi/2), \tag{5.39}$$

where $D^l_{mm'}$ is a Wigner $D$ matrix element. Equation (5.39) yields the modes in a coordinate system in which the particle is on the equator at an azimuthal angle $\phi_p = 0$. An additional rotation brings it to its original position $\phi_p = \Omega t$. The sole effect of that rotation is to introduce the phase $e^{-im\Omega t}$: $\phi_{\ell m} \to \phi_{\ell m} e^{-im\Omega t}$.

Given the modes $\phi^{\mathcal{P}}_{\ell m}$, the rest of the procedure is straightforward. In summary, it involves four steps:[1]

1. Decompose the puncture field (5.22) into $\ell m'$ modes using Eq. (5.38).
2. Use Eq. (5.39) to obtain the $\ell m$ modes $\phi^{\mathcal{P}}_{\ell m}$.
3. Compute the residual-field modes $\phi^{\mathcal{R}}_{\ell m} = \phi^{\rm ret}_{\ell m} - \phi^{\mathcal{P}}_{\ell m}$ [with $\phi^{\rm ret}_{\ell m}$ given in Eqs. (5.15) and (5.16)].
4. Use Eq. (5.31) to compute $S_{\ell m}[\phi^{\mathcal{R}}, \phi^{\mathcal{R}}]$ and $S_{\ell m}[\phi^{\mathcal{R}}, \phi^{\mathcal{P}}]$.

Sections 5.3.2–5.3.6 describe the first three steps, and Sec. 5.3.7 presents and discusses the results of the final step.

[1] We could alternatively compute the modes $S_{\ell m'}[\phi^{\mathcal{R}}, \phi^{\mathcal{R}}]$ and $S_{\ell m'}[\phi^{\mathcal{R}}, \phi^{\mathcal{P}}]$ directly from $\phi^{\mathcal{P}}_{\ell m'}$ using Eq. (5.37). $S_{\ell m}[\phi^{\mathcal{R}}, \phi^{\mathcal{R}}]$ and $S_{\ell m}[\phi^{\mathcal{R}}, \phi^{\mathcal{P}}]$ would then be computed using the analogs of Eq. (5.39).

### 5.3.2 Calculation of $\phi^{\mathcal{P}}_{\ell m}$

Concretely evaluating the integrals (5.38) is a nontrivial task. Before addressing that topic, we make several prefatory remarks.

First, we note that although integrals like (5.38) of local expansions like (5.22) are common in the literature, in our context they introduce a unique challenge. Typically, integrals of this sort appear in mode-sum regularization and puncture schemes [95, 98]. In those contexts, one's primary goal is to compute the Detweiler-Whiting regular field (or some finite number of its derivatives) on the particle's worldline. This gives one considerable leeway: If one is interested in computing $n$ derivatives of the regular field, for example, then so long as one preserves the puncture through order $\lambda^n$, one can smoothly deform the integrand in Eq. (5.38), and one can do so in a different way for each $\ell m'$ mode. Similarly, one can evaluate the integral with a local expansion in the limit $\Delta r \to 0$, which generally simplifies the integration. And since $Y_{\ell m'}$ vanishes at $\alpha = 0$ for $m' \neq 0$, one need only evaluate the $m' = 0$ mode (or in the calculations in Ref. [74], the $m' = 0, \pm 1, \pm 2$ modes); traditionally, this restriction to $m' = 0$ has been a major advantage of using rotated coordinates like $\alpha^{A'}$.

In our calculation, we have none of these luxuries. Because we compute $S_{\ell m}[\phi^{\mathcal{P}}, \phi^{\mathcal{P}}]$ from the 4D expression for $\phi^{\mathcal{P}}$ while we compute $S_{\ell m}[\phi^{\mathcal{R}}, \phi^{\mathcal{P}}]$ and $S_{\ell m}[\phi^{\mathcal{R}}, \phi^{\mathcal{R}}]$ from the modes $\phi^{\mathcal{P}}_{\ell m'}$, the modes must correspond to an *exact* evaluation of Eq. (5.38); otherwise, $S_{\ell m}[\phi^{\mathcal{P}}, \phi^{\mathcal{P}}] + 2S_{\ell m}[\phi^{\mathcal{R}}, \phi^{\mathcal{P}}] + S_{\ell m}[\phi^{\mathcal{R}}, \phi^{\mathcal{R}}]$ would not be equal to $S_{\ell m}[\phi^{\rm ret}, \phi^{\rm ret}]$. This means that if we deform the integrand in Eq. (5.38), then we must make an identical deformation of the 4D expression for $\phi^{\mathcal{P}}$. Similarly, any expansion in powers of $\Delta r$ would have to be performed for both the $\ell m'$ modes and the 4D expression; because we must evaluate these quantities over a range of $\Delta r$ values, we cannot rely on eventually taking the limit $\Delta r \to 0$. And finally, we cannot limit our computation to $m' = 0$; since we do not evaluate any quantities at $\alpha = 0$, there is no *a priori* limit to the number of $m'$ modes we must compute. (If we only required $S$ on the particle, then we would only require the modes $S_{\ell 0'}$, but even these modes depend on all $m'$ modes of $\phi$.)

In brief, we must be exact. We must compute all $\ell m'$ modes of $\phi^{\mathcal{P}}$ without introducing any approximations. The lone exception to this, to be discussed in Sec. 5.3.8, is that in practice we can truncate the number of $m'$ modes at some $|m'| = m'_{\rm max}$. This is possible because the modes fall off rapidly with $|m'|$, allowing us to neglect large-$|m'|$ modes without introducing significant numerical error.

We must address one more issue before detailing the evaluation of Eq. (5.38). As discussed in Ref. [74], our puncture $\phi^{\mathcal{P}}$ is *not* smooth at all points off the particle. The particle sits at the north pole $\alpha = 0$ of the sphere at $\Delta r = 0$, and $\phi^{\mathcal{P}}$ correctly diverges as $1/\lambda$ there. But even away from the particle, for each fixed $\Delta r \neq 0$, $\phi^{\mathcal{P}}$ has a directional discontinuity at the south pole $\alpha = \pi$, inherited from a directional discontinuity in the quantity $\rho$. This discontinuity is nonphysical. $\phi^{\mathcal{P}}$ is originally defined from a local expansion in the neighbourhood of the particle, but in order to evaluate the integrals (5.38), it must be extended over the entire sphere spanned by $\alpha^A$. The particular discontinuity we face is a consequence of the particular manner in which we have performed that extension. Because the total field $\phi^P + \phi^{\mathcal{R}}$ is smooth at all points off the particle, this singularity at $\alpha = \pi$ must be canceled by one in $\phi^{\mathcal{R}}$. And because nonsmoothness of a field leads to slow falloff with $\ell$, this discontinuity limits the convergence rate of $S_{\ell m}[\phi^{\mathcal{P}}, \phi^{\mathcal{R}}]$ and $S_{\ell m}[\phi^{\mathcal{R}}, \phi^{\mathcal{R}}]$ with $\ell_{\max}$. Concretely, the discontinuity introduces terms of the form $\frac{(-1)^\ell}{\ell}$ into $\phi^{\mathcal{R}}_{\ell m'}$ for all $m' \neq 0$.

To eliminate the discontinuity, we must adopt a different extension of $\phi^{\mathcal{P}}$ over the sphere. Following Ref. [74], we do so by introducing a regularizing factor:

$$\phi^{\mathcal{P}}(\Delta r, \alpha^{A'}) \to \mathcal{W}^n_{\mathsf{m}}(\cos\alpha)\phi^{\mathcal{P}}(\Delta r, \alpha^{A'}). \tag{5.40}$$

Here the parameters $n$ and $\mathsf{m}$ are chosen such that $n \geq k$ and $\mathsf{m} \geq m'_{\max}$, where $k$ is the order of the puncture and $m'_{\max}$ is the maximum value of $|m'|$ we use. $\mathcal{W}^n_{\mathsf{m}}$'s dependence on these two parameters is dictated by the required behaviour at the two poles. To control the behaviour at the south pole, we choose a regularizing factor that scales as $\mathcal{W}^n_{\mathsf{m}} = O[(\pi - \alpha)^{\mathsf{m}}]$, which makes $\mathcal{W}^n_{\mathsf{m}}\phi^{\mathcal{P}}$ a $C^{\mathsf{m}-1}$ function at $\alpha = \pi$. For an otherwise smooth function, standard estimation methods [99] show that this degree of smoothness ensures that the modes $|\phi^{\mathcal{P}}_{\ell m'}|$, and hence $|\phi^{\mathcal{R}}_{\ell m'}|$, fall off as $\lesssim \ell^{-\mathsf{m}\pm 1}$; for sufficiently large $\mathsf{m}$, this nonspectral decay will be negligible compared to the slow convergence coming from the singularity at the particle. Now, at the same time as satisfying these conditions at the south pole, we must keep control of the behaviour at the north pole. Specifically, $\mathcal{W}^n_{\mathsf{m}}$ must leave all $k$ orders intact in the $k$th-order puncture, implying that it must behave as $\mathcal{W}^n_{\mathsf{m}} = 1 + O(\alpha^n)$ near $\alpha = 0$. We satisfy the requirements at both poles by choosing

$$\mathcal{W}^n_{\mathsf{m}} \equiv 1 - \frac{n}{2}\binom{(\mathsf{m}+n-2)/2}{n/2} B\left(\frac{1-\cos\alpha}{2}; \frac{n}{2}, \frac{\mathsf{m}}{2}\right), \tag{5.41}$$

where $\binom{p}{q}$ is the Binomial coefficient, and $B(z; a, b)$ is the incomplete Beta function.

This choice has the required properties at the poles provided $n$ and $\mathsf{m}$ are positive integers, and additionally that $\mathsf{m}$ is even. This is not a significant restriction; as discussed below, the $\beta$ integrals ensure that only even $m'$ need be considered in our circular-orbit toy model, and even if this were not the case we could always choose $\mathsf{m}$ to be the smallest even number greater than $m'_{\max}$. With these restrictions on $n$ and $\mathsf{m}$, $\mathcal{W}^n_{\mathsf{m}}$ takes the straightforward form of a polynomial in $y \equiv \frac{1-\cos\alpha}{2}$, whose coefficients and degree both depend on the particular choice of $n$ and $\mathsf{m}$. For example, in all our computations we use

$n = 4$ (equal to the highest order of puncture we use) and $\mathsf{m} = 10$ (equal to the value of $m'_{\max}$ we almost exclusively use), in which case $\mathcal{W}^4_{10} = 1 - 15y^2 + 40y^3 - 45y^4 + 24y^5 - 5y^6$.

Heeding the warnings above about our need for exactness, we must apply this regularization consistently to the 4D puncture in all our calculations, not solely in evaluating the integrals (5.38). So henceforth, we will always use Eq. (5.40) as our puncture, with fixed $n$ and $\mathsf{m}$ independent of the particular $\ell, m'$ mode being considered.

With our preparations out of the way, we now describe our evaluation of the integrals (5.38). We use two methods for computing the double integral (5.38), namely (i) evaluate the $\alpha$ integrals analytically and subsequently evaluate the $\beta$ integrals as numerical elliptic-type integrals, and (ii) evaluate both the $\alpha$ and $\beta$ integrals entirely numerically. The second method is computationally more expensive than the first. However, we used both methods as an internal consistency check. We will describe method (i) first and begin by explaining the steps in the the analytical evaluation of the $\alpha$ integrals.

### 5.3.3 Integration over $\alpha$

We first recall that all of the $\alpha$ dependence of the puncture (5.23) is contained inside the quantity $\rho$. Hence, the integral that we need to evaluate takes the general form

$$\int_{-1}^{1} \mathcal{W}^k_{\mathsf{m}}(x) P^{m'}_{\ell}(x) \rho^n \, dx, \tag{5.42}$$

where $x = \cos\alpha$, $P^{m'}_{\ell}(x)$ are the associated Legendre polynomials, and $n$ is an odd integer.

Furthermore, the simple form of $\mathcal{W}^n_{\mathsf{m}}$ as a power series in $\frac{1-\cos\alpha}{2}$ means that we can use Eq. (5.24) to rewrite it as an even power series in $\Delta r$ and $\rho$. The integrals (5.42) can therefore all be written in the form

$$\int_{-1}^{1} P^{m'}_{\ell}(x) \rho^n \, dx \tag{5.43}$$

for $n$ an odd integer.

Concentrating first on the simplest case of $m' = 0$, the integration can be done analytically using

$$\begin{aligned}\int_{-1}^{1} (\delta^2 + 1 - x)^{n/2} P^0_{\ell}(x) \, dx = &\frac{(-1)^{\frac{n+1}{2}} (\delta^2 + 2)^{\frac{n}{2}+1} \left[\left(\frac{1}{2}\right)_{\frac{n+1}{2}}\right]^2}{\left(\ell - \frac{n}{2}\right)_{n+2}} {}_2F_1(-\ell, \ell+1; -\tfrac{n}{2}; -\tfrac{\delta^2}{2}) \\ &- \frac{2\,|\delta|\,\delta^{n+1}}{n+2} {}_2F_1(-\ell, \ell+1; \tfrac{n}{2}+2; -\tfrac{\delta^2}{2}).\end{aligned} \tag{5.44}$$

For any given odd integer $n$, this is merely a pair of even polynomials of degree $2l$ in $\delta$, one multiplying $(\delta^2+2)^{\frac{p}{2}+1}$ and the other multiplying $|\delta|\delta^{p+1}$.

Turning to the $m' \neq 0$ case, these can now be written in terms of the $m'=0$ result. Using the definition for the associated Legendre polynomials in terms of the Legendre polynomials,

$$P_\ell^m(x) = (-1)^m (1-x^2)^{m/2} \frac{d^m}{dx^m} P_\ell(x), \tag{5.45}$$

the integral (5.43) can be integrated by parts $m'$ times, resulting in an integral of the form (5.44) along with a set of $m'$ boundary terms. These boundary terms are given by

$$\sum_{k=0}^{m'-1} \left[ (-1)^k \frac{d^k \rho^n}{dx^k} \frac{d^{m'-k-1}}{dx^{m'-k-1}} P_\ell(x) \right]_{x=-1}^{x=1}, \tag{5.46}$$

and are therefore power series in $\delta$ of the same kind as in Eq. (5.44). The integrals over $\beta$ then have the same form as for the $m'=0$ case.

### 5.3.4 Alternative method for evaluating $\alpha$ integrals

An alternative, but equivalent strategy for evaluating the $\alpha$ integrals, Eq. (5.42), is based on expressing $\mathcal{W}_{\mathsf{m}}^n(x)$ and $P_\ell^{m'}(x)$ as finite polynomials in $(1+x)$ and $(1-x)$. For example $n=4$ and $\mathsf{m}=10$, Eq. (5.41) can be written as

$$\mathcal{W}_{10}^4(x) = \frac{3}{16}(1+x)^5 - \frac{5}{64}(1+x)^6. \tag{5.47}$$

Similarly, for $m \geq 0$,

$$P_\ell^m(x) = \sum_{p=0}^{\ell} \sum_{q=0}^{m} c_{\ell mpq} (1+x)^{p+q-m/2} (1-x)^{\ell-p-q+m/2}, \tag{5.48}$$

where $c_{\ell mpq}$ are $x$-independent constants given by

$$c_{\ell mpq} = \frac{(-1)^{m+\ell-p+q}}{2^\ell} \binom{\ell}{p}^2 \binom{m}{q} \frac{(\ell-p)!}{(\ell-p-q)!} \frac{p!}{(p-m+q)!}. \tag{5.49}$$

Equation (5.48) can be derived by using the standard representation $P_\ell(x) = \frac{1}{2^\ell}\sum_{p=0}^{\ell}\binom{\ell}{p}^2 (x-1)^{\ell-p}(x+1)^p$ in the formula $P_\ell^m = (-1)^m(1-x^2)^{m/2}\frac{d^m}{dx^m}P_\ell(x)$ and appealing to the Leibniz rule. The analogue of Eq. (5.48) for $m<0$ follows from $P_\ell^{-m} = (-1)^m \frac{(\ell-m)!}{(\ell+m)!}P_\ell^m$; but in practice we need not evaluate the integrals (5.42) for $m'<0$, since for real-valued $\phi^{\mathcal{P}}$ we have $\phi^{\mathcal{P}}_{\ell,-m'} = (-1)^{m'}\phi^{\mathcal{P}*}_{\ell m'}$

Substituting the polynomials (5.47) and (5.48) into (5.42) yields a sum of integrals of the form $F_{abn}(\delta) \equiv \int_{-1}^{1} dx\,(1+x)^{a/2}(1-x)^{b/2}(\delta^2+1-x)^{n/2}$, where $a, b, n$ are positive integers. We write the $\alpha$ integral in Eq. (5.38) as a linear combination of these integrals

$F_{abn}$. Using Wolfram Mathematica, we tabulate analytical formulae for all $F_{abn}$ that appear in this linear combination for $\phi^{\mathcal{P}}_{\ell m'}$ to $\ell = 200$ and $m' = 10$. Each of the tabulated formulae is a finite polynomial in $\delta$, and once tabulated, these formulae allow us to almost instantaneously evaluate the $\alpha$ integral.

### 5.3.5 Integration over $\beta$

We next turn to computing the $\beta$ integrals. The explicit $\beta$-dependent terms in the puncture, Eq. (5.23), appear in the form of positive, even powers of $\sin\beta$. The other dependences on $\beta$ in the integrand appear through $\rho$ (where they appear as powers of $\chi = 1 - r_0^2\Omega^2\sin^2\beta$), through $\chi$ itself, and through the factor of $e^{-im'\beta}$ from the spherical harmonic. With this in mind it can readily be shown that odd-$m'$ modes vanish and all of the non-vanishing modes are purely real.

Furthermore, following from this structure the net dependence on $\beta$ has two possible forms. The first term in Eq. (5.44) above yields integrals of the form

$$\int_0^{2\pi} \left(2 + \frac{\chi_0 \Delta r^2}{2r_0^2\chi}\right)^{\frac{n}{2}+1} \chi^{k/2} d\beta, \tag{5.50}$$

where $n$ is an odd integer. For $n = -1$ and $k = -1$ this can be recognized as a complete elliptic integral of the third kind, with arguments that depend on $\Delta r$, $r_0$, and $\Omega$ (through $\chi_0$). All other values of $n$ and $k$ can be reduced to this case by integrating by parts a sufficient number of times. The second type of integral arises from the second term in Eq. (5.44). This yields integrands involving $\chi^n$ with $n$ an integer; their integral is a polynomial involving $r_0\Omega$. Combining these results, we can therefore compute the integrals over $\beta$ exactly and analytically (in terms of elliptic integrals).

In practice we found it sufficiently efficient (and simpler) to evaluate the $\beta$ integral directly using numerical integration, rather than manipulating it into elliptic integral form. In that case, we used the fact that the integrand is symmetric in the sense that

$$\int_0^{2\pi} f(\beta)_{\ell m'} d\beta = 2\int_0^{\pi} f(\beta)_{\ell m'} d\beta \tag{5.51}$$

to reduce the computational cost. To compute the integrals we used a C++ code employing a 15-point Gauss-Kronrod rule.

### 5.3.6 Two-dimensional numerical integration

As a check on our methods, we also evaluated Eq. (5.38) by computing the double integral entirely numerically. We used a C++ code employing a 25-point Clenshaw-Curtis integration rule. As the azimuthal mode number $m'$ increases, the $\beta$ integrals

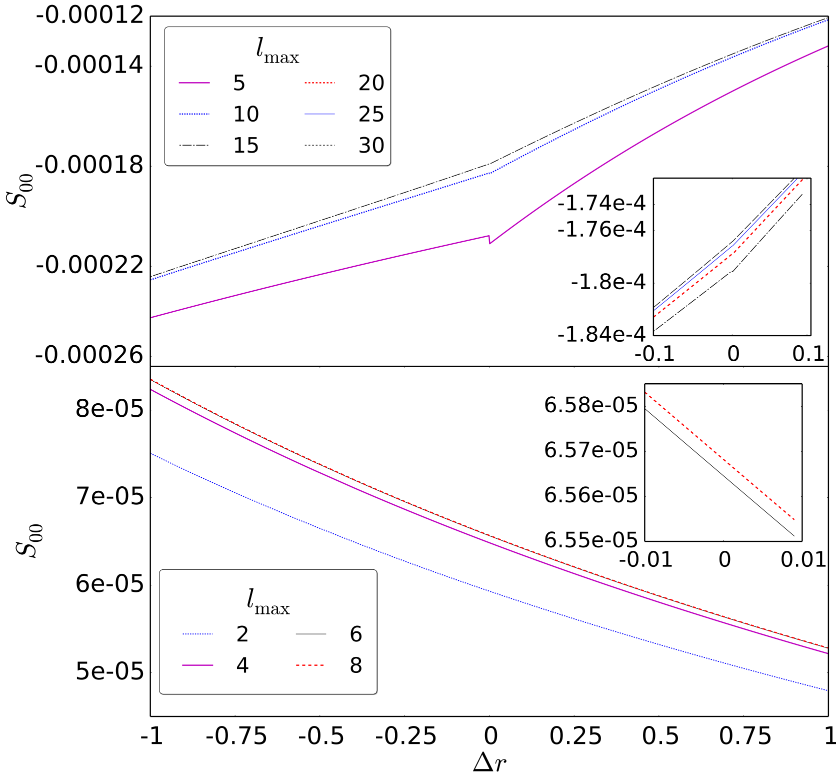


Figure 5.3: Demonstration of rapid convergence of the sum (5.31) for $S_{00}[\phi^{\mathcal{R}}, \phi^{\mathcal{P}}]$ (top panel) and $S_{00}[\phi^{\mathcal{R}}, \phi^{\mathcal{R}}]$ (bottom panel). The mode $S_{00}$ is plotted as a function of $\Delta r$ for a range of values of $\ell_{\max}$. Here we use $r_0 = 10$, $m'_{\max} = 10$, and all four orders in the puncture (5.22).

become highly oscillatory, resulting in loss of accuracy. We found that to improve the accuracy of our results, it was necessary to split the $\beta$ integral, over the range $[0, \pi]$, into a sum of $m'$ separate integrals, each over the range $\beta \in [(i-1)/(m'\pi), i/(m'\pi)]$, where $i$ runs from 1 to $m'$. In all cases, this fully numerical method agreed with the mixed analytical-numerical method described above.

### 5.3.7 Calculation of $S_{\ell m}[\phi^{\mathcal{R}}, \phi^{\mathcal{R}}]$ and $S_{\ell m}[\phi^{\mathcal{R}}, \phi^{\mathcal{P}}]$

After obtaining the modes of $\phi^{\mathcal{P}}$, we implement the final three steps in the strategy outlined at the end of Sec. 5.3.1. The results are shown in Fig. 5.3 for the monopole modes $S_{00}[\phi^{\mathcal{R}}, \phi^{\mathcal{P}}]$ and $S_{00}[\phi^{\mathcal{R}}, \phi^{\mathcal{R}}]$. We see that unlike $S_{\ell m}[\phi^{\rm ret}, \phi^{\rm ret}]$, $S_{\ell m}[\phi^{\mathcal{R}}, \phi^{\mathcal{P}}]$ and $S_{\ell m}[\phi^{\mathcal{R}}, \phi^{\mathcal{R}}]$ both converge rapidly with increasing $\ell_{\max}$. On the scale of the main plot, $S_{\ell m}[\phi^{\mathcal{R}}, \phi^{\mathcal{P}}]$ has numerically converged by $\ell_{\max} = 10$ and $S_{\ell m}[\phi^{\mathcal{R}}, \phi^{\mathcal{R}}]$ by $\ell_{\max} = 6$; the insets show the small changes at larger $\ell_{\max}$.

However, to make useful predictions about how our strategy extends to gravitational fields, we must say more than that it works; we must say something about how and when it works. We do this by considering two important convergence properties of Eq. (5.31):

1. How quickly do $S_{\ell m}[\phi^{\mathcal{R}},\phi^{\mathcal{P}}]$ and $S_{\ell m}[\phi^{\mathcal{R}},\phi^{\mathcal{R}}]$ converge as $m'_{\max}\to\infty$?
2. How does the convergence of $S_{\ell m}[\phi^{\mathcal{R}},\phi^{\mathcal{P}}]$ and $S_{\ell m}[\phi^{\mathcal{R}},\phi^{\mathcal{R}}]$ with $\ell_{\max}$ depend on the order of the puncture $\phi^{\mathcal{P}}$? More pointedly, how high order must the puncture be in order to guarantee convergence with $\ell_{\max}$?

The last of these is the most pertinent: as we shall discuss below, if the puncture is of too low order, then our strategy simply does not work. However, to elucidate that issue, it will be useful to first determine the convergence with $m'_{\max}$.

### 5.3.8 Convergence with $m'_{\max}$

To assess the rate of convergence with $m'_{\max}$, we introduce the finite difference

$$\Delta S_{\ell m}^{m'_{\max}} \equiv S_{\ell m}^{m'_{\max}} - S_{\ell m}^{m'_{\max}-1}, \tag{5.52}$$

where $S_{\ell m}^{m'_{\max}}$ is given by Eq. (5.31) with $\phi^{(1)}_{\ell m'}$ and $\phi^{(2)}_{\ell m'}$ set to zero for $|m'|>m'_{\max}$. Concretely, this means truncating the sum (5.39) at $|m'|=m'_{\max}$.

Figure 5.4 displays the quantity $\Delta S_{00}^{m'_{\max}}[\phi^{\mathcal{R}},\phi^{\mathcal{R}}]$ as a function of $m'_{\max}$ at a fixed value of $\ell_{\max}$ and $\Delta r$. On the semilogarithmic scale of the plot, $\Delta S_{00}^{m'_{\max}}$ falls linearly, indicating exponential decay. Although we do not display it, the behaviour of $\Delta S_{00}^{m'_{\max}}[\phi^{\mathcal{R}},\phi^{\mathcal{P}}]$ is identical, and the behaviour is independent of $\Delta r$. Given this rapid decay, we conclude that in practice, we need include only a small number of $m'$ modes; in all other figures in this paper, we use $m'_{\max}=10$.

$S_{\ell m}$'s rapid convergence with $m'_{\max}$ is a consequence of $\phi^{\mathcal{P}}_{\ell m'}$'s rapid falloff with $m'$. As shown in the inset of Fig. 5.4, this falloff is exponential, like that of $\Delta S_{\ell m}^{m'_{\max}}$. The exponential falloff naturally extends from $\phi^{\mathcal{P}}_{\ell m'}$ to $\phi^{\mathcal{R}}_{\ell m'}$, since $\phi^{\rm ret}$ will never possess worse convergence properties than those of $\phi^{\mathcal{P}}$, and from there it extends to the convergence of the sum (5.39) and finally to Eq. (5.31).

We can best understand this behaviour, and predict its extension to the gravity case, by obtaining analytical estimates of $\phi^{\mathcal{P}}_{\ell m'}$'s falloff. First consider the decomposition into $m'$ modes, without the attendant decomposition into $\ell$ modes. An $m'$ mode is defined by $\phi^{\mathcal{P}}_{m'}=\int_0^{2\pi}e^{-im'\beta}\phi^{\mathcal{P}}d\beta$. For all $\alpha\neq 0$, we can integrate by parts $p$ times to express this as

$$\phi^{\mathcal{P}}_{m'} = \left(\frac{-i}{m'}\right)^p\int_0^{2\pi}e^{-im'\beta}\partial^p_\beta\phi^{\mathcal{P}}d\beta. \tag{5.53}$$

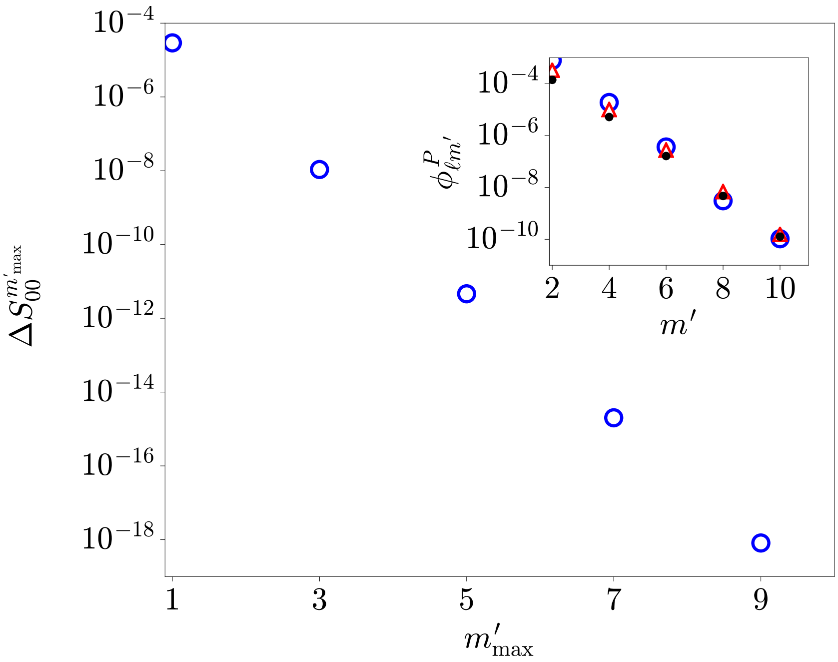


Figure 5.4: Influence of $m'$ modes on $S_{\ell m}$. The main plot shows $\Delta S_{00}^{m'_{\max}}[\phi^{\mathcal{R}},\phi^{\mathcal{R}}]$, which is seen to fall off linearly on the plot's semilog scale, implying exponential decay with $m'_{\max}$. The inset shows $\phi^{\mathcal{P}}_{\ell m'}$ as a function of $m'$ for $\ell=10$ (open blue circles), $\ell=20$ (closed black circles), and $\ell=30$ (open red triangles). In all cases, the modes decay exponentially with $m'$; this behaviour carries over to $\phi^{\mathcal{R}}_{\ell m'}$ and explains the falloff of $\Delta S_{\ell m}^{m'_{\max}}$. To obtain this data we used a fourth-order puncture, $\ell_{\max}=30$, and $\Delta r=10^{-4}$.

Hence,

$$|\phi^{\mathcal{P}}_{m'}|\leq\frac{C(\Delta r,\alpha)}{|m'|^p},\tag{5.54}$$

where $C(\Delta r,\alpha)\equiv 2\pi\max_\beta|\partial^p_\beta\phi^{\mathcal{P}}|$ is independent of $m'$. Since $\phi^{\mathcal{P}}$ is a $C^\infty$ function of $\beta$ at each fixed $\alpha\neq 0,\pi$, the bound (5.54) holds for all integers $p\geq 0$, and we can see by induction that $\phi^{\mathcal{P}}_{m'}$ falls faster than any inverse power of $|m'|$. This rate is uniform in $\Delta r$ for each $\alpha\neq 0,\pi$; it is not uniform in $(\Delta r,\alpha)$ because the divergence at the particle implies $\sup C(\Delta r,\alpha)=\infty$.

Now consider the decomposition into $\ell m'$ modes, which we may write as $\phi^{\mathcal{P}}_{\ell m'}=N_{\ell m'}\int_0^\pi\phi^{\mathcal{P}}_{m'}P^{m'}_\ell(\cos\alpha)\sin\alpha d\alpha$, where $N_{\ell m'}=\sqrt{\frac{2\ell+1}{4\pi}\frac{(\ell-m')!}{(\ell+m')!}}$. Because the exponential falloff of $\phi_{m'}$ is nonuniform, we might worry that it does not extend to $\phi_{\ell m'}$. However, we can quickly deduce that that is not the case. Using the bound [100] $|N_{\ell m'}P^{m'}_\ell|\leq\sqrt{\frac{2\ell+1}{8\pi}}$ and Eq. (5.53), we have

$$|\phi^{\mathcal{P}}_{\ell m'}|\leq\frac{1}{|m'|^p}\sqrt{\frac{2\ell+1}{8\pi}}\int_0^\pi\int_0^{2\pi}|\partial^p_\beta\phi^{\mathcal{P}}\sin\alpha|d\alpha.\tag{5.55}$$

Next we note that $\partial^p_\beta\phi^{\mathcal{P}}$ has the same behaviour as $\phi^{\mathcal{P}}$: it is finite except at $\Delta r = 0$, where it diverges as $\sim 1/\alpha$ at small $\alpha$; the derivatives with respect to $\beta$ do not alter this behaviour. Hence, the $\ell m'$-independent integral $\int_0^\pi\int_0^{2\pi}|\partial^p_\beta\phi^{\mathcal{P}}\sin\alpha|d\alpha$ exists for all integers $p \geq 0$, and we infer by induction that $\phi^{\mathcal{P}}_{\ell m'}$ falls off faster than any power of $|m'|$. Of course, we can only consider large $m'$ if $\ell$ is at least as large. But because the only $\ell$ dependence in the bound (5.55) is the factor $\sqrt{2\ell+1}$, this consideration does not affect our conclusion.

Of course, exponential convergence does not necessarily mean usefully fast convergence. As we have seen, the falloff of $\phi^{\mathcal{P}}_{\ell m}$ with $\ell$ is exponentially fast at all points away from $\Delta r = 0$, but for practical purposes it is slow for small $\Delta r$. However, that is an artefact of the convergence rate being nonuniform. Crucially, the convergence with $m'_{\max}$ *is* uniform in $\Delta r$.

The (uniformly) rapid falloff of $\Delta S^{m'_{\max}}_{\ell m}[\phi^{\mathcal{R}},\phi^{\mathcal{P}}]$ and $\Delta S^{m'_{\max}}_{\ell m}[\phi^{\mathcal{R}},\phi^{\mathcal{R}}]$ with $m'_{\max}$ now follows directly from the rapid falloff of $\phi^{P}_{\ell m'}$. Because this conclusion relies only on generic behaviour of the puncture, it will also apply in the gravity case.

### 5.3.9 Convergence with $\ell_{\max}$

We now turn to the central issue of the convergence rate with $\ell_{\max}$. To assess that, we examine the finite difference

$$\Delta S^{\ell_{\max}}_{\ell m} \equiv S^{\ell_{\max}}_{\ell m} - S^{\ell_{\max}-1}_{\ell m}, \tag{5.56}$$

where $S^{\ell_{\max}}_{\ell m}$ is the partial sum in Eq. (5.32).

Figure 5.5 displays $\Delta S^{\ell_{\max}}_{00}[\phi^{\mathcal{R}},\phi^{\mathcal{P}}]$ and $\Delta S^{\ell_{\max}}_{00}[\phi^{\mathcal{R}},\phi^{\mathcal{R}}]$ at a point very near the particle ($\Delta r = 10^{-12}$). We see that when so close to the particle, the sum (5.31) exhibits power law convergence. At large enough $\ell_{\max}$, this will morph into exponential convergence, as $\phi_{\ell m}$'s slow exponential decay with $\ell$ eventually takes over. The further we move from the particle, the less clean the power laws, and the more quickly the exponential convergence dominates.

The most important aspect of the power laws are their dependence on the order of the puncture. As we will discuss below, a subtle competition between power laws makes determining the true asymptotics nontrivial, and the numerical results can be misleading. Nevertheless, the numerics provide a useful frame for the discussion. For a $k$th-order puncture, Fig. 5.5 suggests that $S_{00}[\phi^{\mathcal{R}},\phi^{\mathcal{R}}]$ converges as

$$\Delta S^{\ell_{\max}}_{00}[\phi^{\mathcal{R}},\phi^{\mathcal{R}}] \sim \begin{cases} \ell_{\max}^{-1} & \text{if } k=1, \\ \ell_{\max}^{-3} & \text{if } k=2, \\ \ell_{\max}^{-7} & \text{if } k=3 \text{ or } 4; \end{cases} \tag{5.57}$$

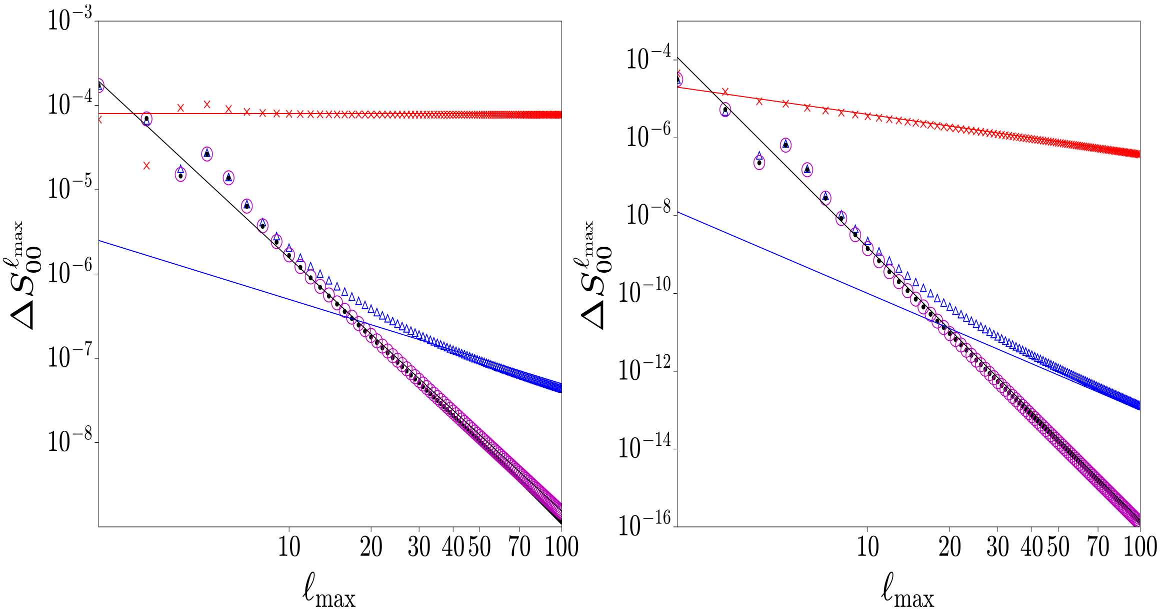


Figure 5.5: The impact of the puncture order $k$ on $S_{\ell m}$'s convergence with $\ell_{\max}$. $\Delta S_{00}^{\ell_{\max}}[\phi^{\mathcal{R}}, \phi^{\mathcal{P}}]$ (left panel) and $\Delta S_{00}^{\ell_{\max}}[\phi^{\mathcal{R}}, \phi^{\mathcal{R}}]$ (right) are plotted as functions of $\ell_{\max}$. In both panels, results are shown for $k = 1$ (red crosses), $k = 2$ (blue triangles), $k = 3$ (solid black circles), and $k = 4$ (open purple circles) and $\Delta r = 10^{-12}$. The straight lines show the asymptotic behaviour $\propto l_{\max}^p$ of the data. In the left panel, listed from top to bottom, they are proportional to $\ell_{\max}^0$, $\ell_{\max}^{-1}$, and $\ell_{\max}^{-3}$; in the right panel, $\ell_{\max}^{-1}$, $\ell_{\max}^{-3}$, and $\ell_{\max}^{-7}$.

we will demonstrate below that for $k = 3$, this inferred falloff is incorrect, and that one would have to go to much larger values of $\ell_{\max}$ to see the true asymptotic behaviour. But the essential facts are unaltered by that: In order for $S_{\ell m}$ to converge with $\ell_{\max}$, $\Delta S_{\ell m}^{\ell_{\max}}$ must fall off at least as $\ell_{\max}^{-1-p}$ with $p > 0$. Hence, to ensure numerical convergence of $S_{00}[\phi^{\mathcal{R}}, \phi^{\mathcal{R}}]$, we must use at least a second-order puncture. Although exponential convergence would eventually manifest, in a concrete situation where we have access to modes up to $\ell = \ell_{\max}$, the exponential convergence would only assist us at distances $|\Delta r| \sim r_0$ from the particle.

Because $\phi^{\mathcal{P}}$ is singular, $S_{00}[\phi^{\mathcal{R}}, \phi^{\mathcal{P}}]$ converges more slowly than $S_{00}[\phi^{\mathcal{R}}, \phi^{\mathcal{R}}]$. According to Fig. 5.5,

$$\Delta S_{00}^{\ell_{\max}}[\phi^{\mathcal{R}}, \phi^{\mathcal{P}}] \sim \begin{cases} \ell_{\max}^{0} & \text{if } k = 1, \\ \ell_{\max}^{-1} & \text{if } k = 2, \\ \ell_{\max}^{-3} & \text{if } k = 3 \text{ or } 4; \end{cases} \tag{5.58}$$

again, the inferred falloff for $k = 3$ is incorrect. But again, we can nevertheless draw the essential conclusions: Because they are slower than those of Eq. (5.57), the falloff rates in Eq. (5.58) are the ultimate determiner of how high order our puncture must be.

To ensure numerical convergence of $S_{00}[\phi^{\mathcal{R}}, \phi^{\mathcal{R}}] + 2S_{00}[\phi^{\mathcal{R}}, \phi^{\mathcal{P}}]$, and hence to allow our overarching strategy to succeed, we must use at least a third-order puncture.

All of the behaviour we have just described is generic; it is not particular to the monopole. We now argue, by way of scaling estimates for arbitrary $k$, that it also extends to the gravitational case. As a byproduct of our derivation, we will also discover, as alluded to above, that the power laws in Eqs. (5.57) and (5.58) are not the true asymptotic falloffs for $k = 3$.

First let us continue to focus on $S_{00}$. We will afterward generalize to arbitrary $\ell m$. Although in practice we use Eq. (5.31) to compute $S_{\ell m}$, Eq. (5.37) will be more useful for our argument. For $\ell = 0$, Eq. (5.29) simplifies to

$$C^{000}_{\ell_1 m_1 s_1 \ell_2 m_2 s_2} = \frac{(-1)^{m_1+s_1}}{\sqrt{4\pi}} \delta^{\ell_1}_{\ell_2} \delta^{m_1}_{-m_2} \delta^{s_1}_{-s_2}, \tag{5.59}$$

where $\delta^i_j$ is a Kronecker delta. Substituting this into Eq. (5.37) and simplifying, we find

$$\begin{aligned} S_{00} = \frac{1}{\sqrt{4\pi}} \sum_{\ell m'} \bigg[ & \partial_r \phi^{(1)}_{\ell m'} \partial_r \phi^{(2)*}_{\ell m'} + \frac{\ell(\ell+1)}{r^2} \phi^{(1)}_{\ell m'} \phi^{(2)*}_{\ell m'} \\ & + \frac{\Omega^2}{4} (\mu^-_{\ell m'} \phi^{(1)}_{\ell, m'+1} - \mu^+_{\ell m'} \phi^{(1)}_{\ell, m'-1})(\mu^-_{\ell m'} \phi^{(2)*}_{\ell, m'+1} - \mu^+_{\ell m'} \phi^{(2)*}_{\ell, m'-1}) \bigg]. \end{aligned} \tag{5.60}$$

Based on the result that $\phi_{\ell m'}$ decays exponentially with $m'$, we may disregard the sum over $m'$ for the purpose of finding the scaling with $\ell_{\max}$. We then obtain the estimate

$$\Delta S^{\ell_{\max}}_{00} \sim \partial_r \phi^{(1)}_{\ell_{\max} 0'} \partial_r \phi^{(2)}_{\ell_{\max} 0'} + l^2_{\max} \phi^{(1)}_{\ell_{\max} 0'} \phi^{(2)}_{\ell_{\max} 0'}. \tag{5.61}$$

Note that the $t$ derivatives in the original source simply contribute to the second term here. They appear in Eq. (5.60) as the term proportional to $\Omega^2$, the dominant piece of which is given by $\frac{1}{2}\Omega^2 \ell(\ell+1) \phi^{(1)}_{\ell 0'} \phi^{(2)}_{\ell 0'}$.

We now appeal to standard results for the large-$\ell$ behaviour of $\phi^{\mathcal{P}}_{\ell 0'}$ and $\phi^{\mathcal{R}}_{\ell 0'}$ [88]. It is well known that when evaluated on the particle, (a) $\partial^n_r \phi^{\mathcal{P}}_{\ell 0'} Y_{\ell 0'} \sim \ell^n$ and $\partial^n_r \phi^{\mathcal{R}}_{\ell 0'} Y_{\ell 0'} \sim \ell^{n-k}$ for a $k$th-order puncture, and (b) the odd negative powers of $\ell$ in $\partial^n_r \phi^{\mathcal{R}}_{\ell 0'} Y_{\ell 0'}$ identically vanish. Noting that $Y_{\ell 0'}(0, \beta) \sim \ell^{1/2}$, we infer that $\phi^{\mathcal{P}}_{\ell 0'} \sim \ell^{-1/2}$, $\partial_r \phi^{\mathcal{P}}_{\ell 0'} \sim \ell^{1/2}$, $\phi^{\mathcal{R}}_{\ell 0'} \sim \ell^{-5/2 - 2\lfloor \frac{k-1}{2} \rfloor}$, and $\partial_r \phi^{\mathcal{R}}_{\ell 0'} \sim \ell^{-1/2 - 2\lfloor \frac{k}{2} \rfloor}$, where $\lfloor s \rfloor$ denotes the largest integer less than or equal to $s$. These results hold at $\Delta r = 0$; at finite $\Delta r$, they transition into exponential decay in the now familiar manner. Substituting this behaviour into Eq. (5.61) yields

$$\Delta S^{\ell_{\max}}_{00}[\phi^{\mathcal{R}}, \phi^{\mathcal{R}}] \sim \ell^{-1-4\lfloor \frac{k}{2} \rfloor}_{\max} + \ell^{-3-4\lfloor \frac{k-1}{2} \rfloor}_{\max} \tag{5.62a}$$

$$\sim \ell^{1-2k}_{\max} \tag{5.62b}$$

and

$$\Delta S_{00}^{\ell_{\max}}[\phi^{\mathcal{R}}, \phi^{\mathcal{P}}] \sim \ell_{\max}^{-2\lfloor\frac{k}{2}\rfloor} + \ell_{\max}^{-1-2\lfloor\frac{k-1}{2}\rfloor} \tag{5.63a}$$
$$\sim \ell_{\max}^{1-k}. \tag{5.63b}$$

In Eqs. (5.62a) and (5.63a), the first term arises from $(\partial_r\phi)^2$ and the second arises from $(\partial_t\phi)^2 + \frac{1}{r^2}\partial_A\phi\partial^A\phi$; these two terms alternate in dominance from one $k$ to the next.

To extend our estimates to generic $\ell m$ modes, we note that in Eq. (5.32), when $\ell_1 \sim \ell_{\max} \gg l$, the triangle inequality also enforces $\ell_2 \sim \ell_{\max} \gg \ell$. We can then appeal to the approximation

$$\begin{pmatrix} \ell & \ell_1 & \ell_2 \\ m & m_1 & m_2 \end{pmatrix} \approx (-1)^{\ell_2+m_2}\frac{d^{\ell}_{m,\ell_2-\ell_1}(\gamma)}{\sqrt{\ell_1+\ell_2+1}} \sim \frac{1}{\ell_{\max}^{1/2}} \tag{5.64}$$

for $\ell \ll \ell_1, \ell_2$, where $\cos\gamma = (m_1 - m_2)/(\ell_1+\ell_2+1)$. This implies

$$C^{\ell m s}_{\ell_1 m' s_1 \ell_2 m_2 s_2} \sim \ell_{\max}^0. \tag{5.65}$$

Given this, we can apply the same arguments as above and find the same scaling estimates: $\Delta S_{\ell m}^{\ell_{\max}}[\phi^{\mathcal{R}}, \phi^{\mathcal{R}}] \sim \ell_{\max}^{1-2k}$ and $\Delta S_{\ell m}^{\ell_{\max}}[\phi^{\mathcal{R}}, \phi^{\mathcal{P}}] \sim \ell_{\max}^{1-k}$. From this, we again conclude that at least a third-order puncture is needed to ensure convergence.

We now return to the numerically determined scalings in Eqs. (5.57) and (5.58). Comparing them to Eqs. (5.62b) and (5.63b), we see that the numerical estimates agree with the analytical ones except in the case of $k = 3$, as mentioned previously. This discrepancy stems from Eqs. (5.62a) and (5.63a). There we see that for a given $k$, two power laws compete for dominance. In practice, we find that the coefficients of these power laws can dramatically differ. Let us focus on $\Delta S_{00}^{\ell_{\max}}[\phi^{\mathcal{R}}, \phi^{\mathcal{R}}]$ for concreteness. For $k = 3$, the dominant power in Eq. (5.62a) is $\ell_{\max}^{-5}$, and it arises from $(\partial_r\phi)^2$; the subdominant power is $\ell_{\max}^{-7}$, and it arises from $(\partial_t\phi)^2 + \frac{1}{r^2}\partial_A\phi\partial^A\phi$. In our numerical results, we only see the latter, subdominant behaviour. Why? Because it comes with an enormously larger numerical coefficient. This is demonstrated in Fig. **??**, which plots the contributions from $(\partial_r\phi)^2$ and $(\partial_t\phi)^2 + \frac{1}{r^2}\partial_A\phi\partial^A\phi$ separately. Each of the separate terms is in agreement with Eqs. (5.62a) and (5.63a), but we see that for $k = 3$, $\Delta[(\partial_r\phi)^2]_{00}^{\ell_{\max}}$ is hugely suppressed relative to $\Delta[(\partial_t\phi)^2 + \frac{1}{r^2}\partial_A\phi\partial^A\phi]_{00}^{\ell_{\max}}$, even though $\Delta[(\partial_r\phi)^2]_{00}^{\ell_{\max}}$ is decaying more slowly. In fact, by fitting the curves, we can estimate that for $k = 3$ and $r_0 = 10$, the true asymptotic behaviour would only become numerically apparent at $\ell_{\max} > 450$.

This competition between terms appears to be a robust feature of the model: numerical investigations show that it is independent of $\ell$ and $m$ and largely independent of $r_0$, though it subsides at smaller values of $r_0$. Furthermore, the underlying cause is not confined to $k = 3$, as we find that the coefficients of various powers of $1/\ell_{\max}$ in $\Delta S_{\ell m}^{\ell_{\max}}$

often differ by factors of $10^4$ or more. Indeed, this is true not just in $\Delta S^{\ell_{\max}}_{\ell m}$, but also within the individual contributions $\Delta[(\partial_r\phi)^2]^{\ell_{\max}}_{\ell m}$, $\Delta[(\partial_t\phi)^2]^{\ell_{\max}}_{\ell m}$, and $\frac{1}{r^2}[\partial_A\phi\partial^A\phi]^{\ell_{\max}}_{\ell m}$. We have no reason to believe that this is particular to our model. Wildly disparate coefficients of the powers of $1/\ell_{\max}$ could very well occur in the gravitational case as well. Because of this, in principle, one might encounter a situation in which one's numerical results had *appeared* to converge, when in fact a divergent power of $1/\ell_{\max}$ was still waiting to emerge at larger $\ell_{\max}$. One can only eliminate this possibility by appealing to analytical estimates of the sort in Eqs. (5.62b) and (5.63b).

With this additional impetus, we now extend our estimates to the gravitational case. Because $\delta^2 G_{i\ell m}$ has the same form as $S_{\ell m}$, and because $h^{1\mathcal{R}}_{il m'}$ and $h^{1\mathcal{P}}_{il m'}$ have the same behaviour as $\phi^{\mathcal{P}}_{\ell m'}$ and $\phi^{\mathcal{R}}_{\ell m'}$, similar estimates will apply. The only difference between the two cases is that $\delta^2 G$ contains terms of the form $h\partial^2 h$ and terms that mix $t, r, \theta^A$ derivatives. Assume we can account for these changes by adopting a generic form

$$\begin{aligned}\Delta\delta^2 G^{\ell_{\max}}_{i\ell m} \sim \partial_r h_{j\ell_{\max}0'}\partial_r h_{k\ell_{\max}0'} + {\ell_{\max}}^2 h_{j\ell_{\max}0'}h_{k\ell_{\max}0'} + \ell_{\max} h_{j\ell_{\max}0'}\partial_r h_{k\ell_{\max}0'}\\ + h_{j\ell_{\max}0'}\partial_r^2 h_{k\ell_{\max}0'}\end{aligned} \tag{5.66}$$

in place of Eq. (5.61). Using $\partial_r^2 h^{\mathcal{P}}_{i\ell 0'} \sim \ell^{3/2}$, $\partial_r^2 h^{\mathcal{R}}_{i\ell 0'} \sim \ell^{1/2}$ for $k=1$, $\partial_r^2 h^{\mathcal{R}}_{i\ell 0'} \sim \ell^{-1/2-2\lfloor\frac{k-1}{2}\rfloor}$ for $k>1$, and the scalings given above for the lower derivatives, we find that $\Delta\delta^2 G^{\ell_{\max}}_{i\ell m}[h^{\mathcal{R}}, h^{\mathcal{P}}] \sim {\ell_{\max}}^{1-k}$ and $\Delta\delta^2 G^{\ell_{\max}}_{i\ell m}[h^{\mathcal{R}}, h^{\mathcal{R}}] \sim {\ell_{\max}}^{-k-2\lfloor\frac{k-1}{2}\rfloor}$. The first of these convergence rates is the slower of the two, and it is identical to the scalar model. Therefore, we conclude that like in the scalar model, for our strategy to be effective in the gravitational case, *it requires at least a third-order puncture* $h^{1\mathcal{P}}_{\mu\nu}$.

## 5.4 Computing $S_{\ell m}[\phi^{\mathcal{P}}, \phi^{\mathcal{P}}]$

The only term that remains to be computed in Eq. (5.8) is $S_{\ell m}[\phi^{\mathcal{P}}, \phi^{P}]$. As we described in the outline of our strategy, we calculate the modes of $S_{\ell m}[\phi^{\mathcal{P}}, \phi^{P}]$ by substituting the 4D expression (5.40) into the 4D expression for $S$ and then integrating against spherical harmonics to obtain the modes.

More precisely, our procedure is summarized by the following four steps:

1. Begin with the puncture field (5.40) in the rotated coordinates $\alpha^{A'}$.
2. Construct the 4D expression $S[\phi^{\mathcal{P}}, \phi^{\mathcal{P}}]$ in $\alpha^{A'}$ coordinates using Eq. (5.33).
3. Decompose $S[\phi^{\mathcal{P}}, \phi^{\mathcal{P}}]$ into $\ell m'$ modes $S_{\ell m'}[\phi^{\mathcal{P}}, \phi^{\mathcal{P}}]$ by evaluating the integrals (5.34).
4. Use Eq. (5.39) to obtain the $\ell m$ modes $S_{\ell m}[\phi^{\mathcal{P}}, \phi^{\mathcal{P}}]$.

The nontrivial step in this procedure is the evaluation of the integrals (5.34). We perform that evaluation in the same manner as we did the integrals in Sec. 5.3.2. Again we use two independent methods of evaluation: fully numerical and mixed analytical-numerical. The only new features of the integrals is that the integrand now contains explicit factors of $\sin\alpha$ and $\cos\alpha$ as well as higher powers, and even powers, of $\rho$ in their denominator. Because Eq. (5.44) is defined only for odd $n$, the method described in Sec. 5.3.3 is not immediately applicable; an even-$n$ analog of Eq. (5.44) would be required. However, the even powers of $n$ are readily handled by the methods described in Secs. 5.3.4 and 5.3.6.

After performing the integrals, we arrive at our promised result displayed in Fig. 5.2. There we see that near the particle, where $S_{\ell m}[\phi^{\rm ret}, \phi^{\rm ret}]$ converges too slowly with $\ell_{\rm max}$ to see any singularity at $\Delta r = 0$, our computed $S_{\ell m}$ correctly behaves as $1/(\Delta r)^2$. Further from the particle, where $S_{\ell m}[\phi^{\rm ret}, \phi^{\rm ret}]$ rapidly converges with $\ell_{\rm max}$, our computed $S_{\ell m}$ correctly recovers $S_{\ell m}[\phi^{\rm ret}, \phi^{\rm ret}]$.

## 5.5 Conclusion

We have now demonstrated that our strategy successfully circumvents the problem of slow convergence described in the introduction. This success is encapsulated by Fig. 5.2.

The core tools in our strategy are adopted from mode-sum regularization and effective-source schemes, but our analysis has highlighted several unforeseen complications in applying these standard methods. Specifically, we have found that notable intricacies arise in computing mode decompositions in rotated coordinates that place the particle at the north pole. Traditionally, the time dependence of the rotation could be treated cavalierly, but in the calculations described here, it must be handled with care; traditionally, as explained in Sec. 4.6 only the $m = 0, \pm1, \pm2$ azimuthal modes are required in the rotated coordinates (see the mode-decomposition of the puncture given in Eq. (C.16)), but here a significant number must be computed; and traditionally, the relevant Legendre integrals can often be simplified by analyzing them in the limit $r \to r_0$, but here they must be evaluated *exactly* in some finite range of $r$ around $r_0$.

Although our implementation has been in a simple scalar toy model, our strategy and computational tools are not in any way specific to that model, and they can be applied directly to the physically relevant gravitational problem. This strategy will be implemented in Chapter 8.

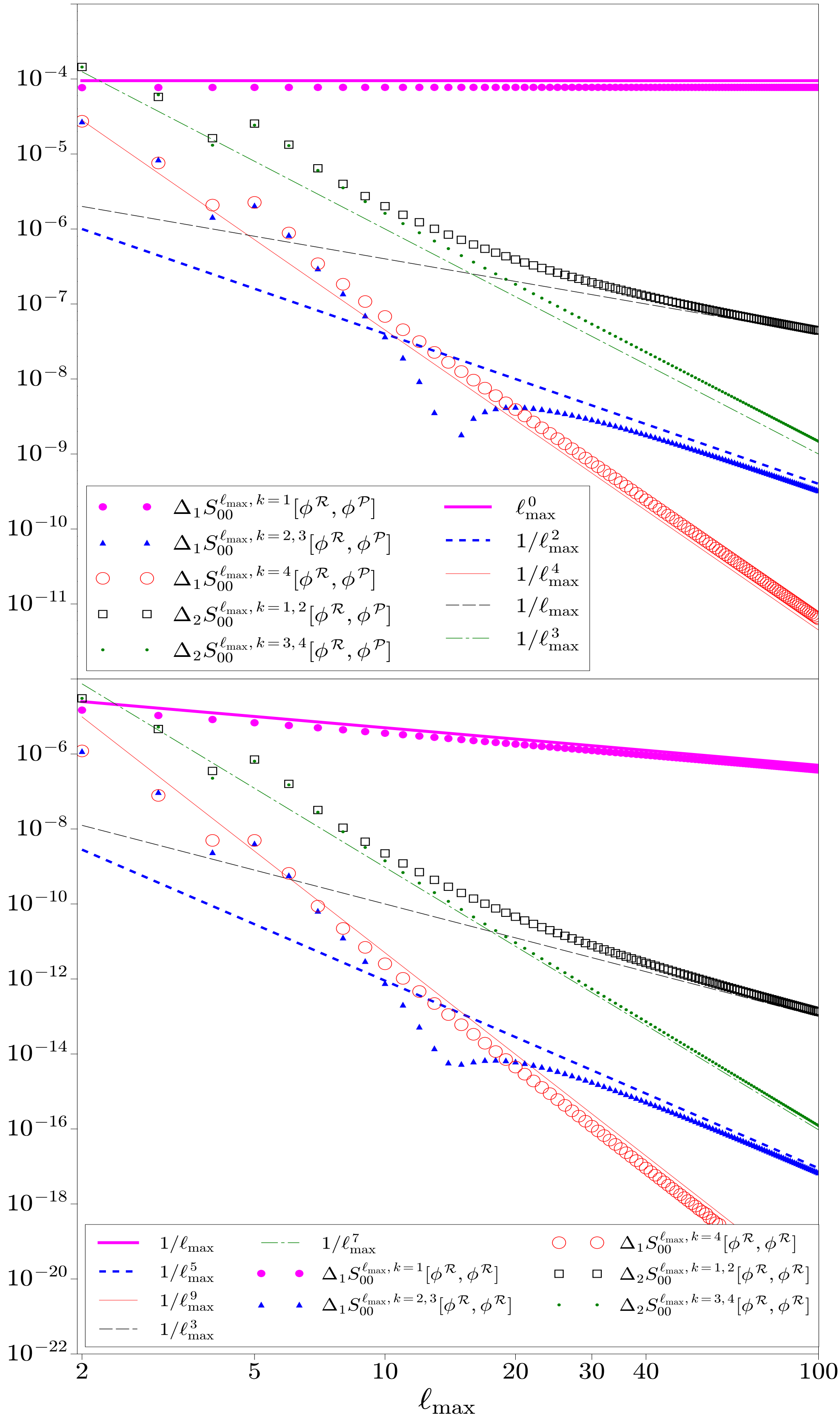


Figure 5.6: Comparison of two contributions to $\Delta S_{00}^{\ell_{\rm max}}[\phi^{\mathcal{R}},\phi^{\mathcal{P}}]$ (upper panel) and $\Delta S_{00}^{\ell_{\rm max}}[\phi^{\mathcal{R}},\phi^{\mathcal{R}}]$ (lower), using the same parameters as in Fig. 5.5. $\Delta_1 S_{00}^{\ell_{\rm max}}[\phi^{(1)},\phi^{(2)}]$ represents the contribution from $\partial_r\phi^{(1)}\partial_r\phi^{(2)}$ and $\Delta_2 S_{00}^{\ell_{\rm max}}[\phi^{(1)},\phi^{(2)}]$ represents the contribution from $\partial_t\phi^{(1)}\partial_t\phi^{(2)} + \frac{1}{r^2}\Omega^{AB}\partial_A\phi^{(1)}\partial_B\phi^{(2)}$. For $k=1$, the dominant contribution comes from large solid magenta circles; for $k=2$, from open black squares; for $k=4$, from small solid green circles. For $k=3$, the dominant contribution appears to come from small solid green circles, but because the solid blue triangles are falling more slowly, they will eventually become dominant at sufficiently large $\ell_{\rm max}$.

# Chapter 6

# Second-order perturbation theory in a scalar-field toy model: the problem of infrared divergences

In Chapter 4, we have computed the first-order field by treating the source orbit as circular, based on looking at a short interval of time. But going to second order, we cannot calculate the field with a geodesic source orbit over long timescales.

On the orbital timescale, $T = 2\pi/\Omega \sim \epsilon^0$, deviations from a geodesic in the background are small ($\sim \epsilon$) and can be neglected in the first-order field $h^1_{\mu\nu}(x;\gamma)$. As such we can solve the linearized Einstein equations with a geodesic source orbit. Conveniently, such a source has a discrete frequency spectrum, allowing us to solve the equations in the frequency domain as we did in Chapter 4.

But if we want to model the EMRI over long timescales, we will not have the luxury of this method because the deviation from geodesic motion grows large in both the past and the future. Because this deviation contributes to the second-order source, the accumulated error due to this approximation manifests as a secular growth in the second-order field. We can quantify this effect by appealing to (1.28). On the orbital timescale ($\Delta t_{\text{orbit}} \sim \epsilon^0$), the deviation, $\delta z^\mu$ from a geodesic due to first-order self-force effects, is small [$\sim O(\epsilon)$]. But during the time of inspiral ($\Delta t_{\text{inspiral}} \sim 1/\epsilon$), the deviation $\delta z^\mu$ (specifically, the error in the orbital phase, $\delta\varphi_p$) grows to be much larger.

Even more, because errors propagate at finite speeds, secular errors at large past times cause growing errors at large distances at fixed time. This is illustrated in Fig. 6.1. Consider a hypersurface of constant time, $t = t_0$, and some point along the worldline at some time $t_{\text{past}}$ to its past. The radial extent of the domain of influence of the event $t_{\text{past}}$ within that hypersurface grows linearly with the time interval $t_0 - t$. Thus, secular errors in the far past can produce large errors at large distances at present.

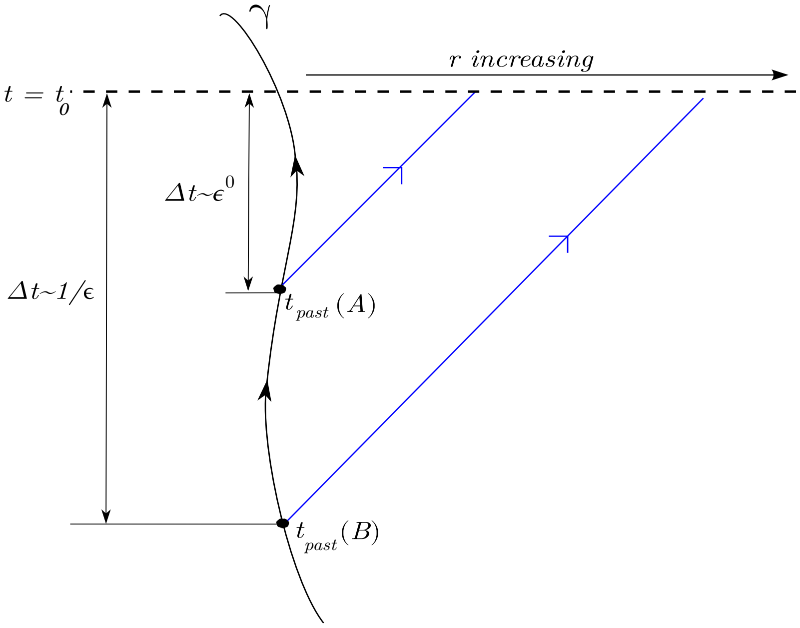


Figure 6.1: At a fixed time $t_0$, fields from source-points on $\gamma$ within the time scale $\Delta t \sim 1/\epsilon$ (such as $B$), propagate along null lines to points at larger $r$ than the fields from source points within the time scale $\Delta t \sim \epsilon^0$ along $\gamma$, such as $A$.

An obvious workaround would be to restrict ourselves to small timescales, in which we can approximate the source orbit to be bound and periodic. But this leads to a second problem. Such a bound periodic source at first order, leads to an everywhere-divergent retarded solution at second order. These divergences are a feature of the fact that the first-order field itself generates curvature, which induces a non-compact source at second order, in the sense that it propagates from every point in spacetime. Mathematically this manifests in a source whose leading-order behaviour falls off too slowly to form a convergent integral against the retarded Green's function over all spacetime. This results in an infrared divergence.

In this chapter, which is entirely based on [75], we show how to overcome both problems that arise at large $r$. In doing so we develop a framework that includes all the physical effects, works on both short and long timescales, and still allows us to work in the frequency domain. We resolve the problem of secular growth using a two-timescale expansion of the field. An infrared divergence of the type just described still arises in this approximation. We cure it by cutting off the retarded integral over $r$ at some large-$r$ cutoff, and adding a homogeneous solution with a constant coefficient, to account for the piece of the field that was removed. We refer to the region beyond the cutoff as the far zone; the region below the cutoff, as the near zone. The coefficient is fixed by matching to an exact solution in the far zone, derived via a post-Minkowski (PM) expansion. We use the scalar-field toy model introduced in Chapter 5 to do the hard work of developing an approach for resolving these obstacles. We will carry this strategy over to the full field equations in gravity, when we come to solving them in Chapters 7 and 8.

## 6.1 Multiscale expansion

In a multiscale expansion of a function $f(\lambda,\epsilon)$, where $\epsilon \ll 1$, we define a fast time $\lambda_{\text{fast}}(\lambda,\epsilon) \sim \epsilon^0\lambda$, and a slow time $\lambda_{\text{slow}}(\lambda,\epsilon) \sim \epsilon\lambda$. We then assume that the function can be uniformly approximated as

$$f\left(\lambda,\epsilon\right) = \sum_n \epsilon^n \tilde{f}_n(\lambda_{\text{fast}},\lambda_{\text{slow}}). \tag{6.1}$$

We may calculate derivatives of $f\left(\lambda,\epsilon\right)$ with respect to $\lambda$ using the chain rule

$$\frac{d\tilde{f}}{d\lambda} = \frac{\partial \tilde{f}}{\partial \lambda_{\text{fast}}}\frac{d\lambda_{\text{fast}}}{d\lambda} + \frac{\partial \tilde{f}}{\partial \lambda_{\text{slow}}}\frac{d\lambda_{\text{slow}}}{d\lambda}. \tag{6.2}$$

Then, in order to solve differential equations in the dependent variable $f(\lambda,\epsilon)$, we substitute Eq. (6.1) for $f(\lambda,\epsilon)$, write derivatives as in Eq. (6.2) and we treat $\lambda_{\text{fast}}$ and $\lambda_{\text{slow}}$ as independent variables.

In our problem, we adopt $\tilde{t} \equiv \epsilon t$ as the slow variable on the worldline $z^\mu$, and as the fast variable we adopt the azimuthal angle $\varphi_p$. The extension away from the worldline will be discussed below. Writing everything in terms of these two timescales, we expand in powers of $\epsilon$ at fixed $\tilde{t}$ and $\varphi_p$. The slow-time $\tilde{t}$ only changes appreciably over the radiation-reaction time scale $t \sim 1/\epsilon$; on that scale, $\tilde{t} \sim 1$.

### 6.1.1 Expansion of the worldline

We assume that the worldline depends on a small parameter $\epsilon \ll 1$ analogous to $\mu/M$. By analogy with the equation of motion (1.37), we write the equation of motion that is coupled to the toy-model field equations (5.4) and (5.7), as

$$\frac{D^2 z^\mu}{d\tau^2} = f^\mu_{\text{ext}} + \epsilon f^{1\mu}_{\text{self}} + \epsilon^2 f^{2\mu}_{\text{self}} + O(\epsilon^3), \tag{6.3}$$

where

$$f^\mu_{\text{ext}} = -\frac{U^2}{r_p^2}\delta^\mu_r \tag{6.4}$$

is a relativistic Coulomb-type radial force per unit mass, where $U(t) \equiv u^t(t)$ and $u^\mu = dz^\mu/d\tau$ is the four velocity of the worldline, $\tau$ being proper time on the worldline. $f^{n\mu}_{\text{self}}$ is the $n$th-order SF per unit mass.

We write the worldline in the parametric form

$$z^{\mu}(t,\epsilon)=\{t,r_p(t,\epsilon),\pi/2,\varphi_p(t,\epsilon)\}. \tag{6.5}$$

From the normalisation $u^{\mu}u^{\nu}\eta_{\mu\nu}=-1$ in flat space, we straightforwardly find that

$$U(t,\epsilon)=1/\sqrt{1-r_p(t,\epsilon)^2\Omega(t,\epsilon)^2}, \tag{6.6}$$

where $\Omega(t,\epsilon)\equiv d\varphi_p(t,\epsilon)/dt$.

We next write the worldline coordinates in Eq. (6.5) in terms of a slow-time $\tilde{t}\equiv\epsilon t$, as $r_p(t,\epsilon)=\tilde{r}_p(\tilde{t},\epsilon)$ and $\varphi_p(t,\epsilon)=\tilde{\varphi}_p(\tilde{t},\epsilon)$. Since the orbital radius and frequency evolve slowly, we may write $\tilde{r}_p(\tilde{t},\epsilon)$ and $\Omega(t,\epsilon)=\tilde{\Omega}(\tilde{t},\epsilon)$ as

$$\tilde{r}_p(\tilde{t},\epsilon)=\tilde{r}_0(\tilde{t})+\epsilon\tilde{r}_1(\tilde{t})+O(\epsilon^2), \tag{6.7}$$

$$\tilde{\Omega}(\tilde{t},\epsilon)=\tilde{\Omega}_0(\tilde{t})+\epsilon\tilde{\Omega}_1(\tilde{t})+O(\epsilon^2). \tag{6.8}$$

The orbital phase, $\varphi_p(t,\epsilon)=\tilde{\varphi}_p(\tilde{t},\epsilon)$, is recovered from the frequency as

$$\begin{aligned}\tilde{\varphi}_p(\tilde{t},\epsilon)=&\frac{1}{\epsilon}\int_0^{\tilde{t}}d\tilde{s}\left[\tilde{\Omega}_0(\tilde{s})+\epsilon\tilde{\Omega}_1(\tilde{s})\right]+O(\epsilon)\\=&\frac{1}{\epsilon}\left[\tilde{\varphi}_0(\tilde{t})+\epsilon\tilde{\varphi}_1(\tilde{t})+O(\epsilon^2)\right].\end{aligned} \tag{6.9}$$

Similarly, writing $U(t,\epsilon)$ in terms of slow time as $U(t,\epsilon)=\tilde{U}(\tilde{t},\epsilon)$ and inserting the expansions (6.7) and (6.9) into (6.6), we may derive the expansion

$$\tilde{U}(\tilde{t},\epsilon)=\tilde{U}_0(\tilde{t})+\epsilon\tilde{U}_1(\tilde{t})+O(\epsilon^2), \tag{6.10}$$

where $\tilde{U}_0=1/\sqrt{1-\tilde{r}_0^2\tilde{\Omega}_0^2}$ and $\tilde{U}_1(\tilde{t})=\epsilon\frac{\partial\tilde{U}(\tilde{t},\epsilon)}{\partial\epsilon}(\tilde{t},0)$.

Expressions for the $\tilde{r}_n$ and $\tilde{\Omega}_n$ may be derived in terms of $f^{n\mu}_{\text{self}}$, by solving the equation of motion order by order in $\epsilon$. Because there is no motion in the $\theta$ direction and $\left(D^2z^{\mu}/d\tau^2\right)u_{\mu}=0$, only two components of the equation of motion are independent, which we select to be the $t$ and $r$ directions, following the choice in [75]. Inserting the expansions (6.7) and (6.8) and using $d/dt=\epsilon d/d\tilde{t}$, we find that the $t$ component of (6.3) reads

$$\epsilon\frac{dU}{d\tilde{t}}=\frac{1}{U}\left[\epsilon f^{1t}_{\text{self}}+\epsilon^2f^{2t}_{\text{self}}+O(\epsilon^3)\right], \tag{6.11}$$

and the $r$ component reads

$$\epsilon^2\frac{d^2r_p}{d\tilde{t}^2}+\epsilon^2\frac{1}{U}\frac{dU}{d\tilde{t}}\frac{dr_p}{d\tilde{t}}-r_p\Omega^2=-\frac{1}{r_p^2}+\frac{1}{U^2}\left[\epsilon f^{1r}_{\text{self}}+\epsilon^2f^{2r}_{\text{self}}+O(\epsilon^3)\right]. \tag{6.12}$$

Following the approach in [75], on the right hand side of (6.11) and (6.12), we write the self-forces as a function of slow time, as $f^{n\mu}_{\rm self}(t,\epsilon) = \tilde{f}^{n\mu}_{\rm self}(\tilde{t},\epsilon)$ and expand them in powers of $\epsilon$ at fixed slow time, to yield

$$\epsilon f^{1\mu}_{\rm self}(t,\epsilon) + \epsilon^2 f^{2\mu}_{\rm self}(t,\epsilon) = \epsilon \tilde{f}^{1\mu}(\tilde{t}) + \epsilon^2 \tilde{f}^{2\mu}(\tilde{t}), \tag{6.13}$$

where

$$\tilde{f}^{1\mu}(\tilde{t}) \equiv \tilde{f}^{1\mu}_{\rm self}(\tilde{t},0), \tag{6.14}$$

$$\tilde{f}^{2\mu}(\tilde{t}) \equiv \tilde{f}^{2\mu}_{\rm self}(\tilde{t},0) + \frac{\partial \tilde{f}^{1\mu}_{\rm self}}{\partial \epsilon}(\tilde{t},0). \tag{6.15}$$

Explicit expressions for $\tilde{f}^{n\mu}$ can be found in [75]. Substituting the expansions (6.7), (6.9) and (6.13) into the equations of motion (6.11) and (6.12), we may derive expressions for $\tilde{r}_n(\tilde{t})$ and $\tilde{\Omega}_n(\tilde{t})$ in terms of $\tilde{f}^{\mu}_n$.

At zeroth order in $\epsilon$, (6.11) is trivial but (6.12) yields

$$\tilde{\Omega}_0(\tilde{t}) = \sqrt{\frac{1}{\tilde{r}_0(\tilde{t})^3}}. \tag{6.16}$$

At linear order in $\epsilon$, (6.11) yields an equation for the slow evolution of $\tilde{r}_0$, as

$$\frac{d\tilde{r}_0}{d\tilde{t}} = -\frac{2\tilde{r}_0^2}{\tilde{U}_0^4}\tilde{f}^t_1. \tag{6.17}$$

This slow evolution is caused by the dissipative piece of the SF, as the right hand side of (6.17) implies. At linear order in $\epsilon$, (6.12) yields an equation for $\tilde{\Omega}_1$

$$\tilde{\Omega}_1 = -\frac{1}{2\tilde{r}_0^{5/2}}\left[(1-\tilde{r}_0)\,\tilde{r}_0^2\tilde{f}^{1r} - 3\tilde{r}_1\right]. \tag{6.18}$$

### 6.1.2 Expansion of the field

For the expansion of the scalar field, we require an extension of the two-timescale coordinates away from the worldline. This requires slow and fast variables as fields on spacetime, not only on the worldline. The first-order source is an oscillatory function of $\varphi_p$, with an amplitude that varies slowly with time $t$. The retarded Green's function propagates this behaviour outward along null cones, leading to a first-order solution that (at least at large distances) oscillates with a phase $\varphi_p(u)$ and has an amplitude that varies slowly with $u$, where $u = t - r$. With this in mind, for our slow and fast variables we adopt $\tilde{u} \equiv \epsilon u$ and $\tilde{\varphi}_p(\tilde{u},\epsilon)$. For conciseness, we refer to the latter as $\tilde{\varphi}_p(\tilde{u})$.

Using the same notation as in Chapter 5 for the first- and second-order fields, we write them as harmonic expansions, $\phi_n(x,\epsilon) = \sum_{\ell m}\phi^n_{\ell m}(t,r,\epsilon)Y^{\ell m}(\theta^A)$, and then write the coefficients in terms of two-timescale coordinates, as

$$\phi^n_{\ell m}(t,r,\epsilon) = \tilde{\phi}^n_{\ell m}(\tilde{u},r,\tilde{\varphi}_p(\tilde{u}),\epsilon). \tag{6.19}$$

Now expand the coefficients in powers of $\epsilon$ at fixed $\tilde{u}$ and fixed $\tilde{\varphi}_p(\tilde{u})$, to yield

$$\tilde{\phi}^n_{\ell m}(\tilde{u},r,\tilde{\varphi}_p(\tilde{u}),\epsilon) = \tilde{\phi}^n_{\ell m}(\tilde{u},r,\tilde{\varphi}_p(\tilde{u}),0) + \epsilon\frac{\partial\tilde{\phi}^n_{\ell m}}{\partial\epsilon}(\tilde{u},r,\tilde{\varphi}_p(\tilde{u}),0) + O(\epsilon^2). \tag{6.20}$$

We may then define new first- and second-order fields:

$$\tilde{\phi}^1_{\ell m}(\tilde{u},r,\tilde{\varphi}_p(\tilde{u})) = \tilde{\phi}^1_{\ell m}(\tilde{u},r,\tilde{\varphi}_p(\tilde{u}),0), \tag{6.21}$$

$$\tilde{\phi}^2_{\ell m}(\tilde{u},r,\tilde{\varphi}_p(\tilde{u})) = \tilde{\phi}^2_{\ell m}(\tilde{u},r,\tilde{\varphi}_p(\tilde{u}),0) + \epsilon\frac{\partial\tilde{\phi}^1_{\ell m}}{\partial\epsilon}(\tilde{u},r,\tilde{\varphi}_p(\tilde{u}),0). \tag{6.22}$$

We may write each of the variables $\tilde{\phi}^n_{\ell m}$ explicitly in terms of $\tilde{\varphi}_p(\tilde{u})$ as

$$\tilde{\phi}^n_{\ell m}(\tilde{u},r,\tilde{\varphi}_p(\tilde{u})) = \tilde{R}^n_{\ell m}(\tilde{u},r)e^{-im\tilde{\varphi}_p(\tilde{u})}. \tag{6.23}$$

Similarly, we may expand the source-term, $\varrho$, in Eq. (5.4) as the harmonic expansion $\varrho(x,\epsilon) = \sum_{\ell m}\varrho_{\ell m}(t,r,\epsilon)Y^{\ell m}\left(\theta^A\right)$, and write the coefficients in terms of two-timescale coordinates, as $\varrho_{\ell m}(t,r,\epsilon) = \tilde{\varrho}_{\ell m}(\tilde{u},r,\tilde{\varphi}_r(\tilde{u}),\epsilon)$. We may then define the new source variables

$$\tilde{\varrho}^1_{\ell m}(\tilde{u},r,\tilde{\varphi}_p(\tilde{u})) = \tilde{\varrho}_{\ell m}(\tilde{u},r,\tilde{\varphi}_p(\tilde{u}),0), \tag{6.24}$$

$$\tilde{\varrho}^2_{\ell m}(\tilde{u},r,\tilde{\varphi}_p(\tilde{u})) = \tilde{\varrho}_{\ell m}(\tilde{u},r,\tilde{\varphi}_p(\tilde{u}),0) + \epsilon\frac{\partial\tilde{\varrho}_{\ell m}}{\partial\epsilon}(\tilde{u},r,\tilde{\varphi}_p(\tilde{u}),0), \tag{6.25}$$

with

$$\tilde{\varrho}^n_{\ell m}(\tilde{u},r,\tilde{\varphi}_p(\tilde{u})) = \tilde{\varrho}^n_{\ell m}(\tilde{u},r)e^{-im\tilde{\varphi}_p(\tilde{u})}. \tag{6.26}$$

Explicit expressions are found by substituting Eqs. (6.7)-(6.9) into Eq. (5.9), and then expanding functions of $\tilde{t}$ around $\tilde{u} = \tilde{t} - \epsilon r$, which yields

$$\tilde{\varrho}^1_{\ell m}(\tilde{u},r) = N_{\ell m}\tilde{U}_0^{-1}(\tilde{u})\frac{e^{-im\tilde{\Omega}_0(\tilde{u})r}}{r^2}\delta(r-\tilde{r}_0(\tilde{u})), \tag{6.27}$$

$$\begin{aligned}\tilde{\varrho}^2_{\ell m}(\tilde{u},r) = -N_{\ell m}\tilde{U}_0^{-1}(\tilde{u})\frac{e^{-im\tilde{\Omega}_0(\tilde{u})r}}{r^2}\bigg\{&\left[\tilde{r}_1(\tilde{u}) + r\dot{\tilde{r}}_0(\tilde{u})\right]\delta'(r-\tilde{r}_0(\tilde{u}))\\ &+ \tilde{U}_0^{-1}(\tilde{u})\left[\tilde{U}_1(\tilde{u}) + r\dot{\tilde{U}}_0(\tilde{u})\right]\delta(r-\tilde{r}_0(\tilde{u}))\\ &+ im\left[r\tilde{\Omega}_1(\tilde{u}) + \frac{1}{2}r^2\dot{\tilde{\Omega}}_0(\tilde{u})\right]\delta(r-\tilde{r}_0(\tilde{u}))\bigg\},\end{aligned} \tag{6.28}$$

with $N_{\ell m}$ given by Eq. (5.17).

After combining all of the above expansions in Eqs. (5.4) and (5.7), we group terms by powers of $\epsilon$ at fixed $\tilde{u}$ and $\tilde{\varphi}_p(\tilde{u},\epsilon)$. This leads to the equations

$$\partial_r^2 \tilde{R}^n_{\ell m} + \frac{2}{r}\left(1 + im\tilde{\Omega}_0 r\right)\partial_r \tilde{R}^n_{\ell m} + \frac{1}{r^2}\left[2im\tilde{\Omega}_0 r - \ell(\ell+1)\right]\tilde{R}^n_{\ell m} = \tilde{\mathcal{S}}^n_{\ell m}, \tag{6.29}$$

where the sources are

$$\tilde{\mathcal{S}}^1_{\ell m} = -4\pi\tilde{\varrho}^1_{\ell m}, \tag{6.30}$$

$$\tilde{\mathcal{S}}^2_{\ell m} = \tilde{S}^2_{\ell m} - 4\pi\tilde{\varrho}^2_{\ell m} + 2(\partial_{\tilde{u}} - im\tilde{\Omega}_1)\left(\partial_r \tilde{R}^1_{\ell m} + \frac{1}{r}\tilde{R}^1_{\ell m}\right). \tag{6.31}$$

$\tilde{S}^2_{\ell m}$ are the modes of the nonlinear source term $t^{\alpha\beta}\partial_\alpha\phi^1\partial_\beta\phi^1$ in Eq. (5.7). We have dropped $\Box\phi^{(2)\mathcal{P}}$ , where $\phi^{(2)\mathcal{P}}$ is the puncture at the particle from Eq. (5.7), because we will solve for the second-order field in a large-$r$ region in which $\phi^{(2)\mathcal{P}}$ vanishes. We will define this region more precisely, when we come to solve for the second-order field in Sec. 6.3.

An explicit formula for $\tilde{S}^2_{\ell m}$ may be derived by setting $t^{\alpha\beta}\partial_\alpha\phi^1\partial_\beta\phi^1 = \sum_{\ell m} Y_{\ell m}\tilde{S}^2_{\ell m} e^{-im\tilde{\phi}_p(\tilde{u})}$, and substituting Eq. (6.23) into the left hand side. Integrating both sides against $Y^*_{\ell m}$ over the unit two-sphere, the formula for $\tilde{S}^2_{\ell m}$ is readily obtained. The details of the derivation can be found in Sec. 5.2.1. The result is

$$\begin{aligned}\tilde{S}^2_{\ell m} = \sum_{\ell' m'}\sum_{\ell'' m''}\Bigg[&C^{\ell m0}_{\ell' m' 0 \ell'' m'' 0}\Big(-2m'm''\tilde{\Omega}_0^2\tilde{R}^1_{\ell' m'}\tilde{R}^1_{\ell'' m''} + im'\tilde{\Omega}_0\tilde{R}^1_{\ell' m'}\partial_r\tilde{R}^1_{\ell'' m''}\\ &+im''\tilde{\Omega}_0\partial_r\tilde{R}^1_{\ell' m'}\tilde{R}^1_{\ell'' m''} + \partial_r\tilde{R}^1_{\ell' m'}\partial_r\tilde{R}^1_{\ell'' m''}\Big)\\ &-\frac{1}{2r^2}(C^{\ell m0}_{\ell' m' -1 \ell'' m'' 1} + C^{\ell m0}_{\ell' m' 1 \ell'' m'' -1})\sqrt{\ell'(\ell'+1)\ell''(\ell''+1)}\,\tilde{R}^1_{\ell' m'}\tilde{R}^1_{\ell'' m''}\Bigg].\end{aligned} \tag{6.32}$$

where $C^{\ell m s}_{\ell_1 m_1 s_1 \ell_2 m_2 s_2}$ is given by Eq. (5.29).

## 6.2 First-order solution

We obtain the first-order solution to Eq. (6.29) via the method of variation of parameters, just as in Chapter 4. The solution has the form

$$\tilde{R}^1_{\ell m}(r) = \tilde{c}^{1+}_{\ell m}(r)\tilde{R}^+_{\ell m}(r) + \tilde{c}^{1-}_{\ell m}(r)\tilde{R}^-_{\ell m}(r), \tag{6.33}$$

where $\tilde{R}^-_{\ell m}(r)$ is a homogeneous solution regular at the origin, and where $\tilde{R}^+_{\ell m}(r)$ is a homogeneous solution regular at $r\to\infty$. The coefficients are

$$\tilde{c}^{1+}_{\ell m}(r) = \int_0^r \frac{\tilde{R}^-_{\ell m}(r')\tilde{\mathcal{S}}^1_{\ell m}(r')}{\tilde{W}_{\ell m}(r')}dr', \tag{6.34}$$

$$\tilde{c}^{1-}_{\ell m}(r) = \int_r^\infty \frac{\tilde{R}^+_{\ell m}(r')\tilde{\mathcal{S}}^1_{\ell m}(r')}{\tilde{W}_{\ell m}(r')}dr'. \tag{6.35}$$

For $m \neq 0$ the homogeneous solutions are

$$\tilde{R}^+_{\ell m} = e^{-im\tilde{\Omega}_0 r} h^{(1)}_\ell(m\tilde{\Omega}_0 r), \tag{6.36}$$
$$\tilde{R}^-_{\ell m} = e^{-im\tilde{\Omega}_0 r} j_\ell(m\tilde{\Omega}_0 r), \tag{6.37}$$

where $h^{(1)}_\ell$ is the spherical Hankel function of the first kind, $j_\ell$ is the spherical Bessel function of the first kind, and the Wronskian is

$$\tilde{W}_{\ell m} = -\frac{e^{-2im\tilde{\Omega}_0 r}}{im\tilde{\Omega}_0 r^2}. \tag{6.38}$$

For $m = 0$, the homogeneous solutions are

$$\tilde{R}^+_{\ell 0} = \frac{1}{r^{\ell+1}}, \tag{6.39}$$
$$\tilde{R}^-_{\ell 0} = r^\ell, \tag{6.40}$$

and the Wronskian is

$$W_{\ell 0} = -\frac{2\ell+1}{r^2}. \tag{6.41}$$

## 6.3 Infrared divergence in the second-order source

To characterize the behaviour of the second-order solution, we split it into two terms, namely $\tilde{\phi}_2 = \tilde{\psi} + \delta\tilde{\phi}_1$, with a corresponding split

$$\tilde{R}^2_{\ell m} = \tilde{R}^{\tilde{\psi}}_{\ell m} + \tilde{R}^{\delta\tilde{\phi}_1}_{\ell m}. \tag{6.42}$$

The first term is generated by $\tilde{S}^2_{\ell m}$ in Eq. (6.31). $\tilde{R}^{\delta\tilde{\phi}_1}_{\ell m}$ is sourced by the remaining terms in Eq. (6.31), which arise due to the slow evolution of the worldline. The infrared divergence of the source comes solely from the $\tilde{S}^2_{\ell m}$ piece, as we will now show.

The equation for $\tilde{R}^{\tilde{\psi}}_{\ell m}$ reads

$$\partial_r^2 \tilde{R}^{\tilde{\psi}}_{\ell m} + \frac{2}{r}\left(1 + im\tilde{\Omega}_0 r\right)\partial_r \tilde{R}^{\tilde{\psi}}_{\ell m} + \frac{1}{r^2}\left[2im\tilde{\Omega}_0 r - \ell(\ell+1)\right]\tilde{R}^{\tilde{\psi}}_{\ell m} = \tilde{S}^2_{\ell m}. \tag{6.43}$$

We solve (6.43) using the method of variation of parameters, to yield the retarded solution. We restrict our solution to $r > r_+$ for some very large $r_+$, which ensures that the dominant piece of $\tilde{R}^2_{\ell m}$ comes from the leading-order, $1/r^2$ piece of $S^2_{\ell m}$ (see Eq. (6.46) below). $r_+$ is a function of slow retarded-time, as $r_+ = \tilde{r}_+(\tilde{u})$, but to save on notation we suppress this dependence. Ignoring the contribution of the source in the region $r < r_+$, we write the solution as

$$\tilde{R}^{\tilde{\psi}}_{\ell m}(r) = \left[\int_{r_+}^{r} \frac{\tilde{R}^-_{\ell m}(r')\tilde{S}^2_{\ell m}(r')}{W_{\ell m}(r')}dr'\right]\tilde{R}^+_{\ell m}(r) + \left[\int_{r}^{\infty} \frac{\tilde{R}^+_{\ell m}(r')\tilde{S}^2_{\ell m}(r')}{W_{\ell m}(r')}dr'\right]\tilde{R}^-_{\ell m}(r). \quad (6.44)$$

The homogeneous solutions $\tilde{R}^{\pm}_{\ell m}$ are precisely the same as the ones given in Eqs. (6.36), (6.37),(6.39) and (6.40). If we take a look at the asymptotic behaviour of (6.32), and note that the $3j$-symbols impose $m = m' + m''$, we find that the slowest decaying terms in $\tilde{S}^2_{\ell m}$ behave as

$$\frac{e^{im'\tilde{\Omega}_0 r}}{r}\frac{e^{im''\tilde{\Omega}_0 r}}{r} = \frac{e^{im\tilde{\Omega}_0 r}}{r^2}, \quad (6.45)$$

coming from the terms $\partial_t \tilde{R}^1_{\ell' m'}\partial_t \tilde{R}^1_{\ell'' m''} \sim \partial_t\left(r^{-1}e^{-im'\tilde{\Omega}_0(t-r)}\right)\partial_t\left(r^{-1}e^{-im''\tilde{\Omega}_0(t-r)}\right)$ and $\partial_r \tilde{R}^1_{\ell' m'}\partial_t \tilde{R}^1_{\ell'' m''} \sim \partial_r\left(r^{-1}e^{-im'\tilde{\Omega}_0(t-r)}\right)\partial_r\left(r^{-1}e^{-im''\tilde{\Omega}_0(t-r)}\right)$. Note that only oscillatory, $m \neq 0$ modes in $\tilde{\phi}_1$ contribute to the $1/r^2$ piece of the source. The stationary modes, which are $t$-independent, do not contribute at order $1/r^2$, but rather decay as $1/r^4$. Eq. (6.45) is exactly the bad behaviour which emerges in the second-order gravitational source $\delta^2 R_{\mu\nu}$. The toy-model source was designed in order to exhibit this behaviour.

We will show now how a source term of the form (6.45) leads to a badly behaved retarded solution in (6.44). Let us write the source modes as

$$\tilde{S}^2_{\ell m} = \frac{\tilde{S}^{(-2)}_{\ell m}e^{im\tilde{\Omega}_0 r}}{r^2} + O(1/r^3), \quad (6.46)$$

where $\tilde{S}^{(-2)}_{\ell m}$ is a constant. With this in mind, let $\tilde{R}^{(-2)}_{\ell m}$ be the part of the solution sourced by $r^{-2}\tilde{S}^{(-2)}_{\ell m}e^{im\tilde{\Omega}_0 r}$ at points $r > r^+$. Then,

$$\tilde{R}^{(-2)}_{\ell m}(r) = \tilde{S}^{(-2)}_{\ell m}\left[\tilde{R}^+_{\ell m}(r)\int_{r_+}^{r}\frac{\tilde{R}^-_{\ell m}(r')e^{im\tilde{\Omega}_0 r'}}{r'^2\tilde{W}_{\ell m}(r')}dr' + \tilde{R}^-_{\ell m}(r)\int_{r}^{\infty}\frac{\tilde{R}^+_{\ell m}(r')e^{im\tilde{\Omega}_0 r'}}{r'^2\tilde{W}_{\ell m}(r')}dr'\right]. \quad (6.47)$$

We are primarily interested in the integral that extends to infinity, the part of the solution which draws information about the first-order solution over large distances. For $m \neq 0$, Eq. (6.47) reads

$$\tilde{R}^{(-2)}_{\ell m} = -im\tilde{\Omega}_0\tilde{S}^{(-2)}_{\ell m}\left[h^{(1)}_\ell(\tilde{r})\int_{r_+}^{r} j_\ell(\tilde{r}')e^{i\tilde{r}'}dr' + j_\ell(\tilde{r})\int_{r}^{\infty} h^{(1)}_\ell(\tilde{r}')e^{i\tilde{r}'}dr'\right], \quad (6.48)$$

where $\tilde{r}' = m\tilde{\Omega}_0 r'$. At large $r$, the behaviour of $h^{(1)}_\ell$ and $j_\ell$ is

$$h^{(1)}_\ell(z) = (-i)^{\ell+1}\frac{e^{iz}}{z} + O(1/z^2), \quad (6.49)$$

and

$$j_\ell(z) = \begin{cases} (-1)^{\ell/2}\dfrac{\sin(z)}{z} + O(1/z^2) & \text{for even } \ell, \\ (-1)^{(\ell+1)/2}\dfrac{\cos(z)}{z} + O(1/z^2) & \text{for odd } \ell. \end{cases} \tag{6.50}$$

These asymptotic expressions show that

$$\int_{r^+}^{r} j_\ell(\tilde{r}')e^{i\tilde{r}'}dr' = \frac{i^{\ell+1}\ln r}{2m\tilde{\Omega}_0} + O(r^0), \tag{6.51}$$

$$\int_{r}^{\infty} h_\ell^{(1)}(\tilde{r}')e^{i\tilde{r}'}dr' = \frac{(-1)^\ell e^{2im\tilde{\Omega}_0 r}}{2m^2\tilde{\Omega}_0^2 r} + O(1/r^2). \tag{6.52}$$

Hence,

$$\tilde{R}^{(-2)}_{\ell m} = \frac{\left[C'_{\ell m} + \tilde{S}^{(-2)}_{\ell m}\ln r\right]e^{im\tilde{\Omega}_0 r}}{2im\tilde{\Omega}_0 r} + O\left(r^{-2}\ln r\right), \tag{6.53}$$

for some constant $C'_{\ell m}$. Due to the logarithm, this behaviour is not smooth at null infinity. In the gravitational problem, such terms would violate asymptotic flatness at future null infinity. However, when we apply the matching procedure in Sec. 6.4, we will find out that this behaviour correctly describes solution in the large-$r$ region of the near zone. In PM theory [101, 102], terms with this type of behaviour arise due to the metric perturbation deforming light cones, along which the solution to the wave equation propagates. They can be removed through a gauge transformation to an asymptotically regular gauge [102].

The most worrisome case is when $m = 0$, for which Eq. (6.46) reduces to

$$\tilde{S}^2_{\ell 0} = \frac{\tilde{S}^{(-2)}_{\ell 0}}{r^2} + O(1/r^3). \tag{6.54}$$

Eq. (6.54) is stationary and non-oscillatory, and stems from destructive interference from waves of opposite phase in the coupling formula (6.32). The contribution from (6.54) to the source leads to the infrared divergence problem in the second-order field, as we will now show.

Substituting Eqs. (6.39)–(6.40) into Eq. (6.47) yields

$$\tilde{R}^{(-2)}_{\ell 0} = -\frac{1}{r^{\ell+1}}\tilde{S}^{(-2)}_{\ell 0}\int_{r^+}^{r}\frac{r'^\ell}{2\ell+1}dr' - r^\ell \tilde{S}^{(-2)}_{\ell 0}\int_{r}^{\infty}\frac{r'^{-\ell-1}}{2\ell+1}dr'. \tag{6.55}$$

For $\ell > 0$ Eq. (6.55) evaluates to

$$\tilde{R}^{(-2)}_{\ell 0} = -\frac{\tilde{S}^{(-2)}_{\ell 0}}{\ell(\ell+1)} + O(1/r^{\ell+1}). \tag{6.56}$$

Hence, every $m = 0$, $\ell > 0$ mode approaches a constant at large $r$. In the gravity problem, this seemingly corresponds to a lack of asymptotic flatness. But like the behaviour for $m \neq 0$, we will find that it is physically correct in the large-$r$ limit of the near zone.

For the $\ell = 0$ mode, Eq. (6.55) yields

$$\tilde{R}^{(-2)}_{00} = \left(\frac{r^+}{r} - 1 + \lim_{\mathcal{R}\to\infty} \ln\frac{r}{\mathcal{R}}\right)\tilde{S}^{(-2)}_{00}. \tag{6.57}$$

The final term is infinite and the solution diverges at all values of $r$. In the next section we will shed light on the origin of the divergence and explain how to rectify it.

## 6.4 Curing the divergence using matched asymptotic expansions

### 6.4.1 Boundary conditions at infinity

To cure the infrared divergence of the source, we choose a large-$r$ boundary at $r = \mathcal{R}$, cut off the retarded integrals at that point, and then add a homogeneous solution to account for the part of the source that lies at $r > \mathcal{R}$, multiplied by some unknown constant. The constant is determined by matching the multiscale expansion in the near zone to the exact solution for the retarded field at large distances, as found from the PM methods of Blanchet and Damour [101–106]. The matching procedure will be the subject of Sec. 6.4.2.

To ensure regularity at $r = 0$, the added homogeneous solution must be regular there. In terms of the variables $\tilde{R}^2_{\ell m}$, this implies

$$\tilde{R}^2_{\ell m} = \tilde{c}^{2+}_{\ell m}(r)\tilde{R}^+_{\ell m} + [\tilde{c}^{2-}_{\ell m}(r) + k_{\ell m}]\tilde{R}^-_{\ell m}, \tag{6.58}$$

with coefficients

$$\tilde{c}^{2+}_{\ell m}(r) = \int_{r_+}^{r} \frac{\tilde{R}^-_{\ell m}(r')\tilde{S}^2_{\ell m}(r')}{\tilde{W}_{\ell m}(r')}dr', \tag{6.59}$$

$$\tilde{c}^{2-}_{\ell m}(r) = \int_{r}^{\mathcal{R}} \frac{\tilde{R}^+_{\ell m}(r')\tilde{S}^2_{\ell m}(r')}{\tilde{W}_{\ell m}(r')}dr', \tag{6.60}$$

and some unknown, $r$-independent functions $k_{\ell m}(\tilde{u}, \mathcal{R})$ that are to be determined by matching. This is the most general solution compatible with (i) the assumptions of the multiscale expansion and the ansatz (6.23), (ii) retarded propagation inside the near zone, and (iii) regularity at $r = 0$. We then find that the analogues of Eqs. (6.53) and (6.56) are

$$\tilde{R}^{(-2)}_{\ell m} = \frac{(\tilde{C}_{\ell m} + \tilde{S}^{(-2)}_{\ell m}\ln r)}{2im\tilde{\Omega}_0 r} + k_{\ell m}(\tilde{u}, \mathcal{R})j_\ell(m\tilde{\Omega}_0 r) + O(r^{-2}\ln r) \tag{6.61}$$

for the $m \neq 0$ modes, and

$$\tilde{R}^{(-2)}_{\ell 0} = -\frac{\tilde{S}^{(-2)}_{\ell 0}}{\ell(\ell+1)} + k_{\ell 0}(\tilde{u}, \mathcal{R}) r^{\ell} + O(1/r^{\ell+1}) \tag{6.62}$$

for the $m = 0$, $\ell > 0$ modes. From the matching procedure to be described in Sec. 6.4.2, the following result is derived [75]:

$$k_{\ell m}(\tilde{u}, \mathcal{R}) = 0 \quad \text{for } \ell \neq 0. \tag{6.63}$$

In other words, for $\ell \neq 0$ we need not have restricted the solution to the near zone, and we may simply send $\mathcal{R} \to \infty$. For $\ell = 0$ we cannot send $\mathcal{R}$ to $\infty$, because the result for the field reads

$$\tilde{R}^{(-2)}_{00} = \left(\frac{r^+}{r} - 1 + \ln\frac{r}{\mathcal{R}}\right) \tilde{S}^{(-2)}_{00} + k_{00}(\tilde{u}, \mathcal{R}). \tag{6.64}$$

Instead we write the total monopole mode as

$$\begin{aligned}\tilde{R}^{2}_{00} &= \left(\frac{r^+}{r} - 1\right) \tilde{S}^{(-2)}_{00} + \ln(r)\tilde{S}^{(-2)}_{00} + k_{00}(\tilde{u}, \mathcal{R}) - \ln(\mathcal{R})\tilde{S}^{(-2)}_{00} \\ &= \ln(r)\tilde{S}^{(-2)}_{00} + \tilde{k}_{00} + O(r^{-1}\ln r),\end{aligned} \tag{6.65}$$

where

$$\tilde{k}_{00}(\tilde{u}) \equiv k_{00}(\tilde{u}, \mathcal{R}) - \ln(\mathcal{R})\tilde{S}^{(-2)}_{00} \tag{6.66}$$

must be independent of $\mathcal{R}$. We will calculate $\tilde{k}_{00}$ using the matching procedure in Sec. 6.4.2.

Thus, for all modes $\ell > 0$, we can set $\mathcal{R} = \infty$. While this is not the case for the $\ell = 0$ mode, we can nevertheless find a more convenient form for dealing with the $\ln r$-divergence in (6.65), by introducing a puncture.

We define the puncture at infinity as

$$\tilde{R}^{\mathcal{P}\infty}(\tilde{u}, r) = \theta(r - r^{\infty}) \ln(r) \tilde{S}^{(-2)}_{00}(\tilde{u}), \tag{6.67}$$

where $r^{\infty}(\tilde{u}) > r^{+}(\tilde{u})$ is arbitrary. Then we can define an effective variable, similar to the residual field defined in Chapter 3, as

$$\tilde{R}^{\text{eff}}_{00} \equiv \tilde{R}^{2}_{00} - \tilde{R}^{\mathcal{P}\infty} - \tilde{k}_{00}. \tag{6.68}$$

Then we transfer $\tilde{R}^{\mathcal{P}\infty}$ to the right-hand side of the field equation (6.29), leading to the equation

$$(\partial_r^2 + 2r^{-1}\partial_r)\tilde{R}^{\text{eff}}_{00} = \tilde{\mathcal{S}}^{\text{eff}}_{00} \tag{6.69}$$

where $\tilde{\mathcal{S}}^{\text{eff}}_{00}$ is the effective source given by

$$\tilde{\mathcal{S}}^{\text{eff}}_{00} = \tilde{\mathcal{S}}^{2}_{00} - (\partial_r^2 + 2r^{-1}\partial_r)\tilde{R}^{\mathcal{P}\infty} \tag{6.70}$$

$$= \tilde{\mathcal{S}}^{2}_{00} - \frac{\tilde{S}^{(-2)}_{00}}{r^2} \quad \text{for } r > r^{\infty}. \tag{6.71}$$

The effective source, $\tilde{\mathcal{S}}^{\text{eff}}_{00}$, falls off as $1/r^3$, and we can write the solution using the standard method of variation of parameters as

$$\tilde{R}^{\text{eff}}_{00} = \tilde{c}^{\text{eff}+}_{00}\tilde{R}^{+}_{00} + \tilde{c}^{\text{eff}-}_{00}\tilde{R}^{-}_{00}, \tag{6.72}$$

where

$$\tilde{c}^{\text{eff}+}_{00} = \int_0^r \frac{\tilde{R}^{-}_{00}(r')\tilde{\mathcal{S}}^{\text{eff}}_{00}(r')}{\tilde{W}_{00}(r')}dr', \tag{6.73}$$

$$\tilde{c}^{\text{eff}-}_{200} = \int_r^\infty \frac{\tilde{R}^{+}_{00}(r')\tilde{\mathcal{S}}^{\text{eff}}_{00}(r')}{\tilde{W}_{00}(r')}dr'. \tag{6.74}$$

The Wronskian $\tilde{W}_{00}(r') = \partial_r\tilde{R}^{+}_{00}(r)\tilde{R}^{-}_{00}(r) - \partial_r\tilde{R}^{-}_{00}(r)\tilde{R}^{+}_{00}(r)$ is given in Eq. (6.41). The physical field can then be recovered using

$$\tilde{R}^{2}_{00} = \tilde{R}^{\text{eff}}_{00} + \tilde{R}^{\mathcal{P}\infty} + \tilde{k}_{00}. \tag{6.75}$$

### 6.4.2 Matching to the exact solution in the far zone

To determine the constant $\tilde{k}_{00}$, we will match to the known PM solution using an approach developed by Blanchet and Damour [103]. They derived a general formula [101–104, 106] for the retarded solution to the PM field equations, which is valid at all points outside of the source. They also showed [103] how to construct a global solution, by matching this general form to an expansion in a suitable, smaller zone containing the matter. Our method in the discussion below closely follows their approach.

The general retarded solution to the first-order equation (5.4) at all points $r > r_p(u)$, is given by

$$\phi_1 = \sum_\ell \frac{(-1)^\ell}{\ell!}\partial_L \frac{F^1_L(u)}{r}, \tag{6.76}$$

where $L = i_1 \dots i_\ell$ is a multi-index, $\partial_L = \partial_{i_1}\dots\partial_{i_\ell}$, and summation over the $\ell$ contracted indices is implied. This is the generic form of a homogeneous solution containing no incoming waves. When the matching procedure is applied, the set of functions $F^1_L(u)$ may be determined by matching to the expansion at large $r$ in the near zone.

Again at points $r > r_p(u)$, the retarded solution to the second-order equation (5.5) reads

$$\phi_2 = \phi^{\text{part}} + \phi^{\text{hom}}, \tag{6.77}$$

where

$$\phi^{\rm hom} = \sum_\ell \frac{(-1)^\ell}{\ell!}\partial_L \frac{F_L^2(u)}{r} \tag{6.78}$$

is another homogeneous solution containing no incoming radiation, and

$$\phi^{\rm part} = {\rm FP}\Box_{\rm ret}^{-1}(r^B S[F_L^1]) \tag{6.79}$$

is a particular solution also containing no incoming radiation. In the region $r > r^+(u)$ where the puncture field vanishes, $S[F_L^1]$ is the source $t^{\alpha\beta}\nabla_\alpha\phi_1\nabla_\beta\phi_1$ with $\phi_1$ given by Eq. (5.4), $\Box_{\rm ret}^{-1}$ denotes integration against the standard retarded Green's function over all spacetime, and "FP" denotes the "finite part", obtained by extracting the coefficient of $B^0$ in the Laurent series around $B = 0$.

Physically speaking, Eqs. (6.77) and (6.79) are the same thing as taking a particular solution $\Box_{\rm ret}^{-1}S(x')|_{r_+}^{\infty}$ where $\mathcal{R} = r_+$, whose source $S$ is valid in the region $r > r_+(u)$, and then in the region $r < r_+$ we replace the physical source with the analytical extension of the source from $r > r_+$. We can see this from the fact that Eq. (6.79) can be written as the sum of the retarded integral of the true source over the region $r > r_+$ and a homogeneous solution given by the finite part of the retarded integral of the fictitious source $r^B S[F_L^1]$ .

Based on (6.76) for $\phi_1$, the source $S$ can be conveniently written as a sum in explicit powers of $r$ as

$$S = \sum_\ell \sum_{k\geq 2} \frac{1}{r^k} S_L^{(-k)}(u)\hat{n}^L. \tag{6.80}$$

As described in [103], for each term in the source (6.80), the retarded integral appearing in Eq. (6.79) can be simplified to

$$\begin{aligned}&{\rm FP}\Box_{\rm ret}^{-1}\left(r^{B-k}S_L^{(-k)}\hat{n}^L\right)\\ &= {\rm FP}\frac{1}{K(B,k)}\int_r^\infty dz\, S_L^{(-k)}(t-z)\hat{\partial}_L\left[\frac{(z-r)^{B-k+\ell+2}-(z+r)^{B-k+\ell+2}}{r}\right],\end{aligned} \tag{6.81}$$

where

$$K(B,k) = 2^{B-k+3}\frac{(B-k+2)!}{(B-k-\ell+1)!}. \tag{6.82}$$

We are only concerned with the most slowly falling term in the source, $r^{-2}S_L^{(-2)}\hat{n}^L$. As discussed above, terms that fall off faster than $1/r^2$ generate retarded solutions that fall off as $\sim 1/r$. With this in mind, we will specialize Eq. (6.81) to $k = 2$. Since $1/r^2$ is integrable at $r = 0$, for this term in the source the FP operation is equivalent to taking the limit $B \to 0$. Thus, the retarded integral of the leading-order term in (6.80), which we may denote as $\Psi_\ell$, can be written as

$$\Psi_\ell \equiv \Box_{\rm ret}^{-1}\left(r^{-2}S_L^{(-2)}\hat{n}^L\right). \tag{6.83}$$

The details of how to evaluate the integral (6.83) for the case of $\ell = 0$ are left for the Appendix F. The final result, which is derived in Eq. (F.17), reads

$$\Psi_{\ell=0} = \left(\ln\frac{2r}{\epsilon} - 1\right)\tilde{S}^{(-2)}_{00}(\tilde{u}) - \int_0^\infty d\tilde{s}\,\dot{\tilde{S}}^{(-2)}_{00}(\tilde{u}-\tilde{s})\ln\tilde{s} + o(\epsilon^0), \tag{6.84}$$

where "$o(\epsilon^p)$" means "goes to zero faster than $\epsilon^p$". Since $\phi^2_{00} = \Box^{-1}_{\rm ret}\left(r^{-2}S^{(-2)}_{00}\right) + O(1/r)$, Eq. (6.84) provides the leading large-$r$ behaviour of the second-order monopole. It must agree with the previous expression (6.65) from the multiscale expansion, which fixes the previously unknown function $\tilde{k}_{00}(\tilde{u})$. A direct comparison with Eq. (6.65) leads to the conclusion that

$$\tilde{k}_{00} = -\tilde{S}^{(-2)}_{00}(\tilde{u})\left(1 + \ln\frac{\epsilon}{2}\right) - \int_0^\infty d\tilde{s}\,\dot{\tilde{S}}^{(-2)}_{00}(\tilde{u}-\tilde{s})\ln\tilde{s}. \tag{6.85}$$

Equipped with this result, the infrared divergence is resolved. The final term in Eq. (6.85) shows that the divergence was caused by neglecting hereditary effects in the wave propagation, which could not have been determined within the near-zone expansion. The first term in Eq. (6.85) shows that these hereditary effects introduce $\ln\epsilon$ terms into the field, a well-known fact in PN theory. Again, this logarithm could not have been determined without knowledge of the solution outside the near zone.

The integrals for $\ell > 0, m = 0$ and $\ell > 0, m > 0$ are evaluated following similar steps to those outlined in Appendix F. We just quote the results here and refer the reader to [75] for details:

$$\Psi_{\ell 0} = -\frac{\tilde{S}^{(-2)}_{\ell 0}(\tilde{u})}{\ell(\ell+1)} + o(\epsilon^0), \tag{6.86}$$

$$\Psi_{\ell m} = -\frac{\ln(r)\,\tilde{S}^{(-2)}_{\ell m}e^{-im\tilde{\varphi}_p(\tilde{u})}}{2im\tilde{\Omega}_0 r} + O\left(r^{-1}\right) + o(\epsilon^0), \tag{6.87}$$

where the $O(r^{-1})$ remainder has the form "constant/$r$" $+O(r^{-2}\ln r)$. Comparison of (6.86) with (6.62) shows that $k_{\ell 0} = 0$, because no terms of the form $r^\ell$ appear in (6.86). Similarly, comparison of (6.87) with (6.61) shows that $k_{\ell m} = 0$, since no terms of the form "oscillation/$r$" appear in (6.87).

# Chapter 7

# Computational framework for second-order gravitational self-force

In the previous two chapters we developed a treatment in the scalar toy-model for resolving the problems we encounter on the particle and at large $r$. In this chapter we show how to apply the lessons we learned in the scalar toy-model to the gravity case, and set up the equations that we will solve for the monopole piece of the second-order field, in Chapter 8. The material in this chapter was developed in collaboration with Adam Pound but its implementation in Chapter 8 was entirely my work.

We divide the spacetime outside the black hole into three zones: The near-horizon zone where we expand around $r \sim 2M$, the near zone $|r^* - r^*_p| \ll M/\epsilon$ where we use a multiscale expansion, and finally the far zone $r^* \gg M$ where we use a Post-Minkowski expansion. In this chapter we derive the multiscale expansion of the field equations explicitly, for the monopole piece of the second-order field. The expansions in the near-horizon zone and the far-zone provide boundary conditions for these equations. One could apply these these expansions to calculate physical quantities including the flux, total mass and angular-momentum of the system, and the multipole moments of the black hole.

This chapter is structured in the following way. In Sec. 7.1 we describe the multiscale expansion, based largely on the material of the previous chapter. In Sec. 7.2 we derive the multiscale expansion of the equation of motion. In Sec. 7.3 we present the multiscale expansion of the field equations for generic $\ell$-modes of the second-order field. Such an expansion was first suggested by Hinderer and Flanagan [107], but this represents the first time it has been worked out in detail. In Sec. 7.4 we discuss boundary conditions near the horizon. Physical boundary conditions at the horizon have not yet been worked out, but in the meantime, we present a method of deriving boundary conditions that at least avoids the infrared divergence of the retarded integral. Sec. 7.5 describes the Post-Minkowski expansion in the far zone, used to construct boundary conditions at $r \to \infty$. This section also draws most of its results from the previous chapter. Appendix G contains a number of asymptotic results for the monopole piece of the second-order source, from which we derive a formula for the energy flux at null infinity.

## 7.1 Multiscale expansion

### 7.1.1 Multiscale expansion of the worldline

We write the coordinates $z^\mu$ on the worldline of the particle, moving along a quasicircular orbit, as in Eq. (6.5), and we use the same two-timescale coordinates described in Section 6.1.1. That is, we adopt $\tilde{t} \equiv \epsilon t$ as the slow time and $\varphi_p(t,\epsilon)$ as the fast time. Then, the coordinates on the worldline may be written in the slowly evolving, quasicircular form $r_p(t,\epsilon) = \tilde{r}_p(\tilde{t},\epsilon)$ and $\varphi_p(t,\epsilon) = \tilde{\varphi}_p(\tilde{t},\epsilon)$, where $\tilde{r}_p(\tilde{t},\epsilon)$ and $\tilde{\varphi}_p(\tilde{t},\epsilon)$ are given by the two-timescale expansions in Eqs. (6.7) and (6.9), respectively. The orbital phase is recovered from the frequency, as in Eq. (6.8).

### 7.1.2 Multiscale expansion of the fields

Just like we constructed a multiscale expansion of the scalar field in Sec. 6.1.2, we expand the fields $\bar{h}^n_{\mu\nu}$ in gravity in a multiscale form. We use a slow time, $\tilde{w}$, defined as [108] [1]

$$\tilde{w} = \epsilon\left[t - k(r)\right]. \tag{7.1}$$

Surfaces of constant $\tilde{w}$ foliate the spacetime as horizon-penetrating hyperboloidal slices, as shown in Fig. 7.1. $k(r)$ is chosen such that $\tilde{w}$ tends towards slow retarded time, $\epsilon u$, close to future null infinity, and slow advanced time, $\epsilon v$, close to the future horizon of the background BH. Elsewhere over a large spatial region, $\tilde{w}$ is close to $\epsilon t$. In our numerical computation of the monopole piece of $\bar{h}^2_{\mu\nu}$, we use the simpler choice of $\tilde{t} = \epsilon t$. We will come to this in Sec. 7.3. As the fast time we adopt $\varphi_p(t,\epsilon)$. We write it in slowly evolving form in terms of $\tilde{w}$ as $\varphi_p(t,\epsilon) = \tilde{\varphi}(\tilde{w},\epsilon)$.

In analogy with the multiscale expansion in Eqs. (6.19)–(6.20), we write the gravitational field $\bar{h}^n_{\mu\nu} = \tilde{h}^n_{\mu\nu}(\tilde{w}, r, \theta^A, \tilde{\varphi}_p, \epsilon)$ as

$$\tilde{h}^n_{\mu\nu}(\tilde{w}, r, \theta^A, \tilde{\varphi}_p, \epsilon) = \tilde{h}^n_{\mu\nu}(\tilde{w}, r, \theta^A, \tilde{\varphi}_p, 0) + \epsilon\partial_\epsilon \tilde{h}^n_{\mu\nu}(\tilde{w}, r, \theta^A, \tilde{\varphi}_p, 0) + O(\epsilon^2). \tag{7.2}$$

[1] In [108] the notation $h(r)$ is used instead of $k(r)$ in the definition of $\tilde{w}$. We choose $k(r)$ to avoid confusion with the metric perturbation.

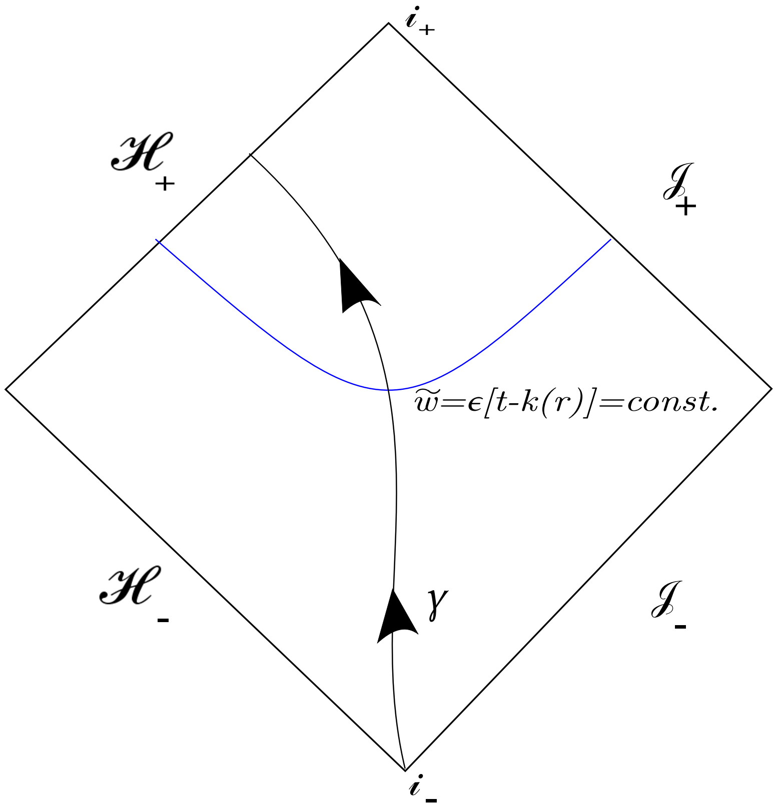


Figure 7.1: Penrose diagram of Schwarzschild spacetime illustrating the slow-time coordinate $\tilde{w}$. $\gamma$ is the particle's inspiralling worldline.

This yields new first- and second-order fields, analogous to Eqs. (6.21) and (6.22):

$$\tilde{h}^1_{\mu\nu}(\tilde{w}, r, \theta^A, \tilde{\varphi}_p) \equiv \tilde{h}^1_{\mu\nu}(\tilde{w}, r, \theta^A, \tilde{\varphi}_p, 0), \tag{7.3}$$

$$\tilde{h}^2_{\mu\nu}(\tilde{w}, r, \theta^A, \tilde{\varphi}_p) \equiv \tilde{h}^2_{\mu\nu}(\tilde{w}, r, \theta^A, \tilde{\varphi}_p, 0) + \partial_\epsilon \tilde{h}^1_{\mu\nu}(\tilde{w}, r, \theta^A, \tilde{\varphi}_p, 0). \tag{7.4}$$

We decompose Eqs. (7.3)–(7.4) into tensor spherical-harmonic modes, as

$$\tilde{h}^n_{\mu\nu} = \frac{\mu}{r} \sum_{i\ell m} a_{i\ell} \tilde{h}^n_{i\ell m}(r, \tilde{w}) e^{-im\tilde{\varphi}_p(\tilde{w})} Y^{i\ell m}_{\mu\nu}, \tag{7.5}$$

where $Y^{i\ell m}_{\mu\nu}$ are the Barack-Sago basis of tensor spherical harmonics, given explicitly in Eqs. (4.15).

Substituting the two-timescale expansion of the field leads to a two-timescale expansion of the second-order Ricci tensor. We may write it as a decomposition into tensor-harmonic modes, in a form analogous to (7.5), as

$$\delta^2 \tilde{R}_{\mu\nu}[\tilde{h}^1, \tilde{h}^1] = \sum_{i=1}^{10} \sum_{\ell=0}^{\infty} \sum_{m=-\ell}^{\ell} \delta^2 \tilde{R}^0_{i\ell m}[\tilde{h}^1, \tilde{h}^1] e^{-im\tilde{\varphi}_p(\tilde{w})} Y^{i\ell m}_{\mu\nu} + O(\epsilon). \tag{7.6}$$

The mode coefficients $\delta^2\tilde{R}^0_{i\ell m}[\,\tilde{h}^1,\tilde{h}^1\,]$ depend on $r$ and $\tilde{w}$. They only include the leading order piece, $\tilde{\Omega}_0$ of the frequency, and do not include any slow time derivatives. An explanation of how to compute these modes is postponed until Chapter 8.

## 7.2 Multiscale expansion of the equation of motion

The equation of motion in Schwarzschild coordinates reads

$$\frac{d^2z^\mu}{dt^2}+U^{-1}\frac{dU}{dt}\frac{dz^\mu}{dt}+\Gamma^\mu_{\beta\gamma}\frac{dz^\beta}{dt}\frac{dz^\gamma}{dt}=U^{-2}F^\mu, \tag{7.7}$$

where $U\equiv dt/d\tau$, with $\tau$ being proper time on the worldline, and $F^\mu$ is the self-force per unit mass. Our goal is to substitute the form of (6.5) for the worldline coordinates, and derive expressions for them at each order of $\epsilon$.

$F^\mu$ is a functional of $z^\mu$, so we write it in the form

$$F^\mu(t,\epsilon)=\epsilon F^\mu_1(z;\gamma)+\epsilon^2F^\mu_2(z;\gamma)+O(\epsilon^3), \tag{7.8}$$

where on the right-hand side, $z=z(t)$, and each $F^\mu_n$ is a functional of the worldline $\gamma$. The self-force through second order, $\epsilon F^\mu_1(z;\gamma)+\epsilon^2F^\mu_1(z;\gamma)$ is given by the right-hand side of Eq. (2.69), in terms of the regular field. By substituting for the regular field the form of Eq. (7.5) and then evaluating all the derivatives, the $\varphi$ and $\varphi_p$ dependence has the same form as the right-hand side of Eq. (7.5). With that, on $\gamma$, $\varphi=\varphi_p$ and the $e^{-im\varphi_p}$ cancels with the $\varphi_p$ dependence in the tensor spherical-harmonic. So, we end up with an expression for the self-force independent of fast-time. The self-force is then a sum over modes $\tilde{h}^n_{i\ell m}(r,\tilde{w})$, their derivatives, and terms like $\tilde{\Omega}(\tilde{w})\tilde{h}^n_{i\ell m}(r,\tilde{w})$. $\tilde{h}^n_{i\ell m}(r,\tilde{w})$ depends on slow time through the source-modes' dependence on the orbital radius, and the explicit powers of frequency that appear in the field equations. Like in Sec. 6.1.1, the frequency can be written in terms of the orbital radius. Therefore, we can express the $\tilde{w}$ dependence of the self-force in terms of the orbital radius, and write it as

$$F^\mu(t,\epsilon)=\epsilon F^\mu_1(\tilde{r}_p;\tilde{r}_p)+\epsilon^2F^\mu_2(\tilde{r}_p;\tilde{r}_p)+O(\epsilon^3). \tag{7.9}$$

Here, $\tilde{r}_p=\tilde{r}_p(\tilde{w})$. The first argument refers to the radius at which we evaluate the regular field in the self-force formula. The second argument refers to the implicit dependence on the radius of the source orbit.

By substituting the expansions (6.7) and (6.9) into Eq. (7.9), we find that

$$F^\mu(t,\epsilon)=\epsilon F^\mu_1(r_0;r_0)+\epsilon^2\hat{F}^\mu_2(r_0;r_0,r_1)+O(\epsilon^3), \tag{7.10}$$

where

$$\hat{F}_2^\mu \equiv F_2^\mu(r_0;r_0) + \left[\frac{\partial}{\partial r_0} F_1^\mu(r_0;r_0) + \frac{\delta}{\delta r_0} F_1^\mu(r_0;r_0)\right] r_1, \tag{7.11}$$

where $\frac{\partial}{\partial r_0}$ acts on the first argument in $F_1^\mu(r_0;r_0)$, and $\frac{\delta}{\delta r_0}$ on the second.

Substituting Eqs. (6.5), (6.7), (6.8), and Eq. (7.10) into Eq. (7.7) leads to a sequence of equations for the terms $\tilde{r}_n(\tilde{t})$ and $\tilde{\Omega}_n(\tilde{t})$ in the expansions of the orbital radius and frequency. At order $\epsilon^0$, the only nontrivial piece of Eq. (7.7) is the $r$ component, which yields

$$\tilde{\Omega}_0 = \sqrt{\frac{M}{\tilde{r}_0^3}}. \tag{7.12}$$

This is precisely the same result derived in Eq. (4.11) for the frequency $\Omega$ of an exactly circular orbit with radius $r_0$.

At higher order in $\epsilon$ we will need an expansion for $U$, which can be found from the normalization condition $U^2 g_{\mu\nu}\dot{z}^\mu \dot{z}^\nu = -1$. By substituting Eqs. (6.5) and (7.12) into this expression, we derive

$$U^{-2} = 1 - \frac{3M}{\tilde{r}_0} - 2\epsilon \tilde{r}_0^2 \tilde{\Omega}_0 \tilde{\Omega}_1 + O(\epsilon^3). \tag{7.13}$$

At linear order in $\epsilon$, from the $t$ component of Eq. (7.7), we find an equation for the slow evolution of $r_0$ as

$$\frac{d\tilde{r}_0}{d\tilde{t}} = \frac{2(\tilde{r}_0 - 3M)^2(\tilde{r}_0 - 2M)}{M(\tilde{r}_0 - 6M)} F_1^t(\tilde{r}_0;\tilde{r}_0). \tag{7.14}$$

This tells us that the slow evolution of the radius is because of the dissipative piece of the first-order self-force. From the $r$ component of Eq. (7.7), we obtain an equation for $\tilde{\Omega}_1$ as

$$\tilde{\Omega}_1 = -\frac{1}{2\tilde{r}_0 f_0 \tilde{\Omega}_0}\left[U_0^{-2} F_1^r(\tilde{r}_0;\tilde{r}_0) + \frac{3M}{\tilde{r}_0^3} f_0 \tilde{r}_1\right], \tag{7.15}$$

where $U_0^{-2} = 1 - 3M/\tilde{r}_0$ and $f_0 = 1 - 2M/\tilde{r}_0$. Eq. (7.15) relates the first-order correction to the radius, $\tilde{r}_1$, and the first-order correction to the orbital frequency, $\tilde{\Omega}_1$, to the conservative piece of the first-order self-force.

At second order in $\epsilon$, from the $t$ component of Eq. (7.7), we obtain an equation for the slow evolution of $\tilde{r}_1$ as

$$\begin{aligned}\frac{2M}{\tilde{r}_0^2 f_0}\frac{d\tilde{r}_1}{d\tilde{t}} + \left(\frac{\tilde{r}_0}{U_0}\right)^2 \tilde{\Omega}_0 \frac{d\tilde{\Omega}_1}{d\tilde{t}} + \left[\frac{(\tilde{r}_0 + 3M)(\tilde{r}_0 - 3M)^2 \tilde{r}_0 f_0}{M(\tilde{r}_0 - 6M)} + 2\tilde{r}_0^2\right] \tilde{\Omega}_0 \tilde{\Omega}_1 F_1^t(r_0;r_0) \\ = U_0^{-2} \hat{F}_2^t(\tilde{r}_0;\tilde{r}_0,\tilde{r}_1). \end{aligned} \tag{7.16}$$

This tells us that the slow evolution of $\tilde{r}_1$ and $\tilde{\Omega}_1$ are due to the dissipative piece of the second-order self-force.

In Chapter 4, at first order we fixed the orbital frequency, but at second order we cannot expand the orbit at fixed frequency, because all quantities are evolving with slow time due to dissipative self-force effects. We only have the freedom to fix the frequency if we choose a preferred value of slow time $\tilde{t}$(=const). In our calculation of the monopole piece of the second-order field, we do just that. This affords us the freedom to set $\tilde{\Omega} = \tilde{\Omega}_0$ and $\tilde{\Omega}_1 = 0$. As a result, a formula for $\tilde{r}_1$ in terms of $F_1^r$ emerges from Eq. (7.15), as

$$\tilde{r}_1 = -\frac{\tilde{r}_0^3 F_1^r(\tilde{r}_0; \tilde{r}_0)}{3MU_0^2 f_0}. \tag{7.17}$$

## 7.3 Multiscale expansion of the field equations

The equations that we want to solve through second order are given in Eqs. (3.9). While we are primarily interested in solving the second-order equations (3.9c) and (3.9d), we include the first-order equations (3.9a) and (3.9b) in the discussion because the two-timescale expansion yields second-order contributions from them. We remind the reader that we solve for the trace-reversed field variable $\bar{h}^2_{\mu\nu}$, as we did at first order for reasons explained in Sec. 4.2. With this in mind, the wave equations obtained by trace-reversing Eqs. (3.9) are

$$E_{\alpha\beta}[\,\bar{h}^{\mathcal{R}1}\,] = -E_{\alpha\beta}[\,\bar{h}^{\mathcal{P}1}\,] \qquad \text{inside } \Gamma, \tag{7.18a}$$

$$E_{\alpha\beta}[\,\bar{h}^{1}\,] = 0 \qquad \text{outside } \Gamma, \tag{7.18b}$$

$$E_{\alpha\beta}[\,\bar{h}^{\mathcal{R}2}\,] = 2\delta^2 \bar{R}_{\alpha\beta}[\,h^1, h^1\,] - E_{\alpha\beta}[\,\bar{h}^{\mathcal{P}2}\,] \qquad \text{inside } \Gamma, \tag{7.18c}$$

$$E_{\alpha\beta}[\,\bar{h}^{2}\,] = 2\delta^2 \bar{R}_{\alpha\beta}[\,h^1, h^1\,] \qquad \text{outside } \Gamma. \tag{7.18d}$$

Now we want to replace $\bar{h}^n_{\mu\nu}(t, r, \theta^A)$ with its counterpart $\tilde{h}^n_{\mu\nu}(\tilde{t}, r, \theta^A, \tilde{\varphi}_p)$. Then we want to substitute the decomposition (7.5) into Eqs. (7.18), in much the same way as we did in Chapter 4. To do the substitution, we note that the derivatives take the form

$$\partial_t\left(\tilde{h}^n_{i\ell m} e^{-im\tilde{\varphi}_p}\right) = \left(-im\tilde{\Omega}\tilde{h}^n_{i\ell m} + \epsilon\partial_{\tilde{w}}\tilde{h}^n_{i\ell m}\right) e^{-im\tilde{\varphi}_p(\tilde{w})}, \tag{7.19a}$$

$$\partial_r\left(\tilde{h}^n_{i\ell m} e^{-im\tilde{\varphi}_p}\right) = \left(\partial_r\tilde{h}^n_{i\ell m} + im\tilde{\Omega}Hf^{-1}\tilde{h}^n_{i\ell m} - \epsilon Hf^{-1}\partial_{\tilde{w}}\tilde{h}^n_{i\ell m}\right) e^{-im\tilde{\varphi}_p(\tilde{w})}, \tag{7.19b}$$

where $\tilde{\Omega}$ is given by the expansion (6.8), $f = 1 - 2M/r$, and following the notation in Ref. [108], we have defined $H(r) \equiv dk(r)/dr^*$. The first term in parentheses on the right-hand side of Eq. (7.19a), and the first term in parentheses on the right-hand side of (7.19b), are precisely the same derivatives that appear in the frequency-domain equations (4.25). The second term in parentheses in Eq. (7.19b) arises from our use of $w = t - k$ instead of $t$; the same term would appear if we used an expansion in Fourier modes $e^{-im\Omega w}$, without a two-timescale expansion. The final terms in Eqs. (7.19) arise from the slow evolution of the system

In this way we derive new first- and second-order equations, as

$$
\begin{aligned}
\tilde{E}^0_{i\ell m}[\,\tilde{h}^{\mathcal{R}1}\,] =& -\tilde{E}^0_{i\ell m}[\,\tilde{h}^{\mathcal{P}1}\,] && \text{inside } \Gamma, && \text{(7.20a)}\\
\tilde{E}^0_{i\ell m}[\,\tilde{h}^{1}\,] =& 0 && \text{outside } \Gamma, && \text{(7.20b)}\\
\tilde{E}^0_{i\ell m}[\,\tilde{h}^{\mathcal{R}2}\,] =& -\frac{r}{2a_{i\ell}}\delta^2\tilde{R}^0_{i\ell m}[\,\tilde{h}^1,\tilde{h}^1\,] - \tilde{E}^0_{i\ell m}[\,\tilde{h}^{\mathcal{P}2}\,] - \tilde{E}^1_{i\ell m}[\,\tilde{h}^{\mathcal{P}1}\,] && \text{inside } \Gamma, && \text{(7.20c)}\\
\tilde{E}^0_{i\ell m}[\,\tilde{h}^{2}\,] =& -\frac{r}{2a_{i\ell}}\delta^2\tilde{R}^0_{i\ell m}[\,\tilde{h}^1,\tilde{h}^1\,] - \tilde{E}^1_{i\ell m}[\,\tilde{h}^{1}\,] && \text{outside } \Gamma. && \text{(7.20d)}
\end{aligned}
$$

Here, $\tilde{h}^{\mathcal{P}n}_{\mu\nu}$ and $\tilde{h}^{\mathcal{R}n}_{\mu\nu}$ are two-timescale expansions of $\bar{h}^{\mathcal{P}n}_{\mu\nu}$ and $\bar{h}^{\mathcal{R}n}_{\mu\nu}$, that appear in Eqs. (7.18). They have forms analogous to (7.5), with corresponding mode coefficients $\tilde{h}^{\mathcal{P}n}_{i\ell m}(r,\tilde{w})$ and $\tilde{h}^{\mathcal{R}n}_{i\ell m}(r,\tilde{w})$. $\tilde{E}^0$ and $\tilde{E}^1$ are given by

$$
\begin{aligned}
\tilde{E}^0_{i\ell m}[\,\tilde{h}\,] &\equiv \tilde{\Box}^0\tilde{h}_{i\ell m}(r,\tilde{w}) + \widetilde{\mathcal{M}}^{ij}_0\tilde{h}_{j\ell m}(r,\tilde{w}), && \text{(7.21a)}\\
\tilde{E}^1_{i\ell m}[\,\tilde{h}\,] &\equiv \tilde{\Box}^1\tilde{h}_{i\ell m}(r,\tilde{w}) + \widetilde{\mathcal{M}}^{ij}_1\tilde{h}_{j\ell m}(r,\tilde{w}), && \text{(7.21b)}
\end{aligned}
$$

where

$$
\tilde{\Box}^0 \equiv -\frac{1}{4}\left[f^2\partial_r^2 + \frac{2M}{r^2 f}\partial_r + im\tilde{\Omega}_0 Hf\partial_r + im\tilde{\Omega}_0 fH' - m^2\tilde{\Omega}_0^2\right] + V_\ell(r), \qquad \text{(7.22a)}
$$

$$
\begin{aligned}
\tilde{\Box}^1 \equiv& -\frac{1}{4}\Big[2m^2\tilde{\Omega}_0\tilde{\Omega}_1 - im\tilde{\Omega}_1 fH' im\tilde{\Omega}_1 fH\partial_r\\
&+2im\tilde{\Omega}_0\partial_{\tilde{w}} + fH'\partial_{\tilde{w}} + fH\partial_r\partial_{\tilde{w}}\Big], \qquad \text{(7.22b)}
\end{aligned}
$$

with $H' = \partial_r H$ and $V_\ell$ given in Eq. (4.28). $\widetilde{\mathcal{M}}^{ij}_0$ are given by $\mathcal{M}^{ij}$ in Eqs. (D.1) with the replacements $\partial_r \to \partial_r + im\tilde{\Omega}_0 H/f$ and $\omega_m = m\Omega \to m\tilde{\Omega}_0$. The terms $\widetilde{\mathcal{M}}^{ij}_1$ are given by $\mathcal{M}^{ij}$ with the replacements $\partial_r \to im\tilde{\Omega}_1 Hf^{-1} - Hf^{-1}\partial_{\tilde{w}}$, $i\omega_m \to im\tilde{\Omega}_1 - \partial_{\tilde{w}}$ and $\omega_m^2 = 2im\tilde{\Omega}_0\tilde{\Omega}_1 - im\tilde{\Omega}_0\partial_{\tilde{w}}$, and including only terms containing exactly one $\tilde{w}$ derivative or factor of $\tilde{\Omega}_1$.

To satisfy the Einstein equations, the solution to the wave equations must also satisfy the gauge condition $\nabla^\mu\tilde{h}^n_{\mu\nu} = 0$. By substituting the mode decomposition (7.5), we derive gauge conditions analogous to Eqs. (4.29), as

$$
\begin{aligned}
\mathscr{D}^0_n[\,\tilde{h}^1\,] =& 0, && \text{(7.23a)}\\
\mathscr{D}^0_n[\,\tilde{h}^2\,] =& -\mathscr{D}^1_n[\,\tilde{h}^1\,], && \text{(7.23b)}
\end{aligned}
$$

$n = 1,2,3,4$, where

$$
\begin{aligned}
\mathscr{D}^0_1[\,\tilde{h}\,] \equiv& im\tilde{\Omega}_0\tilde{h}_{1\ell m}\\
&+ f\left[im\tilde{\Omega}_0\tilde{h}_{3\ell m} + \partial_r\tilde{h}_{2\ell m} + im\tilde{\Omega}_0 Hf^{-1}\tilde{h}_{2\ell m} + \frac{\tilde{h}_{2\ell m}}{r} - \frac{\tilde{h}_{4\ell m}}{r}\right], \qquad \text{(7.24a)}\\
\mathscr{D}^0_2[\,\tilde{h}\,] \equiv& -im\tilde{\Omega}_0\tilde{h}_{2\ell m} - f\partial_r\tilde{h}_{1\ell m} - im\tilde{\Omega}_0 H\tilde{h}_{1\ell m} + f^2\partial_r\tilde{h}_{3\ell m} + im\tilde{\Omega}_0 Hf\tilde{h}_{3\ell m}
\end{aligned}
$$

$$
\begin{aligned}
&-\frac{f}{r}\left[\tilde{h}_{1\ell m}-\tilde{h}_{5\ell m}-f\tilde{h}^{1}_{3\ell m}-2f\tilde{h}_{6\ell m}\right], && (7.24b)\\
\mathscr{D}^0_3[\,\tilde{h}\,]\equiv{}&-im\tilde{\Omega}_0\tilde{h}_{4\ell m}\\
&-\frac{f}{r}\left[r\partial_r\tilde{h}_{5\ell m}+im\tilde{\Omega}_0Hf^{-1}r\tilde{h}_{5\ell m}+2\tilde{h}_{5\ell m}+\ell(\ell+1)\tilde{h}_{6\ell m}-\tilde{h}_{7\ell m}\right], && (7.24c)\\
\mathscr{D}^0_4[\,\tilde{h}\,]\equiv{}&-im\tilde{\Omega}_0\tilde{h}_{8\ell m}-\frac{f}{r}\left[r\partial_r\tilde{h}_{9\ell m}+im\tilde{\Omega}_0Hf^{-1}r\tilde{h}_{9\ell m}+2\tilde{h}_{9\ell m}-\tilde{h}_{10\ell m}\right], && (7.24d)
\end{aligned}
$$

and

$$
\begin{aligned}
\mathscr{D}^1_1[\,\tilde{h}\,]\equiv{}&im\tilde{\Omega}_1\tilde{h}_{1\ell m}-\partial_{\tilde{w}}\tilde{h}_{1\ell m}\\
&+f\left(im\tilde{\Omega}_1\tilde{h}_{3\ell m}-\partial_{\tilde{w}}\tilde{h}_{3\ell m}+im\tilde{\Omega}_1Hf^{-1}\tilde{h}_{2\ell m}-Hf^{-1}\partial_{\tilde{w}}\tilde{h}_{2\ell m}\right), && (7.25a)\\
\mathscr{D}^1_2[\,\tilde{h}\,]\equiv{}&-im\tilde{\Omega}_1\tilde{h}_{2\ell m}+\partial_{\tilde{w}}\tilde{h}_{2\ell m}-im\tilde{\Omega}_1H\tilde{h}_{1\ell m}\\
&-H\partial_{\tilde{w}}\tilde{h}_{1\ell m}-im\tilde{\Omega}_1Hf\tilde{h}_{3\ell m}+Hf\partial_{\tilde{w}}\tilde{h}_{3\ell m}, && (7.25b)\\
\mathscr{D}^1_3[\,\tilde{h}\,]\equiv{}&im\tilde{\Omega}_1\tilde{h}_{4\ell m}-\partial_{\tilde{w}}\tilde{h}_{4\ell m}-im\tilde{\Omega}_1H\tilde{h}_{9\ell m}+H\partial_{\tilde{w}}\tilde{h}_{9\ell m}, && (7.25c)\\
\mathscr{D}^1_4[\,\tilde{h}\,]\equiv{}&-im\tilde{\Omega}_1\tilde{h}_{8\ell m}+\partial_{\tilde{w}}\tilde{h}_{8\ell m}-im\tilde{\Omega}_1H\tilde{h}_{5\ell m}+H\partial_{\tilde{w}}\tilde{h}_{5\ell m}. && (7.25d)
\end{aligned}
$$

Combining the expansion of the equation of motion with the expansion of the field equations, we end up with frequency-domain equations (7.20) that can be solved at each fixed value of slow time, plus evolution equations (7.14), (7.16), and (7.23b) that determine the evolution with slow time. The wave equations (7.20c)–(7.20d) and gauge condition (7.23b) have different roles in that respect: because the wave equation can be solved for any source, slow-time derivatives in (7.20) do not constrain the evolution, instead simply acting as sources; the gauge condition (7.23b) then serves to determine the evolution, just as it served to determine the equation of motion in Chapter 2.

### 7.3.1 General retarded solutions

To find a solution we use the same method of variation of parameters used in Chapter 4, but with different boundary conditions. These boundary conditions will be absorbed into punctures, allowing us to use the methods of Chapter 4 even more directly.

We can write the general solution in this domain as

$$
\tilde{\psi}^n_{\ell m}(\tilde{w},r)=\left(C^{n-}_{\ell m}(\tilde{w},r)+K^{n-}_{\ell m}(\tilde{w})\right)\tilde{\psi}^-_{\ell m}(r)+\left(C^{n+}_{\ell m}(\tilde{w},r)+K^{n+}_{\ell m}(\tilde{w})\right)\tilde{\psi}^+_{\ell m}(r), \quad (7.26)
$$

where $\tilde{\psi}^n_{\ell m}(\tilde{w},r)$ is a column vector of $d$ solutions, $\tilde{h}^n_{i\ell m}(\tilde{w},r)$, whose elements are in the format of (4.59). Likewise, $\tilde{\psi}^\pm_{\ell m}(r)$ is a column vector of $d$ homogeneous solutions, $\tilde{h}^\pm_{i\ell m}(r)$, whose elements follow the same format. $\tilde{h}^+_{i\ell m}(r)$ are regular at infinity and $\tilde{h}^-_{i\ell m}(r)$ are regular at the horizon. The weighting coefficients, $C^{n\pm}_{\ell m}(\tilde{w},r)$ are $d\times d$ matrices, determined using the method of variation of parameters. $K^{n\pm}_{\ell m}$ in Eq. (7.26) are $d \times d$ matrices of constants that are determined by matching the general solution in the near-zone to an exact solution in the far zone, which we calculate using a Post-Minkowski expansion, as described in Sec. 7.5. $K^{n-}_{\ell m}$ in Eq. (7.26) are $d \times d$ matrices of constants that are determined by matching the general solution in the near-zone to an exact solution in the near-horizon zone. Unlike the former, the latter are yet to be obtained. We will return to a discussion of this in Sec. 7.4.

The $C^{n\pm}_{\ell m}(\tilde{w}, r)$ are computed by first defining the $2d \times 2d$ matrix

$$\tilde{\Phi}(\tilde{w}, r) = \left(\begin{array}{c|c} \tilde{\psi}^-(\tilde{w}, r)^T & \tilde{\psi}^+(\tilde{w}, r)^T \\ \hline \partial_r \tilde{\psi}^-(\tilde{w}, r)^T & \partial_r \tilde{\psi}^+(\tilde{w}, r)^T \end{array}\right), \tag{7.27}$$

and then using the standard variation of parameters approach:

$$C^{n-}_{\ell m}(\tilde{w}, r) = \left[\int_r^{\mathcal{R}_+} dr' \tilde{\Phi}^{-1}(\tilde{w}, r') \begin{pmatrix} \mathbf{0}_d \\ \tilde{J}^n_{\ell m}(\tilde{w}, r') \end{pmatrix}\right]_{\text{top } d \text{ entries}}, \tag{7.28}$$

$$C^{n+}_{\ell m}(\tilde{w}, r) = \left[\int_{\mathcal{R}_-}^{r} dr' \tilde{\Phi}^{-1}(\tilde{w}, r') \begin{pmatrix} \mathbf{0}_d \\ \tilde{J}^n_{\ell m}(\tilde{w}, r') \end{pmatrix}\right]_{\text{bottom } d \text{ entries}}, \tag{7.29}$$

where $\tilde{J}^n_{\ell m}$ is a column vector of modes of the source $\tilde{S}^{n\,\text{eff}}_{i\ell m}$, where $\tilde{S}^{1\,\text{eff}}_{i\ell m}$ is defined to be the effective source on the right-hand side of either Eq. (7.20a) or (7.20b), and $\tilde{S}^{2\,\text{eff}}_{i\ell m}$ is defined to be the effective source on the right-hand side of either Eq. (7.20c) or (7.20d). $\mathcal{R}_+$ is a suitably chosen radial position of the outer boundary of the near zone at which we match the general solution in the near-zone to a physical solution in the far-zone, and $\mathcal{R}_-$ is a suitably chosen radial position of the inner boundary of the near zone at which we match the general solution in the near zone to a physical solution in the near-horizon zone. The elements of $\tilde{J}^n_{\ell m}$ are in the format of (4.59), and $V_{\text{top (bottom) } d \text{ entries}}$ means the $d$-vector formed by taking the top (bottom) $d$ elements of the $2d$-vector $V$.

### 7.3.2 The first-order solution

We begin by considering whether the first-order solution in Chapter 4 remains valid in the context of our two-timescale expansion. Rather than moving directly to the general solution (7.26) in the Lorenz gauge, we start by writing the most general, first-order solution valid in any gauge, as

$$\tilde{\psi}^1_{\ell m}(\tilde{w}, r) = \tilde{\psi}^{\text{hom}}_{\ell m}(\tilde{w}, r) + \tilde{\psi}^{1\text{pp}}_{\ell m}(\tilde{w}, r), \tag{7.30}$$

where $\tilde{\psi}^{\text{hom}}_{\ell m}(\tilde{w}, r)$ is any homogeneous solution in an arbitrary gauge, and $\tilde{\psi}^{1\text{pp}}_{\ell m}(\tilde{w}, r)$ is the particular Lorenz-gauge solution, obtained in Chapter 4. The superscript "pp" refers to it being the solution for a point-particle. Now, as mentioned above, unlike in the far zone, we do not yet have a physical retarded solution to match with near the horizon.

However, we assume that a complete matching procedure would establish that in some gauge, the near-zone solution $\tilde{\psi}^1_{\ell m}$ must be regular at the future horizon; the matching procedure in Chapter 6, extended to gravity, already establishes that it must be regular at future null infinity. The no-hair theorem tells us that any pure homogeneous solution (i.e. any vacuum solution) with a discrete Fourier spectrum can only be regular at both boundaries if it is comprised solely of a mass perturbation, a spin perturbation and terms that are pure gauge (see pp.875–876 of Ref. [109]). Thus, the globally regular solution in some gauge has the form

$$\tilde{\psi}^1_{\ell m}(\tilde{w}, r) = \tilde{\psi}^{\text{pure gauge}}_{\ell m}(\tilde{w}, r) + \tilde{\psi}^{1\text{pp}}_{\ell m}(\tilde{w}, r) + \tilde{\psi}^{\delta M}_{\ell m}(\tilde{w}, r) + \tilde{\psi}^{\delta J}_{\ell m}(\tilde{w}, r). \tag{7.31}$$

Now we want to write Eq. (7.31) in the Lorenz gauge. We already know from our discussion in Chapter 4 that $\tilde{\psi}^{1\text{pp}}_{\ell m}(\tilde{w}, r)$ is very close to being the only Lorenz-gauge solution that is globally regular. The only freedom to alter it, while maintaining regularity at the boundaries, comes precisely in the freedom to add an angular-momentum perturbation $\tilde{\psi}^{\delta J}_{\ell m}$. (In Chapter 4 we eliminated that freedom by specifying that the only angular momentum in the system was the orbital angular momentum of the particle.) Crucially, that freedom does not extend to the mass perturbation: it is impossible to make $\tilde{\psi}^{\delta M}_{\ell m}$ regular at both boundaries in the Lorenz gauge. We choose it to be regular at $r \to \infty$ and sacrifice regularity at the horizon, because we already have a known physical solution to match to in the far zone, whereas we have not yet obtained a physical solution to match to in the near-horizon zone. So, we write the Lorenz-gauge solution as

$$\tilde{\psi}^{1,\text{LG}}_{\ell m}(\tilde{w}, r) = \tilde{\psi}^{\text{pure gauge,LG}}_{\ell m}(\tilde{w}, r) + \tilde{\psi}^{1\text{pp}}_{\ell m}(\tilde{w}, r) + \tilde{\psi}^{\delta M,\text{LG}}_{\ell m}(\tilde{w}, r) + \tilde{\psi}^{\delta J,\text{LG}}_{\ell m}(\tilde{w}, r). \tag{7.32}$$

where the superscript "LG" denotes that the solution is now in the Lorenz gauge.

If we allow our near-horizon and far-zone solutions to differ from our near-zone solution by a gauge transformation then we can freely set $\tilde{\psi}^{\text{pure gauge,LG}}_{\ell m} = 0$. With that, and dropping the "LG" superscript, we write the Lorenz-gauge solution at first order, as

$$\tilde{\psi}^1_{\ell m}(\tilde{w}, r) = \tilde{\psi}^{1\text{pp}}_{\ell m}(\tilde{w}, r) + \tilde{\psi}^{\delta M}_{\ell m}(\tilde{w}, r) + \tilde{\psi}^{\delta J}_{\ell m}(\tilde{w}, r). \tag{7.33}$$

In Chapter 4 we only considered the particular solution $\tilde{\psi}^{1\text{pp}}$ and ignored $\tilde{\psi}^{\delta M}_{\ell m}$ and $\tilde{\psi}^{\delta J}_{\ell m}$. Physically, these additional perturbations arise from the slow change of the large BH's mass and angular momentum due to the gravitational-wave fluxes into the horizon. The content of $\tilde{\psi}^{\delta M}_{\ell m}$ bears special note. $\tilde{\psi}^{\delta M}_{\ell m}$ adds mass to the solution, which we will denote $\delta M^{\text{pert}}(\tilde{w})$. But the slow evolution of the BH mass also draws a contribution from $\tilde{\psi}^{1\text{pp}}$, because in the Lorenz gauge, this solution includes a nonzero mass content even inside the orbital radius, which is ascribed to the BH. We will denote this mass as

$\delta M_{<}^{\mathrm{pp}}$. Through $\delta M_{<}^{\mathrm{pp}}(\tilde{r}_0)$ being a function of the orbital radius, its evolution with slow time is entirely determined by Eq. (7.14). $\delta M^{\mathrm{pert}}(\tilde{w})$ adds to $\delta M_{<}^{\mathrm{pp}}(\tilde{r}_0)$ to ensure that the total increase in the BH's mass,

$$\delta M_{BH}(\tilde{w}) = \delta M_{<}^{\mathrm{pp}}(\tilde{w}) + \delta M^{\mathrm{pert}}(\tilde{w}), \tag{7.34}$$

satisfies the Einstein equations (7.20d) and (7.23b).

Now let us analyze the exact form of the first-order solution. $\tilde{\psi}_{\ell m}^{1\mathrm{pp}}$ was calculated in Chapter 4. By analogy with Eq. (4.76), we write its mass content $\delta M_{<}^{\mathrm{pp}}$ inside the region $r < \tilde{r}_0$, and its mass content $\delta M_{>}^{\mathrm{pp}}$ outside the region $r > \tilde{r}_0$, as

$$\delta M_{>}^{\mathrm{pp}}(\tilde{w}) = \frac{\mu\mathscr{E}(\tilde{w})(\tilde{r}_0 - 3M)}{(\tilde{r}_0 - 2M)}, \qquad r > \tilde{r}_0, \tag{7.35a}$$

$$\delta M_{<}^{\mathrm{pp}}(\tilde{w}) = \mu\mathscr{E}(\tilde{w})\left[\frac{(\tilde{r}_0 - 3M)}{(\tilde{r}_0 - 2M)} - 1\right], \qquad r < \tilde{r}_0, \tag{7.35b}$$

where $\mu\mathscr{E}(\tilde{w})$ is the energy of the orbit of the small object. As we mentioned above, they are explicit functions of the orbital radius $\tilde{r}_0$, which is determined by Eq. (7.14). So, we write them simply as functions of slow-time, as $\delta M_{\gtrless} = \delta M_{\gtrless}(\tilde{w})$.

We construct the mass-perturbation term $\tilde{\psi}_{\ell m}^{\delta M}$ by writing a linear combination of the four solutions $H_A$, $H_B$, $H_C$, and $H_D$ given in (4.42). Imposing asymptotic flatness eliminates both $H_A$ and $H_B$. Imposing that the mass is $\delta M^{\mathrm{pert}}$ then restricts the solution to the form $\tilde{c}H_C + 2/3\delta M^{pert}H_D$, where $\tilde{c} = \tilde{c}(\tilde{w})$ can be chosen arbitrarily.

We write the total mass content of the complete first-order solution, $\tilde{\psi}_{\ell m}^{1}$, as

$$\delta M_{>}(\tilde{w}) = \mu\mathscr{E}(\tilde{w}) + \delta M_{BH}(\tilde{w}), \qquad r > \tilde{r}_0, \tag{7.36a}$$

$$\delta M_{<}(\tilde{w}) = \delta M_{BH}(\tilde{w}), \qquad r < \tilde{r}_0. \tag{7.36b}$$

$\delta M_{BH}(\tilde{w})$ describes the physical evolution of the BH's mass with slow time. The fact that $\delta M_{<}(\tilde{w})$ is nonzero reflects the fact that the first-order field carries a flux of energy through the future horizon, causing the mass of the BH to evolve with time as $M_{BH} = M + \delta M_{BH}$. $\delta M_{BH}(\tilde{w})$ is determined by the Einstein equation to satisfy

$$\frac{d\delta M_{BH}(\tilde{w})}{d\tilde{w}} = \dot{E}_H(\tilde{w}), \tag{7.37}$$

where $\dot{E}_H$ is the flux of energy into the horizon.

The perturbation $\tilde{\psi}_{\ell m}^{\delta J}$ is more easily obtained. By linearizing the Kerr metric with respect to $J = Ma$ in Boyer-Lindquist coordinates, we get an angular-momentum perturbation in the Lorenz gauge. The result is purely an $i = 8$ term. Adding a homogeneous $i = 9$ solution to satisfy the regularity condition (4.33), we obtain

$$\tilde{h}^{\delta J}_{i=8,\ell=0,m=0} = -8\sqrt{\frac{\pi}{3}}\frac{\delta J^{\rm pert}(\tilde{w})}{r}, \tag{7.38a}$$

$$\tilde{h}^{\delta J}_{i=9,\ell=0,m=0} = -8\sqrt{\frac{\pi}{3}}\frac{\delta J^{\rm pert}(\tilde{w})}{r}. \tag{7.38b}$$

The analog of Eq. (7.36) is

$$\delta J_<(\tilde{w}) = \delta J_{BH}(\tilde{w}), \tag{7.39a}$$

$$\delta J_>(\tilde{w}) = \mu\mathscr{L}(\tilde{w}) + \delta J_{BH}(\tilde{w}). \tag{7.39b}$$

where $\mu\mathscr{L}(\tilde{w})$ is the angular momentum of the orbit, and $\delta J_{BH} = \delta J^{\rm pert}$, the angular momentum content of $h^{\delta J}_{\ell m}$ in Eq. (7.33).

### 7.3.3 Field equations for the monopole piece of the second-order field

In this section we will write down a simple example of the general equations (7.20), for the monopole ($\ell = m = 0$) mode. Solving these will be our focus in Chapter 8. When we come to compute the monopole mode of the field in Chapter 8, we use $\tilde{w} = \tilde{t}$ for our slow time coordinate.

Let us first write the field equations (7.20) with $\tilde{w} = \tilde{t}$. With this choice, $H(r) = 0$ and we find that

$$\begin{aligned}\tilde{E}^0_{i\ell m}[\,\tilde{h}\,] = &-\frac{1}{4}\left[f^2\partial_r^2 + \frac{2M}{r^2 f}\partial_r - m^2\tilde{\Omega}_0^2\right]\tilde{h}_{i\ell m}(r,\tilde{t}) + V_\ell(r)\tilde{h}_{i\ell m}(r,\tilde{t})\\ &+ \widetilde{\mathcal{M}}^{ij}_0\tilde{h}_{j\ell m}(r,\tilde{t}),\end{aligned} \tag{7.40a}$$

$$\tilde{E}^1_{i\ell m}[\,\tilde{h}\,] = -\frac{1}{2}m^2\tilde{\Omega}_0\tilde{\Omega}_1\tilde{h}_{i\ell m}(r,\tilde{t}) - \frac{im}{2}\tilde{\Omega}_0\partial_{\tilde{t}}\tilde{h}_{i\ell m}(r,\tilde{t}) + \widetilde{\mathcal{M}}^{ij}_1\tilde{h}_{j\ell m}(r,\tilde{t}), \tag{7.40b}$$

where $\widetilde{\mathcal{M}}^{ij}_1$ has the form described above but with $H(r) = 0$, and $\tilde{t}$ derivatives instead of $\tilde{w}$ derivatives. $\tilde{E}^0_{i\ell m}$ is equal to $E_{i\ell m}$ given in (4.26). Hence, Eqs. (7.20a) and (7.20b) are identical to the frequency-domain field equations (4.25).

Now we turn to the monopole ($\ell = 0$) second-order equations (7.20c) and (7.20d). The non-vanishing modes of the monopole piece of the field are $i = 1, 2, 3, 6$. We need not solve an ordinary differential equation to find $\tilde{h}_{600}$, but rather we can obtain it algebraically using the gauge condition (7.43a), given below. For the $i = 1, 2, 3$ modes we solve the ordinary differential equations (7.20c) and (7.20d). They have the form

$$\Delta_{i00}[\,\tilde{h}^{\mathcal{R}2}\,] = \frac{\sqrt{2}r}{f}\delta^2\tilde{R}^0_{i00} - \Delta_{i00}[\,\tilde{h}^{\mathcal{P}2}\,] + \frac{4M}{r^2f^2}\delta_{i2}\partial_{\tilde{t}}\tilde{h}^{\mathcal{P}1}_{100} \qquad \text{inside } \Gamma, \tag{7.41a}$$

$$\Delta_{i00}[\,\tilde{h}^{2}\,] = \frac{\sqrt{2}r}{f}\delta^2\tilde{R}^0_{i00} + \frac{4M}{r^2f^2}\delta_{i2}\partial_{\tilde{t}}\tilde{h}^{1}_{100} \qquad \text{outside } \Gamma, \tag{7.41b}$$

where all terms depend on $r$ and $\tilde{t}$, and

$$\Delta_{100}[\,\tilde{h}\,] \equiv \partial_r^2 \tilde{h}_{100} + \frac{1}{rf}\left(1 - \frac{4M}{r}\right)\partial_r \tilde{h}_{100} - \frac{f}{r}\partial_r \tilde{h}_{300} - \frac{1}{r^2 f}\tilde{h}_{100} + \frac{f}{r^2}\tilde{h}_{300}, \tag{7.42a}$$

$$\Delta_{200}[\,\tilde{h}\,] \equiv \partial_r^2 \tilde{h}_{200} - \frac{f'}{f}\partial_r \tilde{h}_{200} - \frac{2\,(r-M)}{r^3 f}\tilde{h}_{200}, \tag{7.42b}$$

$$\Delta_{300}[\,\tilde{h}\,] \equiv \partial_r^2 \tilde{h}_{300} - \frac{1}{rf^2}\left(1 - \frac{4M}{r}\right)\partial_r \tilde{h}_{100} - \frac{1}{r}\partial_r \tilde{h}_{300} + \frac{1}{r^2 f^2}\tilde{h}_{100} - \frac{1}{r^2}\tilde{h}_{300}, \tag{7.42c}$$

$$\begin{aligned}\Delta_{600}[\,\tilde{h}\,] \equiv{}& \partial_r^2 \tilde{h}_{600} + \frac{1}{rf^2}\left(1 - \frac{4M}{r}\right)\partial_r\left(f\partial_r \tilde{h}_{300} - \frac{f}{r}\tilde{h}_{300} - \partial_r \tilde{h}_{100}\right) + \frac{1}{r^2 f^2}\tilde{h}_{100}\\ &+ \frac{f'}{rf}\left(r\partial_r \tilde{h}_{600} - \tilde{h}_{600}\right).\end{aligned} \tag{7.42d}$$

As we mentioned above, the $i = 6$ mode is obtained by solving the gauge conditions (7.23). For the monopole, the non-trivial conditions at second order are $\mathscr{D}^0_n[\,\tilde{h}^2\,] = -\mathscr{D}^1_n[\,\tilde{h}^1\,]$, $n = 1, 2$. Explicitly they read

$$-f\partial_r \tilde{h}^2_{100} + f^2 \partial_r \tilde{h}^2_{300} - \frac{f}{r}\left(\tilde{h}^2_{100} - f\tilde{h}^2_{300} - 2f\tilde{h}^2_{600}\right) = 0, \tag{7.43a}$$

$$f\partial_r \tilde{h}^2_{200} + \frac{f}{r}\tilde{h}^2_{200} - \partial_{\tilde{t}} \tilde{h}^1_{100} - f\partial_{\tilde{t}} \tilde{h}^1_{300} = 0. \tag{7.43b}$$

Then, $\tilde{h}^2_{600}$ is determined from Eq. (7.43a).

The dependence on $\tilde{t}$ in Eq. (7.41) and in the gauge condition is entirely contained in two quantities: $r_0(\tilde{t})$ and $\delta M(\tilde{t})$. In the $i = 1, 3, 6$ equations, only $\tilde{r}_0$ appears. So we can solve Eq. (7.41) for $\tilde{h}^2{}_{i=1,3,6}$ as functions of $r$ and $\tilde{r}_0$. Their $\tilde{t}$ evolution is then determined by Eq. (7.14). We note that by substituting the general first-order solution (7.33) into the $i = 2$ wave equation (7.41) and the $i = 2$ gauge condition (7.43b), the slow-time derivative of the mass, $\delta\dot{M} \equiv \partial_{\tilde{t}} M$ appears in both. We can solve those two equations for the $i = 2$ field as a function of $r$ and $\tilde{r}_0$ and for $\delta\dot{M}$ as a function of $\tilde{r}_0$. The entire evolution of all four fields ($i = 1, 2, 3, 6$) is then governed by Eq. (7.14).

## 7.4 Near-horizon expansion

In the region close to the horizon at $r = 2M$, we could derive boundary conditions at the horizon, in analogy with how we construct boundary conditions at the far zone, namely by matching to a known analytical retarded solution in the far zone , as described below in Sec. 7.5. We have not yet formulated a way to do this. Instead, what we have done is derived formulas for a set of particular solutions to Eqs. (7.41), by writing an expansion in powers of $(r - 2M)$ and fixing the coefficients by solving Eqs. (7.41) order by order. The resulting particular solutions act as punctures at the horizon in the manner explained below in this section.

In preparation for the computations in Chapter 8, we focus on $\ell = 0$. Let $\tilde{h}^{\mathcal{P}H}_{i00}$ denote the $i, \ell = 0, m = 0$ mode of the puncture near the horizon. Then in a region close to the horizon we may write the monopole piece of the retarded field as $\tilde{h}^{\mathcal{P}H}_{i00}$ plus a residual piece, which we will denote as $\tilde{h}^{\mathcal{R}H}_{i00}$:

$$\tilde{h}_{i00} = \tilde{h}^{\mathcal{P}H}_{i00} + \tilde{h}^{\mathcal{R}H}_{i00}. \tag{7.44}$$

From the form of the second-order Ricci tensor in (2.18), it is comprised of smooth combinations of the background metric and the perturbations, all of which are smooth at the horizon (in regular coordinates). With that, we found that we can write any particular solution as an expansion in powers of $r - 2M$ and $\ln(r - 2M)$. In this vein, we substitute the following ansatz into Eqs (7.41):

$$\tilde{h}^{\mathcal{P}H}_{i00} = \tilde{h}^{\mathcal{P}H\text{nolog}}_{i00} + \tilde{h}^{\mathcal{P}H\text{log}}_{i00} \ln(r - 2M), \tag{7.45}$$

where $\tilde{h}^{\mathcal{P}H\text{nolog}}_{i00}$ and $\tilde{h}^{\mathcal{P}H\text{log}}_{i00}$ are power series in $r - 2M$. Using this approach the following results are readily derived:

$$\begin{aligned}
\tilde{h}^{\mathcal{P}H}_{100} =& -\sqrt{2}s_{200}(r-2M) + \frac{1}{\sqrt{2}M}\left[2M^2\delta^2\tilde{R}^0_{300}(2M) + s_{200}\right](r-2M)^2 \\
&+ \frac{1}{6}\left[-\frac{3s_{200}}{\sqrt{2}M^2} - 2\sqrt{2}\tilde{B}_{100}(2M) + 4\sqrt{2}M\delta^2\tilde{R}^{0\prime}_{300}(2M) + \sqrt{2}\delta^2\tilde{R}^0_{300}(2M)\right. \\
&\left.+4\sqrt{2}\delta^2\tilde{R}^0_{600}(2M)\right](r-2M)^3, && (7.46a)\\
\tilde{h}^{\mathcal{P}H}_{200} =& -\sqrt{2}s_{200}(r-2M), && (7.46b)\\
\tilde{h}^{\mathcal{P}H}_{300} =& -\sqrt{2}rs_{200}\log(r-2M) + \frac{\sqrt{2}}{M}\left[2M^3\delta^2\tilde{R}^{0\prime}_{300}(2M) - M^2\tilde{B}_{100}(2M)\right. \\
&\left.+4M^2\delta^2\tilde{R}^0_{300}(2M) + s_{200}\right](r-2M)^2, && (7.46c)\\
\tilde{h}^{\mathcal{P}H}_{600} =& \sqrt{2}rs_{200}\log(r-2M) \\
&+ \frac{1}{\sqrt{2}M}\left[8M^5\delta^2\tilde{R}^{0\prime}_{600}(2M) - 8M^4r\delta^2\tilde{R}^{0\prime}_{600}(2M) + 2M^3r^2\delta^2\tilde{R}^{0\prime}_{600}(2M)\right. \\
&+2M^2\left(12M^2 - 6Mr + r^2\right)\delta^2\tilde{R}^0_{300}(2M) + 12M^2s_{200} \\
&\left.+\left(2M^2r^2 - 8M^4\right)\delta^2\tilde{R}^0_{600}(2M) - 7Mrs_{200} + r^2s_{200}\right]. && (7.46d)
\end{aligned}$$

Here, $\delta^2\tilde{R}^0_{i00}(2M)$ and $\delta^2\tilde{R}^{0\prime}_{i00}(2M)$ are the values of $\delta^2\tilde{R}^0_{i00}(r)$ and its first derivative with respect to $r$ at $r = 2M$, respectively. $\tilde{B}_{100}(r)$ is a $C^\infty$ function, related to $\delta^2\tilde{R}^0_{100}$ and $\delta^2\tilde{R}^0_{200}$ through

$$\delta^2\tilde{R}_{200} = \delta^2\tilde{R}_{100} + f^2\tilde{B}_{100}(r), \tag{7.47}$$

analogous to Eq. (4.34). $s_{200}$ is the constant in the formula $\delta^2\tilde{R}^0_{200} = s_{200}/r^2$, which stems from the property that $\delta^2\tilde{R}^0_{200}(r)$ behaves exactly as $1/r^2$, as we show in Appendix G. $\delta^2\tilde{R}^0_{i00}(2M)$, $\delta^2\tilde{R}^{0\prime}_{i00}(2M)$ and $s_{200}$ are determined by matching to the numerical data, as we will describe in Chapter 8.

Equipped with the punctures at the horizon, the divergence in the source term on the right hand side of Eq. (7.41b) at $r = 2M$, gets canceled by the action of the differential operator $\Delta_{i00}$ defined in (7.42) acting on the puncture at the horizon. Note that $\delta^2\tilde{R}^0_{i00}$ itself is regular at $r = 2M$, rather the divergence comes from the factor of $1/f$ in front. We may then solve an effective source equation near the horizon:

$$\Delta_{i00}[\,\tilde{h}^{\mathcal{R}H}\,] = S^{\text{eff}\,H}_{i00}, \tag{7.48}$$

where the effective source is given by

$$S^{\text{eff}\,H}_{i00} = \frac{\sqrt{2}r}{f}\delta^2\tilde{R}^0_{i00}(r) - \delta_{i2}\frac{4M}{r^2 f^2}\partial_{\tilde{t}}\tilde{h}^1_{i00} - \Delta_{i00}[\,\tilde{h}^{\mathcal{P}H}\,]. \tag{7.49}$$

Although our puncture is not physically motivated, we can justify our use of it at a particular value of slow time. Because $h^{\mathcal{P}H}$ must be a particular solution to the field equations, altering it can only change our final result for $h^{\mathcal{P}H} + h^{\mathcal{R}H}$ by a homogeneous solution. But an $\ell = 0$ homogeneous solution only has mass content and pure gauge, which we can always absorb into the background mass.

However, this argument will no longer apply to the higher-$\ell$ modes. It will also no longer be the case once we are doing an evolution, because once the mass is varying with time, it can no longer be absorbed into the background mass. Therefore, we will eventually require a thorough matching procedure at the horizon.

## 7.5 Post-Minkowski expansion

The last remaining region to consider is the far zone. In this section we will construct a post-Minkowski (PM) solution valid in the far zone, closely following the method described in Sec. 6.4.2. In order to find the solution at large $r$, we will restrict the range of spatial coordinates to points outside of $\text{supp}(h^{2\mathcal{P}})$, namely $r > \mathcal{R}_+$. In this region the field equations (7.18) reduce to

$$E_{\mu\nu}[\,\bar{h}^1\,] = 0, \tag{7.50}$$

$$E_{\mu\nu}[\,\bar{h}^2\,] = 2\delta^2\bar{R}_{\mu\nu}[h^1, h^1]. \tag{7.51}$$

We then write $g_{\mu\nu}$ and $\bar{h}^n_{\mu\nu}$ in a PM form by expanding in powers of $M$, using the following approach.

We expand at fixed Cartesian coordinates $(u \equiv t - r, x^i)$ and at fixed $z^\mu$. After performing the expansion, we adopt background coordinates $(t, x^i)$, where $t = u + r$ (which differs from the Schwarzschild time coordinate by a gauge transformation of order $M \ln M$). The expansion puts the operators $E$ and $\delta^2\bar{R}$ in the form

$$E = \Box + \sum_{n\geq 1} M^n E^n, \tag{7.52}$$

$$\delta^2\bar{R} = \sum_{n\geq 0} M^n \delta^2\bar{R}^n, \tag{7.53}$$

and the metric perturbations in the form

$$\bar{h}^n_{\mu\nu} = \sum_{p\geq 0} M^p \bar{h}^{n,p}_{\mu\nu}(t, x^i; z). \tag{7.54}$$

Here, all components are in coordinates $(t, x^i)$, in which $\Box = \eta^{\mu\nu}\partial_\mu\partial_\nu$ and $\eta^{\mu\nu} = \mathrm{diag}(-1, 1, 1, 1)$. In particular, we choose the $\bar{h}^1$ solutions in the far zone such that as $r \to \infty$, the leading oscillatory term in $\bar{h}^{1,p+1}$ falls off faster than the leading oscillatory term in $\bar{h}^{1,p}$. Then the "oscillation $/r$" term in $\bar{h}^{1,0}$ will be identical to the "oscillation $/r$" term in $\bar{h}^1$. This point is key to the discussion in Appendix G.

With these expansions, the field equations become a sequence of equations, one at each order in $M$. The leading-order equations read

$$\Box\bar{h}^{1,0}_{\mu\nu} = 0, \tag{7.55}$$

$$\Box\bar{h}^{2,0}_{\mu\nu} = 2\delta^2\bar{R}^0_{\mu\nu}[h^{1,0}, h^{1,0}]. \tag{7.56}$$

The retarded solution to Eq. (7.55) can be written as

$$\bar{h}^{1,0}_{tt} = 4\sum_{\ell\geq 0} \frac{(-1)^\ell}{\ell!}\partial_L \frac{F_L(u)}{r}, \tag{7.57a}$$

$$\bar{h}^{1,0}_{ti} = 4\sum_{\ell\geq 0} \frac{(-1)^\ell}{\ell!}\partial_L \frac{G_{iL}(u)}{r}, \tag{7.57b}$$

$$\bar{h}^{1,0}_{ij} = 4\sum_{\ell\geq 0} \frac{(-1)^\ell}{\ell!}\partial_L \frac{H_{ijL}(u)}{r}, \tag{7.57c}$$

where $r = \sqrt{\delta_{ij}x^i x^j}$ and $u = t - r$, and the STF multipole moments $F_L$, $G_{iL}$, and $H_{ijL}$ are to be determined by matching to the near-zone solution. The notation used here is the same notation employed in Sec. 6.4.2.

The retarded solution to Eq. (7.56) can be written, in the same way that we wrote Eq. (6.77), as

$$\bar{h}^{2,0}_{\mu\nu} = \bar{h}^{\mathrm{part}}_{\mu\nu} + \bar{h}^{\mathrm{hom}}_{\mu\nu}, \tag{7.58}$$

where the homogeneous solution $\bar{h}^{\mathrm{hom}}_{\mu\nu}$ has a form identical to Eq. (7.57), and the particular solution is

$$\bar{h}^{\mathrm{part}}_{\mu\nu} = \mathrm{FP}\Box^{-1}_{\mathrm{ret}}(r^B S_{\mu\nu}), \tag{7.59}$$

with $S_{\mu\nu} \equiv 2\delta^2 \bar{R}_{\mu\nu}$ being the source term on the right-hand side of (7.51).

To determine boundary conditions for our near-zone expansion we need only examine the part of the solution sourced by the most slowly falling piece of the source term, $2\delta^2 \bar{R}^0_{\mu\nu}$, on the right-hand side of Eq. (7.56), as described in Chapter 6. We may write the source by isolating the leading-order piece that falls off as $1/r^2$ plus terms that fall off faster than that, in the form

$$2\delta^2 \bar{R}^0_{\mu\nu} = \frac{s_{\mu\nu}(u, n^i)}{r^2} + O(1/r^3). \tag{7.60}$$

In the same style of notation as Sec. 6.4.2, we define $j_{\mu\nu}$ to be the finite part of the retarded integral of the slowest decaying piece of the source against the Green's function,

$$j_{\mu\nu} = \mathrm{FP}\Box^{-1}_{\mathrm{ret}}(r^{B-2} s_{\mu\nu}) = \Box^{-1}_{\mathrm{ret}}(r^{-2} s_{\mu\nu}). \tag{7.61}$$

Our original field variable $\bar{h}^2_{\mu\nu}$ can then be written as

$$\bar{h}^2_{\mu\nu} = j_{\mu\nu} + O(\ln r/r). \tag{7.62}$$

### 7.5.1 Calculation of the monopole piece of $j_{\mu\nu}$

Now we turn to deriving an expression for the monopole ($\ell = 0$) piece of $j_{\mu\nu}$. In Chapter 6 it was shown that for a scalar field, only the monopole ($\ell = 0$) mode of (the analog of) Eq. (7.61) is required for matching. We will carry this result over to the 4D second-order field, and use the matching procedure for the monopole mode to determine $j_{\mu\nu}$. To begin, we write the components of $j_{\mu\nu}$ as an expansion in terms of irreducible symmetric trace-free pieces, analogous to Eqs. (2.38), as

$$j_{tt} = \sum_{\ell\geq 0} \hat{A}^{\ell}_{L} \hat{n}^L, \tag{7.63a}$$

$$j_{ta} = \sum_{\ell\geq 0} \hat{B}^{\ell+1}_{L} \hat{n}_a{}^L + \sum_{\ell\geq 1} \left[ \hat{C}^{\ell-1}_{aL-1} \hat{n}^{L-1} + \epsilon_{ab}{}^c \hat{D}^{\ell}_{cL-1} \hat{n}^{bL-1} \right], \tag{7.63b}$$

$$\begin{aligned} j_{ab} = {} & \delta_{ab} \sum_{\ell\geq 0} \hat{K}^{\ell}_{L} \hat{n}^L + \sum_{\ell\geq 0} \hat{E}^{\ell+2}_{L} \hat{n}_{ab}{}^L + \sum_{\ell\geq 1} \left[ \hat{F}^{\ell}_{L-1\langle a} \hat{n}_{b\rangle}{}^{L-1} + \epsilon^{cd}{}_{(a} \hat{n}_{b)c}{}^{L-1} \hat{G}^{\ell+1}_{dL-1} \right] \\ & + \sum_{\ell\geq 2} \left[ \hat{H}^{\ell-2}_{abL-2} \hat{n}^{L-2} + \epsilon^{cd}{}_{(a} \hat{I}^{\ell-1}_{b)dL-2} \hat{n}_c{}^{L-2} \right]. \end{aligned} \tag{7.63c}$$

We will use the notation $\bar{\ell}$ for the superscript on the coefficients, for example in the term $\hat{A}^{\ell}_{L} \hat{n}^L$, $\bar{\ell} = \ell$, and for the term $\hat{B}^{\ell+1}_{L} \hat{n}_a{}^L$, $\bar{\ell} = \ell + 1$, and so on. We may write analogous STF expansions for the components $s_{\mu\nu}$. We will refer to the coefficients in that expansion as $\hat{\hat{A}}^{\bar{\ell}}_{L}$, $\hat{\hat{B}}^{\bar{\ell}}_{L}$, and so on. Let $\hat{j}^{\bar{\ell}}_{L}$ be an element of the set $\left\{ \hat{A}^{\bar{\ell}}_{L}, \hat{B}^{\bar{\ell}}_{L}, \ldots \right\}$ and $\hat{s}^{\bar{\ell}}_{L}$ be an element of the set $\left\{ \hat{\hat{A}}^{\bar{\ell}}_{L}, \hat{\hat{B}}^{\bar{\ell}}_{L}, \ldots \right\}$. From the analysis in Chapter 6, the quasistationary pieces of the retarded solutions are given by

$$\hat{j}_L^{\bar{\ell}} = \begin{cases} F[\hat{s}_L^{\bar{\ell}}] & \text{if } \bar{\ell} = 0, \\ -\dfrac{\hat{s}_L^{\bar{\ell}}}{\bar{\ell}(\bar{\ell}+1)} & \text{if } \bar{\ell} > 0, \end{cases} \tag{7.64}$$

where in analogy with Eqs. (6.65) and (6.85),

$$F[\hat{s}](\tilde{w}) \equiv \hat{s}(\tilde{w}) \ln r - \hat{s}(\tilde{w}) + k[\hat{s}](\tilde{w}) \tag{7.65}$$

and

$$k[\hat{s}](\tilde{w}) \equiv -\hat{s}(\tilde{w}) \ln \frac{2}{\epsilon} - \int_0^\infty d\tilde{z}\ \dot{\hat{s}}(\tilde{w} - \tilde{z}) \ln \tilde{z}. \tag{7.66}$$

Explicitly, for the $\ell = 0$ terms, we derive

$$\begin{aligned} \hat{A}^0 &= F[\hat{\hat{A}}^0], \quad \hat{K}^0 = F[\hat{\hat{K}}^0], \\ \hat{B}^1 &= -\frac{1}{2}\hat{\hat{B}}^1, \quad \hat{E}^2 = -\frac{1}{6}\hat{\hat{E}}^2. \end{aligned} \tag{7.67}$$

We may extract the $\ell = 0$ scalar, spherical harmonic of any of these components by integrating them against $Y_{00}^*$ over the unit two-sphere. Then, we find that the scalar spherical-harmonic monopole of the components is

$$j_{tt}^{00} = 2\sqrt{\pi}\hat{A}^0, \tag{7.68a}$$
$$j_{tr}^{00} = 2\sqrt{\pi}\hat{B}^1, \tag{7.68b}$$
$$j_{rr}^{00} = 2\sqrt{\pi}\left(\hat{K}^0 + \frac{2}{3}\hat{E}^2\right), \tag{7.68c}$$
$$j^{00} = 2\sqrt{\pi}\left(\hat{K}^0 - \frac{1}{3}\hat{E}^2\right), \tag{7.68d}$$

where $j_{\mu\nu}^{00} \equiv \oint d\Omega j_{\mu\nu} Y_{00}^*$ and $j^{00} \equiv \oint d\Omega j Y_{00}^*$, where $j$ is the trace. We find a similar set of relations for $s_{tt}^{00}$,$s_{tr}^{00}$, $s_{rr}^{00}$ and $s^{00}$ in terms of $\hat{\hat{A}}^0$, $\hat{\hat{B}}^1$, $\hat{\hat{K}}^0$ and $\hat{\hat{E}}^2$, where $s_{\mu\nu}^{00}$ is defined analogously to $j_{\mu\nu}^{00}$. By analogy with the above discussion, the scalar harmonic monopole of $s_{\mu\nu}$ is

$$s_{tt}^{00} = 2\sqrt{\pi}\hat{\hat{A}}^0, \tag{7.69a}$$
$$s_{tr}^{00} = 2\sqrt{\pi}\hat{\hat{B}}^1, \tag{7.69b}$$
$$s_{rr}^{00} = 2\sqrt{\pi}\left(\hat{\hat{K}}^0 + \frac{2}{3}\hat{\hat{E}}^2\right), \tag{7.69c}$$
$$s^{00} = 2\sqrt{\pi}\left(\hat{\hat{K}}^0 - \frac{1}{3}\hat{\hat{E}}^2\right). \tag{7.69d}$$

Combining Eqs. (7.67)–(7.69), we obtain relationships between the monopole pieces of the $j_{\mu\nu}$ and $s_{\mu\nu}$ as

$$j^{00}_{tt} = s^{00}_{tt} \ln r - s^{00}_{tt} + k\left[s^{00}_{tt}\right], \tag{7.70a}$$

$$j^{00}_{tr} = -\frac{1}{2} s^{00}_{tr}, \tag{7.70b}$$

$$j^{00}_{rr} = \frac{1}{3}\left(s^{00}_{rr} + 2s^{00}\right)\ln r - \frac{4}{9}s^{00}_{rr} - \frac{5}{9}s^{00} + \frac{1}{3}k\left[s^{00}_{rr} + 2s^{00}\right], \tag{7.70c}$$

$$j^{00} = \frac{1}{3}\left(s^{00}_{rr} + 2s^{00}\right)\ln r - \frac{1}{18}\left(5s^{00}_{rr} + 13s^{00}\right) + \frac{1}{3}k\left[s^{00}_{rr} + 2s^{00}\right]. \tag{7.70d}$$

Using the relations

$$s^{00}_{tt} = s_{100} + s_{300}, \quad s^{00}_{tr} = s_{200}, \quad s^{00}_{rr} = s_{100} - s_{300}, \quad s^{00} = s_{600}, \tag{7.71}$$

with a similar set of expressions for $\{j^{00}_{tt}, j^{00}_{tr}, j^{00}_{rr}, j^{00}\}$ in terms of $\{j_{100}, j_{200}, j_{300}, j_{600}\}$, we derive that

$$j_{100} = \frac{2}{3}s_{100}\ln r - \frac{1}{18}s_{100} + 2\kappa, \tag{7.72a}$$

$$j_{200} = \frac{1}{2}s_{100}, \tag{7.72b}$$

$$j_{300} = j_{600} = \frac{1}{3}s_{100}\ln r + \frac{1}{18}s_{100} + \kappa, \tag{7.72c}$$

where

$$\kappa \equiv -\frac{1}{3}\left(1 + \ln\frac{\epsilon}{2}\right)s_{100} - \frac{1}{3}\int_0^\infty d\tilde{z}\,\dot{s}_{100}(\tilde{u} - \tilde{z})\ln\tilde{z}. \tag{7.73}$$

In Appendix G we derive a physically informative expression for $s_{100}$. The $j_{i00}$ are used to define a puncture at infinity, as in the previous chapter.

### 7.5.2 Punctures at infinity

The punctures at infinity are constructed using the analogous method for the scalar case, outlined in Sec. 6.4.1. The expressions for the monopole modes are

$$\bar{h}^{\mathcal{P}\infty}_{100} = \sqrt{2}r j_{100}(r) + \frac{1}{3}\left(8\sqrt{2}\right)M s_{200}\log(r) + \frac{2}{9}\sqrt{2}M(11s_{200} - 36\kappa), \tag{7.74a}$$

$$\bar{h}^{\mathcal{P}\infty}_{200} = \sqrt{2}r j_{200}(r), \tag{7.74b}$$

$$\bar{h}^{\mathcal{P}\infty}_{300} = \sqrt{2}r j_{300}(r), \tag{7.74c}$$

$$\bar{h}^{\mathcal{P}\infty}_{600} = \sqrt{2}r j_{600}(r) + 2\sqrt{2}M s_{200}, \tag{7.74d}$$

where the factor of $\sqrt{2}r$ arises from the factor $a_{i\ell}/r$ in Eq. (4.14), where the $j_{i00}$ and $\kappa$ were derived in Eqs. (7.72) and (7.73), respectively. $s_{200}$ is the proportionality constant in $\delta^2\bar{R}_{200}[h^1, h^1] = s_{200}/r^2$. Its value may be extracted from the numerical data for $\delta^2\bar{R}_{200}[h^1, h^1]$, which is discussed in Sec. 8.4.

The punctures in (7.74) include terms one order higher in $1/r$ than those derived in (7.72). Those extra terms were derived following an approach similar to the one we used near the horizon, by inserting an expansion of the form $\bar{h}_{i00} = \sqrt{2} r j_{i00}(r) + A_i \log(r) + B_i$, with $A_i$ and $B_i$ independent of $r$. The terms in addition to $j_{i00}$ ensure that subleading terms (terms that decay slower than $1/r^2$) also cancel in Eq. (7.51). Our puncture can be altered by adding an asymptotically flat homogeneous solution. However, changing the puncture by such a solution merely moves terms between the puncture and the residual field, leaving the total field unaltered.

To summarise, in this chapter we have constructed boundary conditions at the horizon in Eqs. (7.46), and at infinity in Eqs. (7.74). In the next chapter, we are going to use these boundary conditions to solve equations (7.41), for the monopole mode of the second-order field.

# Chapter 8

# Results for the monopole mode of the second-order field

In this chapter we describe our calculation of the monopole piece of the second-order field, and present our results. In Sec. 8.1 we give an overview of the puncture scheme used in the calculation. Next, in Sec. 8.2 we go into detail about how we implement the puncture scheme to solve the second-order field equations. In Sec. 8.3, we move on to explain how the modes of the second-order source are computed. This follows from the technique described in Chapter 5 for computing the modes of the source in the toy model. We extend that technique to the computation of the second-order source in gravity. In Sec. 8.4, we present our numerical results for the source, and compare our findings with analytical predictions derived in Appendix G. In Sec. 8.5 we give formulas for the punctures at the particle. In Sec. 8.6 we describe how we compute the effective source. Putting all this together, we calculate the monopole piece of the second-order field, and present our results in Sec. 8.7.

## 8.1 Overview of the calculation

Our goal is to compute the monopole mode of the second-order field, for an orbit of radius $\tilde{r}_0$. We remind the reader that $\tilde{r}_0$ is the leading-order contribution to the orbital radius in the context of the two-timescale expansion of the worldline. The field equations are comprised of equations at fixed slow time, $\tilde{t}$, and equations that describe the evolution of the system with $\tilde{t}$. We will only concentrate on the equations at some fixed $\tilde{t} = \tilde{t}_0$ in this chapter. At this fixed time, we make several simplifications. As mentioned in Chapter 7, we choose $\tilde{\Omega}_1(\tilde{t}_0) = 0$. We also choose $\delta M^{\rm pert}(\tilde{t}_0) = \delta J^{\rm pert}(\tilde{t}_0) = 0$, such that the first-order solution $\tilde{\psi}^1_{\ell m}$ described in Sec. 7.3.2 reduces to the solution $\tilde{\psi}^{\rm 1pp}_{\ell m}$ obtained in Chapter 4. But note that we do not have the freedom to set slow-time derivatives of these quantities to zero.

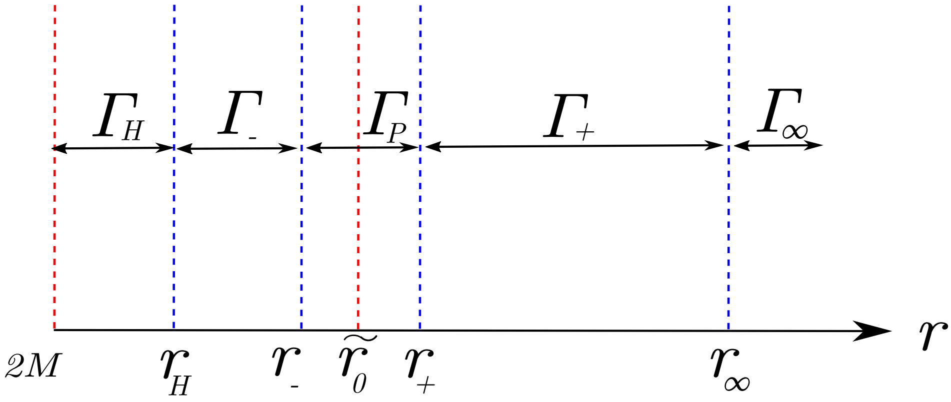


Figure 8.1: The worldtube boundaries in the second-order puncture scheme. $\Gamma_H$ is the region $r \in (2M, r_H)$, where $r_H$ is chosen to be suitably close to the horizon in a way which we will describe below. $\Gamma_{\rm P}$ is the worldtube centered on the particle at $\tilde{r}_0$, as $r \in (r_-, r_+)$. $\Gamma_\infty$ refers to the asymptotic region $r \in (r_\infty, \infty)$.

We also emphasize that in our expressions (7.74) for the punctures near infinity, we set $\kappa = 0$. We have the freedom to do this, since picking a particular value for $\kappa$ is equivalent to adding a homogeneous solution. Because the only invariant content in a homogeneous solution is mass, we can absorb it into the background mass $M$. The reason for setting it to zero is because it introduces a $\ln(\epsilon)$ into our solution, hence, we would no longer be calculating the coefficient of $\epsilon^2$; our results would depend on the specific value of the mass ratio.

We now want to generalise Eqs. (7.41) to a set of equations that include punctures at the horizon and at infinity. With this in mind we define the following regions $\Gamma_H, \Gamma_-, \Gamma_{\rm P}, \Gamma_+, \Gamma_\infty$ , as illustrated in Fig. 8.1. In $\Gamma_H$ we use the puncture at the horizon, $\tilde{h}^{\mathcal{P}H}_{\mu\nu}$ given in Eqs. (7.46), in $\Gamma_{\rm P}$ we use the puncture at the particle, $\tilde{h}^{\mathcal{P}\rm P}_{\mu\nu}$ given below in Eq. (8.28), and in $\Gamma_\infty$ we use the puncture at infinity, $\tilde{h}^{\mathcal{P}\infty}_{\mu\nu}$ given in Eqs. (7.74). We remind the reader that $\tilde{h}_{\mu\nu}$ refers to the trace reverse of the field written in two-timescale coordinates, in the manner described in Chapter 7.

We may define residual fields in these regions, analogous to (3.4), as

$$\tilde{h}^{\mathcal{R}H}_{\mu\nu} \equiv \tilde{h}^2_{\mu\nu} - \tilde{h}^{\mathcal{P}H}_{\mu\nu}, \tag{8.1a}$$
$$\tilde{h}^{\mathcal{R}\rm P}_{\mu\nu} \equiv \tilde{h}^2_{\mu\nu} - \tilde{h}^{\mathcal{P}\rm P}_{\mu\nu}, \tag{8.1b}$$
$$\tilde{h}^{\mathcal{R}\infty}_{\mu\nu} \equiv \tilde{h}^2_{\mu\nu} - \tilde{h}^{\mathcal{P}\infty}_{\mu\nu}. \tag{8.1c}$$

The non-punctured regions are $\Gamma_-$, where $r \in (r_H, r_-)$, and $\Gamma_+$, where $r \in (r_+, r_\infty)$.

Proceeding as we did at first order, we write each of the fields $\tilde{h}^2_{\mu\nu}$, $\tilde{h}^{\mathcal{P}H}_{\mu\nu}$, $\tilde{h}^{\mathcal{P}\rm P}_{\mu\nu}$, $\tilde{h}^{\mathcal{P}\infty}_{\mu\nu}$, $\tilde{h}^{\mathcal{R}H}_{\mu\nu}$, $\tilde{h}^{\mathcal{R}\rm P}_{\mu\nu}$, $\tilde{h}^{\mathcal{R}\infty}_{\mu\nu}$ as a decomposition into modes analogous to Eq. (7.5). We will use the notation $\tilde{h}_{i\ell m}$ for the harmonic modes of $\tilde{h}^2_{\mu\nu}$, and $\tilde{h}^{\mathcal{P}H}_{i\ell m}$, $\tilde{h}^{\mathcal{P}\mathrm{P}}_{i\ell m}$, $\tilde{h}^{\mathcal{P}\infty}_{i\ell m}$, $\tilde{h}^{\mathcal{R}H}_{i\ell m}$, $\tilde{h}^{\mathcal{R}\mathrm{P}}_{i\ell m}$, $\tilde{h}^{\mathcal{R}\infty}_{i\ell m}$ for the modes of $\tilde{h}^{\mathcal{P}H}_{\mu\nu}$, $\tilde{h}^{\mathcal{P}\mathrm{P}}_{\mu\nu}$, $\tilde{h}^{\mathcal{P}\infty}_{\mu\nu}$, $\tilde{h}^{\mathcal{R}H}_{\mu\nu}$, $\tilde{h}^{\mathcal{R}\mathrm{P}}_{\mu\nu}$, $\tilde{h}^{\mathcal{R}\infty}_{\mu\nu}$, respectively. $\delta^2\tilde{R}^0_{\mu\nu}[h^1,h^1]$ is decomposed in an analogous way, as given in Eq. (7.6). The exact form of the modes $\delta^2\tilde{R}^0_{i\ell m}$ will be discussed in Sec. 8.3.

The non-vanishing modes of the monopole ($\ell=0$) piece of the field are $i=1,2,3,6$. Unlike at first order, the $i=2$, $\ell=m=0$ effective source is non-zero and the inhomogeneous solutions are not trivially zero. So, we need to obtain solutions for this mode at second order. The $i=2$ equations (7.41) and (7.43b) differ from the others in that they contain slow-time derivatives of the first-order field; Adam Pound has separately solved these equations for $i=2$ analytically. Given that the $i=2$ mode is not coupled to the $i=1,3,6$ modes, we will neglect the $i=2$ equation in this work and focus only on the $i=1,3,6$ modes. For these modes, the effective-source equations (7.41), generalised to include punctures at the horizon and at infinity, are given explicitly by

$$\Delta_{i00}[\,\tilde{h}^{\mathcal{R}s}\,]=S^{\mathrm{eff}\,s}_{i00}(r)\qquad\text{inside }\Gamma_s,\tag{8.2}$$

where $s\in\{H,-,\mathrm{P},+,\infty\}$,

$$S^{\mathrm{eff}\,s}_{i00}(r)\equiv\frac{\sqrt{2}r}{f}\delta^2\tilde{R}^0_{i00}-\Delta_{i00}[\,\tilde{h}^{\mathcal{P}s}\,],\tag{8.3}$$

and the $\Delta_{i00}[\,\tilde{h}\,]$ are defined in Eqs. (7.42). We note that $h^{\mathcal{P}\pm}=0$ in the non-punctured regions, $\Gamma_\pm$. Just like at first order, we can solve the gauge constraint given in Eq. (7.43a) for $\tilde{h}_{600}$, and we need not solve the $i=6$ equation (8.2).

## 8.2 The worldtube method for punctures at the particle and at the boundaries

In this section we will outline the worldtube method for solving the puncture-scheme equations (8.2), which is an extension of the worldtube method used in Sec. 4.5, to include punctures at the horizon and at infinity. The worldtube method for solving the second-order equations was developed in collaboration with Adam Pound, but its implementation in the later sections of this chapter was entirely my work.

Let $\psi(r)$ be a column vector comprised of $\ell=m=0$ modes of the retarded field, given by

$$\psi(r)=\begin{pmatrix}\tilde{h}_{100}(r)\\ \tilde{h}_{300}(r)\end{pmatrix}.\tag{8.4}$$

We define

$$\psi^{\mathcal{R}s}(r)\equiv\psi(r)-\psi^{\mathcal{P}s}(r),\tag{8.5}$$

where $s \in \{H, -, \mathrm{P}, +, \infty\}$. $\psi^{\mathcal{R}s}$ is defined by

$$\psi^{\mathcal{R}s}(r) \equiv \begin{pmatrix} \tilde{h}^{\mathcal{R}s}_{100}(r) \\ \tilde{h}^{\mathcal{R}s}_{300}(r) \end{pmatrix} \tag{8.6}$$

for $s \in \{H, -, \mathrm{P}, +, \infty\}$, $\psi^{\mathcal{P}s}$ is defined by

$$\psi^{\mathcal{P}s}(r) \equiv \begin{pmatrix} \tilde{h}^{\mathcal{P}s}_{100}(r) \\ \tilde{h}^{\mathcal{P}s}_{300}(r) \end{pmatrix} \tag{8.7}$$

for $s \in \{H, \mathrm{P}, \infty\}$, and $\psi^{\mathcal{P}+} = \psi^{P-} \equiv (0, 0, 0)^T$. We define the column vector

$$J^{\mathrm{eff}\,s}(r) \equiv \begin{pmatrix} S^{\mathrm{eff}\,s}_{100}(r) \\ S^{\mathrm{eff}\,s}_{300}(r) \end{pmatrix}. \tag{8.8}$$

While this discussion focuses on the monopole modes, we can apply it to generic $\ell > 0$ modes, by using the format of Eq. (4.59) for column vectors instead of Eqs. (8.4)-(8.8). $d(= 2)$ shall denote the number of elements in each vector. Keeping $d$ symbolic is convenient for the next part of the discussion and allows us to easily generalise to $\ell > 0$ modes, for which $d$ is different.

Then, analogous to Eqs. (4.62) and (4.63), we may write Eqs. (8.2) as

$$\frac{d\hat{\psi}^s}{dr} + \hat{A}\hat{\psi}^s = \hat{J}^s \qquad \text{inside } \Gamma_s, \tag{8.9}$$

where $\hat{\psi}^s = \begin{pmatrix} \psi^s \\ \partial_r \psi^s \end{pmatrix}$ is a column vector with $2d$ elements, $\hat{A}$ is a $2d \times 2d$ matrix and the source term $\hat{J}^s = \begin{pmatrix} \mathbf{0}_d \\ J^{\mathrm{eff}\,s} \end{pmatrix}$ has $2d$ elements. The general solution in each region is

$$\hat{\psi}^s = \hat{\Phi}\left(\int_{r_s}^{r} \hat{\Phi}^{-1}\hat{J}^s dr + a^s\right), \tag{8.10}$$

where $\hat{\Phi} = \begin{pmatrix} \hat{\psi}_{[1]} & \cdots & \hat{\psi}_{[2d]} \end{pmatrix}$ is a $2d \times 2d$ matrix of independent homogeneous solutions $\hat{\psi}_{[k]} = \begin{pmatrix} \psi_{[k]} \\ \partial_r \psi_{[k]} \end{pmatrix}$, $a^s$ is an $r$-independent $d$-vector to be determined by jump conditions at the boundaries of $\Gamma_s$ in the manner described below, and $r_s \in \{2M, r_H, r_-, r_+, r_\infty\}$ is the left boundary of the domain of $\hat{\psi}^s$.

The jump conditions are

$$a^H - a^- = -\int_{2M}^{r_H} \hat{\Phi}^{-1}\hat{J}^H dr - \hat{\Phi}^{-1}\hat{\psi}^{\mathcal{P}H}(r_H), \tag{8.11a}$$

$$a^{\mathrm{P}} - a^- = \int_{r_H}^{r_-} \hat{\Phi}^{-1}\hat{J}^- dr - \hat{\Phi}^{-1}\hat{\psi}^{\mathcal{P}\mathrm{P}}(r_-), \tag{8.11b}$$

$$a^{\mathrm{P}} - a^{+} = -\int_{r^{-}}^{r_{+}} \hat{\Phi}^{-1} \hat{J}^{\mathrm{P}} dr - \hat{\Phi}^{-1} \hat{\psi}^{\mathcal{P}\mathrm{P}}(r_{+}), \tag{8.11c}$$

$$a^{\infty} - a^{+} = \int_{r_{+}}^{r_{\infty}} \hat{\Phi}^{-1} \hat{J}^{\infty} dr - \hat{\Phi}^{-1} \hat{\psi}^{\mathcal{P}\infty}(r_{\infty}), \tag{8.11d}$$

and the regularity conditions are

$$a^{H} = (a_1^{H}, \ldots, a_d^{H}, 0, \ldots, 0)^{T}, \tag{8.12a}$$

$$a^{\infty} = -\int_{r_{\infty}}^{\infty} \Phi^{-1} \hat{J}^{\infty} dr + (0, \ldots, 0, a_1^{\infty}, \ldots, a_d^{\infty})^{T}. \tag{8.12b}$$

We first solve for $a^{\infty-H} \equiv \left(-a_1^{H}, \ldots, -a_d^{H}, a_1^{\infty}, \ldots, a_d^{\infty}\right)^{T}$ by taking the difference of Eqs. (8.11d) and (8.11a) and substituting the difference of Eqs. (8.11c) and (8.11b). This yields

$$\begin{aligned} a^{\infty-H} = &\int_{2M}^{\infty} \Phi^{-1} \hat{\mathcal{J}} dr + \Phi^{-1} \hat{\psi}^{\mathcal{P}H}(r_H) - \Phi^{-1} \hat{\psi}^{\mathcal{P}\mathrm{P}}(r_{-}) \\ &+ \Phi^{-1} \hat{\psi}^{\mathcal{P}\mathrm{P}}(r_{+}) - \Phi^{-1} \hat{\psi}^{\mathcal{P}\infty}(r_{\infty}), \end{aligned} \tag{8.13}$$

where in the first integral on the right-hand side, going from $r = 2M$ to $r \to \infty$, $\hat{\mathcal{J}} = \hat{J}^{s}$ when $r \in \Gamma_s$. Substituting this result back into Eqs. (8.11a) and (8.11d), we find

$$a^{-} = \begin{pmatrix} -\int_{r_H}^{\infty} \Phi_{\mathrm{top}}^{-1} \hat{\mathcal{J}} dr + \Phi_{\mathrm{top}}^{-1} \hat{\psi}^{\mathcal{P}\mathrm{P}}(r_{-}) - \Phi_{\mathrm{top}}^{-1} \hat{\psi}^{\mathcal{P}\mathrm{P}}(r_{+}) + \Phi_{\mathrm{top}}^{-1} \hat{\psi}^{\mathcal{P}\infty}(r_{\infty}) \\ \int_{2M}^{r_H} \Phi_{\mathrm{bot}}^{-1} \hat{\mathcal{J}} dr + \Phi_{\mathrm{bot}}^{-1} \hat{\psi}^{\mathcal{P}H}(r_H) \end{pmatrix}, \tag{8.14}$$

$$a^{+} = \begin{pmatrix} -\int_{r_{+}}^{\infty} \Phi_{\mathrm{top}}^{-1} \hat{\mathcal{J}} dr + \Phi_{\mathrm{top}}^{-1} \hat{\psi}^{\mathcal{P}\infty}(r_{\infty}) \\ \int_{2M}^{r_{+}} \Phi_{\mathrm{bot}}^{-1} \hat{\mathcal{J}} dr + \Phi_{\mathrm{bot}}^{-1} \hat{\psi}^{\mathcal{P}H}(r_H) - \Phi_{\mathrm{bot}}^{-1} \hat{\psi}^{\mathcal{P}\mathrm{P}}(r_{-}) + \Phi_{\mathrm{bot}}^{-1} \hat{\psi}^{\mathcal{P}\mathrm{P}}(r_{+}) \end{pmatrix}, \tag{8.15}$$

where $\hat{\Phi}_{\mathrm{top}}$ and $\hat{\Phi}_{\mathrm{bot}}$, as defined in Sec. 4.5, are the top and bottom $d$ rows of the matrix $\hat{\Phi}(r)$. Finally, substitution of $a^{-}$ into Eq. (8.11b) gives us

$$a^{\mathrm{P}} = \begin{pmatrix} -\int_{r_{-}}^{\infty} \Phi_{\mathrm{top}}^{-1} \hat{\mathcal{J}} dr + \Phi_{\mathrm{top}}^{-1} \hat{\psi}^{\mathcal{P}\infty}(r_{\infty}) - \Phi_{\mathrm{top}}^{-1} \hat{\psi}^{\mathcal{P}\mathrm{P}}(r_{+}) \\ \int_{2M}^{r_{-}} \Phi_{\mathrm{bot}}^{-1} \hat{\mathcal{J}} dr + \Phi_{\mathrm{bot}}^{-1} \hat{\psi}^{\mathcal{P}H}(r_H) - \Phi_{\mathrm{bot}}^{-1} \hat{\psi}^{\mathcal{P}\mathrm{P}}(r_{-}) \end{pmatrix}. \tag{8.16}$$

Given homogeneous solutions, we may compute the residual fields using Eq. (8.10). But we still need a strategy for computing the modes of the source. We will address this in the next section.

## 8.3 Computation of the source

In this section we will outline how to calculate the mode coefficients $\delta^2\tilde{R}^0_{i\ell m}[\tilde{h}^1, \tilde{h}^1]$.

### 8.3.1 Summary of the computation strategy

To compute the modes $\delta^2\tilde{R}^0_{i\ell m}[\tilde{h}^1, \tilde{h}^1]$, we apply an analogous strategy to the one used to calculate the toy-model source, as explained in Chapter 5. We write the first-order retarded field as the sum of the puncture plus the residual field, as $\tilde{h}^1 = \tilde{h}^{1\mathcal{R}} + \tilde{h}^{1\mathcal{P}}$. The steps involved in the calculation are as follows:

1. We begin with two ingredients:

   (a) numerically computed tensor-harmonic modes $\tilde{h}^1_{i\ell m}$ of the first-order retarded field in the unrotated coordinates $(t, r, \theta^A)$,

   (b) a 4D expression for the puncture $\tilde{h}^{1\mathcal{P}}_{\mu\nu}$ in the rotated coordinates $(t, r, \alpha^{A'})$.

   For a given numerical accuracy target, the higher the order of the puncture, the fewer modes $\tilde{h}^1_{i\ell m}$ are required; correspondingly, the more modes of $\tilde{h}^1_{i\ell m}$ are computed, the lower the necessary order of the puncture. We use a puncture that is quadratic in order of distance from the particle.

2. Using the coupling formula, given schematically below in Eq. (8.23) and explicitly in [94], we compute the modes $\delta^2\tilde{R}^0_{i\ell m}[\tilde{h}^1, \tilde{h}^1]$. They are computed over the entire numerical domain except in the worldtube region $\Gamma_{\rm P}$ around the particle (as defined in Sec. 8.2), choosing $\Gamma_{\rm P}$ such that it contains all points at which the sums in the coupling formula fail to numerically converge.

3. In the region $\Gamma_{\rm P}$, we compute the tensor-harmonic modes $\tilde{h}^{1\mathcal{P}}_{i\ell m'}$ in the rotated system and then use Wigner D matrices to obtain the modes $\tilde{h}^{1\mathcal{P}}_{i\ell m}$ in the unrotated system, as described in Appendix C. From the result, we compute the modes $\tilde{h}^{1\mathcal{R}}_{i\ell m} = \tilde{h}^1_{i\ell m} - \tilde{h}^{1\mathcal{P}}_{i\ell m}$ of the residual field.

4. Using the coupling formula we compute the modes $\delta^2\tilde{R}^0_{i\ell m}[\tilde{h}^{1\mathcal{P}}, \tilde{h}^{1\mathcal{R}}]$, $\delta^2\tilde{R}^0_{i\ell m}[\tilde{h}^{1\mathcal{R}}, \tilde{h}^{1\mathcal{P}}]$ and $\delta^2\tilde{R}^0_{i\ell m}[\tilde{h}^{1\mathcal{R}}, \tilde{h}^{1\mathcal{R}}]$ in $\Gamma_{\rm P}$.

5. Following the treatment of time derivatives in Appendix E, we express $\delta^2\tilde{R}^0_{\mu\nu}[\tilde{h}^{1\mathcal{P}}, \tilde{h}^{1\mathcal{P}}]$ in the rotated coordinates $(t, r, \alpha^{A'})$. In $\Gamma_{\rm P}$, we compute the modes $\delta^2\tilde{R}^0_{i\ell m}[\tilde{h}^{1\mathcal{P}}, \tilde{h}^{1\mathcal{P}}]$ in the same manner that we computed $\tilde{h}^{1\mathcal{P}}_{i\ell m}$.

6. We sum the results $\delta^2\tilde{R}^0_{i\ell m}[\tilde{h}^{1\mathcal{P}}, \tilde{h}^{1\mathcal{P}}] + \delta^2\tilde{R}^0_{i\ell m}[\tilde{h}^{1\mathcal{P}}, \tilde{h}^{1\mathcal{R}}] + \delta^2\tilde{R}^0_{i\ell m}[\tilde{h}^{1\mathcal{R}}, \tilde{h}^{1\mathcal{P}}] + \delta^2\tilde{R}^0_{i\ell m}[\tilde{h}^{1\mathcal{R}}, \tilde{h}^{1\mathcal{R}}]$ to obtain the complete $\delta^2\tilde{R}^0_{i\ell m}$ in the region $\Gamma_{\rm P}$. Combined with the result from step 2, this provides $\delta^2\tilde{R}^0_{i\ell m}$ everywhere in the numerical domain.

### 8.3.2 The mode-coupling formula

In this section we give a brief description of the mode-coupling formula for the modes of $\delta^2 R_{\mu\nu}[\, h^1, h^1\,]$ and its derivation. Full details can be found in a forthcoming paper [77]. The derivation and the end result are analogous to that of the coupling formula (5.31) for the toy-model source, described in Chapter 5.

Our starting point is the explicit formula for $\delta^2 R_{\mu\nu}[\, h^1, h^1\,]$, given in Eq. (2.18). Because we will use the coupling formula to calculate the pieces $\delta^2 R_{\mu\nu}[\, h^{1\mathcal{R}}, h^{1\mathcal{P}}\,]$ and $\delta^2 R_{\mu\nu}[\, h^{1\mathcal{R}}, h^{1\mathcal{R}}\,]$ of the second-order Ricci tensor, it will be useful to re-state the formula for $\delta^2 R_{\mu\nu}$ in the form

$$
\begin{aligned}
\delta^2 R_{\mu\nu}\,[\, h^{1(A)}, h^{1(B)}\,] = {} & \frac{1}{2}\nabla_\rho \bar{h}^{1(A)\,\rho\tau}\left(2\nabla_{(\mu} h^{1(B)}_{\nu)\tau} - \nabla_\tau h^{1(B)}_{\mu\nu}\right) \\
& + \frac{1}{4}\nabla_\mu h^{1(A)\,\rho\tau}\nabla_\nu h^{1(B)}_{\rho\tau} + \frac{1}{2}\nabla^\tau h_\nu^{1(A)\,\rho}\nabla_\tau h^{1(B)}_{\rho\mu} - \frac{1}{2}\nabla^\tau h_\nu^{1(A)\,\rho}\nabla_\rho h^{1(B)}_{\tau\mu} \\
& - \frac{1}{2} h^{A\,\rho\tau}\left(2\nabla_\rho\nabla_{(\mu} h^{1(B)}_{\nu)\tau} - \nabla_\rho\nabla_\tau h^{1(B)}_{\mu\nu} - \nabla_\mu\nabla_\nu h^{1(B)}_{\rho\tau}\right). \qquad (8.17)
\end{aligned}
$$

After expressing $h^1_{\mu\nu}$ in terms of $\bar{h}^1_{\mu\nu}$, we substitute the expansion (7.5). In terms of the trace-reversed field, the first term that appears in Eq. (8.17) is $\delta^2 R^{[1]}_{\mu\nu}[\, \bar{h}^{1(A)}, \bar{h}^{1(B)}\,] \equiv \nabla_\rho \bar{h}^{1(A)\,\rho\tau}\nabla_{(\mu}\bar{h}^{1(B)}_{\nu)\tau}$. Substituting the multiscale expansion yields

$$
\begin{aligned}
\delta^2 \tilde{R}^{[1]}_{\mu\nu}[\, \tilde{h}^{1(A)}, \tilde{h}^{1(B)}\,] = {} & \sum_{\substack{i_1\ell_1 m_1\\ i_2\ell_2 m_2}} a_{i_1\ell_1} a_{i_2\ell_2} \\
\nabla_\rho\left(\frac{1}{r} Y^{\rho\tau\, i_1\ell_1 m_1}\tilde{h}^{1(A)}_{i_1\ell_1 m_1} e^{-im_1\varphi_p}\right) & \nabla_{(\mu}\left(\frac{1}{r} Y^{i_2\ell_2 m_2}_{\nu)\tau}\tilde{h}^{1(B)}_{i_2\ell_2 m_2} e^{-im_2\varphi_p}\right), \qquad (8.18)
\end{aligned}
$$

where $1 \le i_j \le 10$, $0 \le \ell_j \le \infty$, $-\ell_j \le m_j \le \ell_j$ for the summation limits. Let us write the left-hand side as the mode sum

$$
\delta^2 \tilde{R}^{[1]}_{\mu\nu}\,[\, \tilde{h}^{1(A)}, \tilde{h}^{1(B)}\,] = \sum_{i\ell m} Y^{i\ell m}_{\mu\nu}\,\delta^2 \tilde{R}^{[1]}_{i\ell m}[\, \tilde{h}^{1(A)}, \tilde{h}^{1(B)}\,]\, e^{-im\varphi_p}, \qquad (8.19)
$$

with the modes given by

$$
\begin{aligned}
\delta^2 \tilde{R}^{[1]}_{i\ell m}[\, \tilde{h}^{1(A)}, \tilde{h}^{1(B)}\,] = {} & \frac{\kappa_i}{2\pi}\int_0^{2\pi} d\varphi_p e^{im\varphi_p}\int_0^{2\pi} d\varphi \int_0^{\pi} d\theta \sin\theta \\
& \delta^2 \tilde{R}^{[1]}_{\mu\nu}[\, \tilde{h}^{1(A)}, \tilde{h}^{1(B)}\,]\, Y^{*i\ell m}_{\rho\tau}\,\eta^{\rho\mu}\,\eta^{\nu\tau}, \qquad (8.20)
\end{aligned}
$$

where $\kappa_i$ is defined in Eq. (4.18). By substituting Eq. (8.18) into Eq. (8.20), we find that

$$
\delta^2 \tilde{R}^{[1]}_{i\ell m}[\, \tilde{h}^{1(A)}, \tilde{h}^{1(B)}\,] = \frac{\kappa_i}{2\pi}\int_0^{2\pi} d\varphi_p e^{im\varphi_p}\int_0^{2\pi} d\varphi \int_0^{\pi} d\theta \sin\theta \sum_{\substack{i_1\ell_1 m_1\\ i_2\ell_2 m_2}} a_{i_1\ell_1} a_{i_2\ell_2} Y^{*i\ell m}_{\rho\tau}\,\eta^{\rho\gamma}\,\eta^{\tau\sigma}
$$

$$\nabla_\mu\left(\frac{1}{r}Y^{\mu\nu\, i_1\ell_1 m_1}\,\tilde{h}^{1(A)}_{i_1\ell_1 m_1}e^{-im_1\varphi_p}\right)\times\nabla_{(\gamma}\left(\frac{1}{r}Y^{\ \ i_2\ell_2 m_2}_{\sigma)\nu}\,\tilde{h}^{1(B)}_{i_2\ell_2 m_2}e^{-im_2\varphi_p}\right). \tag{8.21}$$

Applying the same strategy to the remaining terms in Eq. (2.18), we obtain expressions similar to Eq. (8.21). The result can be written, in schematic form, as

$$\delta^2\tilde{R}^0_{i\ell m}[\,\tilde{h}^{1(A)},\tilde{h}^{1(B)}\,]=\sum_{\substack{s\\ i_1\ell_1 m_1 s_1\\ i_2\ell_2 m_2 s_2}}\mathscr{R}^{i\ell m}_{\substack{i_1\ell_1 m_1\\ i_2\ell_2 m_2}}\left(\tilde{h}^{1(A)}_{i_1\ell_1 m_1},\tilde{h}^{1(B)}_{i_2\ell_2 m_2}\right)$$
$$\int_0^{2\pi}d\varphi\int_0^{\pi}d\theta\sin\theta\ {}_sY^*_{\ell m}\ {}_{s_1}Y_{\ell_1 m_1}\ {}_{s_2}Y_{\ell_2 m_2}, \tag{8.22}$$

where ${}_sY^*_{\ell m}$ are spin-weighted spherical harmonics. The summation limits for the $i,\ell,m$ are the same as in Eq. (8.18), $s$ ranges from $-2$ to 2 and $s_1$, $s_2$ range between $-4$ and 4. We may substitute the formula (5.28) for the integral in (8.22), with $C^{\ell ms}_{\ell_1 m_1 s_1\ell_2 m_2 s_2}$ given by Eq. (5.29). Then we may write Eq. (8.22) as

$$\delta^2\tilde{R}^0_{i\ell m}[\,\tilde{h}^{1(A)},\tilde{h}^{1(B)}\,]=\sum_{\substack{i_1\ell_1 m_1 s_1\\ i_2\ell_2 m_2 s_2}}\mathscr{R}^{i\ell m}_{\substack{i_1\ell_1 m_1\\ i_2\ell_2 m_2}}\left(\tilde{h}^{1(A)}_{i_1\ell_1 m_1},\tilde{h}^{1(B)}_{i_2\ell_2 m_2}\right)C^{\ell ms}_{\ell_1 m_1 s_1\ell_2 m_2 s_2}. \tag{8.23}$$

Eq. (8.23) gives the form of the mode-coupling formula for the modes of $\delta^2\tilde{R}^0_{\mu\nu}[\,\tilde{h}^{1(A)},\tilde{h}^{1(B)}\,]$, in terms of modes of $\tilde{h}^{1(A)}$ and $\tilde{h}^{1(B)}$. We will use this method to compute the modes $\delta^2\tilde{R}^0_{i\ell m}[\,\tilde{h}^{1\mathcal{R}},\tilde{h}^{1\mathcal{P}}\,]$, $\delta^2\tilde{R}^0_{i\ell m}[\,\tilde{h}^{1\mathcal{P}},\tilde{h}^{1\mathcal{R}}\,]$ and $\delta^2\tilde{R}^0_{i\ell m}[\,\tilde{h}^{1\mathcal{R}},\tilde{h}^{1\mathcal{R}}\,]$. But this method will not work for the modes of $\delta^2\tilde{R}^0_{i\ell m}[\,\tilde{h}^{1\mathcal{P}},\tilde{h}^{1\mathcal{P}}\,]$, for reasons explained in Chapter 5. Rather we compute this piece as explained in the coming subsection.

### 8.3.3 Calculation of the divergent piece of the source

The modes $\delta^2\tilde{R}^0_{i\ell m}[\tilde{h}^{1\mathcal{P}},\tilde{h}^{1\mathcal{P}}]$ are computed by directly integrating $\delta^2\tilde{R}^0_{\mu\nu}[\,\tilde{h}^{1\mathcal{P}},\tilde{h}^{1\mathcal{P}}\,]$, against the tensor harmonics over the two-sphere, as

$$\delta^2\tilde{R}^0_{i\ell m'}[\,\tilde{h}^{1\mathcal{P}},\tilde{h}^{1\mathcal{P}}]=\int_0^{2\pi}d\alpha\int_0^{\pi}d\beta\sin\beta\ \delta^2\tilde{R}^0_{\mu\nu}[\,\tilde{h}^{1\mathcal{P}},\tilde{h}^{1\mathcal{P}}]\,Y^{*(i\ell m)}_{\rho\tau}\eta^{\mu\rho}\eta^{\nu\tau}. \tag{8.24}$$

Here, $\delta^2\tilde{R}^0_{\mu\nu}[\,\tilde{h}^{1\mathcal{P}},\tilde{h}^{1\mathcal{P}}]$ is calculated by inserting the expressions for $\tilde{h}^{1\mathcal{P}}_{\mu\nu}$, whose leading order pieces are given in Eqs. (C.13), into Eq. (8.17). The $\alpha$-integral may be evaluated analytically and the $\beta$-integral numerically, using an analogous approach to the one described in Chapter 5. This part of the computation has been performed in collaboration with Barry Wardell. We calculate $\delta^2\tilde{R}^0_{i\ell m}[\,\tilde{h}^{1\mathcal{P}},\tilde{h}^{1\mathcal{P}}]$ in unrotated coordinates from $\delta^2\tilde{R}^0_{i\ell m'}[\,\tilde{h}^{1\mathcal{P}},\tilde{h}^{1\mathcal{P}}]$ in rotated coordinates as $\delta^2\tilde{R}^0_{i\ell m}[\,\tilde{h}^{1\mathcal{P}},\tilde{h}^{1\mathcal{P}}]=\sum_{m'}D_{\ell mm'}\left(\pi,\frac{\pi}{2},\frac{\pi}{2}\right)\delta^2\tilde{R}^0_{i\ell m'}[\,\tilde{h}^{1\mathcal{P}},\tilde{h}^{1\mathcal{P}}]$, where the $D_{\ell mm'}$ are Wigner-D matrices.

| $i$ | $k$ | $B^i_k$ |
|---|---|---|
| 1 | 0 | $-1.5385411580401104172152043636 5 \times 10^{-5}$ |
| | 1 | $-R^1_1$ |
| | 2 | 3.16104669037757890492912338232 |
| | 3 | $-10.4725537977717966242607872118$ |
| | 4 | 18.4561479788650437683372729225 |
| 2 | 0 | $R^1_0$ |
| | 1 | $R^1_1$ |
| | 2 | $-1.15390586853008281291140327274 \times 10^{-5}$ |
| | 3 | $7.69270579020055378014191632685 \times 10^{-6}$ |
| | 4 | $-4.80794111887534547731398726356 \times 10^{-6}$ |
| 3 | 0 | 15.8951030477012764663413690869 |
| | 1 | $-101.194324286140172830528172199$ |
| | 2 | 281.453610014203604805516079068 |
| | 3 | $-529.893514220868496522598434240$ |
| | 4 | 789.411581933436082181287929416 |
| 6 | 0 | $-3.76837738717146741862507042242$ |
| | 1 | 0.517507257215248483994685102516 |
| | 2 | 28.2745219170346828718720644247 |
| | 3 | $-89.2706023395906100859065190889$ |
| | 4 | 172.065492328370112318225437775 |

Table 8.1: Table of values for coefficients in the the near-horizon expansion of $\delta^2\tilde{R}^0_{i00}$ given in Eq. (8.25). The coefficients were computed from data for the modes of the first-order field, $h^1_{i\ell m}$ sourced by a quasicircular orbit of radius $r_0 = 6M$.

## 8.4 Numerical results for the second-order source

In this section we present our results from a numerical computation of the modes $\delta^2\tilde{R}^0_{i00}[h^1, h^1]$, using the strategy described in the previous section. Although we do not solve the $i = 2$ equations, we include the computation of the source as it has a distinct analytical behaviour, given by Eq. (G.3); comparing to that prediction provides a strong check of our numerics. For all numerical calculations in this chapter, we use data for the modes of the first-order field, with $\tilde{r}_0 = 6M$, on a grid of $r$-values from $r_{\rm in} = (2 + 10^{-7})M$ up to $r_{\rm out} = 10^4 M$.

In the region $r \lessapprox \left(2 + 10^{-5}\right) M$, numerical errors in our first-order fields lead to numerical errors in $\delta^2\tilde{R}^0_{i00}[h^1, h^1]$ that accumulate as we approach the horizon. The net result is that the modes, $\delta^2\tilde{R}^0_{i00}[h^1, h^1]$ blow up in the region $r \lessapprox \left(2 + 10^{-5}\right) M$ as we approach the horizon. We found two methods to overcome this, that both work and give the same result. The first strategy is to replace the numerical computation with a near-horizon expansion for $\delta^2\tilde{R}^0_{i00}[h^1, h^1]$, provided by Adam Pound. This is obtained by substituting for the modes of the first-order field in the coupling formula, the asymptotic solutions given in Eqs. (4.56) and (4.58). This leads to the near-horizon expansion for the second-order Ricci tensor:

$$\delta^2 \tilde{R}^0_{i00}[\, h^1, h^1 \,] = \sum_{k=0}^{k_{\max}} B^i_k \, (r - 2M)^k \,, \tag{8.25}$$

where the $B^i_k$ are $r$-independent coefficients. They depend on the coefficients $b^i_k$ from Eqs. (4.56) and (4.58), which we have already computed to obtain boundary conditions for the first-order solutions, as we explained in Chapter 4. We found that for $k_{\max} \geq 4$ our results did not change beyond the 16th significant figure, so, we set $k_{\max} = 4$. Our results for the values of the coefficients in (8.25) are given above in Table 8.1.

The second method is to generate data for the first-order modes themselves, to an accuracy beyond machine precision. To do so, instead of using the GSL ODE solver as reported in Sec. 4.6.1, we employ the Boost ODE solver [110] that allows us to go to arbitrary precision. Because the latter method is computationally very expensive, we wanted to apply it to as few modes as possible. We found that it sufficed to use the Boost ODE solver for $\ell \leq 6$ and then revert back to the GSL ODE solver for the $\ell > 6$ modes. But owing to the computational burden of this method, we used the near-horizon expansion of the second-order Ricci tensor to resolve the issue.

Fig. 8.2 shows that $\delta^2 \tilde{R}^0_{100}[\, h^1, h^1 \,]$ behaves like $1/r^2$ with increasing $r$, in agreement with the prediction of Eq. (G.4). $\delta^2 \tilde{R}^0_{100}[\, h^1, h^1 \,]$ is dominated by behaviour proportional to $f^2$ as $r$ decreases, but approaches a constant value near the horizon. Fig. 8.2 also shows that $\delta^2 \tilde{R}^0_{200}[\, h^1, h^1 \,]$ is proportional to $1/r^2$ for the entire range of $r$ values, which agrees with the analytical prediction in Eq. (G.3). Fig. 8.2 shows that both the $\delta^2 \tilde{R}^0_{300}[\, h^1, h^1 \,]$ and $\delta^2 \tilde{R}^0_{600}[\, h^1, h^1 \,]$ behave like $1/r^4$ at large $r$. This is consistent with but much stronger than the prediction (G.5). In the data for $\delta^2 \tilde{R}_{i00}$ displayed in Fig. 8.2 and used in all of the computations described in this chapter, we used the near-horizon expansion in the region $r \leq 2.1M$ and the coupling formula everywhere else. We found agreement of at least 16 significant figures, i.e. up to all digits available at machine precision between the data from the coupling formula and data from the near-horizon expansion, as can be seen from the smooth transition in the plots in Fig. 8.2 at $r = 2.1M$. We observe that $\delta^2 \tilde{R}^0_{100}$ passes through zero at a certain value $r = r_c$ between $2.001M$ and $2.01M$, in the region where the near-horizon expansion is applied. We calculated $r_c$ by finding the real roots of the polynomial in (8.25). The relevant root is the one that is real and greater than $2M$, yielding $r_c = 2.00221M$.

We observe from Fig. 8.2 that $\delta^2 \tilde{R}^0_{100}$ and $\delta^2 \tilde{R}^0_{200}$ tend to the same constant approaching the horizon, which is consistent with the condition for regularity given in Eq. (7.47). We also note that they tend to the same magnitude at $r \to \infty$. This is to be expected, because, at large $r$, $\delta^2 \tilde{R}^0_{200}$ and $-\delta^2 \tilde{R}^0_{100}$ are both equal to the energy flux at null infinity (up to a numerical factor over $r^2$). Since $\delta^2 \tilde{R}^0_{300}$ is proportional to the

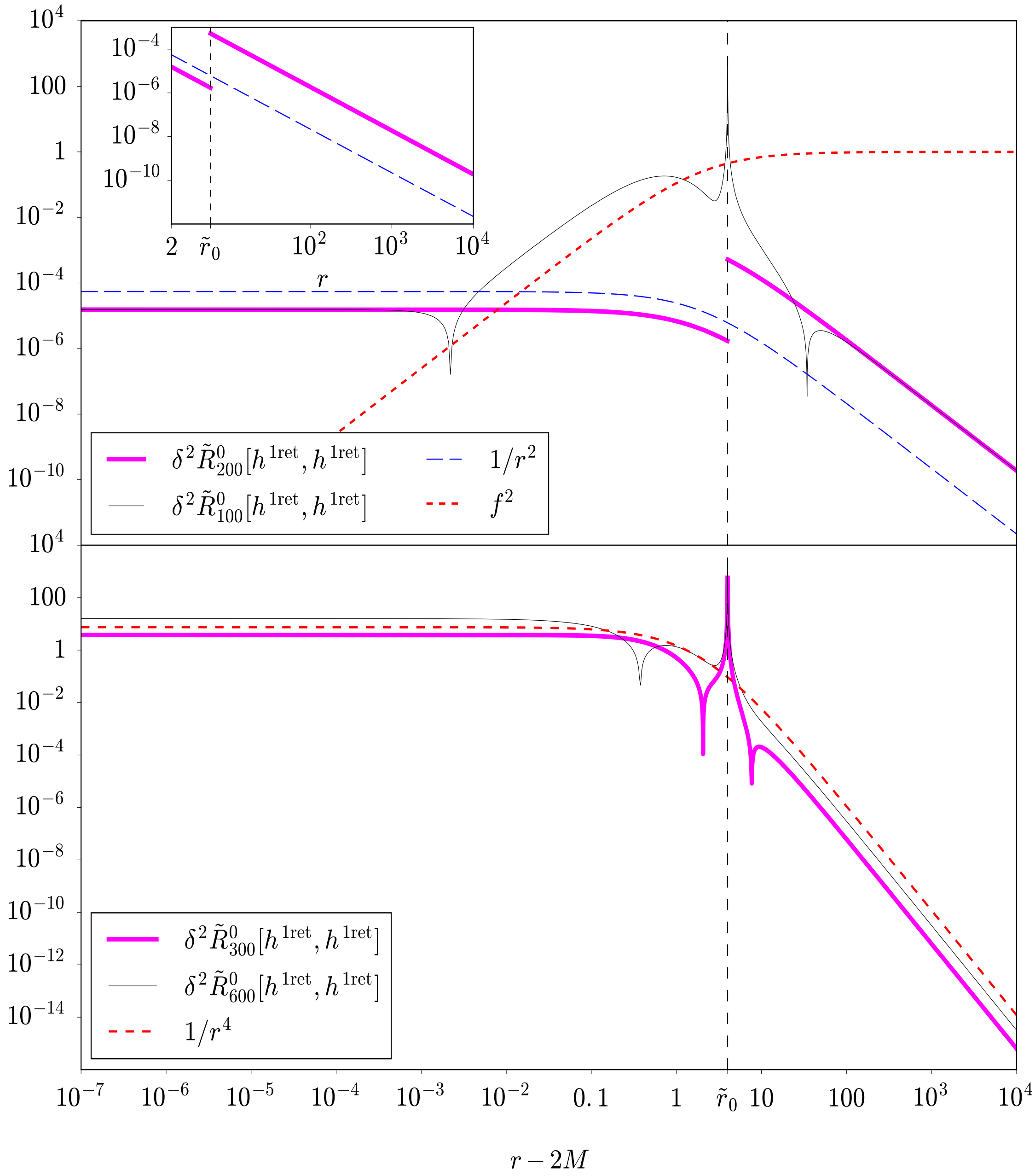


Figure 8.2: Monopole modes of the second-order Ricci tensor, where all plots are shown on a log-log scale. The $i = 1$ mode tends to a constant near the horizon and behaves as $1/r^2$ at large $r$. Elsewhere it behaves as $f^2$. The $i = 2$ mode behaves as $1/r^2$ across the entire domain; this is shown most starkly in the inset inside the upper plot. Both the $i = 3$ and $i = 6$ modes behave like $1/r^4$ at large $r$. All features of the plot are consistent with analytical predictions in Eqs. (G.3)–(G.5).

trace of $\delta^2\tilde{R}^0_{\alpha\beta}$, then $\delta^2\tilde{R}^0_{300} \sim 1/r^4$ tells us that the trace of the curvature due to the small object decays more rapidly than the trace-free part.

Using the definition of the flux of gravitational energy (see Eq. (B.2) in [111]),

$$\dot{E} = -\epsilon r^2 f \oint d\Omega \left(\frac{-1}{8\pi}\right) \delta^2 R_{tr}, \tag{8.26}$$

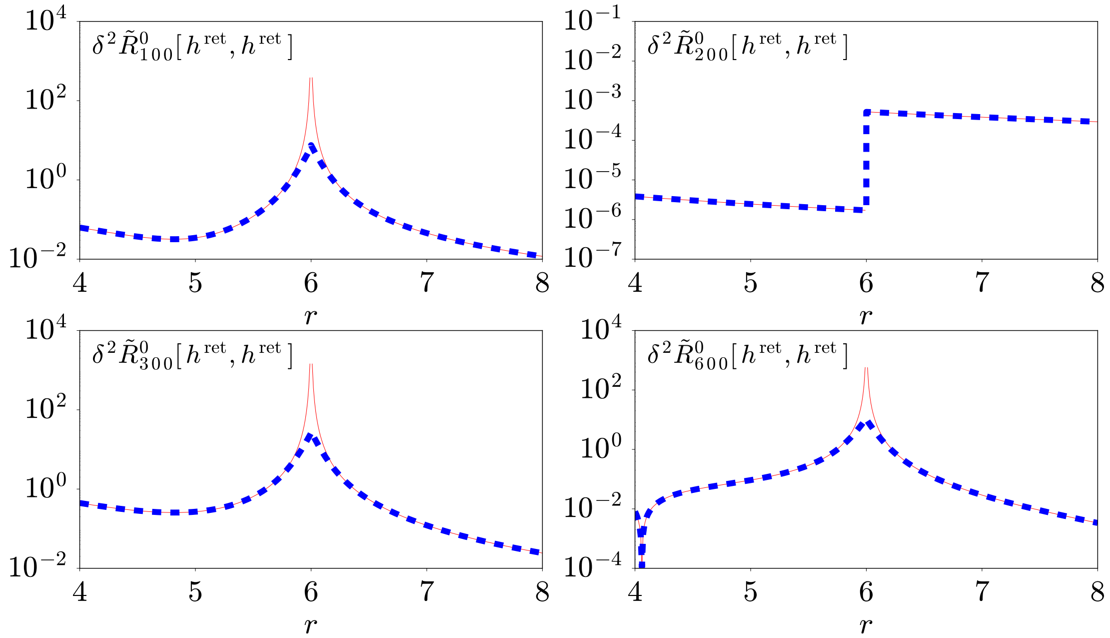


Figure 8.3: $\delta^2\tilde{R}^0_{i00}[h^{\rm ret}, h^{\rm ret}]$ calculated in two different ways: (1) 2D integral for SS part and the coupling formula for SR and RR parts (solid line), and (2) the result of a direct application of the coupling formula (dashed line).

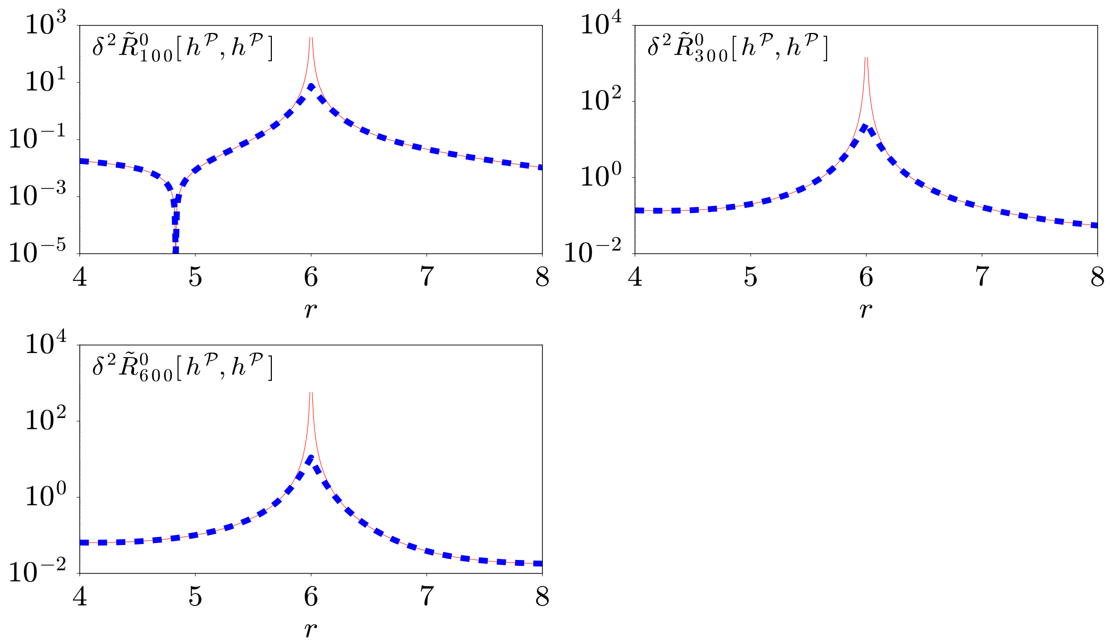


Figure 8.4: $\delta^2\tilde{R}_{i00}[h^{\mathcal{P}}, h^{\mathcal{P}}]$ calculated via the 2D-integral versus the coupling formula. The dashed line is data from the coupling formula, and the solid line is data from the 2D-integral.

where for the flux at $\infty$, $\epsilon = 1$ and the flux through the horizon, $\epsilon = -1$, we may derive the following relation between the $i = 2$ monopole mode and $\dot{E}$. From the result (G.3), we may replace $\delta^2 R_{tr} = s_{200}Y^{00}/(\sqrt{2}fr^2)$ (plus higher modes, which integrate to zero). $s_{200}$ is a constant that takes different values for $r < \tilde{r}_0$ and $r > \tilde{r}_0$. Then, straightforwardly evaluating the spherical integral, we determine these two values for

$s_{200}$ either side of the particle, such that

$$\delta^2 \tilde{R}^0_{200} = \begin{cases} -2\sqrt{8\pi}\dfrac{\dot{E}_H}{r^2} & r < \tilde{r}_0, \\ +2\sqrt{8\pi}\dfrac{\dot{E}_\infty}{r^2} & r > \tilde{r}_0. \end{cases} \tag{8.27}$$

We have numerically checked that our numerical result for $\delta^2 \tilde{R}^0_{200}$ agrees with the formulas (8.27).

In Figs. 8.3 we have plotted the monopole modes $\delta^2 \tilde{R}^0_{i00}[h^{1\mathrm{ret}}, h^{1\mathrm{ret}}] = \delta^2 \tilde{R}^0_{i00}[\,h^{1\mathcal{P}}, h^{1\mathcal{P}}\,] + \delta^2 \tilde{R}^0_{i00}[\,h^{1\mathcal{R}}, h^{1\mathcal{P}}\,] + \delta^2 \tilde{R}^0_{i00}[\,h^{1\mathcal{P}}, h^{1\mathcal{R}}\,] + \delta^2 \tilde{R}^0_{i00}[\,h^{1\mathcal{R}}, h^{1\mathcal{R}}\,]$, using two different methods of computation: calculating the most divergent piece at the particle, $\delta^2 \tilde{R}^0_{i00}[\,h^{1\mathcal{P}}, h^{1\mathcal{P}}\,]$ using the mode-coupling formula, and by direct integration against the tensor harmonics over the 2D sphere as in (8.24), while the remaining three pieces are computed using the coupling formula. While the two methods agree sufficiently far away from the particle, closer and closer to the particle the lack of convergence of the coupling formula becomes worse and worse, except for $i = 2$. The lack of convergence of the sum in the coupling formula is isolated to the $\delta^2 \tilde{R}^0_{i00}[\,h^{1\mathcal{P}}, h^{1\mathcal{P}}\,]$ piece. For $i = 2$, $\delta^2 \tilde{R}^0_{200}[\,h^{1\mathcal{P}}, h^{1\mathcal{P}}\,] = 0$, and therefore there is no issue of non-convergence for this mode and the two methods agree.

In Figs. 8.4 we have plotted data of the contribution from $\delta^2 \tilde{R}^0_{i00}[h^{1\mathcal{P}}, h^{1\mathcal{P}}]$, computed using the two different approaches. In these plots we clearly see that the coupling formula does not converge close to the particle, as opposed to the 2D integral (8.24) which does, while both methods agree sufficiently far away from the particle.

## 8.5 Punctures at the particle

The second-order puncture fields at the particle are derived in an analogous way to the method used to derive the first-order punctures. We start with the covariant expressions for pieces of the second-order singular field, namely $\tilde{h}^{\mathrm{SS}}_{\mu\nu}$, $\tilde{h}^{\mathrm{SR}}_{\mu\nu}$, $\tilde{h}^{\delta m}_{\mu\nu}$ and $\tilde{h}^{\delta z}_{\mu\nu}$, derived in Sec. 3.2.7. We write them as coordinate expansions in Schwarzschild coordinates, for a quasicircular orbit around a Schwarzschild black hole, using the prescription given in Appendix C. We do this in rotated Schwarzschild coordinates $(t, r, \tilde{\alpha}, \tilde{\beta})$. We obtain the tensor-harmonic modes by integrating the full punctures over $\tilde{\alpha}$ and $\tilde{\beta}$, against the tensor spherical-harmonics, as described in detail in Appendix C.

We use expressions that are $O(\lambda^0)$ for $\tilde{h}^{\mathrm{SR}}_{\mu\nu}$, $\tilde{h}^{\delta m}_{\mu\nu}$ and $\tilde{h}^{\delta z}_{\mu\nu}$, in order to obtain an effective source that is continuous at the particle (we remind the reader that we use $\lambda(\equiv 1)$ to count powers of distance from the particle). To understand this, first observe that since the left-hand side of Eq. (8.2) is obtained by taking two derivatives and two integrals of the residual field, it has the same degree of smoothness as the 4D residual field. Since the effective source modes must also be equal to the left-hand side of Eq. (8.2), they also have that same degree of smoothness. For $\tilde{h}^{\rm SS}_{\mu\nu}$ we use all the available orders through $O(\lambda\ln\lambda)$, because they have a relatively simple form. We then expand these expressions for all pieces of the puncture in powers of $\Delta r$, through $O(\Delta r^2)$.

We give results here for the monopole ($\ell=0, m=0$) modes of the punctures. They have the form

$$\tilde{h}^{\mathcal{P}\rm P}_{i00} = h^{\rm SS}_{i00} + h^{\rm SR}_{i00} + h^{\delta m}_{i00} + h^{\delta z}_{i00}. \tag{8.28}$$

We have derived explicit formulas for $\tilde{h}^{\rm SR}_{\mu\nu}$, $\tilde{h}^{\delta m}_{\mu\nu}$, $h^{\delta z}_{i00}$ through order $O(\lambda^0)$, as expansions in powers of $\Delta r$ up to quadratic order. Similarly, we have derived an explicit formula for $\tilde{h}^{\rm SS}_{\mu\nu}$ through $O(\lambda\ln\lambda)$ as an expansion in powers of $\Delta r$ up to quadratic order. These expressions are too long to include in this thesis, so we only state the result through $O(\log(\Delta r))$:

$$\tilde{h}^{\rm SS}_{100} = \sqrt{\frac{3M-\tilde{r}_0}{2M-\tilde{r}_0}}\left(\frac{19M-6\tilde{r}_0}{4\sqrt{\pi}}\right)\log(|\Delta r|) + O(\Delta r), \tag{8.29a}$$

$$\tilde{h}^{\rm SS}_{200} = 0, \tag{8.29b}$$

$$\tilde{h}^{\rm SS}_{300} = \sqrt{\frac{3M-\tilde{r}_0}{2M-\tilde{r}_0}}\left(\frac{41M-14\tilde{r}_0}{4\sqrt{\pi}(3M-\tilde{r}_0)\tilde{r}_0}\right)\log(|\Delta r|) + O(\Delta r), \tag{8.29c}$$

$$\tilde{h}^{\rm SS}_{600} = \sqrt{\frac{3M-\tilde{r}_0}{2M-\tilde{r}_0}}\left(\frac{19M-6\tilde{r}_0}{4\sqrt{\pi}(3M-\tilde{r}_0)\tilde{r}_0}\right)\log(|\Delta r|) + O(\Delta r), \tag{8.29d}$$

$$\begin{aligned}
\tilde{h}^{\rm SR}_{100} =& \frac{E(\mathcal{K})}{3\pi^{3/2}\tilde{r}_0^3(3M-\tilde{r}_0)} \\
&\Big(3M\tilde{r}_0^3 h^{\rm 1R}_{tt} - 2\tilde{r}_0^4 h^{\rm 1R}_{tt} + 12M\tilde{\Omega}_0\tilde{r}_0^3 h^{\rm 1R}_{r\theta} - 6\tilde{\Omega}_0\tilde{r}_0^4 h^{\rm 1R}_{r\theta} + 12M^3\tilde{r}_0 h^{\rm 1R}_{rr} \\
&-20M^2\tilde{r}_0^2 h^{\rm 1R}_{rr} + 11M\tilde{r}_0^3 h^{\rm 1R}_{rr} - 2\tilde{r}_0^4 h^{\rm 1R}_{rr} + 6M^2 h^{\rm 1R}_{\theta\theta} - 3M\tilde{r}_0 h^{\rm 1R}_{\theta\theta} \\
&-6M^2 h^{\rm 1R}_{\varphi\varphi} + 3M\tilde{r}_0 h^{\rm 1R}_{\varphi\varphi}\Big) + O(\Delta r, |\Delta r|),
\end{aligned} \tag{8.30a}$$

$$\begin{aligned}
\tilde{h}^{\rm SR}_{200} =& \frac{2h^{\rm 1R}_{tr}\left(6M^2-7M\tilde{r}_0+2\tilde{r}_0^2\right)E(\mathcal{K})}{3\pi^{3/2}\tilde{r}_0(\tilde{r}_0-3M)} + \frac{2h^{\rm 1R}_{r\theta}\tilde{\Omega}_0(\tilde{r}_0-2M)^2E(\mathcal{K})}{\pi^{3/2}\tilde{r}_0(\tilde{r}_0-3M)} \\
&+ 2E(\mathcal{K})\frac{1}{3\pi^{3/2}\tilde{r}_0(3M-\tilde{r}_0)} + O(\Delta r, |\Delta r|),
\end{aligned} \tag{8.30b}$$

$$\begin{aligned}
\tilde{h}^{\rm SR}_{300} =& -\frac{2\tilde{r}_0 h^{\rm 1R}_{t\theta}\tilde{\Omega}_0E(\mathcal{K})}{\pi^{3/2}(\tilde{r}_0-3M)} + \frac{h^{\rm 1R}_{\theta\theta}(3M-2\tilde{r}_0)E(\mathcal{K})}{3\pi^{3/2}\tilde{r}_0^2(\tilde{r}_0-3M)} \\
&+ \frac{h^{\rm 1R}_{\varphi\varphi}(3M-2\tilde{r}_0)E(\mathcal{K})}{3\pi^{3/2}\tilde{r}_0^2(\tilde{r}_0-3M)} - \frac{\tilde{r}_0 h^{\rm 1R}_{tt}(3M-2\tilde{r}_0)E(\mathcal{K})}{3\pi^{3/2}(2M-\tilde{r}_0)(\tilde{r}_0-3M)} \\
&+ \frac{h^{\rm 1R}_{rr}(\tilde{r}_0-2M)(2\tilde{r}_0-3M)E(\mathcal{K})}{3\pi^{3/2}\tilde{r}_0(\tilde{r}_0-3M)} + O(\Delta r, |\Delta r|)),
\end{aligned} \tag{8.30c}$$

$$\tilde{h}^{\rm SR}_{600} = \frac{\tilde{r}_0 h^{R(1)}_{tt}(3M-2\tilde{r}_0)E(\mathcal{K})}{3\pi^{3/2}\left(6M^2-5M\tilde{r}_0+\tilde{r}_0^2\right)} + \frac{2\tilde{r}_0 h^{R(1)}_{t\theta}\tilde{\Omega}_0E(\mathcal{K})}{\pi^{3/2}(3M-\tilde{r}_0)}$$

$$
\begin{aligned}
&- \frac{h^{R(1)}_{\theta\theta}(3M-2\tilde{r}_0)E\left(\mathcal{K}\right)}{3\pi^{3/2}\tilde{r}_0^2(3M-\tilde{r}_0)} - \frac{h^{R(1)}_{\varphi\varphi}(3M-2\tilde{r}_0)E\left(\mathcal{K}\right)}{3\pi^{3/2}\tilde{r}_0^2(3M-\tilde{r}_0)} \\
&- \frac{h^{R(1)}_{rr}(3M-2\tilde{r}_0)(2M-\tilde{r}_0)E\left(\mathcal{K}\right)}{3\pi^{3/2}\tilde{r}_0(3M-\tilde{r}_0)} + O(\Delta r, |\Delta r|)),
\end{aligned} \tag{8.30d}
$$

where $E$ is the elliptic function of the first kind and $\mathcal{K} \equiv \tilde{r}_0/\left(\tilde{r}_0 - 2M\right)$ and $\tilde{\Omega}_0 \equiv \sqrt{M/\tilde{r}_0^3}$. We also obtain

$$
\tilde{h}^{\delta z}_{100} = - \frac{2\left(\delta r\left(-4M^2 - 3M\tilde{r}_0 + 2\tilde{r}_0^2\right)E\left(\mathcal{K}\right)\right)}{\pi^{3/2}\tilde{r}_0^2(\tilde{r}_0-3M)} + O(\Delta r, |\Delta r|), \tag{8.31a}
$$

$$
\tilde{h}^{\delta z}_{200} = 0, \tag{8.31b}
$$

$$
\tilde{h}^{\delta z}_{300} = - \frac{2\left(\delta r\left(-4M^2 - 3M\tilde{r}_0 + 2\tilde{r}_0^2\right)E\left(\mathcal{K}\right)\right)}{\pi^{3/2}\tilde{r}_0^2(\tilde{r}_0-3M)} + O(\Delta r, |\Delta r|), \tag{8.31c}
$$

$$
\begin{aligned}
\tilde{h}^{\delta z}_{600} =& \frac{2\delta r E\left(\mathcal{K}\right)}{\pi^{3/2}\tilde{r}_0(2M-\tilde{r}_0)(3M-\tilde{r}_0)}\left(4M^2 - 2\tilde{r}_0^2 + 3M\tilde{r}_0\right) \\
&+ \frac{\Delta r\delta r}{\pi^{3/2}\tilde{r}_0^2(2M-\tilde{r}_0)^2(3M-\tilde{r}_0)}E\left(\mathcal{K}\right)\left(16M^3 + 4M^2\tilde{r}_0 + 2\tilde{r}_0^3 - 9M\tilde{r}_0^2\right) \\
&+ O(\Delta r, |\Delta r|).
\end{aligned} \tag{8.31d}
$$

where

$$
\delta r \equiv \left(\frac{\tilde{r}_0^3(\tilde{r}_0-3M)}{3M(\tilde{r}_0-2M)}\right)F^{1r}, \tag{8.32}
$$

with $F^{1r}$ being the $r$-component of the self-force at first order. $\tilde{h}^{\delta z}_{i00}$ in Eqs.(8.31) relates to the two-timescale expansion by the fact that $\delta r$ is the first-order correction, $\tilde{r}_1$, to the orbital radius, as we have already seen in Eq. (7.17). We have ignored terms that include $\dot{\tilde{r}}_0$, which would otherwise appear in the two-timescale expansion of the $i = 2$ punctures. Finally

$$
\begin{aligned}
\tilde{h}^{\delta m}_{100} =& \frac{4E\left(\mathcal{K}\right)}{3\pi^{3/2}\tilde{r}_0^3(3M-\tilde{r}_0)^2}\left\{36M^4\tilde{r}_0h^{1\mathrm{R}}_{rr} - 60M^3\tilde{r}_0^2h^{1\mathrm{R}}_{rr} + 12M^3h^{1\mathrm{R}}_{\varphi\varphi}\right. \\
&-15M^2\tilde{r}_0^3h^{1\mathrm{R}}_{tt} - 12M^2\tilde{r}_0^3h^{1\mathrm{R}}_{t\varphi}\tilde{\Omega}_0 + 37M^2\tilde{r}_0^3h^{1\mathrm{R}}_{rr} - 12M^2\tilde{r}_0h^{1\mathrm{R}}_{\varphi\varphi} \\
&+12M\tilde{r}_0^4h^{1\mathrm{R}}_{tt} - 10M\tilde{r}_0^4h^{1\mathrm{R}}_{rr} + 3M\tilde{r}_0^2h^{1\mathrm{R}}_{\varphi\varphi} + 6M\tilde{r}_0^4h^{1\mathrm{R}}_{t\varphi}\tilde{\Omega}_0 - 2\tilde{r}_0^5h^{1\mathrm{R}}_{tt} \\
&\left.+\tilde{r}_0^5h^{1\mathrm{R}}_{rr} + 72\delta r M^3\tilde{r}_0 - 60\delta r M^2\tilde{r}_0^2 + 12\delta r M\tilde{r}_0^3\right\} + O(\Delta r, |\Delta r|),
\end{aligned} \tag{8.33a}
$$

$$
\begin{aligned}
\tilde{h}^{\delta m}_{200} =& \frac{8(2M-\tilde{r}_0)E\left(\mathcal{K}\right)}{3\pi^{3/2}\tilde{r}_0(3M-\tilde{r}_0)}\left(3Mh^{1\mathrm{R}}_{tr} - 2r0h^{1\mathrm{R}}_{tr} + 6M\tilde{\Omega}_0h^{1\mathrm{R}}_{r\varphi} - 3\tilde{\Omega}_0r0h^{1\mathrm{R}}_{r\varphi}\right) \\
&+ O(\Delta r, |\Delta r|),
\end{aligned} \tag{8.33b}
$$

$$
\begin{aligned}
\tilde{h}^{\delta m}_{300} =& \frac{4E\left(\mathcal{K}\right)}{3\pi^{3/2}\tilde{r}_0^3(3M-\tilde{r}_0)^2}\left(36M^4\tilde{r}_0h^{1\mathrm{R}}_{rr} - 60M^3\tilde{r}_0^2h^{1\mathrm{R}}_{rr} + 12M^3h^{1\mathrm{R}}_{\varphi\varphi} - 15M^2\tilde{r}_0^3h^{1\mathrm{R}}_{tt}\right. \\
&-12M^2\tilde{r}_0^3h^{1\mathrm{R}}_{t\varphi}\tilde{\Omega}_0 + 37M^2\tilde{r}_0^3h^{1\mathrm{R}}_{rr} - 12M^2\tilde{r}_0h^{1\mathrm{R}}_{\varphi\varphi} + 12M\tilde{r}_0^4h^{1\mathrm{R}}_{tt} - 10M\tilde{r}_0^4h^{1\mathrm{R}}_{rr} \\
&+3M\tilde{r}_0^2h^{1\mathrm{R}}_{\varphi\varphi} + 6M\tilde{r}_0^4h^{1\mathrm{R}}_{t\varphi}\tilde{\Omega}_0 - 2\tilde{r}_0^5h^{1\mathrm{R}}_{tt} + \tilde{r}_0^5h^{1\mathrm{R}}_{rr} \\
&\left.+72\delta r M^3\tilde{r}_0 - 60\delta r M^2\tilde{r}_0^2 + 12\delta r M\tilde{r}_0^3\right) + O(\Delta r, |\Delta r|),
\end{aligned} \tag{8.33c}
$$

$$\begin{aligned}\tilde{h}^{\delta m}_{600} =& \frac{4\tilde{r}_0 h^{1\mathrm{R}}_{tt}\left(3M^2-6M\tilde{r}_0+2\tilde{r}_0^2\right)E\left(\mathcal{K}\right)}{3\pi^{3/2}(\tilde{r}_0-3M)^2(\tilde{r}_0-2M)}\\ &-\frac{4\left(6M^2h^{1\mathrm{R}}_{\varphi\varphi}E\left(\mathcal{K}\right)-2\tilde{r}_0^2h^{1\mathrm{R}}_{\varphi\varphi}E\left(\mathcal{K}\right)+3M\tilde{r}_0h^{1\mathrm{R}}_{\varphi\varphi}E\left(\mathcal{K}\right)\right)}{3\pi^{3/2}\tilde{r}_0^2(3M-\tilde{r}_0)^2}\\ &-\frac{8\tilde{r}_0h^{1\mathrm{R}}_{t\varphi}(5M-2\tilde{r}_0)\tilde{\Omega}_0E\left(\mathcal{K}\right)}{\pi^{3/2}(3M-\tilde{r}_0)^2}+\frac{8h^{1\mathrm{R}}_{\theta\theta}E\left(\mathcal{K}\right)}{3\pi^{3/2}\tilde{r}_0^2}\\ &-\frac{4h^{1\mathrm{R}}_{rr}(2M-\tilde{r}_0)E\left(\mathcal{K}\right)}{3\pi^{3/2}\tilde{r}_0}-\frac{16\delta r M E\left(\mathcal{K}\right)}{\pi^{3/2}\tilde{r}_0(3M-\tilde{r}_0)}+O(\Delta r,|\Delta r|).\end{aligned} \tag{8.33d}$$

Barry Wardell provided these formulas for all of the $\ell=0$ modes of the punctures at the particle. Independently, I derived expressions for $h^{\mathrm{SR}}_{i\ell m}$ for generic $i\ell m$ through $O(\lambda)$, and successfully checked my formulas for the $\ell=0$ modes with the formulas of Wardell. Hence, in my computation I use my formulas $\tilde{h}^{\mathrm{SR}}_{i00}$ through $O(\lambda)$. $\tilde{h}^{\mathrm{SR}}_{i00}$ requires data for the 4D components of the first-order regular-field, and its first derivatives and second derivatives, for which I used data that I myself computed using the methodology detailed in Chapter 4. For the remaining pieces, $\tilde{h}^{\mathrm{SS}}_{i00}$, $\tilde{h}^{\delta z}_{i00}$ and $\tilde{h}^{\delta m}_{i00}$, I use the formulas of Wardell.

## 8.6 The effective source

Now that we have derived formulas for the puncture fields, we may calculate the effective source, $S^{\mathrm{eff}}_{i00}$ defined in Eq. (8.3). We will refer to the piece $\sqrt{2}rf^{-1}\delta^2\tilde{R}^0_{i00}$ as the raw source. We computed $S^{\mathrm{eff}}_{i00}$ using our data for $\delta^2\tilde{R}^0_{i00}$, which was presented in Sec. 8.4. We computed $\Delta_{i00}[\,\tilde{h}^{\mathcal{P}s}\,]$ in the punctured regions using the same numerical parameters used for $\delta^2\tilde{R}^0_{i00}$, for a quasicircular orbit of radius $\tilde{r}_0=6M$, on the same grid of $r$-values from $r_{\mathrm{in}}=(2+10^{-7})M$ up to $r_{\mathrm{out}}=10^4M$ that was used to compute $\delta^2\tilde{R}^0_{i00}$. For the boundaries of the regions $\Gamma_s$, we set $r_H=2.1M$, $r_\pm=\tilde{r}_0\pm2M$ and $r_\infty=100M$. The punctures at the particle require data for the components $h^{\mathrm{R}1}_{\alpha\beta}$ on the particle, and data for the first-order self-force. We used our own data for these quantities for $\tilde{r}_0=6M$, obtained using the computation methods described in Chapter 4.

We are confronted by difficulties in the region $r\lessapprox 2.01M$, where we need to subtract two large numbers to compute the effective source, requiring access to a number of significant figures beyond machine precision. To overcome this, in this region we use long double variables to compute the effective source, as part of our C++ code used to carry out the full computation of the monopole second-order field, described in Sec. 8.7.1.

Figs. 8.5–8.10 display numerical results for $S^{\mathrm{eff}}_{i00}$ for the whole range of $r$ values, and for the region $\Gamma_{\mathrm{P}}$, magnified for clarity. Our results show that in the non-punctured regions, $\Gamma_\pm$, the effective source agrees with the raw source. In the region close to the particle, $\Gamma_{\mathrm{P}}$, the raw source diverges at the particle ($r=\tilde{r}_0$), whereas the effective source does not diverge there. We also observe that as we approach the particle, $\Delta_{i00}[\,h^{\mathcal{P}\mathrm{P}}\,]$ and the raw source coincide, because the dominant behaviour in the raw source comes from $\Delta_{i00}[\,h^{\mathcal{P}\mathrm{P}}\,]$ close to the particle.

## 8.7 The second-order monopole field

### 8.7.1 Computational algorithm

We compute the $i = 1, 3, \ell = 0, m = 0$ modes of the second-order field, using the worldtube method outlined in Sec. 8.2, for a quasicircular orbit of radius $\tilde{r}_0 = 6M$, using a grid of $r$-values from $r_{\rm in} = (2 + 10^{-7})M$ up to $r_{\rm out} = 10^4 M$, and setting $r_H = 2.1M$, $r_\pm = \tilde{r}_0 \pm 2M$ and $r_\infty = 100M$. We found that our results are insensitive to the location of the boundaries between regions. To implement this strategy we required two ingredients: homogeneous solutions and data for the effective source. The effective source was computed as described in Sec. 8.6. For the $i = 1, 3$ monopole, homogeneous solutions, we used the basis of solutions given analytically in Eqs. (4.42).

We used a straightforward C++ code to carry out the full computation. Our algorithm follows these steps:

- Input the analytical formulas for the homogeneous solutions, and compute $\hat{\Phi}(r)$ on a grid of $r$ values.
- Compute the effective source $J^s(r)$ on a grid of $r$ values, using the method described in Sec. 8.6.
- Calculate the integrand $\hat{\Phi}^{-1}(r)\hat{J}^s(r)$ everywhere on the grid, using a standard LU-decomposition routine to invert $\hat{\Phi}(r)$.
- Evaluate the integrals $\int_{r_s}^{r} dr'\hat{\Phi}^{-1}(r')J^s(r')$ at all points $r$ along the grid, using Simpson's rule. We found that to obtain results which no longer changed beyond the 16th significant figure, in the region $\Gamma_H$ we required the grid spacing to be no larger than $10^{-8}$ close to $r_{\rm in}$, which can become gradually larger as we approach $r_H$, approaching $10^{-3}$, but even close to $r_H$ the grid spacing cannot be larger than $10^{-3}$. In the regions $\Gamma_{\rm P}$ and $\Gamma_\infty$ we required a grid spacing no larger than $10^{-3}$.
- Calculate the constants $a^s$ from Eqs. (8.13) and (8.16). At this stage we perform a self-consistency check on our code, making sure that the $a^s$ satisfy the jump conditions (8.11) and regularity conditions (8.12).
- Finally, we compute the $i = 1, 3$ residual fields, $\tilde{h}^{\mathcal{R}}_{i00}$, and their $r$ derivatives, using Eq. (8.10).

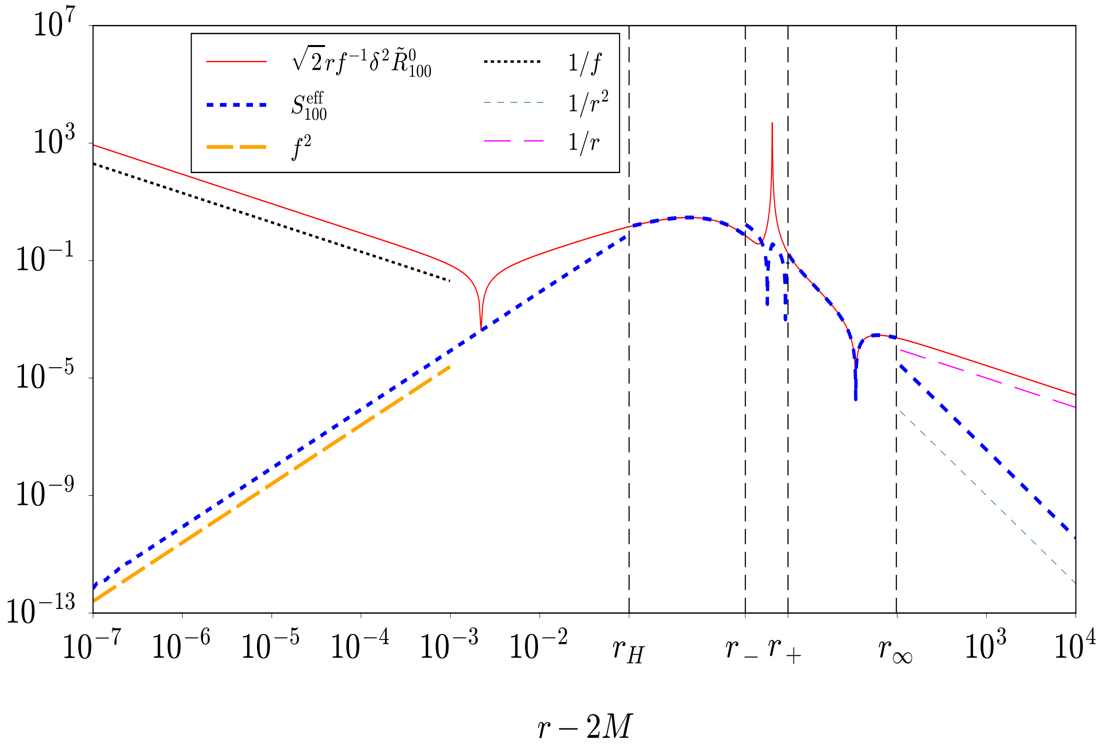


Figure 8.5: Comparison of the $i=1$ raw source with the $i=1$ effective source. Both axes are log scaled. As we approach the horizon the raw source diverges like $1/f$ but the effective source falls off as $f^2$. The region $\Gamma_{\rm P}$ is shown in Fig 8.6. In $\Gamma_\infty$ the raw source decays like $1/r$ and the effective source falls off as $1/r^2$. In the non-punctured regions, $\Gamma_\pm$, the effective source and the raw source agree.

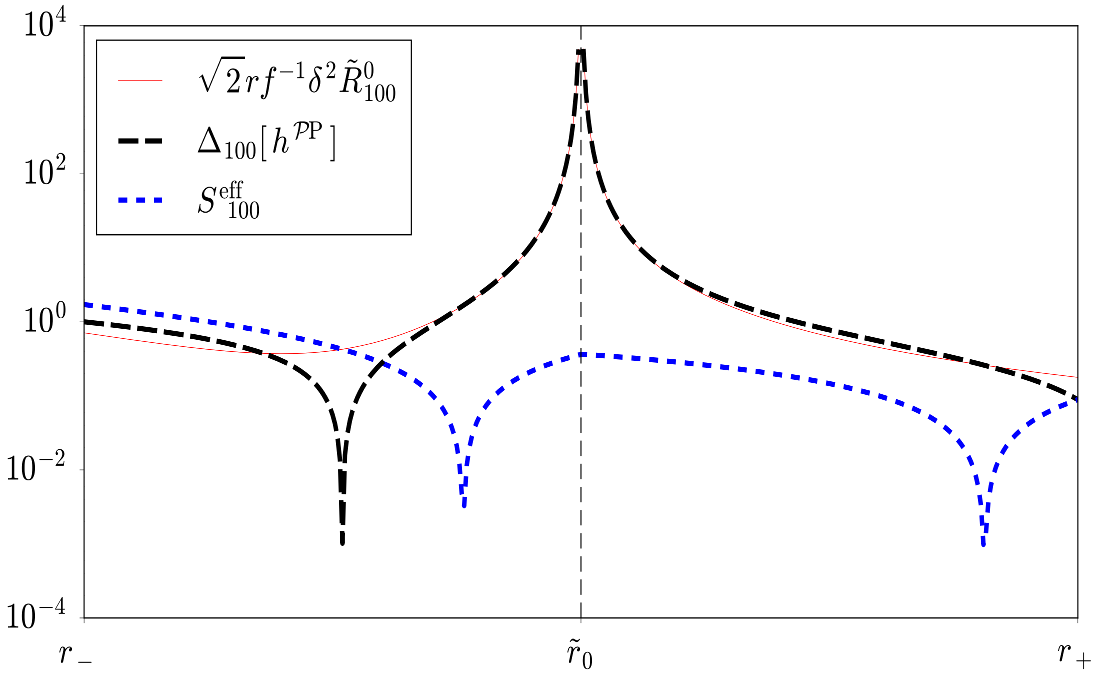


Figure 8.6: Comparison of the $i=1$ raw source with the $i=1$ effective source, in the region $\Gamma_{\rm P}$. The vertical axis is log scaled. The raw source and $\Delta_{100}[h^{\mathcal{P}\rm P}]$ agree close to the particle and diverge at the particle. $S^{\rm eff}_{100}$ does not diverge there.

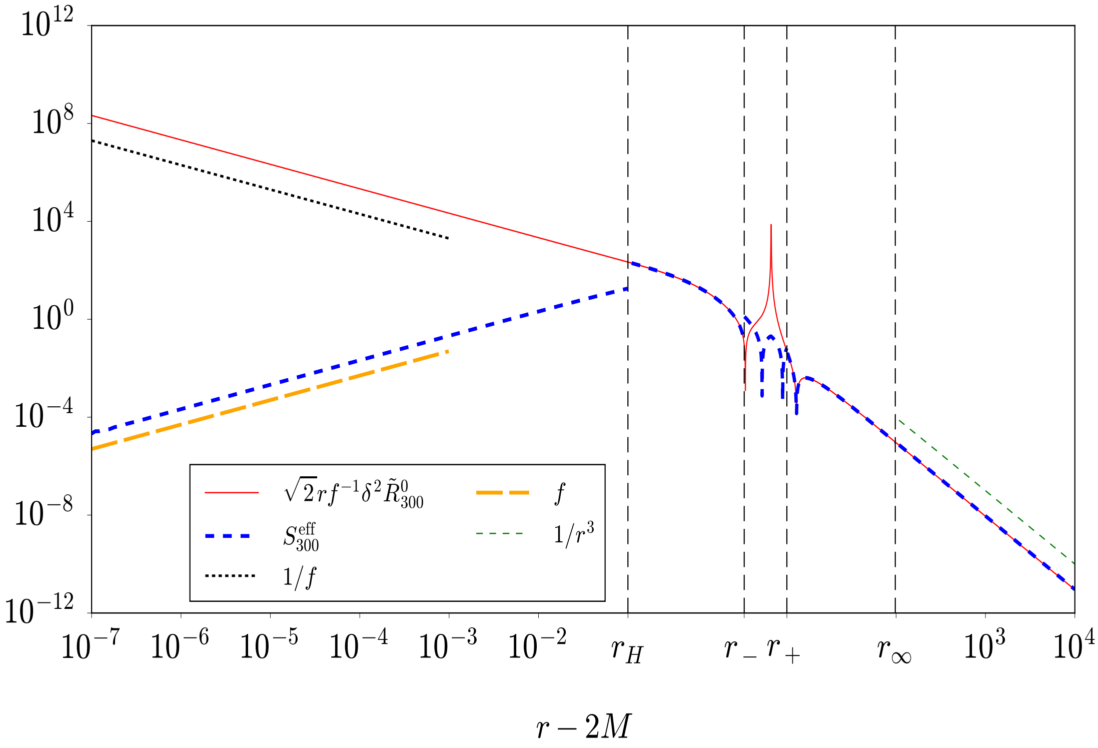


Figure 8.7: Comparison of the $i = 3$ raw source with the $i = 3$ effective source. Both axes are log scaled. As we approach the horizon the raw source diverges like $1/f$ but the effective source falls off as $f$. The region $\Gamma_{\rm P}$ is shown in Fig 8.8. In $\Gamma_\infty$ both the raw source and the effective source fall off as $1/r^3$. In the non-punctured regions, $\Gamma_\pm$, the effective source and the raw source agree.

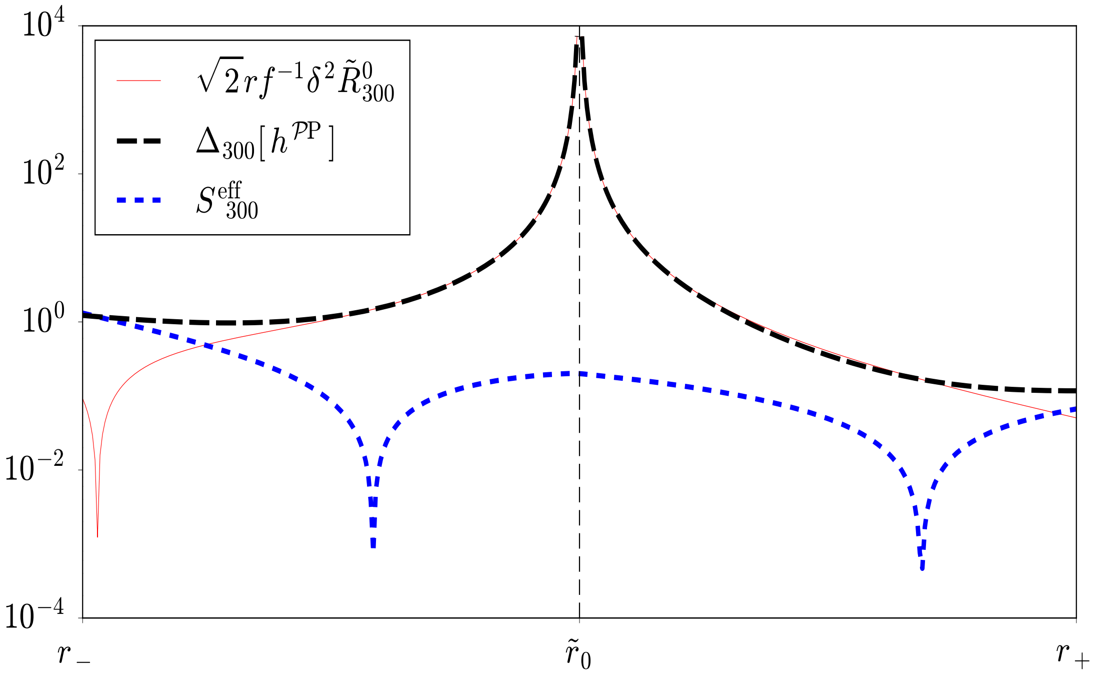


Figure 8.8: Comparison of the $i = 3$ raw source with the $i = 3$ effective source, in the region $\Gamma_P$. The vertical axis is log scaled. The raw source and $\Delta_{300}[h^{\mathcal{PP}}]$ agree close to the particle and diverge at the particle. $S^{\text{eff}}_{300}$ does not diverge there.

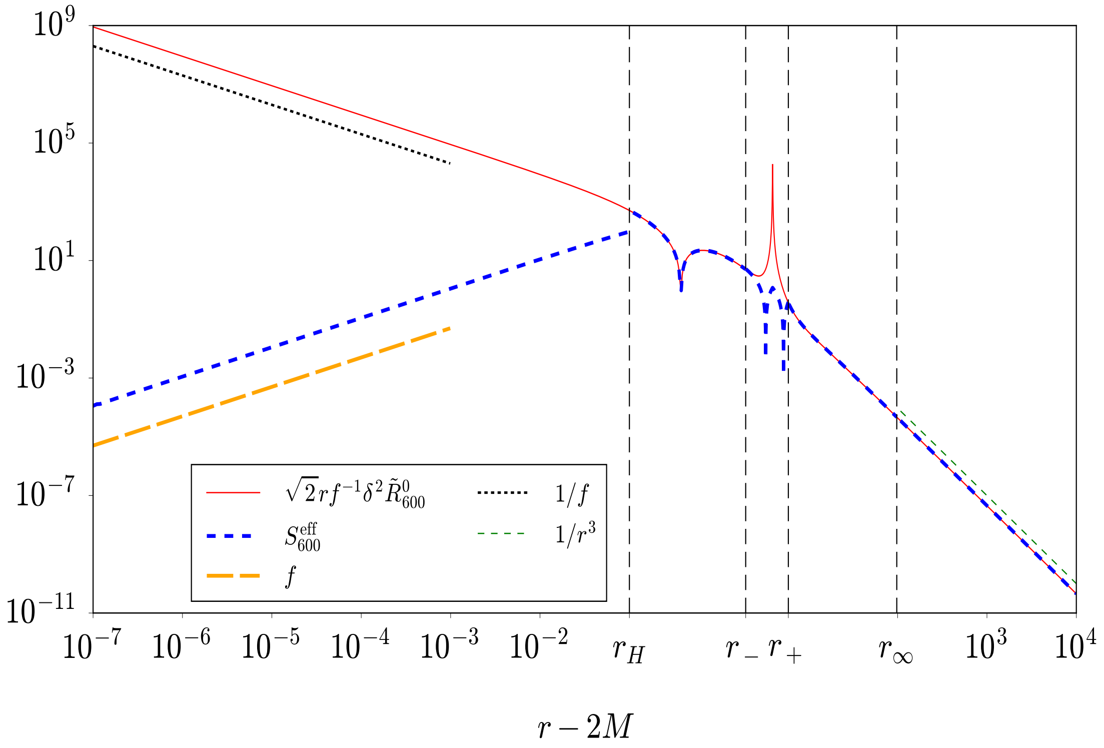


Figure 8.9: Comparison of the $i = 6$ raw source with the $i = 6$ effective source. Both axes are log scaled. As we approach the horizon the raw source diverges like $1/f$ but the effective source falls off as $f$. The region $\Gamma_{\rm P}$ is shown in Fig 8.10. In $\Gamma_\infty$ both the raw source and the effective source fall off as $1/r^3$. In the non-punctured regions, $\Gamma_\pm$, the effective source and the raw source agree.

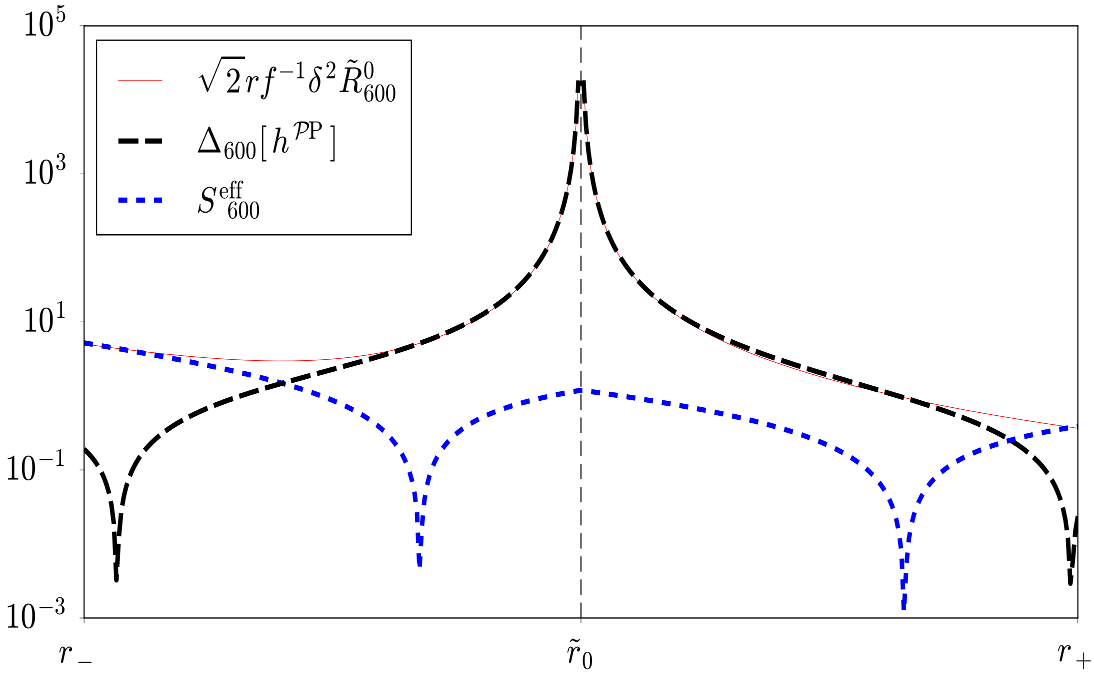


Figure 8.10: Comparison of the $i = 6$ raw source with the $i = 6$ effective source, in the region $\Gamma_P$. The vertical axis is log scaled. The raw source and $\Delta_{600}[h^{\mathcal{P}\rm P}]$ agree close to the particle and diverge at the particle. $S^{\rm eff}_{600}$ does not diverge there.

- We calculate the retarded fields, $\tilde{h}^{\rm ret}_{i00}$ by adding $\tilde{h}^{\mathcal{P}_s}_{i00}$ to the residual field in the punctured regions $\Gamma_s$, for $s = (H, \mathrm{P}, \infty)$. By substituting $\tilde{h}^{\rm ret}_{i00}$ $i = 1, 3$ into the gauge condition (7.43a), we may compute $\tilde{h}^{\rm ret}_{600}$. Then, we calculate $\tilde{h}^{\mathcal{R}}_{600}$ by subtracting the puncture in the punctured regions. But we note that unlike $\tilde{h}^{\rm ret}_{600}$, $\tilde{h}^{\mathcal{R}}_{600}$ will not automatically satisfy the gauge condition.

### 8.7.2 Numerical results

| | $r_0$ | this work | Warburton | rel. diff. |
|---|---|---|---|---|
| $h^{2\mathcal{R}}_{100}(r_{\rm in})$ | 6 | 0 | 0 | |
| $h^{2\mathcal{R}}_{100}(r_0)$ | 6 | $-1.2776905081034842$ | $-1.31223$ | $3 \times 10^{-2}$ |
| $h^{2\mathcal{R}}_{100}(r_{\rm out})$ | 6 | $-2.2896611175870656$ | $-2.36304$ | $3 \times 10^{-2}$ |
| $h^{2\mathcal{R}}_{300}(r_{\rm in})$ | 6 | $-4.6266797468335925$ | $-4.62267$ | $< 10^{-3}$ |
| $h^{2\mathcal{R}}_{300}(r_0)$ | 6 | 6.190042979233179 | 6.1308 | $< 10^{-2}$ |
| $h^{2\mathcal{R}}_{300}(r_{\rm out})$ | 6 | $-2.2890768331107143$ | $-2.36247$ | $3 \times 10^{-2}$ |
| $h^{2\mathcal{R}}_{600}(r_{\rm in})$ | 6 | $-35.871083609313445$ | | |
| $h^{2\mathcal{R}}_{600}(r_0)$ | 6 | 0.5319088368041207 | | |
| $h^{2\mathcal{R}}_{600}(r_{\rm out})$ | 6 | 0.0005317661529034012 | 0.0005320145402265553 | $5 \times 10^{-4}$ |
| $h^{2\mathcal{R}}_{100}(r_{\rm in})$ | 8 | 0 | 0 | |
| $h^{2\mathcal{R}}_{100}(r_0)$ | 8 | $-1.8174057692884025$ | $-1.87312$ | $3 \times 10^{-2}$ |
| $h^{2\mathcal{R}}_{100}(r_{\rm out})$ | 8 | $-1.2758926343764194$ | $-1.36183$ | $6 \times 10^{-2}$ |
| $h^{2\mathcal{R}}_{300}(r_{\rm in})$ | 8 | $-3.4796240776963505$ | $-3.38134$ | $2 \times 10^{-2}$ |
| $h^{2\mathcal{R}}_{300}(r_0)$ | 8 | 5.37093884874699 | 5.31596 | $10^{-2}$ |
| $h^{2\mathcal{R}}_{300}(r_{\rm out})$ | 8 | $-1.2744918717716103$ | $-1.36044$ | $6 \times 10^{-2}$ |
| $h^{2\mathcal{R}}_{600}(r_{\rm in})$ | 8 | $-51.08133309932423$ | | |
| $h^{2\mathcal{R}}_{600}(r_0)$ | 8 | 1.297003784933751 | | |
| $h^{2\mathcal{R}}_{600}(r_{\rm out})$ | 8 | 0.000830180386799384 | 0.0008312334095705864 | $1.2 \times 10^{-3}$ |
| $h^{2\mathcal{R}}_{100}(r_{\rm in})$ | 10 | 0 | 0 | |
| $h^{2\mathcal{R}}_{100}(r_0)$ | 10 | $-2.199972780725526$ | $-2.21554$ | $7 \times 10^{-3}$ |
| $h^{2\mathcal{R}}_{100}(r_{\rm out})$ | 10 | $-0.9388565339196675$ | $-0.962272$ | $2 \times 10^{-2}$ |
| $h^{2\mathcal{R}}_{300}(r_{\rm in})$ | 10 | $-2.7815250036479293$ | $-2.6301$ | $5 \times 10^{-2}$ |
| $h^{2\mathcal{R}}_{300}(r_0)$ | 10 | 5.048353178504122 | 5.06855 | $4 \times 10^{-3}$ |
| $h^{2\mathcal{R}}_{300}(r_{\rm out})$ | 10 | $-0.9370583887302292$ | $-0.960462$ | $2 \times 10^{-2}$ |
| $h^{2\mathcal{R}}_{600}(r_{\rm in})$ | 10 | $-74.07264254530617$ | | |
| $h^{2\mathcal{R}}_{600}(r_0)$ | 10 | 1.7920187427192475 | | |
| $h^{2\mathcal{R}}_{600}(r_{\rm out})$ | 10 | 0.000993626756134347 | 0.001002267487052677 | $< 10^{-2}$ |

Table 8.2: Data for the second-order, monopole piece of the residual field. The absolute error in the data from this work is between $10^{-5}$ to $10^{-6}$ for all quantities.

In Table 8.2 we show data for $h^{\mathcal{R}}_{i00}(r)$ $(i = 1, 3, 6)$ , at points $r = r_{\rm in}$, $r_0$, $r_{\rm out}$, for quasicircular orbits for a variety of radii. We stress that these results are still only provisional. We compare our results to results for the same quantities obtained in parallel by Warburton, using the same worldtube method described in this work. Blank spaces in the table correspond to quantities that I have not compared with Warburton. We believe that the difference in the numerical data between this work and Warburton can be explained by the fact that we have used more grid points than Warburton to evaluate the numerical integrals required for calculating the residual field modes.

Our results for $\tilde{h}^{\text{ret}}_{i00}$, $\tilde{h}^{\mathcal{R}}_{i00}$ and their derivatives are plotted in Figs. 8.11–8.16. In all of the plots we see that $\tilde{h}^{\text{ret}}_{i00}$ and $\tilde{h}^{\mathcal{R}}_{i00}$ agree in the non-punctured regions. In all cases $\tilde{h}^{\text{ret}}_{i00}$ diverges as $r \ln r$, whereas $\tilde{h}^{\mathcal{R}}_{i00}$ either tends to a constant or falls off to zero as $r \to \infty$. We remind the reader that in the sum over frequency-domain tensor-harmonic modes (4.24), there is a factor of $1/r$ outside, so the monopole contribution to the full residual field falls off at least as fast as $1/r$ at large $r$.

The results in this section represent a milestone in self-force research: they are the first direct computation of a mode of the second-order field.

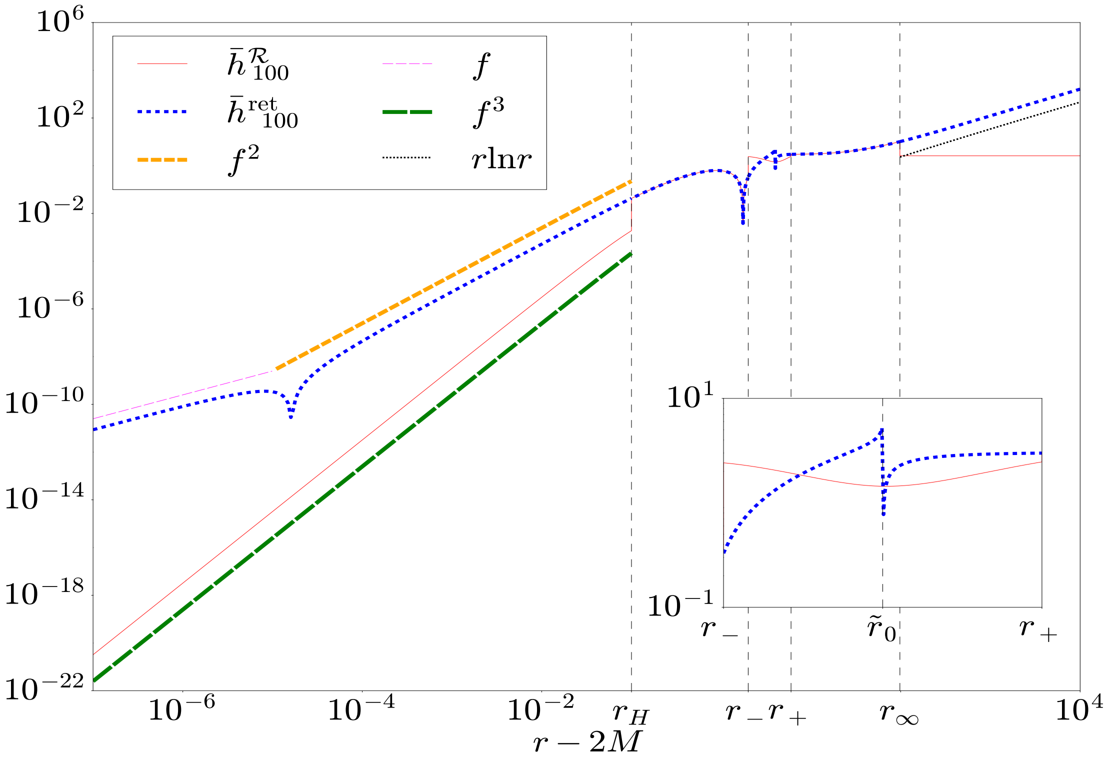


Figure 8.11: $\tilde{h}^{\text{ret}}_{100}$ and $\tilde{h}^{\mathcal{R}}_{100}$ on a log log scale. As we approach the horizon $\tilde{h}^{\text{ret}}_{100}$ falls off like $f$, whereas $\tilde{h}^{\mathcal{R}}_{100}$ falls off faster, as $f^3$. $\tilde{h}^{\text{ret}}_{100}$ diverges like $r\ln r$ but $\tilde{h}^{\mathcal{R}}_{100}$ tends to a constant as $r\to\infty$. In the non-punctured regions, $\Gamma_\pm$, $\tilde{h}^{\text{ret}}_{100}$ and $\tilde{h}^{\mathcal{R}}_{100}$ agree.

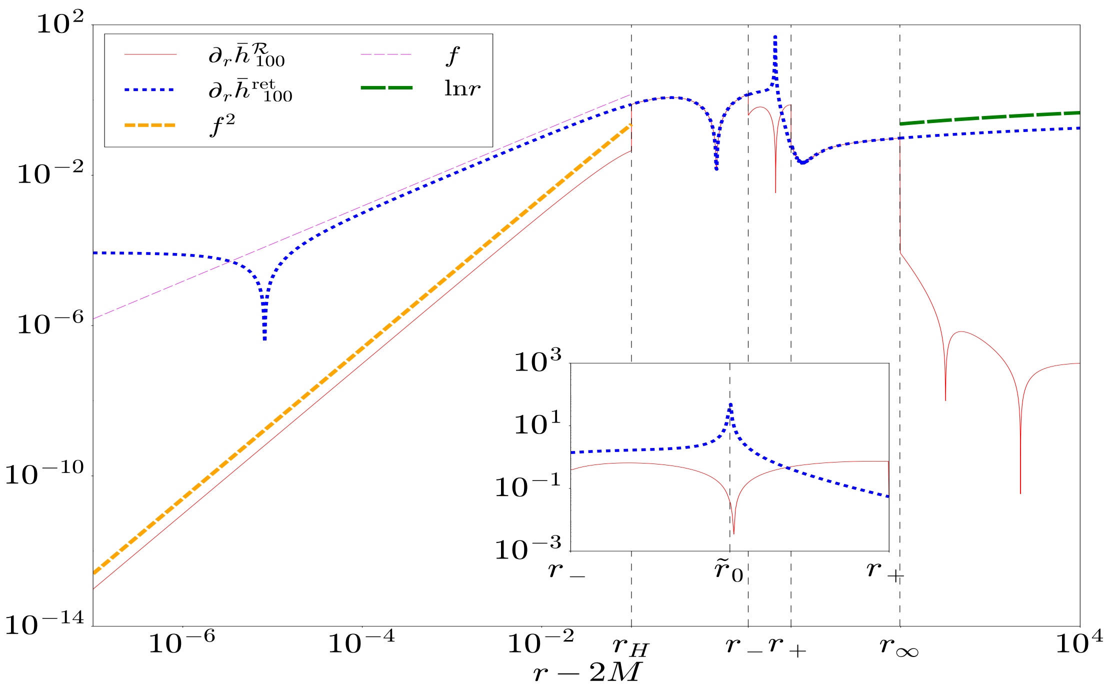


Figure 8.12: $\partial_r\tilde{h}^{\text{ret}}_{100}$ and $\partial_r\tilde{h}^{\mathcal{R}}_{100}$ on a log log scale. As we approach the horizon $\partial_r\tilde{h}^{\text{ret}}_{100}$ tends to a constant whereas $\partial_r\tilde{h}^{\mathcal{R}}_{100}$ falls off as $f^2$. $\partial_r\tilde{h}^{\text{ret}}_{100}$ diverges like $\ln r$ but $\partial\tilde{h}^{\mathcal{R}}_{100}$ approaches zero as $r\to\infty$. In the non-punctured regions, $\Gamma_\pm$, $\partial_r\tilde{h}^{\text{ret}}_{100}$ and $\partial_r\tilde{h}^{\mathcal{R}}_{100}$ agree.

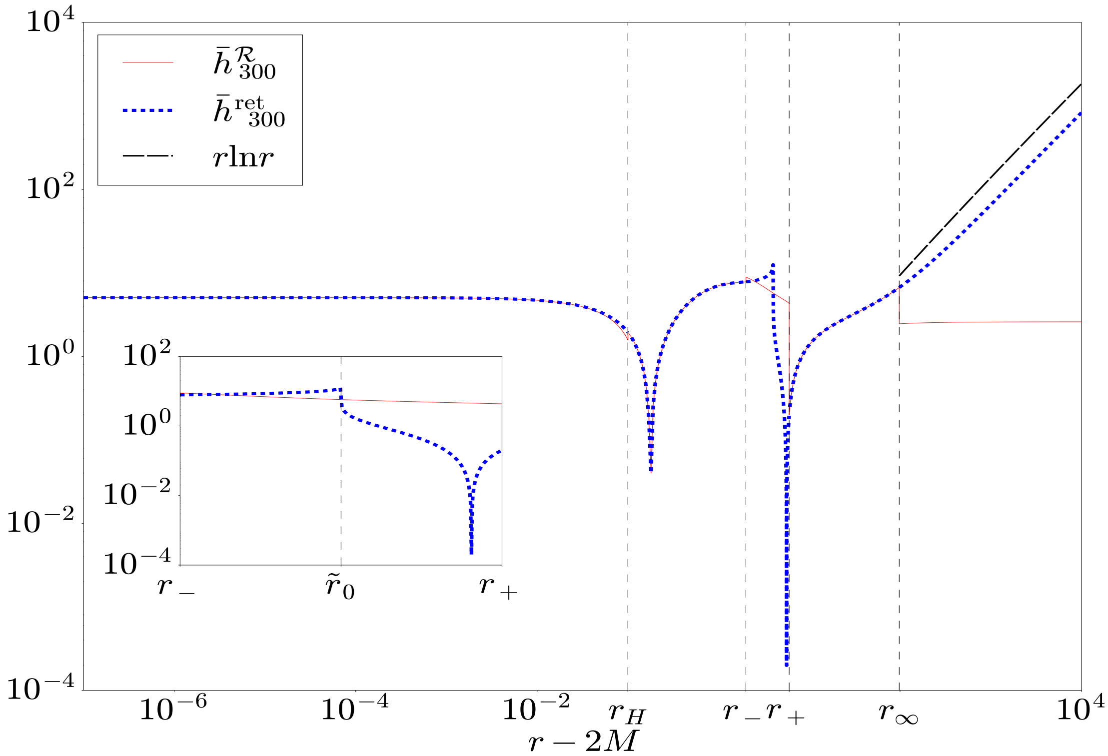


Figure 8.13: $\tilde{h}^{\text{ret}}_{300}$ and $\tilde{h}^{\mathcal{R}}_{300}$ on a log log scale. As we approach the horizon $\tilde{h}^{\text{ret}}_{300}$ and $\tilde{h}^{\mathcal{R}}_{300}$ both tend to a constant. $\tilde{h}^{\text{ret}}_{300}$ diverges like $r\ln r$ but $\tilde{h}^{\mathcal{R}}_{300}$ tends to a constant as $r\to\infty$. In the non-punctured regions, $\Gamma_\pm$, $\tilde{h}^{\text{ret}}_{300}$ and $\tilde{h}^{\mathcal{R}}_{300}$ agree.

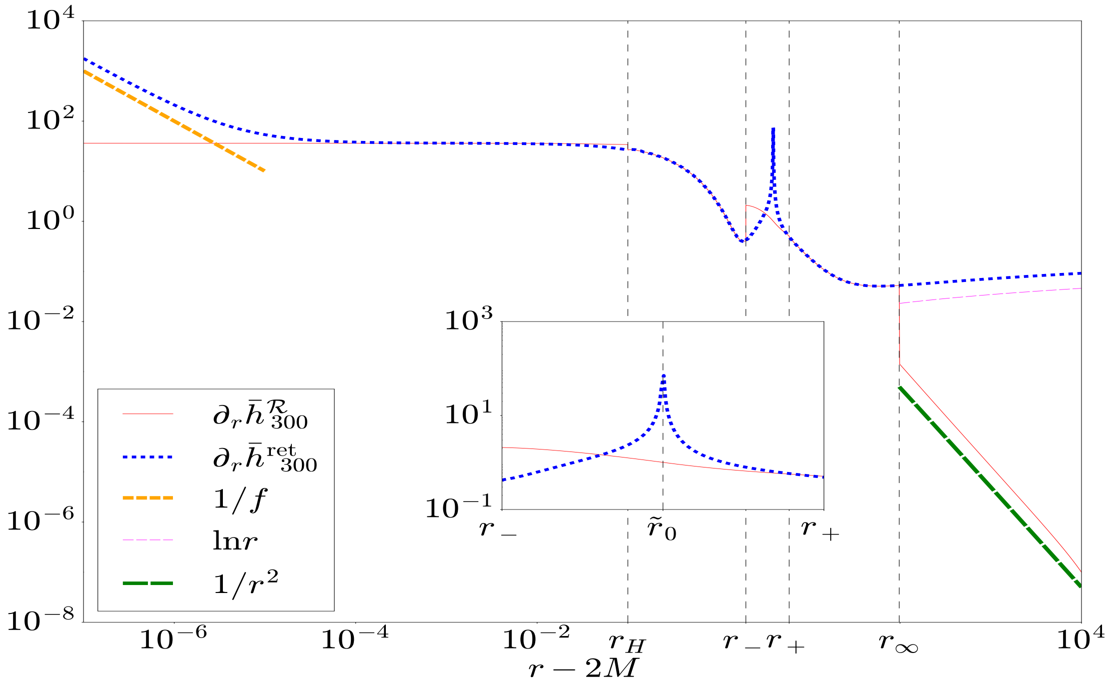


Figure 8.14: $\partial_r\tilde{h}^{\text{ret}}_{300}$ and $\partial_r\tilde{h}^{\mathcal{R}}_{300}$ on a log log scale. As we approach the horizon $\partial_r\tilde{h}^{\text{ret}}_{300}$ blows up as $1/f$ but $\partial_r\tilde{h}^{\mathcal{R}}_{300}$ tends to a constant. $\partial_r\tilde{h}^{\text{ret}}_{300}$ diverges like $\ln r$ but $\partial\tilde{h}^{\mathcal{R}}_{300}$ falls off like $1/r^2$ as $r\to\infty$. In the non-punctured regions, $\Gamma_\pm$, $\partial_r\tilde{h}^{\text{ret}}_{300}$ and $\partial_r\tilde{h}^{\mathcal{R}}_{300}$ agree.

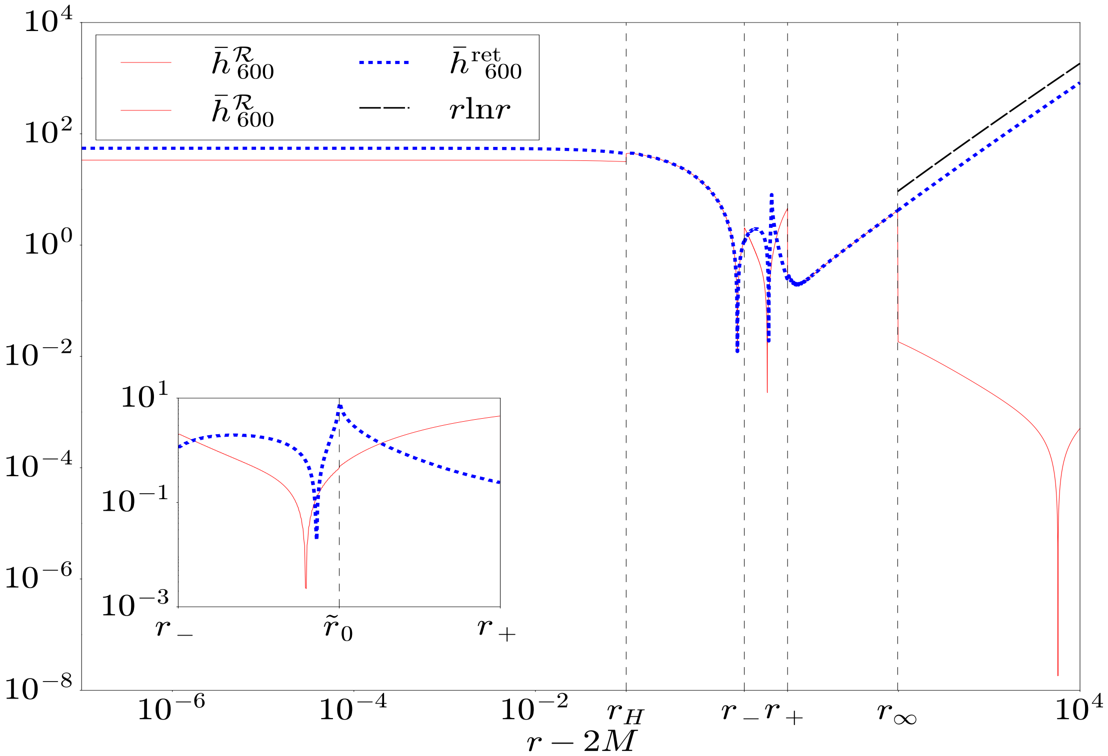


Figure 8.15: $\tilde{h}^{\text{ret}}_{600}$ and $\tilde{h}^{\mathcal{R}}_{600}$ on a log log scale. As we approach the horizon $\tilde{h}^{\text{ret}}_{600}$ and $\tilde{h}^{\mathcal{R}}_{600}$ both tend to a constant. $\tilde{h}^{\text{ret}}_{600}$ diverges like $r\ln r$ but $\tilde{h}^{\mathcal{R}}_{600}$ approaches zero as $r \to \infty$. In the non-punctured regions, $\Gamma_\pm$, $\tilde{h}^{\text{ret}}_{600}$ and $\tilde{h}^{\mathcal{R}}_{600}$ agree.

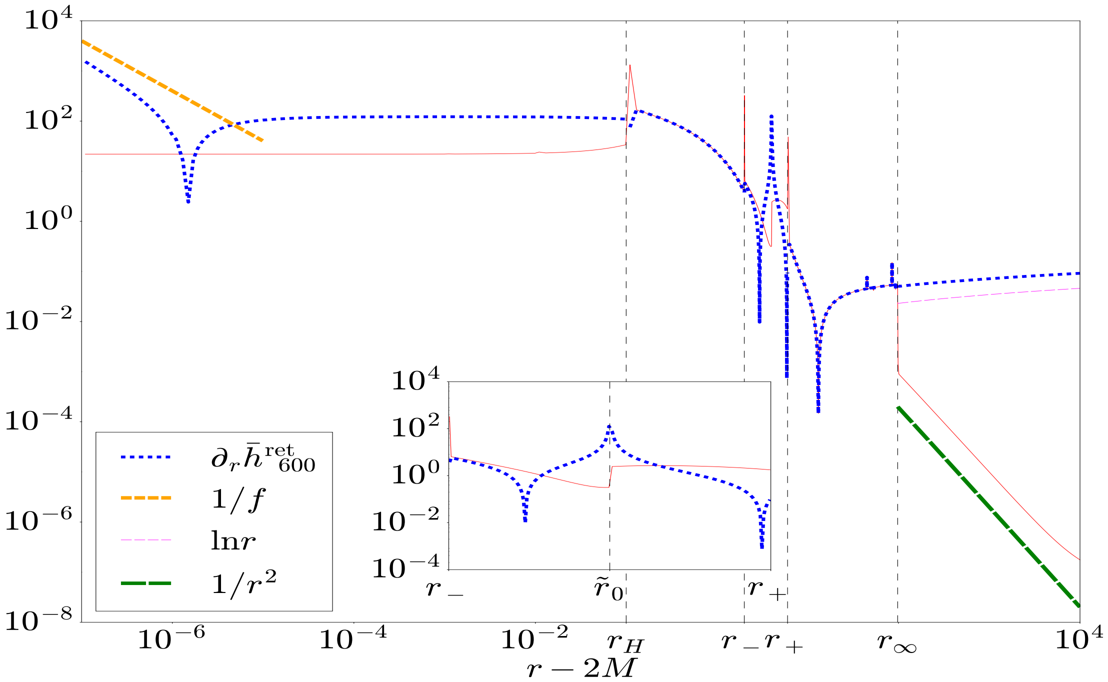


Figure 8.16: $\partial_r\tilde{h}^{\text{ret}}_{600}$ and $\partial_r\tilde{h}^{\mathcal{R}}_{600}$ on a log log scale. As we approach the horizon $\partial_r\tilde{h}^{\text{ret}}_{600}$ blows up as $1/f$ but $\partial_r\tilde{h}^{\mathcal{R}}_{600}$ tends to a constant. $\partial_r\tilde{h}^{\text{ret}}_{600}$ diverges like $\ln r$ but $\partial\tilde{h}^{\mathcal{R}}_{600}$ falls off like $1/r^2$ as $r \to \infty$. In the non-punctured regions, $\Gamma_\pm$, $\partial_r\tilde{h}^{\text{ret}}_{600}$ and $\partial_r\tilde{h}^{\mathcal{R}}_{600}$ agree.

# Chapter 9

# Summary and conclusion

## 9.1 Summary of results

The research of this thesis was motivated by the goal of modeling GWs from binary inspirals. We have discussed different types of binaries, including comparable-mass inspirals, IMRIs and EMRIs. In this work we have focused exclusively on EMRIs, comprised of a small compact object orbiting a MBH. They have a long inspiral time, generating many tens of thousands of GW cycles as the small object orbits very close to the MBH. As such, EMRIs trace out a detailed map of the curved spacetime around the MBH, and this information is encoded in the emitted GWs. The GWs also encode information about the orbital dynamics. For example, EMRI orbits can be eccentric, inclined and rapidly precessing. As such, EMRIs offer a rich set of relativistic phenomena to study, which can be extracted from GW signals.

We have described a number of models available for modeling binary inspirals, including NR, EOB and PN theory. But for EMRIs, PN theory is inaccurate because the system is highly relativistic, and NR cannot accommodate the two very different length scales and large number of orbits in the inspiral. The only model able to accurately model EMRIs is the gravitational self-force model. That is the main motive to calculate the gravitational self-force. The first-order gravitational self-force has been computed, but prior to our research, second-order results were yet to be obtained, and without including the effect of the second-order gravitational self-force we cannot accurately model an EMRI over the inspiral time.

We have discussed different approaches that have been used to calculate the first-order gravitational self-force, including the mode-sum approach, the worldline convolution approach and the puncture-scheme approach. But at second-order, the worldline convolution and mode-sum approaches cannot be implemented, for reasons that were described in the introduction. The only viable method for a computation at second order is the puncture scheme approach. Hence the central goal of this thesis: to develop a new puncture scheme that can be applied at second order and used to calculate the second-order gravitational self-force.

The essential analytical ingredients needed to compute the second-order self-force are (i) a local expression for the small object's self-field $h^{\rm S}_{\mu\nu}$, and (ii) an equation of motion for the small object's center of mass in terms of a certain effective field $h^{\rm R}_{\mu\nu}$. Both of these results were available to us in the beginning of this project, as reviewed in detail in Chapter 2. There we discussed how to derive formulas for the first- and second-order fields of the small object using the methods of matched asymptotic expansions developed in [39, 40]. In that context we found that the fields can be written locally as $h^{n}_{\mu\nu} = h^{{\rm S}n}_{\mu\nu} + h^{{\rm R}n}_{\mu\nu}$ $(n = 1, 2)$, where the self-fields $h^{{\rm S}n}$ encapsulate local information about the object's multipole structure, and the effective fields $h^{{\rm R}n}$ are vacuum perturbations that are determined by global boundary conditions imposed on $h^{n}_{\mu\nu}$. There are different ways of defining this singular-regular split, but in this work we have used the Pound choice [44], as described in Sec. 2.4.

$h^{\rm S}_{\mu\nu}$ and $h^{\rm R}_{\mu\nu}$ are defined locally in a neighbourhood *outside* the object. A puncture scheme proceeds by analytically continuing these fields into the region where the object would lie in the full, physical spacetime. The analytically continued self-field $h^{\rm S}_{\mu\nu}$ diverges at a worldline $\gamma$ that represents the motion of the center of mass of the small object in the background spacetime. It is hence referred to as the singular field. In contrast, the analytically continued field $h^{\rm R}_{\mu\nu}$ is smooth at $\gamma$, and is referred to as the regular field. With our convention for the singular-regular split, the effective metric $g_{\mu\nu} + h^{\rm R}_{\mu\nu}$ is a $C^\infty$ solution to the vacuum Einstein equation, and $\gamma$ is a geodesic in that vacuum metric through second order. Splitting the field in this way, we can replace the field equations with effective source equations. The divergent source has now been replaced with an effective source, which does not diverge at the particle.

More concretely, we define a puncture, $h^{\mathcal{P}}_{\mu\nu}$, which is a truncation of a local expansion of the singular field, in powers of spatial distance from the worldline, at a specified order. We then define a residual field, $h^{\mathcal{R}}_{\mu\nu} \equiv h^{\rm ret}_{\mu\nu} - h^{\mathcal{P}}_{\mu\nu}$, and we construct an effective source for it by moving all terms including the puncture to the right-hand side of the field equations. In this manner, terms involving the puncture get subtracted from the raw source and the divergence at the particle cancels. We are left with an effective source equation, which we may solve for the residual field numerically, using retarded boundary conditions. Then, the self-force may be computed from the equation of motion (2.69), by replacing $h^{\rm R}_{\mu\nu}$ with $h^{\mathcal{R}}_{\mu\nu}$.

We have derived formulas for the first- and second-order puncture fields, as covariant expansions of the first- and second-order singular fields in an arbitrary vacuum background. These are given in Eqs. (3.59)-(3.67). For a practical numerical implementation of a puncture scheme, all we need to do is to write the punctures in a specified coordinate system, and then expand in coordinate distances from the worldline, as in Eqs. (3.70) and (3.71).

As a first test of our puncture scheme, we implemented it to solve the first-order equations for the case of quasicircular orbits in Schwarzschild. We devised a worldtube strategy, in which we solved the effective source equation for the residual field inside a worldtube centered on the worldline, and outside the worldtube we solved the vacuum equations for the retarded field directly. This method can be used to solve the full non-linear equations in 3+1 dimensions, but we approached the problem by decomposing the puncture and the field equations into tensor spherical-harmonic and frequency modes. We have performed numerous checks of our results. For individual modes of the perturbation, we have obtained agreement with results of Warburton up to a relative difference of between $10^{-13}$ and $10^{-9}$, as shown in Fig. 4.4. Our results for the first-order self-force, shown in Table. 4.2, agree with previously published data in [93] up to a relative difference smaller than $10^{-7}$.

After successfully testing our puncture scheme at first order, we progressed to applying it at second order. We encountered two hurdles. Firstly, we found that closer and closer to the particle an arbitrarily large number of modes of the first-order field are needed to calculate a single mode of the Ricci tensor. Rather than facing the problem head-on in gravity, we used a flat-space scalar toy model, whose second-order source was designed to have the same problematic properties as its full counterpart in gravity. Fig. 5.1 illustrates the problem with the example of the monopole mode of the toy-model source $S_{00}\left(\phi^{\rm ret},\phi^{\rm ret}\right)$; near the particle the sum shows no signs of numerical convergence with $\ell_{\rm max}$. In Chapter 5 we sought a way of circumventing the bad convergence of the mode sum near the particle using an analytical approximation for the singular field. The essential idea was to compute the modes of the most singular piece of the source by direct integration of the full 4D expression against the scalar spherical-harmonics, instead of using the coupling formula (5.31), where the non-convergence arises. This strategy was applied in some region around $r = r_0$; outside that region, we simply used the retarded modes in Eq. (5.31) without difficulty. Later, in Chapter 8, we applied the lessons learned from the toy-model source to the second-order Ricci tensor. Our results are displayed in Figs 8.3 and 8.4. This attests to the veracity of our data for the first-order modes and the correctness of our method.

The second problem is that the large-$r$ behaviour of the source prevents the retarded integral from converging. The problem at large $r$ can be divided into two separate issues, which are associated with two separate pieces of the second-order source. The first exhibits secular growth at large $r$. The second piece falls off too slowly, such that its retarded-integral against the Green's function leads to an infrared divergence. The cause of both of these problems is that we assume the trajectory of the small body can be approximated to be a circular orbit in a Schwarzschild background spacetime. The issue of secular growth is resolved by applying a two-timescale expansion to the field.

The infrared divergence is resolved by truncating the retarded integral at some value of $r$, adding a homogeneous field times a constant to account for the piece of the solution removed by truncating the retarded integral, and determining the constant by matching to a known solution. This was discussed in Chapter 6.

In Chapter 7 we have applied the two-timescale method to the field equations in gravity, using the formalism developed in the toy-model in Chapter 6. We derived boundary conditions at the horizon and at infinity, as well as deriving a two-timescale expansion of the second-order field equations. We note that while our boundary conditions at the horizon are a particular solution to the field equations, they are not physically motivated. However, we have argued that we nevertheless obtain a physical solution for $\ell = 0$, at a fixed value of slow time.

Finally, we have implemented our puncture scheme at second-order for calculating the monopole piece of the second-order field. We have computed the second-order Ricci tensor based on our data for the first-order field, and we found that it behaves according to analytical predictions. This reinforces the accuracy of our first-order data and the correctness of the coupling formula itself. We have constructed a second-order puncture scheme that caters for including punctures at the horizon and at infinity, developed in Chapter 7, and punctures at the particle, developed in collaboration with Wardell. Using these punctures we have constructed an effective source, which is precisely as smooth as we would predict from the order of our puncture. It falls off at the horizon, and at infinity, exactly as we would predict from the form of the punctures we use in those regions. We have successfully applied our puncture scheme to directly compute the monopole ($i = 1, 3, 6$) modes of the second-order field. Our results are displayed in Figs. 8.11–8.16. This stands as the first direct computation of a second-order metric perturbation.

In summary, we have constructed a puncture scheme that can be applied at second order, successfully tested it at first order, and implemented it as the first direct computation of a mode of the second-order field. We can use the same strategy to compute the $\ell > 0$ modes of the second-order field, using the second-order puncture scheme set out in Chapter 8. Such results will provide all the numerical ingredients for computing the second-order self-force.

## 9.2 Outlook

In Chapter 8 we focused on obtaining the second-order metric perturbation, an intrinsically gauge-dependent quantity. Going forward, our first goal will be to extract physical quantities from the perturbation. In principle, we already have the necessary ingredients to compute one such quantity: the binding energy of the system. The specific binding energy may be defined as

$$E_{\text{binding}} = \frac{M_{\text{Bondi}} - \mu - M_{BH}}{\nu}, \tag{9.1}$$

where $M_{\text{Bondi}}$ is the total Bondi mass of the system, $M_{BH}$ is the central BH's mass, and $\nu \equiv \mu M_{BH}/(\mu + M_{BH})$ is the reduced mass of the binary. Through first order, $M_{BH}$ is simply $M + \epsilon\delta M_{BH}$, as given by Eq. (7.34). Similarly, the Bondi mass is simply $M + \epsilon(\delta M_{BH} + \mu\mathscr{E})$, as described in Eq. (7.36a). The binding energy at first order is then simply the kinetic energy of the small mass, $\epsilon\mu(\mathscr{E} - 1)$.

At second order, the binding energy measures the energy stored in the field, and its computation becomes more delicate. The second-order contribution to the Bondi mass can be read off of the asymptotic form of the second-order $\ell = 0$ field, but it must be measured at null infinity, not in the near zone; hence, we require a careful application of the matching procedure described in Chapter 7 to determine how the Bondi mass of the full physical field relates to our numerically computed residual field $h^{\mathcal{R}2}_{\mu\nu}$ at $r \to \infty$. We must also decide upon a measure of the slowly evolving BH's mass. A useful choice is to identify it with the irreducible mass $M_{\text{irr}}$, defined as

$$M_{\text{irr}} = \sqrt{\frac{\sigma_{\text{AH}}}{16\pi}}, \tag{9.2}$$

where $\sigma_{AH}$ is the surface area of the apparent horizon that surrounds the BH. Again, the contribution to Eq. (9.2) from the second-order field requires only the $\ell = 0$ mode. However, we must consider whether our ad hoc boundary conditions at the horizon allows a meaningful measurement of mass. A different choice of puncture at the horizon would correspond to a different choice of particular solution, altering our results by the addition of a homogeneous solution. At first glance, it appears that this should not alter the binding energy: a homogeneous solution would add the same mass to $M_{\text{Bondi}}$ as to $M_{BH}$, leaving $E_{\text{binding}}$ in Eq. (9.1) unchanged. However, this demands more careful analysis because our puncture is singular at the horizon, with an unclear contribution to Eq. (9.2). We are currently undertaking a comparison of preliminary results for $E_{\text{binding}}$ with a prediction from the first law of binary mechanics [23].

The puncture scheme that we developed in this thesis can, in principle, be applied to generic orbits in any vacuum spacetime. Aside from quasicircular orbits in Schwarzschild that we focused on, the next simplest scenario would be eccentric orbits in Schwarzschild. But unlike circular orbits which only have one frequency for each $\ell m$ mode, eccentric orbits requires summing over a range of discrete Fourier modes to compute a single $\ell, m$ mode of the field. In this approach we would encounter an already well known problem that the sum over frequency modes does not converge well near the particle. This is an example of a general problem of trying to reconstruct a non-smooth function using Fourier modes, known as the Gibbs phenomenon. A method for resolving this problem that allows one to compute the first-order self-force from eccentric source orbits, is the method of extended homogeneous solutions [112], explained as follows. Analogous to the homogeneous solutions we found for circular source orbits, for eccentric orbits one finds two sets of homogeneous solutions that are regular at the horizon and at $r \to \infty$, and valid for $r \leq r_{\rm min}$ and $r \geq r_{\rm max}$ respectively, where $r_{\rm min}$ and $r_{\rm max}$ are the minimum and maximum values of the radial coordinate along an eccentric orbit. One extends the domain of these solutions from a vacuum region to the entire region $r > 2M$, to include the non-vacuum region where the particle lies. Then, instead of computing $\ell$ modes of the self-force by summing $\ell m\omega$ modes of the inhomogeneous self-field, one computes it using $\ell m\omega$ modes of the extended homogeneous field. This method avoids the lack of convergent summation over frequency modes. While this method works well at first order, at second order difficulties still arise because the second-order source is not localised like it is at first order, rather it has support everywhere. So, the extended homogeneous solutions method will not apply at second order and it is not immediately obvious how to overcome the lack of convergent summation over Fourier modes at second order.

Restricting ourselves to quasicircular orbits but generalizing to Kerr spacetime, our frequency domain approach cannot be directly applied because the wave equations do not separate into ordinary differential equations at each $\ell m$ mode like they do in Schwarzschild. However, the puncture scheme itself does not require us to do any kind of mode decomposition, so we could in principle apply it to the full 3+1D field equations. For this we would need to construct punctures from our covariant expressions constructed in Chapter 3, in a Kerr background. Alternatively, we can decompose the equations into 2+1D equations at each $m$-mode. This type of decomposition was already performed by Barack and Dolan in Schwarzschild [63], and in Kerr, although the latter has not yet been published. If we wanted to solve the equations in the frequency domain we would have to develop a suitable extension of the metric reconstruction formalism in [52, 113, 114] to second order, which is not an easy task.

However, instead of generalizing to eccentric orbits or a Kerr background, our more immediate goal for the future is to compute the higher, $\ell > 0$ modes of the second-order field for quasicircular orbits in Schwarzschild. We have already calculated analytical expressions for the tensor-harmonic-modes of the punctures at the particle for generic $i, \ell, m$. We have also written a code capable of computing the higher modes of the second-order field, using the same worldtube strategy developed in Sec. 8.2. At first sight, based on our data of the higher modes of the second-order Ricci tensor, it seems that we will need punctures at the horizon. These are yet to be constructed. Once we have derived these, we will be in a position to compute the higher modes of the second-order field, which will allow us to calculate the dissipative piece of the second-order self-force. This will enable us to compute the evolution of the orbit of the small object in the inspiral. This would be the first instance of a computation of the orbital evolution in a binary inspiral, taking into account second-order effects. As we argued in the introduction, an accurate model of the evolution can only be done by including second-order effects. Even more, we would be able to accurately model GWs from such an orbital evolution with second-order results. Moreover access to all the modes of the field will afford us the ability to calculate a range of gauge-invariant quantities, including the second-order contribution to the Detweiler redshift, and higher multipole moments, e.g. the quadrupole moment of the system. We will also be able to calculate a number of quantities relevant to the orbital dynamics, such as the ISCO shift, pericenter advance and spin precession.

Further afield, besides the obvious relevance of second-order gravitational self-force results to EMRIs, second-order results will be useful for improving models of other two-body systems, possibly pushing into the IMRI regime. Second-order gravitational self-force data will enable us to fix higher-order terms in PN theory and the EOB model, which describe binary systems of arbitrary mass ratios.

# Appendix A

# The first-order and second-order metric perturbations

In this appendix we give the formulas for the first- and second-order fields, whose derivation was outlined in Chapter 2. $h^1_{\alpha\beta}$ and $h^2_{\alpha\beta}$ split into a singular and a regular piece as

$$h^1_{\alpha\beta} = h^{\rm S1}_{\alpha\beta} + h^{\rm R1}_{\alpha\beta}\,, \tag{A.1a}$$

$$h^2_{\alpha\beta} = h^{\rm S2}_{\alpha\beta} + h^{\rm R2}_{\alpha\beta}\,. \tag{A.1b}$$

The full expressions for the singular field components take the form [1,46]

$$\begin{aligned}
h^{\rm S1}_{tt} &= \frac{2\mu}{r} + 3\mu\, a_i n^i + \mu\, r\left[4a_a a^a + \left(\frac{5}{3}\mathcal{E}_{ab} + \frac{3}{4}a_a a_b\right)\hat{n}^{ab}\right] \\
&\quad + \mu r^2\left[\frac{9}{5}a_a a^a a_b n^b + \frac{87}{20}\mathcal{E}_{ab}a^a n^b + \left(\frac{7}{12}\mathcal{E}_{abc} + \frac{3}{2}\mathcal{E}_{bc}a_a - \frac{1}{8}a_a a_b a_c\right)\hat{n}^{abc}\right] \\
&\quad + O(r^3),
\end{aligned} \tag{A.2a}$$

$$\begin{aligned}
h^{\rm S1}_{ta} &= \mu r\left[\frac{2}{3}\mathcal{B}^{bc}\varepsilon_{acd}\hat{n}^d_b - 2\dot{a}_a\right] \\
&\quad + \mu r^2\Bigg[\left(\frac{7}{30}\mathcal{B}_b{}^d\varepsilon_{acd}a^b - \frac{73}{30}\mathcal{B}_b{}^d\varepsilon_{acd}a^b + \frac{7}{6}\mathcal{B}_a{}^d\varepsilon_{bcd}a^b\right)n^c \\
&\quad + \left(a_b\dot{a}_a - \frac{19}{30}\dot{\mathcal{E}}_{ab} + 2a_a\dot{a}_b\right)n^b - \frac{1}{18}\dot{\mathcal{E}}^{bc}\hat{n}_{abc} + \frac{7}{9}\mathcal{B}^{cd}\varepsilon_{ac}{}^i a^b\hat{n}_{bdi} \\
&\quad - \frac{2}{9}\mathcal{B}^{bcd}\varepsilon_{ab}{}^i\hat{n}_{cdi}\Bigg] + O(r^3),
\end{aligned} \tag{A.2b}$$

$$h^{\rm S1}_{ab} = \frac{2\mu\delta_{ab}}{r} - \mu\delta_{ab}a_i n^i$$

$$
\begin{aligned}
&+\mu r\left[4a_a a_b-\frac{38}{9}\mathcal{E}_{ab}+\frac{4}{3}\mathcal{E}_{(a}{}^{c}\hat{n}_{b)c}+\left(\frac{3}{4}a_c a_d-\mathcal{E}_{cd}\right)\delta_{ab}\hat{n}^{cd}\right]\\
&+\mu r^2\Bigg[\left(\frac{11}{5}\mathcal{E}_{ab}a^c-6a_a a_b a^c\right)n^c-\frac{2}{15}\mathcal{E}_{c(a}a^c\hat{n}_c+\frac{1}{12}\mathcal{E}_{cd}a^c\delta_{ab}n^d\\
&+\left(\frac{58}{15}\mathcal{E}_{c(a}a_{b)}-\frac{31}{15}\mathcal{E}_{abc}-\frac{68}{45}\dot{\mathcal{B}}_{(a}{}^{d}\varepsilon_{b)cd}-\frac{1}{4}\delta_{ab}\ddot{a}_c\right)n^c\\
&+\frac{2}{3}\left(\mathcal{E}_{(a}{}^{cd}-\mathcal{E}_{(a}{}^{d}a^c\right)\hat{n}_{b)cd}+\frac{2}{9}\dot{\mathcal{B}}^{cd}\varepsilon^{i}{}_{c(a}\hat{n}_{b)di}\\
&+\left(\frac{5}{6}\mathcal{E}^{di}a^c-\frac{5}{12}\mathcal{E}^{cdi}-\frac{5}{8}a^c a^d a^i\right)\delta_{ab}\hat{n}_{cdi}\Bigg]+O(r^3). \qquad \text{(A.2c)}
\end{aligned}
$$

The $O(1/r)$ term in Eqs. (A.2) is the Newtonian-like field of the small body. The higher-order terms in Eq. (A.2) are generalisations of the "Newtonian" field to include the acceleration of the small body's worldline and tidal forces due to the external spacetime of the black hole. The first-order regular-field components, in terms of the coefficients in the STF expansion (2.38), are given by [46]

$$
\begin{aligned}
h^{\rm R1}_{tt} &= \hat{A}^{(1,0)}+r\hat{A}^{(1,1)}_i n^i\,, && \text{(A.3a)}\\
h^{\rm R1}_{ta} &= \hat{C}^{(1,0)}_{ta}+r\left(\hat{B}^{(1,1)}n_a+\hat{C}^{(1,1)}_{ia}n^i+\varepsilon_{aij}\hat{D}^{(1,1)j}n^j\right), && \text{(A.3b)}\\
h^{\rm R1}_{ab} &= \delta_{ab}\hat{K}^{(1,0)}+\hat{H}^{(1,0)}_{ab}\\
&\quad+r\left(\delta_{ab}\hat{K}^{(1,1)}_i n^i+\hat{H}^{(1,1)}_{abi}n^i+\varepsilon_{ij(a}\hat{I}^{(1,1)j}_{b)}n^i+\hat{F}^{(1,1)}_{\langle a}n_{b\rangle}\right). && \text{(A.3c)}
\end{aligned}
$$

$h^{\rm R1}_{\alpha\beta}$ is a vacuum solution of the first-order wave equation $E_{\alpha\beta}[h^{\rm R1}]=0$, finite and $C^\infty$ everywhere, including on the worldline. The regular field is unknown analytically. It can be calculated by solving the first-order field equation numerically with retarded boundary conditions. This is explained in more detail in Chapter 4.

The second-order singular field splits into the sum of four pieces [1, 46] as

$$
h^{\rm S2}_{\alpha\beta}=h^{\rm SS}_{\alpha\beta}+h^{\rm SR}_{\alpha\beta}+h^{\delta m}_{\alpha\beta}+h^{\delta z}_{\alpha\beta}. \qquad \text{(A.4)}
$$

The first piece,

$$
\begin{aligned}
h^{\rm SS}_{tt} &= -\frac{2\mu^2}{r^2}-\frac{10\mu^2 a_i n^i}{r}-\mu^2 r^0\left(\frac{7}{3}\mathcal{E}_{ab}+\frac{29}{3}a_a a_b\right)\hat{n}^{ab}\\
&\quad+4\mu^2 a_a a^a\ln r+O(r\ln r)\,, \qquad \text{(A.5a)}
\end{aligned}
$$

$$
h^{\rm SS}_{ta}=\mu^2 r^0\left(\frac{1}{2}\dot{a}_b\hat{n}_a^b-\frac{10}{3}\mathcal{B}^{bc}\varepsilon_{acd}\hat{n}_b{}^d\right)-8\mu^2\dot{a}_a\ln r+O(r\ln r)\,, \qquad \text{(A.5b)}
$$

$$
h^{\rm SS}_{ab}=\frac{8\mu^2\delta_{ab}}{3r^2}-\frac{7\mu^2\hat{n}_{ab}}{3r^2}+\frac{\mu^2}{r}\left[\frac{31}{5}a_{(a}n_{b)}-\frac{37}{5}a^c\delta_{ab}n_c+\frac{14}{3}a^c\hat{n}_{abc}\right]
$$

$$+ \mu^2 r^0 \Bigg[ \left(4\mathcal{E}_{c(a} - a_c a_{(a}\right) \hat{n}_{b)}{}^c - \frac{7}{2} a_c a^c \hat{n}_{ab} + \left(\frac{10}{3} a_c a_d - \frac{4}{3}\mathcal{E}_{cd}\right) \delta_{ab}\hat{n}^{cd}$$
$$+ \left(\frac{7}{5}\mathcal{E}_{cd} - \frac{56}{15} a_c a_d\right) \hat{n}_{ab}{}^{cd} \Bigg]$$
$$+ \mu^2 \left(\frac{68}{15} a_c a^c \delta_{ab} - \frac{16}{15}\mathcal{E}_{ab} - \frac{8}{5} a_a a_b\right) \ln r + O(r \ln r), \tag{A.5c}$$

is a solution to $E_{\alpha\beta}[h^{\rm SS}] = 2\delta^2 R_{\alpha\beta}\,[\,h^{\rm S1}\,,\,h^{\rm S1}\,]$ away from the worldline, i.e. $r \neq 0$. The second piece,

$$h^{\rm SR}_{tt} = -\frac{\mu h^{\rm R1}_{ab}(\gamma)\hat{n}^{ab}}{r} + O(r^0)\,, \tag{A.6a}$$
$$h^{\rm SR}_{ta} = -\frac{\mu h^{\rm R1}_{tb}(\gamma)\hat{n}_a{}^b}{r} + O(r^0)\,, \tag{A.6b}$$
$$h^{\rm SR}_{ab} = \frac{\mu}{r}\left[2h^{\rm R1}_{c(a}(\gamma)\hat{n}_{b)}{}^c - \delta_{ab}h^{\rm R1}_{cd}(\gamma)\hat{n}^{cd} - \left(h^{\rm R1}_{ij}(\gamma)\delta^{ij} + h^{\rm R1}_{tt}(\gamma)\right)\hat{n}_{ab}\right] + O(r^0)\,, \tag{A.6c}$$

is a solution to $E_{\alpha\beta}\,[\,h^{\rm SR}\,] = 2\delta^2 R_{\alpha\beta}\,[\,h^{\rm S1}\,,h^{\rm R1}\,] + 2\delta^2 R_{\alpha\beta}\,[\,h^{\rm R1}\,,h^{\rm S1}\,]$, away from the worldline ($r \neq 0$). In Eqs. (A.6), $h^{\rm R1}(\gamma)$ denotes the first-order regular field evaluated on the worldline $\gamma$. The third piece,

$$h^{\delta m}_{tt} = \frac{\delta m_{tt}}{r} + O(r^0)\,, \tag{A.7a}$$
$$h^{\delta m}_{ta} = \frac{\delta m_{ta}}{r} + O(r^0)\,, \tag{A.7b}$$
$$h^{\delta m}_{ab} = \frac{\delta m_{ab}}{r} + O(r^0)\,, \tag{A.7c}$$

is a solution to the homogeneous wave equation $E_{\alpha\beta}\,[\,h^{\delta m}\,] = 0$ at $r \neq 0$. In a domain that includes $r = 0$ it is a solution to the sourced equation

$$E_{\alpha\beta}[\,h^{\delta m}\,] = -4\pi\delta m_{\alpha\beta}(t)\delta^3(x^i). \tag{A.8}$$

The components $\delta m_{\alpha\beta}$ are constrained by the gauge condition (2.26) at order $O(1/r)$ to be

$$\delta m_{tt} = -2\mu h^{\rm R1}_{tt}(\gamma) - \frac{\mu}{3}\delta^{ab}h^{\rm R1}_{ab}(\gamma)\,, \tag{A.9a}$$
$$\delta m_{ta} = -4\mu\delta\dot{z}_a - \frac{4\mu}{3}h^{\rm R1}_{ta}(\gamma)\,, \tag{A.9b}$$
$$\delta m_{ab} = \frac{2\mu}{3}h^{\rm R1}_{ab}(\gamma) + \frac{\mu}{3}\delta_{ab}\delta^{ij}h^{\rm R1}_{ij}(\gamma) + \frac{2\mu}{3}\delta_{ab}h^{\rm R1}_{tt}(\gamma)\,. \tag{A.9c}$$

The final piece, $h^{\delta z}_{\alpha\beta}$, is given by

$$h^{\delta z}_{tt} = \frac{2\mu\delta z_a n^a}{r^2} + O(r^0), \tag{A.10a}$$
$$h^{\delta z}_{ta} = O(r^0), \tag{A.10b}$$

$$h^{\delta z}_{ab} = \frac{2\mu\delta z_c n^c \delta_{ab}}{r^2} + O(r^0). \tag{A.10c}$$

$h^{\delta z}_{\alpha\beta}$ is a solution to the homogeneous wave equation $E_{\alpha\beta}[\,h^{\delta z}\,] = 0$ off $r = 0$. In a domain including $r = 0$ it is a solution to the wave equation with a source equivalent to that created by the displacement of a point mass,

$$E_{\alpha\beta}[\,h^{\delta z}\,] = 8\pi\mu\delta_{\alpha\beta}\delta z^a \partial_a \delta^3(x^i). \tag{A.11}$$

# Appendix B

# Fermi-Walker coordinates

We begin with a description of Fermi-Walker coordinates and associated notation, relevant to the discussion in Chapter 3. Let $\gamma$ refer to a generic time-like worldline, as depicted in Fig. B.1 and coordinates on $\gamma$ shall be denoted as $\bar{x}$ with a bar on top. We assume that $\bar{x}$ lies within a normal convex neighbourhood of $x$. The spacelike geodesic $\beta$ links the points $x$ and $\bar{x}$, where $\beta$ intercepts $\gamma$ orthogonally at $\bar{x}$. The tangent vector on $\beta$ is $-\sigma^{\bar{\alpha}}$. We will refer to ordinary coordinates off $\gamma$ as $x$ without a bar. Indices of tensor quantities evaluated on $\gamma$ shall be denoted by Greek letters with a bar on top, e.g. $u^{\bar{\alpha}}$ and those evaluated off $\gamma$ shall be denoted by Greek letters, without a bar. Let $u^{\bar{\alpha}}$ be the four-velocity on $\gamma$ and let $\tau$ refer to proper time on $\gamma$. We will use $\beta$ to refer to the unique, spacelike geodesic that connects the points $x$ and $\bar{x}$, and intersects $\gamma$ at $\bar{x}$ orthogonally, as shown in Fig. B.1. The spatial geodesic distance between $x$ and $\bar{x}$ is given by $2\sigma(x,\bar{x})$, where $\sigma(x,\bar{x})$ is the Synge world-function [46]. Note that in this construction $u_{\bar{\alpha}}\sigma^{\bar{\alpha}} = 0$.

We begin by constructing the tetrad

$$e^{\bar{\alpha}}_{\mu}(\bar{x}) = \Big\{ u^{\bar{\alpha}}(\bar{x}), e^{\bar{\alpha}}_{a}(\bar{x}) \Big\} \,, \tag{B.1}$$

and the dual-tetrad

$$\tilde{e}^{\mu}_{\bar{\alpha}}(\bar{x}) = \Big\{ - u_{\bar{\alpha}}(\bar{x}), \tilde{e}^{a}_{\bar{\alpha}}(\bar{x}) \Big\} \tag{B.2}$$

on $\gamma$, such that

$$e^{\bar{\alpha}}_{\nu}\tilde{e}^{\mu}_{\bar{\alpha}} = \delta^{\mu}_{\nu}. \tag{B.3}$$

The tetrad and dual tetrad satisfy the orthogonality relations

$$g_{\bar{\alpha}\bar{\beta}}\, e^{\bar{\alpha}}_{\mu}\, e^{\bar{\beta}}_{\nu} \;=\; \eta_{\mu\nu} \qquad g^{\bar{\alpha}\bar{\beta}}\, \tilde{e}^{\mu}_{\bar{\alpha}}\, \tilde{e}^{\nu}_{\bar{\beta}} \;=\; \eta^{\mu\nu} \,, \tag{B.4}$$

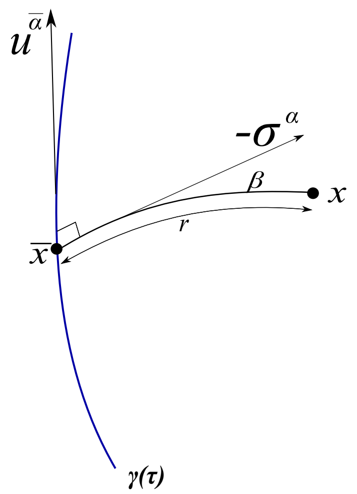


Figure B.1: The point $\bar x$ on the generic timelike worldline $\gamma$, whose tangent vector is $u^{\bar\alpha}$. Proper time on $\gamma$ is $\tau$. The spacelike geodesic $\beta$ links the points $x$ and $\bar x$, where $\beta$ intercepts $\gamma$ orthogonally at $\bar x$, and $r = \sqrt{2\sigma(x,\bar x)}$ is the spatial geodesic distance between $x$ and $\bar x$, where $\sigma(x,\bar x)$ is the Synge world-function [46]. The tangent vector along $\beta$ is $-\sigma^\alpha$. Fermi-Walker coordinates $(t, x^a)$ are constructed at the point $x$, such that $t = \bar\tau$, the proper time on $\gamma$ at $\bar x$, and $x^a = -e^a_{\bar\alpha}\sigma^{\bar\alpha}$, where $(u^{\bar\alpha}, e^{\bar\alpha}_a)$ is the tetrad which is orthogonal Fermi-Walker transported along $\gamma$, according to (B.7).

and the completeness relations,

$$g_{\bar\alpha\bar\beta} = \tilde e^\mu_{\bar\alpha}\,\tilde e^\nu_{\bar\beta}\,\eta_{\mu\nu} \qquad g^{\bar\alpha\bar\beta} = e^{\bar\alpha}_\mu\, e^{\bar\beta}_\nu\,\eta^{\mu\nu}\,. \tag{B.5}$$

The tetrad $e^{\bar\alpha}_a$ is said to be Fermi-Walker transported along $\gamma$ if [46]

$$\frac{De^{\bar\alpha}_a}{d\tau} = a_{\bar\beta}e^{\bar\beta}_a u^{\bar\alpha} - u_{\bar\beta}e^{\bar\beta}_a a^{\bar\alpha} \tag{B.6}$$

holds true, where $a^{\bar\alpha} \equiv Du^{\bar\alpha}/d\tau$ is the four-acceleration of $\gamma$. Eq. (B.6) guarantees that $D(u_{\bar\alpha}e^{\bar\alpha}_a)/d\tau = 0$, such that if $u_{\bar\alpha}e^{\bar\alpha}_a = 0$ at some point $\bar x_0$ on $\gamma$, $u_{\bar\alpha}$ and $e^{\bar\alpha}_a$ will remain orthogonal everywhere on $\gamma$. Hence, for $u_{\bar\alpha}$ and $e^{\bar\alpha}_a$ orthogonal, they are Fermi-Walker transported along $\gamma$ as

$$\frac{De^{\bar\alpha}_a}{d\tau} = a_a u^{\bar\alpha}, \tag{B.7}$$

where $a_a \equiv a_{\bar\alpha}e^{\bar\alpha}_a$ are the spatial components of $\gamma$'s acceleration.

Fermi-Walker coordinates $(t, x^a)$ are constructed from a tetrad $(u^{\bar\alpha}, e^{\bar\alpha}_a)$ established along $\gamma$, which are Fermi-Walker transported according to (B.7). At each instant $\bar\tau$ of proper time, spatial geodesics are sent out orthogonally from the point $\bar{x} = z(\bar{\tau})$ on $\gamma$ (see Fig. B.1). These geodesics generate a spatial hypersurface $\Sigma_{\bar{\tau}}$, and on that hypersurface coordinates $x^a$ are defined as

$$x^a = -e^a_{\bar{\alpha}}\sigma^{\bar{\alpha}}. \tag{B.8}$$

Each of the hypersurfaces is labelled with time $t = \bar{\tau}$, defining the coordinates $(t, x^a)$ at each point in the convex normal neighbourhood of $\gamma$. As such, the time coordinate $t$ at $x$ is equal to the proper time $\tau$ on $\bar{\gamma}$ at the point $\bar{x}$, where $\beta$ intersects $\gamma$ (orthogonally).

Using the definition of the Synge world-function, we may define the spatial unit vector $n^a$ as

$$n^a \equiv \frac{x^a}{r}, \tag{B.9}$$

$$r = \sqrt{2\bar{\sigma}}, \tag{B.10}$$

where we use the notation

$$\bar{\sigma} \equiv \sigma(x, \bar{x}) \tag{B.11}$$

to refer to the world-function $\sigma(x, \bar{x})$.

Consider what happens when the field point shifts from $x$ to $x + \delta x$. Since the field point $x$ and the source point $\bar{x}$ are inextricably linked through $\beta$, this will induce a corresponding variation in the source point, from $\bar{x}$ to $\bar{x} + \delta\bar{x}$. This can be expressed as $\delta\bar{x}^{\bar{\alpha}} = u^{\bar{\alpha}}\delta\tau$, where $\delta\tau$, the proper time difference on $\gamma$ between the points $\bar{x}$ and $\bar{x}+\delta\bar{x}$, is equal to $\delta t$ in Fermi-Walker coordinates.

From Eq. (B.8), the relationship between $\delta x$ and $\delta\bar{x}$ is

$$\begin{aligned} x^a \to x^a + \delta x^a &= -\tilde{e}^a_{\bar{\alpha}}(\bar{x} + \delta\bar{x})\sigma^{\bar{\alpha}}(x + \delta x, \bar{x} + \delta\bar{x}) \\ &= -\tilde{e}^a_{\bar{\alpha}}(\bar{x})\sigma^{\bar{\alpha}}(x, \bar{x}) - u^{\bar{\beta}}\nabla_{\bar{\beta}}\tilde{e}^a_{\bar{\alpha}}\delta t\sigma^{\bar{\alpha}} - \tilde{e}^a_{\bar{\alpha}}\sigma^{\bar{\alpha}}_{\bar{\beta}}\delta u^{\bar{\beta}}\delta t - \tilde{e}^a_{\bar{\alpha}}\sigma^{\bar{\alpha}}_{\beta}\delta x^{\beta}. \end{aligned} \tag{B.12}$$

Equating the coefficients of $\delta x$ yields

$$\delta x^a = -a^a u_{\bar{\alpha}}\sigma^{\bar{\alpha}}\delta t - \tilde{e}^a_{\bar{\alpha}}\sigma^{\bar{\alpha}}_{\bar{\beta}}u^{\bar{\beta}}\delta t - \tilde{e}^a_{\bar{\alpha}}\sigma^{\bar{\alpha}}_{\bar{\beta}}\delta x^{\beta}. \tag{B.13}$$

$\delta t$ is determined by imposing that (3.16) should hold true even after varying $x$, such that

$$\begin{aligned} \sigma_{\bar{\alpha}}(x + \delta x, \bar{x} + \delta\bar{x})u^{\bar{\alpha}}(\bar{x} + \delta\bar{x}) &= \sigma_{\bar{\alpha}}(x, \bar{x})u^{\bar{\alpha}}(\bar{x}) + \sigma_{\bar{\alpha}\beta}u^{\bar{\alpha}}\delta x^{\beta} + \sigma_{\bar{\alpha}\bar{\beta}}u^{\bar{\alpha}}u^{\bar{\beta}}\delta t \\ &\quad + \sigma_{\bar{\alpha}}(\nabla_{\bar{\beta}}u^{\bar{\alpha}})u^{\bar{\beta}}\delta t \\ &= 0. \end{aligned} \tag{B.14}$$

After rearranging terms, we find

$$\delta t = B\sigma_{\bar{\alpha}\beta}u^{\bar{\alpha}}\delta x^{\beta}\,, \qquad\qquad B \equiv -\left(\sigma_{\bar{\alpha}\bar{\beta}}u^{\bar{\alpha}}u^{\bar{\beta}} + \sigma_{\bar{\alpha}}a^{\bar{\alpha}}\right)^{-1}, \tag{B.15}$$

where in the last step, $a^{\bar{\alpha}} \equiv u^{\bar{\alpha}}_{;\bar{\beta}}u^{\bar{\beta}}$ was used. Substituting Eq. (B.15) into Eq. (B.13) yields

$$\delta x^{a} = -\tilde{e}^{a}_{\bar{\alpha}}\left(\sigma^{\bar{\alpha}}_{\beta} + B\sigma^{\bar{\alpha}}_{\bar{\beta}}u^{\bar{\beta}}\sigma_{\beta\bar{\gamma}}u^{\bar{\gamma}}\right)\delta x^{\beta}. \tag{B.16}$$

Eqs. (B.15) and (B.16) give the one-forms $dt$ and $dx^a$, in terms of Fermi-Walker coordinates.

Now let us proceed to derive expressions for $dt$ and $dx^a$ in covariant form. We will make use of the following expressions [46] for the parallel propagator,

$$g^{\bar{\alpha}}_{\beta}(x,\bar{x}) = \tilde{e}^{\mu}_{\beta}(x)e^{\bar{\alpha}}_{\mu}(\bar{x}) = u^{\bar{\alpha}}(\bar{x})\tilde{e}^{0}_{\beta}(x) + e^{\bar{\alpha}}_{a}(\bar{x})\tilde{e}^{a}_{\beta}(x), \tag{B.17}$$

the near-coincidence expansions,

$$\sigma_{\bar{\alpha}\bar{\beta}} = g_{\bar{\alpha}\bar{\beta}} - \frac{1}{3}R_{\bar{\alpha}\bar{\mu}\bar{\beta}\bar{\nu}}\sigma^{\bar{\mu}}\sigma^{\bar{\nu}} - \frac{1}{12}\nabla_{\bar{\gamma}}R_{\bar{\alpha}\bar{\mu}\bar{\beta}\bar{\nu}}\sigma^{\bar{\gamma}}\sigma^{\bar{\mu}}\sigma^{\bar{\nu}} + O(r^4), \tag{B.18}$$

$$\sigma_{\bar{\alpha}\beta} = -g^{\bar{\gamma}}_{\alpha}\left(g_{\bar{\alpha}\bar{\gamma}} + \frac{1}{6}R_{\bar{\alpha}\bar{\mu}\bar{\beta}\bar{\nu}}\sigma^{\bar{\mu}}\sigma^{\bar{\nu}} + \frac{1}{12}\nabla_{\bar{\lambda}}R_{\bar{\alpha}\bar{\mu}\bar{\beta}\bar{\nu}}\sigma^{\bar{\lambda}}\sigma^{\bar{\mu}}\sigma^{\bar{\nu}}\right) + O(r^4), \tag{B.19}$$

and the definitions

$$R_{0\bar{\mu}0\bar{\nu}} = R_{\bar{\alpha}\bar{\mu}\bar{\beta}\bar{\nu}}u^{\bar{\alpha}}u^{\bar{\beta}},\quad R_{\bar{\alpha}a\bar{\beta}b} = R_{\bar{\alpha}\bar{\mu}\bar{\beta}\bar{\nu}}\tilde{e}^{\bar{\mu}}_{a}\tilde{e}^{\bar{\nu}}_{b},\quad a_b = \tilde{e}^{\bar{\alpha}}_{b}a_{\bar{\alpha}},\quad \nabla_c = \tilde{e}^{\bar{\gamma}}_{c}\nabla_{\bar{\gamma}}. \tag{B.20}$$

Inserting Eqs. (B.18) and (B.19) into Eq. (B.15) returns

$$\begin{aligned} B &= \left(1 + \frac{1}{3}R_{0a0b}x^a x^b + \frac{1}{12}\nabla_c R_{0a0b}x^a x^b x^c + a_b x^b\right)^{-1} \\ &= 1 - a_b x^b + (a_b x^b)^2 - \frac{1}{3}R_{0a0b}x^a x^b - (a_b x^b)^3 + \frac{2}{3}a_c R_{0a0b}x^a x^b x^c \\ &\quad - \frac{1}{12}\nabla_c R_{0a0b}x^a x^b x^c + O(x^4). \end{aligned} \tag{B.21}$$

Now, making use of the near-coincidence expansion (B.19), we find that

$$\begin{aligned} \sigma_{\bar{\alpha}\beta}u^{\bar{\alpha}} &= \left(1 - \frac{1}{6}R_{0a0b}x^a x^b - \frac{1}{12}\nabla_c R_{0a0b}x^a x^b x^c\right)\tilde{e}^{0}_{\beta} \\ &\quad - \left(\frac{1}{6}R_{0bac}x^b x^c + \frac{1}{12}\nabla_d R_{0bac}x^b x^c x^d\right)\tilde{e}^{a}_{\beta}. \end{aligned} \tag{B.22}$$

Substituting this and (B.21) into (B.15), and using the covariant form $t_\alpha \equiv \partial_\alpha t$, leads to the result

$$\begin{aligned} t_\alpha = &\Big(1 - a_b x^b + (a_b x^b)^2 - \frac{1}{2}R_{0a0b}x^a x^b - (a_b x^b)^3 + \frac{5}{6}a_c R_{0a0b}x^a x^b x^c \\ &- \frac{1}{6}\nabla_c R_{0a0b}x^a x^b x^c\Big)\tilde{e}^0_\alpha - \Big(R_{0bac}\left(1 - a_d x^d\right)x^b x^c \\ &+ \frac{1}{2}\nabla_d R_{0bac}x^b x^c x^d\Big)\tilde{e}^a_\alpha. \end{aligned} \tag{B.23}$$

From the definition of the parallel propagator (B.17), the near-coincidence expansions (B.18) and (B.19), and the result of Eq. (B.22), we find

$$\begin{aligned} -\tilde{e}^a_{\bar{\alpha}}\sigma^{\bar{\alpha}}_{\beta} = &\left(\delta^a_i + \frac{1}{6}R^a{}_{bic}x^b x^c + \frac{1}{12}\nabla_d R^a{}_{bic}x^b x^c x^d\right)\tilde{e}^i_\beta \\ &+ \left(\frac{1}{6}R^a{}_{b0c}x^b x^c + \frac{1}{12}\nabla_d R^a{}_{b0c}x^b x^c x^d\right)\tilde{e}^0_\beta, \end{aligned} \tag{B.24}$$

and

$$-B\tilde{e}^a_{\bar{\alpha}}\sigma^{\bar{\alpha}}_{\beta}\sigma_{\beta}{}_{\bar{\gamma}}u^{\bar{\beta}}u^{\bar{\gamma}} = \left(\frac{1}{3}R^a{}_{b0c}x^b x^c + \frac{1}{12}\nabla_d R^a{}_{b0c}x^b x^c x^d - \frac{1}{3}a_d R^a{}_{b0c}x^b x^c x^d\right)\tilde{e}^0_\beta. \tag{B.25}$$

Now substituting Eqs. (B.24) and (B.25) into Eq. (B.16), and using the covariant form $x^a_\alpha \equiv \partial_\alpha x^a$, yields

$$\begin{aligned} x^a_\alpha = &\left(\frac{1}{2}R^a{}_{b0c}x^b x^c + \frac{1}{6}\nabla_d R^a{}_{b0c}x^b x^c x^d - \frac{1}{3}a_d R^a{}_{b0c}x^b x^c x^d\right)\tilde{e}^0_\alpha \\ &+ \left(\delta^a_b + \frac{1}{6}R^a{}_{cbd}x^c x^d + \frac{1}{12}\nabla_e R^a{}_{cbd}x^c x^d x^e\right)\tilde{e}^b_\alpha. \end{aligned} \tag{B.26}$$

The formulas in (B.23) and (B.26) are needed in Chapter 3, where we write covariant expressions for the puncture field.

In order to derive expressions for the metric in Fermi-Walker coordinates, the formulas (B.23) and (B.26) need to be inverted to find expressions for $\tilde{e}^0_\alpha$ and $\tilde{e}^a_\alpha$. Write $t_\alpha$ and $x^a_\alpha$ in the format $t_\alpha = A\tilde{e}^0_\alpha + B_a\tilde{e}^a_\alpha$ and $x^a_\alpha = C^a\tilde{e}^0_\alpha + D^a_b\tilde{e}^b_\alpha$. This implies that $\tilde{e}^0_\alpha = A^{-1}(t_\alpha - B_a\tilde{e}^a_\alpha)$ and $\tilde{e}^b_\alpha = (D^a_b - A^{-1}C^a B_b)^{-1}(x^a_\alpha - A^{-1}C^a t_\alpha)$. $A$ and $B_a$ are easily read off Eq. (B.23). Inverting them yields the result

$$\begin{aligned} \tilde{e}^0_\alpha = &\left(1 + a_b x^b + \frac{1}{2}R_{0a0b}x^a x^b + \frac{1}{6}a_c R_{0a0b}x^a x^b x^c + \frac{1}{6}\nabla_d R_{0bac}x^b x^c x^d\right)t_\alpha \\ &+ \frac{1}{6}\left(R_{0bac}x^b x^c + \frac{1}{2}\nabla_d R_{0bac}x^b x^c x^d\right)x^a_\alpha + O(r^4). \end{aligned} \tag{B.27}$$

Likewise, $C^a$ and $D^a_b$ are easily read off Eq. (B.26). The $D^a_b$ are inverted using the expansion $(D^a_b)^{-1} = (\delta^a_b + \Delta^a_b)^{-1} = \delta^b_a - \Delta^b_a + \Delta^b_c\Delta^c_a - \Delta^b_c\Delta^c_d\Delta^d_a + \ldots$. Overall we find

$$\begin{aligned}\tilde{e}^b_\alpha &= \left(\delta^b_a - \frac{1}{6}R^b{}_{cad}x^c x^d - \frac{1}{12}\nabla_e R^b{}_{cad}x^c x^d x^e\right) x^a_\alpha \\ &\quad - \left(\frac{1}{2}R^b{}_{j0k}x^j x^k + \frac{1}{6}a_\ell R^b{}_{j0k}x^j x^k x^\ell + \frac{1}{6}\nabla_\ell R^b{}_{j0k}x^j x^k x^\ell\right) t_\alpha + O(r^4). \qquad \text{(B.28)}\end{aligned}$$

Now substituting Eqs. (B.27) and (B.28) into the completeness relations (B.5), we derive the metric components in Fermi-Walker coordinates as

$$g_{tt} = -1 - 2a_b x^b - (a_b x^b) - \mathcal{E}_{ab}x^a x^b - \frac{4}{3}a_c\mathcal{E}_{ab}x^a x^b x^c - \frac{1}{3}\mathcal{E}_{ab|c}x^a x^b x^c + O(r^4), \quad \text{(B.29a)}$$

$$g_{ta} = -\frac{2}{3}\epsilon_{aci}\mathcal{B}^i_b x^b x^c - \frac{1}{3}\varepsilon_{aci}a_d\mathcal{B}^i_b x^b x^c x^d - \frac{1}{4}\varepsilon_{aci}\mathcal{B}^i_{b|d}x^b x^c x^d + O(r^4), \quad \text{(B.29b)}$$

$$\begin{aligned}g_{ab} &= \delta_{ab} - \frac{1}{3}\delta_{ab}\mathcal{E}_{ij}x^i x^j - \frac{1}{3}\mathcal{E}_{ab}r^2 - \frac{1}{3}\mathcal{E}_{ai}x^i x_b - \frac{1}{3}\mathcal{E}_{bi}x^i x_a \\ &\quad - \frac{1}{6}\delta_{ab}\mathcal{E}_{ab|c}x^a x^b x^c - \frac{1}{6}\mathcal{E}_{ab|c}x^a x^b x^c - \frac{1}{3}\mathcal{E}_{ab|i}x^a x^b x^i + O(r^4). \qquad \text{(B.29c)}\end{aligned}$$

where the notation| refers to covariant differentiation with respect to spatial coordinates, as in Eq. (3.17). For example $\mathcal{E}_{ab|c} = R_{0a0b|c} = R_{0\bar{\alpha}0\bar{\beta};\bar{\mu}}e^{\bar{\alpha}}_a e^{\bar{\beta}}_b e^{\bar{\mu}}_c$. The inverse-metric components are

$$g^{tt} = -1 + 2a_b x^b - 3(a_b x^b) + \mathcal{E}_{ab}x^a x^b + O(r^3), \quad \text{(B.30a)}$$

$$g^{ta} = -\frac{2}{3}\varepsilon^a{}_{ci}\mathcal{B}^i_b x^b x^c + O(r^3), \quad \text{(B.30b)}$$

$$g^{ab} = \delta^{ab} + \frac{1}{3}\delta^{ab}\mathcal{E}_{ij}x^i x^j + \frac{1}{3}\mathcal{E}^{ab}r^2 - \frac{1}{3}\mathcal{E}^{ai}x_i x^b - \frac{1}{3}\mathcal{E}^{bi}x_i x^a + O(r^3). \quad \text{(B.30c)}$$

The Christoffel symbols are readily derived from the metric and inverse-metric components. We find the non-vanishing components to be

$$\Gamma^t_{tt} = \dot{a}_i x^i + O(r^2), \quad \text{(B.31a)}$$

$$\Gamma^t_{bt} = a_b - a_b a_i x^i + \mathcal{E}_{bi}x^i + O(r^2), \quad \text{(B.31b)}$$

$$\Gamma^b_{tt} = a^b + a^b a_i x^i + \mathcal{E}^{bi}x_i + O(r^2), \quad \text{(B.31c)}$$

$$\Gamma^c_{ab} = \frac{2}{3}\delta_{ab}\mathcal{E}^{ci}x_i + \frac{2}{3}\mathcal{E}_{ab}x^c - \frac{2}{3}\delta^c_{(a}\mathcal{E}_{b)i}x^i - \frac{2}{3}x_{(a}\mathcal{E}^c_{b)} + O(r^2), \quad \text{(B.31d)}$$

$$\Gamma^t_{ab} = -\frac{1}{3}\varepsilon_{bij}\mathcal{B}^j_a x^i - \frac{1}{3}\varepsilon_{aij}\mathcal{B}^j_b x^i + O(r^2), \quad \text{(B.31e)}$$

$$\Gamma^a_{tb} = \varepsilon^a{}_{bi}\mathcal{B}^i_j x^j + O(r^2). \quad \text{(B.31f)}$$

This completes our overview of Fermi-Walker coordinates.

# Appendix C

# First-order puncture fields and their harmonic decomposition.

In this appendix we explain how we derive the non-vanishing components of the first-order puncture field, in Schwarzschild coordinates for a circular orbit in a Schwarzschild background spacetime. After obtaining these expressions, we derive the frequency-domain, tensor-harmonic modes. Wardell was the first to derive these formulas for the modes [74], but I independently derived formulas for them and successfully checked my own results with those of Wardell.

We will explain how to write our covariant expression (3.60) for the first-order singular field for a circular orbit in Schwarzschild, using the leading order term as an example. The same method may be applied to all remaining terms. The leading-order piece comes out of the first term in (3.60),

$$h^{\mathrm{S1}\,[1]}_{\mu\nu} = \frac{2\mu}{\mathsf{s}} g^{\tau'}_{\mu} g^{\kappa'}_{\nu} \left(g_{\tau'\kappa'} + 2u_{\tau'}u_{\kappa'}\right), \tag{C.1}$$

where $u^{\mu'}$ is the four velocity of $\gamma$. We remind the reader of the relations in Eqs. (3.30) and (3.31): $\mathsf{s}^2 = \mathsf{r}^2 + 2\sigma$ and $\mathsf{r} = \sigma_{\mu'}u^{\mu'}$, where $\sigma = \sigma(x, x')$ is the Synge world function. We recall from the discussion in Chapter 3 that $x$ denotes the coordinates of a generic point off $\gamma$ and $x'$ denotes coordinates of some point on $\gamma$.

From the coordinate expansions in Eq. (3.68) for $\sigma$, we find that

$$\mathsf{s} = \left[\lambda^2\rho^2 + \lambda^3 A_{\tau'\kappa'\nu'}\Delta x^{\tau'}\Delta x^{\kappa'}\Delta x^{\nu'} + O(\lambda^4)\right]^{1/2}, \tag{C.2}$$

with $\Delta x^{\nu'} \equiv x^{\nu} - x^{\nu'}$, $A_{\tau'\kappa'\nu'} = g_{\tau'\kappa',\nu'}(x')/4$ from [88], and

$$\rho = \left[\left(g_{\mu'\nu'}\Delta x^{\mu'}u^{\nu'}\right)^2 + g_{\mu'\nu'}\Delta x^{\mu'}\Delta x^{\nu'}\right]^{1/2}. \tag{C.3}$$

By inserting Eq. (C.2) and the coordinate expansion (3.69) into (C.1), we find that the leading-order piece of the first-order singular field is

$$h^{\mathrm{S1\,LO}}_{\mu\nu} = \frac{2\mu}{\lambda\rho}\left(g_{\mu\nu} + 2u_\mu u_\nu\right). \tag{C.4}$$

It was pointed out in [115] that the most efficient way to decompose the field into tensor-harmonic modes is to write the components in rotated coordinates $(t, r, \tilde{\alpha}, \tilde{\beta})$, where the particle is momentarily located at the north pole. The advantage is that a large number of modes vanish in these coordinates. After calculating the modes in this frame, we rotate back to our original coordinates, $(t, r, \theta, \varphi)$, where the particle lies on the equator ($\theta = \pi/2$). Note that we used these coordinates in Chapter 5. But here, unlike in Chapter 5, we add tildes to the angular coordinates to distinguish them from Greek letters, in order not to confuse them with spacetime indices.

We follow the formalism in [88] to write $\rho$ in terms of rotated coordinates. We introduce Riemann normal coordinates on the two-sphere, centered on the particle at $x'$, as

$$w_1 = 2\sin\left(\frac{\tilde{\alpha}}{2}\right)\cos\tilde{\beta}, \quad w_2 = 2\sin\left(\frac{\tilde{\alpha}}{2}\right)\sin\tilde{\beta}, \tag{C.5}$$

where $\tilde{\alpha}$ and $\tilde{\beta}$ are rotated angular coordinates given by

$$\sin\theta\cos\varphi = \cos\tilde{\alpha}, \tag{C.6a}$$

$$\sin\theta\sin\varphi = \sin\tilde{\alpha}\cos\tilde{\beta}, \tag{C.6b}$$

$$\cos\theta = \sin\tilde{\alpha}\sin\tilde{\beta}. \tag{C.6c}$$

In Riemann-normal coordinates the Schwarzschild metric takes the form

$$\begin{aligned} dx^2 = &- f dt^2 + \frac{dr^2}{f} + r^2\left(\frac{16 - w_2^2 k_1}{k_2}\right) dw_1^2 + r^2\left(\frac{16 - w_1^2 k_1}{k_2}\right) dw_2^2 \\ &+ 2r^2 \frac{w_1 w_2 k_1}{k_2} dw_1 dw_2, \end{aligned} \tag{C.7}$$

with $f = 1 - 2M/r$, $k_1 \equiv 8 - w_1^2 - w_2^2$ and $k_2 \equiv 16 - 4w_1^2 - 4w_2^2$.

Using the relations $\mathscr{E} = -u_t$ and $\mathscr{L} = u_\varphi$ from Eqs. (4.3), and the components of the metric (C.7), and labeling coordinates on the worldline in the rotated frame as $\left(r_0, t_0, \tilde{\alpha}_0, \tilde{\beta}_0\right)$, we find that [88]

$$\begin{aligned} \rho^2 = &\frac{1}{r_0^2 f_0^2}\left(r_0^2\mathscr{E}^2 - f_0\mathscr{L}^2\right)\Delta r^2 + \left(\mathscr{L}^2 + r_0^2\right)\Delta w_1^2 - 2\mathscr{E}\left(\frac{1}{f_0}\dot{r}_0\Delta r + \mathscr{L}\Delta w_1\right)\Delta t \\ &+ \frac{2}{f_0}\mathscr{L}\dot{r}_0\Delta r\Delta w_1 + \left(\mathscr{E}^2 - f_0\right)\Delta t^2 + r_0^2\Delta w_2^2. \end{aligned} \tag{C.8}$$

Now we let $\gamma$ be an exactly circular orbit with fixed radius $r_0$. Accordingly, we set the specific energy to be that for a circular orbit, $\mathscr{E}_0$, given in (4.9), and the specific angular momentum to be that of a circular orbit, $\mathscr{L}_0$, given in (4.8). If we let $\Delta t = 0$, then

$$\rho^2 = \frac{1}{f_0}\Delta r^2 + \left(\mathscr{L}_0^2 + r_0^2\right)\Delta w_1^2 + r_0^2 \Delta w_2^2, \tag{C.9}$$

where $\Delta r \equiv r - r_0$ is the radial distance from the particle. But $\Delta w_1^2 = 2\left(1-\cos\tilde{\alpha}\right)\cos^2\tilde{\beta}$ and $\Delta w_2^2 = 2\left(1-\cos\tilde{\alpha}\right)\sin^2\tilde{\beta}$, so we may write $\rho$ as

$$\rho \equiv \left(\frac{2r_0^2\left(r_0-2M\right)}{r_0-3M}\chi\right)^{1/2}\left(\delta^2 + 1 - \cos\tilde{\alpha}\right)^{1/2}, \tag{C.10}$$

where the quantities $\chi$ and $\delta$ are defined as

$$\delta^2 \equiv \frac{(r_0-3M)\Delta r^2}{2r_0(r_0-2M)\chi}, \tag{C.11}$$

$$\chi \equiv 1 - \frac{M\sin^2\tilde{\beta}}{r_0-2M}. \tag{C.12}$$

We may write the components of the leading-order piece of the puncture from Eq. (C.4), by substituting the expressions for the non-vanishing components of the four velocity given in Eqs. (4.10). All higher order terms in the puncture can be found in a similar way, and we find that, schematically, the puncture can be written as in Eq. (3.70).

Let us denote the $O(\lambda^n)$ piece of the (trace-reversed) puncture as $\bar{h}^{\mathcal{P}1,n}_{\mu\nu}$. We find that the non-vanishing components of the $O(\lambda^{-1})$ and $O(\lambda^0)$ terms are

$$\begin{aligned}
\bar{h}^{1\mathcal{P},-1}_{tt} &= \frac{4\mathcal{K}^2}{\rho}, & \bar{h}^{1\mathcal{P},-1}_{t\tilde{\alpha}} &= -\frac{1}{\rho}\frac{4r_0^3\mathcal{K}^2\Omega}{(r_0-2M)}\cos\tilde{\beta},\\
\bar{h}^{1\mathcal{P},-1}_{t\tilde{\beta}} &= \frac{1}{\rho}\frac{4r_0^3\mathcal{K}^2\Omega}{(r_0-2M)}\sin\tilde{\alpha}\sin\tilde{\beta}, & \bar{h}^{1\mathcal{P},-1}_{\tilde{\alpha}\tilde{\alpha}} &= \frac{1}{\rho}\frac{4Mr_0^2\mathcal{K}^2}{(r_0-2M)^2}\cos^2\tilde{\beta},\\
\bar{h}^{1\mathcal{P},-1}_{\tilde{\alpha}\tilde{\beta}} &= -\frac{1}{\rho}\frac{4Mr_0^2\mathcal{K}^2}{(r_0-2M)^2}\sin\tilde{\alpha}\sin\tilde{\beta}\cos\tilde{\beta}, & \bar{h}^{1\mathcal{P},-1}_{\tilde{\beta}\tilde{\beta}} &= \frac{1}{\rho}\frac{4Mr_0^2\mathcal{K}^2\sin^2\tilde{\alpha}\sin^2\tilde{\beta}}{(r_0-2M)^2},
\end{aligned} \tag{C.13}$$

where

$$\mathcal{K}^2 \equiv \frac{(r_0-2M)^2}{r_0(r_0-3M)}, \tag{C.14}$$

and

$$\bar{h}^{1\mathcal{P},0}_{tt} = -\frac{1}{\rho}\frac{2\Delta r}{r_0^2\left(r_0-3M\right)}\left[\frac{r_0^2 - 7Mr_0 + 10M^2 - 2M\left(r_0-4M\right)\sin^2\tilde{\beta}}{\chi}\right], \tag{C.15a}$$

$$\bar{h}^{1\mathcal{P},0}_{tr} = -\frac{1}{\rho}\frac{4\,r_0^2\,\Omega\,\mathcal{K}^2\sin\tilde{\alpha}\cos\tilde{\beta}}{(r_0-2M)}, \tag{C.15b}$$

$$\bar{h}^{1\mathcal{P},0}_{t\tilde{\alpha}} = -\frac{1}{\rho}\frac{2\Delta r\, r_0\Omega}{\left(r_0-3M\right)}\left[\frac{r_0^2 - 3Mr_0 + 2M^2 - 2M^2\sin^2\tilde{\beta}}{\left(r_0-2M\right)\chi}\right]\cos\tilde{\beta}, \tag{C.15c}$$

$$\bar{h}^{1\mathcal{P},0}_{t\tilde{\beta}} = \frac{1}{\rho}\frac{2\Delta r\, r_0\Omega}{(r_0-3M)}\left[\frac{r_0^2-3Mr_0+2M^2-2M^2\sin^2\tilde{\beta}}{(r_0-2M)\,\chi}\right]\sin\tilde{\alpha}\sin\tilde{\beta}, \tag{C.15d}$$

$$\bar{h}^{1\mathcal{P},0}_{r\tilde{\alpha}} = \frac{1}{\rho}\frac{4Mr_0\sin\tilde{\alpha}\cos^2\tilde{\beta}}{(r_0-3M)}, \tag{C.15e}$$

$$\bar{h}^{1\mathcal{P},0}_{r\tilde{\beta}} = -\frac{1}{\rho}\frac{4Mr_0\sin^2\tilde{\alpha}\cos\tilde{\beta}\sin\tilde{\beta}}{(r_0-3M)}, \tag{C.15f}$$

$$\bar{h}^{1\mathcal{P},0}_{\tilde{\alpha}\tilde{\alpha}} = \frac{1}{\rho}\frac{2\Delta r\, M\, r_0}{(r_0-3M)}\left[\frac{3r_0-7M-2M^2\sin^2\tilde{\beta}}{(r_0-2M)\,\chi}\right]\cos^2\tilde{\beta}, \tag{C.15g}$$

$$\bar{h}^{1\mathcal{P},0}_{\tilde{\alpha}\tilde{\beta}} = -\frac{1}{\rho}\frac{2\Delta r\, M\, r_0}{(r_0-3M)}\left[\frac{3r_0-7M-2M^2\sin^2\tilde{\beta}}{(r_0-2M)\,\chi}\right]\sin\tilde{\alpha}\sin\tilde{\beta}\cos\tilde{\beta}, \tag{C.15h}$$

$$\bar{h}^{1\mathcal{P},0}_{\tilde{\alpha}\tilde{\beta}} = \frac{1}{\rho}\frac{2\Delta r\, M\, r_0}{(r_0-3M)}\left[\frac{3r_0-7M-2M^2\sin^2\tilde{\beta}}{(r_0-2M)\,\chi}\right]\sin^2\tilde{\alpha}\sin^2\tilde{\beta}. \tag{C.15i}$$

We have derived formulas through $O(\lambda^2)$, but the higher order terms are too long to be included in this work, so we omit them.

Now we want to decompose the full 4D expressions into frequency-domain, tensor harmonic modes. We will use the notation $i\ell m'$ for the modes of quantities defined in terms of coordinates $(t, r, \tilde{\alpha}, \tilde{\beta})$, and $i\ell m$ for modes of quantities defined in terms of $(t, r, \theta, \varphi)$. This choice of notation reflects the fact that the rotation, which takes us from $(t, r, \tilde{\alpha}, \tilde{\beta})$ to $(t, r, \theta, \varphi)$ coordinates, induces a transformation between the corresponding $m$-modes. They have different $m$-mode numbers while the $i\ell$ mode numbers are unaffected by the rotation.

We want to expand the components in the basis of tensor spherical-harmonics in the frequency-domain, as

$$\bar{h}^{\mathcal{P}}_{\mu\nu} = \sum_{\ell=0}^{\infty}\sum_{m'=-\ell}^{\ell}\sum_{i=1}^{10} Y^{i\ell m'}_{\mu\nu}(\tilde{\alpha}, \tilde{\beta}, r)e^{-im'\Omega t}\bar{h}^{\mathcal{P}}_{i\ell m'}(r)\,. \tag{C.16}$$

The coefficients are given by

$$\bar{h}^{\mathcal{P}}_{i\ell m'}(r) = \int_0^{2\pi} d\tilde{\beta}\int_0^{\pi} d\tilde{\alpha}\sin\tilde{\alpha}\; h^{\mathcal{P}}_{\mu\nu}\eta^{\mu\tau}\eta^{\nu\sigma}\, Y^{*i\ell m'}_{\tau\sigma}(\tilde{\alpha}, \tilde{\beta}, r)e^{im'\Omega t}\,. \tag{C.17}$$

At the pole, we find that only the $m' = 0$ for $i = 1, 3, 6$, $m' = \pm 1$ for $i = 4, 8$ and $m' = \pm 2$ for $i = 7, 10$ spherical-harmonics (4.15) are non-zero. As such, (C.16) simplifies to

$$\bar{h}^{\mathcal{P}}_{\mu\nu}(t, r, \tilde{\alpha} = 0, \tilde{\beta}) = \sum_{\ell=0}^{\infty}\sum_{i=1}^{10}\bar{h}^{\mathcal{P}}_{\mu\nu,i\ell}, \tag{C.18}$$

where

$$\bar{h}^{\mathcal{P}}_{\mu\nu,1\ell} = \left(\frac{2\ell+1}{4\pi}\right)^{1/2} \frac{1}{\sqrt{2}} \left(\delta^t_\mu \delta^t_\nu + f^{-2}\delta^r_\mu \delta^r_\nu\right) \bar{h}^{\mathcal{P}}_{1\,\ell\,0}(r), \tag{C.19a}$$

$$\bar{h}^{\mathcal{P}}_{\mu\nu,2\ell} = \left(\frac{2\ell+1}{4\pi}\right)^{1/2} \frac{f^{-1}}{\sqrt{2}} \left(\delta^t_\mu \delta^r_\nu + \delta^r_\mu \delta^t_\nu\right) \bar{h}^{\mathcal{P}}_{2\,\ell 0}(r), \tag{C.19b}$$

$$\bar{h}^{\mathcal{P}}_{\mu\nu,3\ell} = \left(\frac{2\ell+1}{4\pi}\right)^{1/2} \frac{1}{\sqrt{2}} \left(\delta^t_\mu \delta^t_\nu - f^{-2}\delta^r_\mu \delta^r_\nu\right) \bar{h}^{\mathcal{P}}_{3\,\ell 0}(r), \tag{C.19c}$$

$$\bar{h}^{\mathcal{P}}_{\mu\nu,4\ell} = \left(\frac{2\ell+1}{16\pi}\right)^{1/2} \frac{r}{\sqrt{2}} \left(\delta^t_\mu \delta^{\tilde{\alpha}}_\nu + \delta^{\tilde{\alpha}}_\mu \delta^t_\nu\right) \left[e^{-i\tilde{\beta}}\bar{h}^{\mathcal{P}}_{4\,\ell,-1}(r) - e^{i\tilde{\beta}}\bar{h}^{\mathcal{P}}_{4\,\ell,+1}(r)\right], \tag{C.19d}$$

$$\bar{h}^{\mathcal{P}}_{\mu\nu,5\ell} = \left(\frac{2\ell+1}{16\pi}\right)^{1/2} \frac{rf^{-1}}{\sqrt{2}} \left(\delta^t_\mu \delta^{\tilde{\alpha}}_\nu + \delta^{\tilde{\alpha}}_\mu \delta^t_\nu\right) \left[e^{-i\tilde{\beta}}\bar{h}^{\mathcal{P}}_{5\,\ell,-1}(r) - e^{i\tilde{\beta}}\bar{h}^{\mathcal{P}}_{5\,\ell,+1}(r)\right], \tag{C.19e}$$

$$\bar{h}^{\mathcal{P}}_{\mu\nu,6\ell} = \left(\frac{2\ell+1}{4\pi}\right)^{1/2} \frac{r^2}{\sqrt{2}} \left(\delta^{\tilde{\alpha}}_\mu \delta^{\tilde{\alpha}}_\nu + \sin^2\tilde{\alpha}\,\delta^{\tilde{\beta}}_\mu \delta^{\tilde{\beta}}_\nu\right) \bar{h}^{\mathcal{P}}_{6\,\ell 0}(r), \tag{C.19f}$$

$$\bar{h}^{\mathcal{P}}_{\mu\nu,7\ell} = \left(\frac{2\ell+1}{16\pi}\right)^{1/2} r^2 \delta^{\tilde{\alpha}}_\mu \delta^{\tilde{\alpha}}_\nu \left[e^{-2i\tilde{\beta}}\bar{h}^{\mathcal{P}}_{7\,\ell,-2}(r) + e^{2i\tilde{\beta}}\bar{h}^{\mathcal{P}}_{7\,\ell,+2}(r)\right], \tag{C.19g}$$

$$\bar{h}^{\mathcal{P}}_{\mu\nu,8\ell} = i\left(\frac{2\ell+1}{16\pi}\right)^{1/2} \frac{r}{\sqrt{2}} \left(\delta^t_\mu \delta^{\tilde{\alpha}}_\nu + \delta^{\tilde{\alpha}}_\mu \delta^t_\nu\right) \left[e^{-i\tilde{\beta}}\bar{h}^{\mathcal{P}}_{8\,\ell,-1}(r) + e^{i\tilde{\beta}}\bar{h}^{\mathcal{P}}_{8\,\ell,+1}(r)\right], \tag{C.19h}$$

$$\bar{h}^{\mathcal{P}}_{\mu\nu,9\ell} = i\left(\frac{2\ell+1}{16\pi}\right)^{1/2} \frac{rf^{-1}}{\sqrt{2}} \left(\delta^r_\mu \delta^{\tilde{\alpha}}_\nu + \delta^{\tilde{\alpha}}_\mu \delta^r_\nu\right) \left[e^{-i\tilde{\beta}}\bar{h}^{\mathcal{P}}_{9\,\ell,-1}(r) + e^{i\tilde{\beta}}\bar{h}^{\mathcal{P}}_{9\,\ell,+1}(r)\right], \tag{C.19i}$$

$$\bar{h}^{\mathcal{P}}_{\mu\nu,10\,\ell} = -i\left(\frac{2\ell+1}{16\pi}\right)^{1/2} r^2 \delta^{\tilde{\alpha}}_\mu \delta^{\tilde{\alpha}}_\nu \left[e^{-2i\tilde{\beta}}\bar{h}^{\mathcal{P}}_{10\,\ell,-2}(r) - e^{2i\tilde{\beta}}\bar{h}^{\mathcal{P}}_{10\,\ell,+2}(r)\right]. \tag{C.19j}$$

The coefficients are given by

$$\bar{h}^{\mathcal{P}}_{1\ell 0}(r) = N_\ell \oint d\Omega \frac{1}{\sqrt{2}}(\bar{h}^{\mathcal{P}}_{tt} + \bar{h}^{\mathcal{P}}_{rr})P^0_\ell, \tag{C.20a}$$

$$\bar{h}^{\mathcal{P}}_{2\ell 0}(r) = N_\ell \oint d\Omega \sqrt{2}\,\bar{h}^{\mathcal{P}}_{tr}\,P^0_\ell, \tag{C.20b}$$

$$\bar{h}^{\mathcal{P}}_{3\ell 0}(r) = N_\ell \oint d\Omega \frac{1}{\sqrt{2}}(\bar{h}^{\mathcal{P}}_{tt} - \bar{h}^{\mathcal{P}}_{rr})P^0_\ell, \tag{C.20c}$$

$$\bar{h}^{\mathcal{P}}_{4\,\ell\pm 1}(r) = \frac{\mp\sqrt{2}N_\ell}{r\ell(\ell+1)} \oint d\Omega e^{\mp i\tilde{\beta}} \left[\bar{h}^{\mathcal{P}}_{t\tilde{\alpha}} \left(\frac{(\ell+1)^2 P^1_{\ell-1} - \ell^2 P^1_{\ell+1}}{(2\ell+1)\sin\tilde{\alpha}}\right) \pm i\bar{h}^{\mathcal{P}}_{t\tilde{\beta}} \frac{P^1_\ell}{\sin^2\tilde{\alpha}}\right], \tag{C.20d}$$

$$\bar{h}^{\mathcal{P}}_{5\,\ell\pm 1}(r) = \frac{\mp\sqrt{2}N_\ell}{r\ell(\ell+1)} \oint d\Omega e^{\mp i\tilde{\beta}} \left[\bar{h}^{\mathcal{P}}_{r\tilde{\alpha}} \left(\frac{(\ell+1)^2 P^1_{\ell-1} - \ell^2 P^1_{\ell+1}}{(2\ell+1)\sin\tilde{\alpha}}\right) \pm \bar{h}^{\mathcal{P}}_{r\tilde{\beta}} \frac{P^1_\ell}{\sin^2\tilde{\alpha}}\right], \tag{C.20e}$$

$$\bar{h}^{\mathcal{P}}_{6\ell 0}(r) = \frac{N_\ell}{\sqrt{2}r^2} \oint d\Omega \left(\bar{h}^{\mathcal{P}}_{\tilde{\alpha}\tilde{\alpha}} + \csc^2\tilde{\alpha}\,\bar{h}^{\mathcal{P}}_{\tilde{\beta}\tilde{\beta}}\right) P^0_\ell, \tag{C.20f}$$

$$\begin{aligned}\bar{h}^{\mathcal{P}}_{7\ell\pm 2}(r) = &\frac{1}{\sqrt{2}r^2\Lambda^{1/2}} \oint d\Omega e^{-2i\varphi} \\ &\left\{3e^{2i\varphi}\csc\tilde{\alpha}\,Y^{-2}_\ell \left[(\cos 2\tilde{\alpha}+3)(h^{\mathcal{P}}_{\tilde{\alpha}\tilde{\alpha}} - h^{\mathcal{P}}_{\tilde{\beta}\tilde{\beta}}) + 8i\bar{h}^{\mathcal{P}}_{\tilde{\alpha}\tilde{\beta}}\cos\tilde{\alpha}\right]\right. \\ &-4e^{i\varphi}(\ell-1)^{1/2}(\ell+2)^{1/2}\,Y^{-1}_\ell \left[\cos\tilde{\alpha}\left(\bar{h}^{\mathcal{P}}_{\tilde{\alpha}\tilde{\alpha}} - \bar{h}^{\mathcal{P}}_{\tilde{\beta}\tilde{\beta}}\right) + 2i\bar{h}^{\mathcal{P}}_{\tilde{\beta}\tilde{\beta}}\right] \\ &\left.+\sin\tilde{\alpha}\left(\bar{h}^{\mathcal{P}}_{\tilde{\alpha}\tilde{\alpha}} - \bar{h}^{\mathcal{P}}_{\tilde{\beta}\tilde{\beta}}\right)(\ell+2)^{1/2}\,\Lambda^{1/2}Y^0_\ell\right\},\end{aligned} \tag{C.20g}$$

$$\bar{h}^{\mathcal{P}}_{8\,\ell\pm1}(r) = \frac{\mp\sqrt{2}N_\ell}{r\ell(\ell+1)} \oint d\Omega e^{\mp i\tilde{\beta}} \left[ \bar{h}^{\mathcal{P}}_{t\tilde{\alpha}} \left( \frac{(\ell+1)^2 P^1_{\ell-1} - \ell^2 P^1_{\ell+1}}{(2\ell+1)\sin^2\tilde{\alpha}} \right) \mp \bar{h}^{\mathcal{P}}_{t\tilde{\beta}} \frac{P^1_\ell}{\sin\tilde{\alpha}} \right], \quad \text{(C.20h)}$$

$$\bar{h}^{\mathcal{P}}_{9\,\ell\pm1}(r) = \frac{N_\ell \mp \sqrt{2}}{r\ell(\ell+1)} \oint d\Omega e^{\mp i\tilde{\beta}} \left[ \bar{h}^{\mathcal{P}}_{r\tilde{\alpha}} \left( \frac{(\ell+1)^2 P^1_{\ell-1} - \ell^2 P^1_{\ell+1}}{(2\ell+1)\sin^2\tilde{\alpha}} \right) \mp \bar{h}^{\mathcal{P}}_{t\tilde{\beta}} \frac{P^1_\ell}{\sin\tilde{\alpha}} \right], \quad \text{(C.20i)}$$

$$\begin{aligned} \bar{h}^{\mathcal{P}}_{10\,\ell\pm2}(r) = {} & \frac{\sqrt{2}N_\ell}{r^2\Lambda^{1/2}} \oint d\Omega e^{-2i\tilde{\beta}} \csc\tilde{\alpha} \\ & \Big\{ 6e^{2i\tilde{\beta}} Y^{-2}_\ell \left[ -i\cos\tilde{\alpha}(\bar{h}^{\mathcal{P}}_{\tilde{\alpha}\tilde{\beta}} - \bar{h}^{\mathcal{P}}_{\tilde{\beta}\tilde{\beta}}) + \cos^2\tilde{\alpha}\bar{h}^{\mathcal{P}}_{\tilde{\alpha}\tilde{\beta}} + \bar{h}^{\mathcal{P}}_{\tilde{\alpha}\tilde{\beta}} \right] \\ & + \sin\tilde{\alpha} \Big[ \bar{h}^{\mathcal{P}}_{\tilde{\alpha}\tilde{\beta}} \sin\tilde{\alpha} \sqrt{(\ell+1)(\ell+2)} Y^0_\ell \\ & + 2ie^{i\tilde{\beta}} \sqrt{(\ell-1)(\ell+2)} Y^{-1}_\ell \left( \bar{h}^{\mathcal{P}}_{\tilde{\alpha}\tilde{\beta}} + 2i\cos\tilde{\alpha}\bar{h}^{\mathcal{P}}_{\tilde{\alpha}\tilde{\beta}} - \bar{h}^{\mathcal{P}}_{\tilde{\beta}\tilde{\beta}} \right) \Big] \Big\}, \end{aligned} \quad \text{(C.20j)}$$

where $\oint d\Omega \equiv \int_0^{2\pi} d\tilde{\beta} \int_0^\pi d\tilde{\alpha} \sin\tilde{\alpha}$, $N_\ell \equiv [(2\ell+1)/4\pi]^{1/2}$, $P^m_\ell = P^m_\ell(\cos\tilde{\alpha})$ are the associated Legendre polynomials, $Y^m_\ell = Y^m_\ell(\tilde{\alpha}, \tilde{\beta})$ are the scalar spherical-harmonics and $\Lambda \equiv (\ell-1)\,\ell\,(\ell+1)\,(\ell+2)$.

We evaluate the integrals over $\tilde{\alpha}$ analytically, using the following useful results:

$$\int_0^\pi d\tilde{\alpha} \sin\tilde{\alpha} \frac{P^0_\ell}{(\delta^2+1-\cos\tilde{\alpha})} = \frac{2\sqrt{2}}{1+2\ell} A(\delta)^{1/2+\ell}, \quad \text{(C.21a)}$$

$$\begin{aligned} \int_0^\pi d\tilde{\alpha} \sin\tilde{\alpha} \frac{\sin\tilde{\alpha} P^1_\ell}{(\delta^2+1-\cos\tilde{\alpha})} = {} & \frac{2\sqrt{2}\ell\,(\ell+1)!}{(\ell-1)!\,(2\ell+3)\,(2\ell+1)\,(2\ell-1)} A(\delta)^{1/2+\ell} \\ & \left[ -3 - 2\ell + (2\ell-1)\,A(\delta)^2 \right], \end{aligned} \quad \text{(C.21b)}$$

$$\begin{aligned} \int_0^\pi d\tilde{\alpha} \sin\tilde{\alpha} \frac{\sin^2\tilde{\alpha} P^2_\ell}{(\delta^2+1-\cos\tilde{\alpha})} = {} & \frac{2\sqrt{2}\,(\ell+2)!}{3\,(\ell-2)!\,(2\ell+1)} A(\delta)^{\ell-3/2} \\ & \Bigg\{ \frac{\left[A(\delta)^2+1\right]\left[A(\delta)^2(2\ell-1) - 2\ell - 3\right]}{4\ell^2+4\ell-3} \\ & - \frac{2\ell\left[A(\delta)^2(2\ell-3) - 2\ell - 5\right]}{(4\ell^2-4\ell-3)\,(2\ell-1)} \\ & - \frac{2(\ell+1)\left[A(\delta)^2(2\ell+1) - 2\ell - 5\right] A(\delta)^2}{(2\ell+3)\,(4\ell^2+12\ell+5)} \Bigg\}. \end{aligned} \quad \text{(C.21c)}$$

where $A(\delta) \equiv 1 + \delta^2 - |\delta|\left(2+\delta^2\right)^{1/2}$.

We are then left with expressions that depend on the azimuthal angle $\tilde{\beta}$ and $\Delta r$. The most efficient way to evaluate the integral over $\tilde{\beta}$ is to expand in powers of $\Delta r$. This yields an expression in powers of $\sin\tilde{\beta}$, $\cos\tilde{\beta}$ and $\chi$. We re-write powers of $\sin\tilde{\beta}$

and $\cos\tilde{\beta}$, as

$$\sin^n\tilde{\beta} = \left(\frac{r_0-2M}{M}\left[1-\chi\right]\right)^{n/2}, \quad \cos^n\tilde{\beta} = \left(1-\frac{r_0-2M}{M}\left[1-\chi\right]\right)^{n/2}. \tag{C.22}$$

In this approach, we straightforwardly evaluate the integral over $\tilde{\beta}$ using the general formula

$$\int_0^{2\pi} d\tilde{\beta}\chi^n = 2\pi{}_2F_1\left(n, \frac{1}{2}, 1, \frac{M}{r_0-2M}\right), \tag{C.23}$$

where ${}_2F_1$ is the hypergeometric function.

We end up with expressions for the $i\ell m'$ modes, in the rotated frame. We rotate back to unrotated-coordinates, $(t, r, \theta, \varphi)$, where the particle is located on the equator, as

$$\bar{h}^{\mathcal{P}}_{i\ell m}(r) = \sum_{m'} D^{\ell}_{mm'}\left(0, \pi/2, \pi/2\right)\bar{h}^{\mathcal{P}}_{i\ell m'}(r). \tag{C.24}$$

where $D_{\ell,m,m'}$ are the Wigner D-symbols.

Using this strategy we obtain analytical expressions for the modes of the puncture $\bar{h}^{\mathcal{P}}_{i\ell m}(r)$, through order $\Delta r^2$. The expressions themselves are too long to quote here in full. Instead we give them through order $O(\Delta r^0)$. We have the full expressions through order $O(\Delta r^2)$ stored in a *Mathematica* file.

$$\bar{h}^{\mathcal{P}}_{1\,\ell m} = D_{\ell,-m,0}\left(0, \frac{\pi}{2}, \frac{\pi}{2}\right)\frac{2\sqrt{\frac{2}{\pi}}(r_0-2M)^{3/2}E\left(\frac{M}{r_0-2M}\right)}{r_0^2\sqrt{(2\ell+1)(r_0-3M)}} + O(r), \tag{C.25a}$$

$$\bar{h}^{\mathcal{P}}_{2\,\ell m} = O(r), \tag{C.25b}$$

$$\bar{h}^{\mathcal{P}}_{3\,\ell m} = D_{\ell,-m,0}\left(0, \frac{\pi}{2}, \frac{\pi}{2}\right)\frac{2\sqrt{\frac{2}{\pi}}(r_0-2M)^{3/2}E\left(\frac{M}{r_0-2M}\right)}{r_0^2\sqrt{(2\ell+1)(r_0-3M)}} + O(r), \tag{C.25c}$$

$$\begin{aligned}\bar{h}^{\mathcal{P}}_{4\,\ell m} = &\left[D_{\ell,m,1}\left(\pi, \frac{\pi}{2}, \frac{\pi}{2}\right) + D_{\ell,m,-1}\left(\pi, \frac{\pi}{2}, \frac{\pi}{2}\right)\right]\frac{8}{\sqrt{2\ell+1}Mr}\sqrt{\frac{2M(r_0-2M)}{\pi r_0(r_0-3M)}} \\ &\left[\frac{MK\left(\frac{M}{r_0-2M}\right)}{\ell(\ell+1)}\right. \\ &\left.+ 2(r_0-2M)\left(K\left(\frac{M}{r_0-2M}\right) - E\left(\frac{M}{r_0-2M}\right)\right)\right] + O(r),\end{aligned} \tag{C.25d}$$

$$\bar{h}^{\mathcal{P}}_{5\,\ell m} = O(r), \tag{C.25e}$$

$$\begin{aligned}\bar{h}^{\mathcal{P}}_{6\,\ell m} = &D_{\ell,-m,0}\left(0, \frac{\pi}{2}, \frac{\pi}{2}\right) \\ &\frac{8\sqrt{\frac{2}{\pi}}r_0\sqrt{r_0-2M}\left(K\left(\frac{M}{r_0-2M}\right) - E\left(\frac{M}{r_0-2M}\right)\right)}{r^2\sqrt{(2\ell+1)(r_0-3M)}} + O(r),\end{aligned} \tag{C.25f}$$

$$\bar{h}^{\mathcal{P}}_{7\,\ell m} = \left[D_{\ell,m,2}\left(\pi, \frac{\pi}{2}, \frac{\pi}{2}\right) + D_{\ell,m,-2}\left(\pi, \frac{\pi}{2}, \frac{\pi}{2}\right)\right]\frac{4\left(\sqrt{2}r_0\right)}{3\sqrt{2\ell+1}Mr^2\sqrt{\pi(r_0-2M)(r_0-3M)}}$$

$$
\begin{aligned}
&\left[\frac{12(2\ell+1)^2M^2K\left(\frac{M}{r_0-2M}\right)}{5(\ell-1)\ell(\ell+1)(\ell+2)}+2\left(51M^2-40Mr_0+8r_0^2\right)K\left(\frac{M}{r_0-2M}\right)\right.\\
&\left.-8(2r_0-5M)(r_0-2M)E\left(\frac{M}{r_0-2M}\right)\right]+O(r)\,, \qquad \text{(C.25g)}\\
\bar{h}^{\mathcal{P}}_{8\,\ell m}=&\left[D_{\ell,m,1}\left(\pi,\frac{\pi}{2},\frac{\pi}{2}\right)+D_{\ell,m,-1}\left(\pi,\frac{\pi}{2},\frac{\pi}{2}\right)\right]\frac{(8i)}{\sqrt{2\ell+1}Mr}\sqrt{\frac{2M(r_0-2M)}{\pi r_0(r_0-3M)}}\\
&\left[\left(2(r_0-3M)K\left(\frac{M}{r_0-2M}\right)-2(r_0-2M)E\left(\frac{M}{r_0-2M}\right)\right)\right.\\
&\left.-\frac{MK\left(\frac{M}{r_0-2M}\right)}{\ell(\ell+1)}\right]+O(r), \qquad \text{(C.25h)}\\
\bar{h}^{\mathcal{P}}_{9\,\ell m}=&O(r), \qquad \text{(C.25i)}\\
\bar{h}^{\mathcal{P}}_{10\,\ell m}=&\left[D_{\ell,m,2}\left(\pi,\frac{\pi}{2},\frac{\pi}{2}\right)+D_{\ell,m,-2}\left(\pi,\frac{\pi}{2},\frac{\pi}{2}\right)\right]\frac{4\left(\sqrt{2}ir_0\right)}{3\sqrt{2\ell+1}Mr^2\sqrt{\pi(r_0-2M)(r_0-3M)}}\\
&\left[-\frac{12(2\ell+1)^2M^2K\left(\frac{M}{r_0-2M}\right)}{5(\ell-1)\ell(\ell+1)(\ell+2)}+16(r_0-2M)(r_0-3M)K\left(\frac{M}{r_0-2M}\right)\right.\\
&\left.-8(2r_0-5M)(r_0-2M)E\left(\frac{M}{r_0-2M}\right)\right]+O(r)\,, \qquad \text{(C.25j)}
\end{aligned}
$$

where $E$ is the elliptic function of the first kind and $K$ is the elliptic function of the second kind.

# Appendix D

# Field equations

The explicit formulas for the coupling terms $\mathcal{M}^{ij}$'s in the frequency-domain field equations (4.25) are (see Appendix A of [62]), using the shortform notation $\bar{h}_i = \bar{h}_{i\ell m}$,

$$\mathcal{M}^{1j}\bar{h}_j = \frac{Mf^2}{r^2}\partial_r\bar{h}_3 + \frac{f}{2r^2}\left(1-\frac{4M}{r}\right)\left(\bar{h}_1-\bar{h}_5-f\bar{h}_3\right) - \frac{f^2}{2r^2}\left(1-\frac{6M}{r}\right)\bar{h}_6, \tag{D.1a}$$

$$\mathcal{M}^{2j}\bar{h}_j = \frac{Mf}{r^2}\partial_r\bar{h}_2 + \frac{M}{r^2}i\omega_m\bar{h}_1 + \frac{f^2}{2r^2}\left(\bar{h}_2-\bar{h}_4\right), \tag{D.1b}$$

$$\mathcal{M}^{3j}\bar{h}_j = -\frac{f}{2r^2}\left[\bar{h}_1-\bar{h}_5-\left(1-\frac{4M}{r}\right)\left(\bar{h}_3+\bar{h}_6\right)\right], \tag{D.1c}$$

$$\mathcal{M}^{4j}\bar{h}_j = \frac{M}{2r^2}\left(i\omega_m\bar{h}_5-i\omega_m\bar{h}_4+\partial_r\bar{h}_4-\partial_r\bar{h}_5\right) - \frac{1}{2}\,\ell\,(\ell+1)\;\frac{f}{r^2}\bar{h}^{(2)} - \frac{Mf}{2r^3}\left[3\bar{h}_4+2\bar{h}_5-\bar{h}_7+\ell\,(\ell+1)\,\bar{h}_6\right], \tag{D.1d}$$

$$\mathcal{M}^{5j}\bar{h}_j = \frac{f}{r^2}\left[\left(1-\frac{9M}{2r}\right)\bar{h}_5-\frac{1}{2}\ell\,(\ell+1)\left(\bar{h}_1-f\bar{h}_3\right) + \frac{1}{2}\left(1-\frac{3M}{r}\right)\left(\ell\,(\ell+1)\,\bar{h}_6-\bar{h}_7\right)\right], \tag{D.1e}$$

$$\mathcal{M}^{6j}\bar{h}_j = -\frac{f}{2r^2}\left[\bar{h}_1-\bar{h}_5-\left(1-\frac{4M}{r}\right)\left(\bar{h}_3+\bar{h}_6\right)\right], \tag{D.1f}$$

$$\mathcal{M}^{7j}\bar{h}_j = -\frac{f}{2r^2}\left(\bar{h}_7+\lambda\,\bar{h}_5\right), \tag{D.1g}$$

$$\mathcal{M}^{8j}\bar{h}_j = \frac{M}{2r^2}\left(i\omega_m\bar{h}_9 - i\omega_m\bar{h}_8 + \partial_r\bar{h}_8 - \partial_r\bar{h}_9\right) - \frac{1}{4}\frac{Mf}{2r^3}\left(3\bar{h}_8 + 2\bar{h}_9 - \bar{h}_{10}\right), \tag{D.1h}$$

$$\mathcal{M}^{9j}\bar{h}_j = \frac{f}{r^2}\left(1 - \frac{9M}{2r}\right)\bar{h}_9 - \frac{f}{2r^2}\left(1 - \frac{3M}{r}\right)\bar{h}_{10}, \tag{D.1i}$$

$$\mathcal{M}^{10j}\bar{h}_j = -\frac{f}{2r^2}\left(\bar{h}_{10} + \lambda\bar{h}_9\right). \tag{D.1j}$$

where $\lambda \equiv (\ell-1)(\ell+2)$.

# Appendix E

# Rotations

In Sec. 5.4, we require a 4D representation of $S = t^{\mu\nu}\partial_\mu\phi^{1\mathcal{P}}\partial_\nu\phi^{1\mathcal{P}}$, given only the expression (5.22) for $\phi^{1\mathcal{P}}$, an expression written in a coordinate system in which the particle is instantaneously at the north pole. This is nontrivial because there is no explicit time dependence in Eq. (5.22),[1] making it unclear how to evaluate the $t$ derivatives in $S$. Here we consider two ways of tackling this problem: via a time-dependent rotation and via a one-parameter family of rotations. We will refer to the first as the 4D method, the second as the 2D method. To assist the discussion, we split the unrotated coordinates into $x^\mu = (x^a, \theta^A)$, where $x^a = (t, r)$ and $\theta^A = (\theta, \varphi)$, thereby splitting the manifold into the Cartesian product $\mathcal{M}^2 \times S^2$, where $\mathcal{M}^2$ is the $x^a$ plane and $S^2$ is the unit sphere.

In the first approach, we would use a 4D coordinate transformation $x^\mu \to x^{\mu'} = (x^{a'}, \alpha^{A'})$ given by $x^{a'} = x^a$ and $\alpha^{A'} = \alpha^{A'}(\theta^A, t)$, where $\alpha^{A'} = (\alpha, \beta)$, such that at each fixed $t$, the transformation would be a 2D rotation that placed the particle at the north pole. In this case, all tensors would transform in the usual 4D way, including tensors tangent $\mathcal{M}^2$; the transformation mixes $\mathcal{M}^2$ with $S^2$. For example, for a dual vector $w_\mu$ we would have $w_t \to w_{t'} = w_t + \dot{\theta}^A w_A$, $w_r \to w_{r'} = w_r$, and $w_A \to w_{A'} = \Omega^A{}_{A'} w_A$, where

$$\dot{\theta}^A := \frac{\partial\theta^A}{\partial t'}, \tag{E.1}$$

$$\Omega^A{}_{A'} := \frac{\partial\theta^A}{\partial\alpha^{A'}}. \tag{E.2}$$

In the coordinates $x^{\mu'}$, the particle would be permanently at the north pole, with four-velocity $u^{a'} = u^a$ and $u^{A'} = 0$. [Since the coordinates are singular at the particle's position at the north pole, $u^{A'}$ is not strictly well defined. But if we introduce local Cartesian coordinates $x^{i'} = (r_0\alpha\cos\beta, r_0\alpha\sin\beta)$, then we can establish $u^{i'} = 0$, allowing us to freely set $u^{A'} = 0$.] In this method, all components would be expressed in the primed coordinate system, meaning the only time derivatives appearing in $S$ would

[1] This fact is specific to circular orbits. For noncircular orbits, even in these rotated coordinates, $\phi^{1\mathcal{P}}$ would depend on time through its dependence on the orbital radius $r_p(t)$.

be $\partial_{t'}\phi^{1\mathcal{P}}$. For circular orbits, these derivatives would trivially vanish because $\phi^{1\mathcal{P}}$ contains no explicit dependence on $t'$; the $t$ dependence would be entirely encoded in the transformation law's dependence on $\dot{\theta}^A$.

Although the 4D method is practicable, we henceforth adopt the second, 2D method, for reasons described below. In this approach, instead of a 4D coordinate transformation, we consider a different 2D rotation at each instant of $t$. We may write this as $\alpha_t^{A'} = \alpha^{A'}(\theta^A, t)$. This is superficially the same as the 4D method, but the time at which the rotation is performed is now a parameter of the rotation rather than a coordinate, and for each value of the parameter, we have a different coordinate system; for example, if the rotation is performed at time $t_0$, it induces a coordinate system $(t, r, \alpha_{t_0}^{A'})$. Because the transformation is restricted to $S^2$, tensors tangent to $\mathcal{M}^2$ transform as scalars and those tangent to $S^2$ transform as tensors on $S^2$: for the same dual vector $w_\mu$ mentioned above, we now have $w_a \to w_a$ and $w_A \to w_{A'} = \Omega^A{}_{A'} w_A$. Unlike in the 4D method, where the particle was permanently at the north pole, here it is only there at the particular instant at which the rotation is performed, with an instantaneous four-velocity $(u^a, u^{A'}) = (u^a, u^\varphi, 0)$ at that time. [As above, this value of $u^{A'}$ comes from consideration of the locally Cartesian components, which can be established to be $u^{i'} = (r_0 u^\varphi, 0)$.] Time derivatives in this method are evaluated as derivatives with respect to the parameter $t$: $\partial_t\phi^{1\mathcal{P}} = \dot{\alpha}^{A'}\partial_{A'}\phi^{1\mathcal{P}}$, where

$$\dot{\alpha}^{A'} := \frac{\partial \alpha^{A'}}{\partial t} = -\Omega^{A'}{}_A \dot{\theta}^A. \tag{E.3}$$

Here $\Omega^{A'}{}_A := \frac{\partial\theta^{A'}}{\partial\theta^A} = (\Omega^A{}_{A'})^{-1} = \Omega^{A'B'}\Omega_{AB}\Omega^B{}_{B'}$, and the second equality in Eq. (E.3) follows from the implicit function theorem.

In our toy model, the above two methods both lead to the result

$$S = (\partial_r\phi^P)^2 + (r^{-2}\Omega^{A'B'} + \dot{\alpha}^{A'}\dot{\alpha}^{B'})\partial_{A'}\phi^P\partial_{B'}\phi^P. \tag{E.4}$$

However, in gravity the two methods would lead to quite different calculations when performing decompositions into tensor harmonics. Furthermore, only the 2D method is immediately applicable to the decomposition strategy of Ref. [74].[2] Hence, the 2D method is preferred here.

All of the above is fairly general. When we specialize to our particular case of circular orbits with frequency $\Omega$, the transformation is given by

$$\theta = \arccos(\sin\alpha\sin\beta), \tag{E.5}$$

[2]To see this, consider $\delta^2 G_{\mu\nu}[h^{1\mathcal{P}}, h^{1\mathcal{P}}]$. In the strategy used in Ref. [74], as in our 2D method described here, a quantity such as $\delta^2 G_{tt}$ is treated as a scalar, that scalar is then written in terms of the coordinates $\alpha^{A'}$, and it is decomposed into scalar harmonics by integrating against $Y_{lm}(\alpha^{A'})$. Contrary to this, in the 4D method, the scalar-harmonic decomposition of $\delta^2 G_{tt}$ would be constructed from the scalar, vector, and tensor-harmonic decompositions of $\delta^2 G_{t't'}$, $\delta^2 G_{t'A'}$, and $\delta^2 G_{A'B'}$, using the transformation $\delta^2 G_{tt} = \delta^2 G_{t't'} + 2\dot{\alpha}^{A'}\delta^2 G_{t'A'} + \dot{\alpha}^{A'}\dot{\alpha}^{B'}\delta^2 G_{A'B'}$.

$$\varphi = \arccos\{\cos\alpha / \sin[\arccos(\sin\alpha\sin\beta)]\} + \Omega t, \tag{E.6}$$

which implies $(u^a, u^{A'}) = u^t(1, 0, \Omega, 0)$ and

$$\dot{\theta}^A = (0, \Omega), \tag{E.7}$$

$$\dot{\alpha}^{A'} = \Omega(-\cos\beta, \cot\alpha\sin\beta). \tag{E.8}$$

The final expression for $S$, used in our computations in Sec. 5.4, is given by Eq. (E.4) with Eq. (E.8).

# Appendix F

# Retarded integral of the leading-order monopole source in the far-zone

In this appendix we outline the steps of how to evaluate the retarded integral of Eq. (6.81), for the case $\ell = 0$, which provides the solution for the monopole piece of the second-order field in the far-zone. The analysis here follows the derivation given in Ref. [75], which stems from the original work of Blanchet and Damour given in Ref. [103]. For convenience we restate the integral Eq. (6.81) to be evaluated:

$$\mathrm{FP}\Box^{-1}_{\mathrm{ret}}\left(r^{B-k}S_L^{(-k)}\hat{n}^L\right) = \mathrm{FP}\frac{1}{K(B,k)}\int_r^{\infty} dz\, S_L^{(-k)}(t-z)$$
$$\hat{\partial}_L\left[\frac{(z-r)^{B-k+\ell+2}-(z+r)^{B-k+\ell+2}}{r}\right], \tag{F.1}$$

where

$$K(B,k) \equiv 2^{B-k+3}\frac{(B-k+2)!}{(B-k-\ell+1)!}. \tag{F.2}$$

The first step is to introduce a cutoff in the integral at $\tilde{T} \equiv T/\epsilon^{n+1}$, where $T > 0$ and $n > 0$ are $\epsilon$-independent constants. The motivation for the cutoff is that the contribution from the range $z \in [\tilde{T}, \infty]$ is negeligibly small compared to the contribution from the range $z \in [r, \tilde{T}]$, as will be shown below. Before proceeding to show that this is true, we remind the reader that we are only interested in the slowest falling term in the source, $r^{-2}S_L^{(-2)}\hat{n}^L$. In light of this we will specialise to the case of $k = 2$ in the integral of Eq. (F.1). Since $1/r^2$ is integrable at $r = 0$, for this term in the source the FP operation is equivalent to taking the limit $B \to 0$.

Using the expansion $x^B = 1 + B\ln x + O(B^2)$ the integrand reduces to

$$\begin{aligned}
&\mathrm{FP}\frac{1}{K(B,2)}\hat{\partial}_L\left[\frac{(z-r)^{B+\ell}-(z+r)^{B+\ell}}{r}\right] \\
&= K_\ell\hat{\partial}_L\left[\frac{(z-r)^{\ell}\ln(z-r)-(z+r)^{\ell}\ln(z+r)}{r}\right],
\end{aligned} \tag{F.3}$$

where $K_\ell \equiv (-1)^\ell/2(\ell!)$. Using the result [101] that $\hat{\partial}_L r^k = 0$ for even integers $0 \le k < 2\ell$, Eq. (F.3) simplifies to

$$\mathrm{FP}\frac{1}{K(B,2)}\hat{\partial}_L\left[\frac{(z-r)^{B+\ell}-(z+r)^{B+\ell}}{r}\right] = K_\ell\frac{r^\ell}{z^{\ell+1}} + O(1/z^{\ell+2}). \tag{F.4}$$

Given that the leading-order behaviour of the first-order fields is $1/r$, then from the coupling formula (6.32) we may deduce that $S^2 \sim \tilde{\Omega}_p^2\left(\tilde{R}^1\right)^2 + O(1/r^3) \sim \left(\tilde{R}^1\right)^2/r_p^3$, where the last step follows from the fact that $\tilde{\Omega}_p \sim \sqrt{1/r_p^3}$. From Eqs. (6.33)-(6.38), $\tilde{R}^1 \sim j_\ell(m\tilde{\Omega}_p r_p)/r = j_\ell(m/r_p^{1/2})/r$. Noting that $j_\ell(z) \sim z^\ell$ for large $z$ and that the dominant term is the $\ell = 1$ term, $\tilde{R}^1 \sim r_p^{-1/2}/r$. Overall, $S^2 \sim r_p^{-4}/r^2 + O(1/r^3)$. Therefore,

$$S_L^{(-2)} \sim \frac{1}{r_p^5} \sim \frac{1}{(\epsilon z)^5}. \tag{F.5}$$

Thus, substituting Eqs. (F.4) and (F.5) into Eq. (F.1), we find that the integral for the range $z \in [\tilde{T}, \infty]$ reads

$$\frac{K_\ell}{\epsilon^5}\int_{T/\epsilon^{n+1}}^{\infty} dz\frac{r^\ell}{z^{6+\ell}} = K_\ell\epsilon^{(5+\ell)n+\ell}\int_T^\infty d\tilde{z}\frac{r^\ell}{\tilde{z}^{6+\ell}}. \tag{F.6}$$

For $n > 0$, this is negligible.

We may now limit our analysis to the integration range $z \in [r, \tilde{T}]$ in Eq. (F.1). Definining

$$\Psi_\ell := \square_{\mathrm{ret}}^{-1}\left(r^{-2}S_L^{(-2)}\hat{n}^L\right), \tag{F.7}$$

we may rewrite Eq. (F.1) as

$$\begin{aligned}
\Psi_\ell = \mathrm{FP}\frac{K_\ell}{B}\int_r^{\tilde{T}} dz\, S_L^{(-2)}(t-z)\hat{\partial}_L&\left[\frac{(z-r)^{B+\ell}\ln(z-r)-(z+r)^{B+\ell}\ln(z+r)}{r}\right] \\
&+ o(\epsilon^0).
\end{aligned} \tag{F.8}$$

where "$o(\epsilon^p)$" means "goes to zero faster than $\epsilon^p$".

The following relations, given in Appendix A of Ref. [101], allow conversion to ordinary scalar spherical-harmonics:

$$F_L^n\hat{n}^L = \sum_m F_{\ell m}^n Y_{\ell m}, \tag{F.9}$$

$$S_L^{(-k)}\hat{n}^L = \sum_m S_{\ell m}^{(-k)} Y_{\ell m}. \tag{F.10}$$

Using Eq. (F.10), for the case $\ell = 0$ we find that Eq. (F.8) reduces to

$$\begin{aligned}\Psi_0 =& \frac{Y_{00}}{2}\int_r^{\tilde{T}} dz\, S_{00}^{(-2)}(t-z)\frac{\ln(z-r)}{r} - \frac{Y_{00}}{2}\int_r^{\tilde{T}} dz\, S_{00}^{(-2)}(t-z)\frac{\ln(z+r)}{r} \\ &+ o(\epsilon^0) \\ =& \frac{Y_{00}}{2r}\int_0^{\tilde{T}} ds\, S_{00}^{(-2)}(t-s-r)\ln(s) - \frac{Y_{00}}{2r}\int_{2r}^{\tilde{T}} ds\, S_{00}^{(-2)}(t-s+r)\ln(s) \\ &+ o(\epsilon^0),\end{aligned} \tag{F.11}$$

where in the second step, we changed variables to $s = z - r$ in the first integral, and $s = z + r$ in the second integral. Strictly speaking, the change of variables alters the upper integration limits to $\tilde{T} - r$ and $\tilde{T} + r$ in the first and second integrals, respectively. But since $\tilde{T}$ is large, this change has a negligible effect, so we ignore it. By writing the integrand in terms of retarded time $u = t - r$, we find that Eq. (F.11) becomes

$$\begin{aligned}\Psi_0 =& \frac{Y_{00}}{2r}\int_0^{\tilde{T}} ds\Big[S_{00}^{(-2)}(u-s) - S_{00}^{(-2)}(u-s+2r)\Big]\ln s \\ &+ \frac{Y_{00}}{2r}\int_0^{2r} ds\, S_{00}^{(-2)}(u-s+2r)\ln s + o(\epsilon^0).\end{aligned} \tag{F.12}$$

We remind the reader, as mentioned in the discussion in Sec. 6.4.2, that through $S$ being a functional of $F_L^1$, so too $S^{(-2)} = S^{(-2)}[F_L^1]$. We then substitute the multiscale expansion of $F_L^1(u,\epsilon)$, implying $S_{00}^{(-2)}(t) = \tilde{S}_{00}^{(-2)}(\epsilon t) + O(\epsilon)$, and similarly, $S_{00}^{(-2)}(u - 2s + 2r) = \tilde{S}_{00}^{(-2)}(\tilde{u} - \epsilon s + 2\epsilon r) + O(\epsilon)$. We then expand $\tilde{S}_{00}^{(-2)}(\tilde{u} - \epsilon s + 2\epsilon r)$ around $\tilde{u} - \epsilon s + 2\epsilon r = \tilde{u} - \epsilon s$, as

$$\tilde{S}_{00}^{(-2)}(\tilde{u} - \epsilon s + 2\epsilon r) = \tilde{S}_{00}^{(-2)}(\tilde{u} - \epsilon s) + 2\epsilon r \dot{\tilde{S}}^{(-2)}(\tilde{u} - \epsilon s) + O(\epsilon^2), \tag{F.13}$$

yielding

$$\Psi_0 = -Y_{00}\int_0^{\tilde{T}} ds\, \epsilon \dot{\tilde{S}}_{00}^{(-2)}(\tilde{u} - \epsilon s)\ln s + \frac{Y_{00}}{2r}\int_0^{2r} ds\, \tilde{S}_{00}^{(-2)}(\tilde{u} - \epsilon s)\ln s + o(\epsilon^0). \tag{F.14}$$

After a change of integration variable to $\tilde{s} = \epsilon s$, the first integral becomes

$$\int_0^{\tilde{T}} ds\, \epsilon \dot{\tilde{S}}_{00}^{(-2)}(\tilde{u} - \epsilon s)\ln s = \int_0^{T/\epsilon^n} d\tilde{s}\, \dot{\tilde{S}}_{00}^{(-2)}(\tilde{u} - \tilde{s})\ln \tilde{s} - \tilde{S}_{00}^{2}(\tilde{u})\ln \epsilon + o(\epsilon^0). \tag{F.15}$$

With the expansion $\tilde{S}_{00}^{(-2)}(\tilde{u} - \epsilon s) = \tilde{S}_{00}^{(-2)}(\tilde{u}) + O(\epsilon)$, the second integral evaluates to

$$\frac{1}{2r}\int_0^{2r} ds\, \tilde{S}_{00}^{(-2)}(\tilde{u} - \epsilon s)\ln s = [\ln(2r) - 1]\, \tilde{S}_{00}^{(-2)}(\tilde{u}) + O(\epsilon). \tag{F.16}$$

Collecting the results of Eqs. (F.15) and (F.16) and inserting them into Eq. (F.12), we arrive at the result

$$\Box^{-1}_{\rm ret}\left(r^{-2}S^{(-2)}_{00}\right) = \left(\ln\frac{2r}{\epsilon} - 1\right)\tilde{S}^{(-2)}_{00}(\tilde{u}) - \int_0^\infty d\tilde{s}\,\dot{\tilde{S}}^{(-2)}_{00}(\tilde{u}-\tilde{s})\ln\tilde{s} + o(\epsilon^0). \tag{F.17}$$

Eq. (F.17) is the main result of this appendix. It is used in Eq. (6.31) to compute $\Psi_{\ell=0}$. Note that we have changed the upper integration limit from $T/\epsilon^n$ to $\infty$, which has the effect of adding a $o(\epsilon^0)$ term. The final result for the retarded integral of the monopole piece of the source is given by the right hand side of Eq. (F.17).

# Appendix G

# Asymptotics of the second-order source

In this Appendix we derive various analytical predictions for the behaviour of the second-order source, which provide an important check of our numerics in Sec. 8.4. Certain behaviours of the monopole modes of the source can be determined from the Bianchi identities, $\nabla^\alpha G_{\alpha\beta}[\mathrm{g}] = \nabla^\alpha \bar{R}_{\alpha\beta}[\mathrm{g}] = 0$, where $\mathrm{g} = g + h$ is the full spacetime, $g$ being the metric of the background and $h$ being the perturbation due to the small body. Substituting the expansion of the Ricci tensor (2.12), we find analogous identities at each order. Indeed, at points away from the worldline (where $\delta R_{\mu\nu}[h^1] = 0$),

$$\nabla^\alpha \delta^2 \bar{R}_{\alpha\beta} = 0. \tag{G.1}$$

Writing the second-order Ricci tensor as in (7.6), the Bianchi-identities in (G.1) separate into four separate equations analogous to Eqs. (4.29). We note that the mode sum (7.6) has an extra factor of $r$ in front compared to (4.24), so to construct gauge conditions for $\delta^2 \bar{R}_{i\ell m}$ analogous to Eqs. (4.29), we replace $\bar{h}_{i\ell m}$ with $r\delta^2 \bar{R}_{i\ell m}$. In this way, we find that for $\ell = m = 0$, the non-trivial equations are

$$r\partial_r \delta^2 \bar{R}_{200}(r) + 2\delta^2 \bar{R}_{200} = 0, \tag{G.2a}$$
$$-rf\partial_r \delta^2 \bar{R}_{100} + rf^2 \partial_r \delta^2 \bar{R}_{300} - f\left(2\delta^2 \bar{R}_{100} - 2f\delta^2 \bar{R}_{300} - 2f\delta^2 \bar{R}_{600}\right) = 0. \tag{G.2b}$$

The unique solution to Eq. (G.2a) is

$$\delta^2 \bar{R}_{200} = \frac{s_{200}}{r^2}, \tag{G.3}$$

where $s_{200}$ is a constant. We show below that for $\delta^2 \bar{R}_{100}$ we have the asymptotic behaviour

$$\delta^2 \bar{R}_{100} \sim 1/r^2 \qquad \text{for } r \gg 2M. \tag{G.4}$$

From the Bianchi identity Eq. (G.2b), by inserting the asymptotic behaviour of Eqs. (G.3) and (G.4), we find that

$$\delta^2 \bar{R}_{600} \text{ falls off least as fast as } \frac{1}{r^3}. \tag{G.5}$$

We can also express the large-$r$ behaviour of $\delta^2 \bar{R}_{i00}$ in terms of the flux of energy to infinity. We are interested in the behaviour of the source at large $r$, which is comprised of terms of the schematic form $h^1 \partial^2 h^1$ and $(\partial h^1)^2$. With this in mind we write the first-order field in terms of its leading-order piece plus terms that fall off faster than $1/r$, in Cartesian coordinates, as

$$h^1_{\mu\nu} = \frac{c_{\mu\nu}(u, n^i)}{r} + O(1/r^2). \tag{G.6}$$

Similarly we may write the second-order source on the right-hand side of (7.51) by isolating the leading-order piece that falls off as $1/r^2$ plus terms that fall off faster than that, in the form

$$2\delta^2 R_{\mu\nu}[h^1, h^1] = \frac{s_{\mu\nu}(u, n^a)}{r^2} + O(1/r^3), \tag{G.7}$$

where $s_{\mu\nu}(u, n^a)$ are the coefficients of the $1/r^2$ piece of $\delta^2 R_{\mu\nu}[\,h^1, h^1\,]$. As we mentioned in Sec. 7.5, the "oscillation $/r$" term in $h^{1,0}$ in the post-Minkowski expansion in (7.54) will be identical to the "oscillation $/r$" term in $h^1$. Because of this, the leading $1/r^2$ term in the two sources, $\delta^2 R^0_{\mu\nu}$ and $\delta^2 R_{\mu\nu}$, are identical, and we can identify the $s_{\mu\nu}$ in (G.7) with that of Eq. (7.61). We may derive a useful expression for the source by writing, in Cartesian coordinates,

$$c_{\mu\nu} = z_{\mu\nu}(u, n^a) + 2\delta M_{>}\delta_{\mu\nu}. \tag{G.8}$$

The first term, $z_{\mu\nu}$, is the nonstationary part of $c_{\mu\nu}$, and the mass term is the stationary part which appears in the result derived in (2.47). Because $\ell > 0$ (tensor-harmonic) stationary modes fall faster than $1/r$, the only stationary part of $c_{\mu\nu}$ is the mass term.

To simplify the source, we make use of the the Lorenz gauge condition, which reads

$$\dot{z}_{\mu\nu} k^\nu = \frac{1}{2}\dot{z} k_\mu, \tag{G.9}$$

where $z \equiv \eta^{\alpha\beta} z_{\alpha\beta}$, a dot indicates differentiation with respect to $u$, and $k_\mu \equiv -\partial_\mu u = (-1, n_a)$ is the principal outgoing null vector. Note that we neglect derivatives that act on the $n^a$ dependence in $z_{\mu\nu}$, because $\partial_i n^a \sim 1/r$. Integrating this with the initial condition $z_{\mu\nu}(-\infty) = 0$ gives us

$$z_{\mu\nu} k^\nu = \frac{1}{2} z k_\mu. \tag{G.10}$$

Substituting Eq. (G.8) into the formula (2.18) for $2\delta^2 R_{\mu\nu}$ in Cartesian coordinates, using Eq. (G.10), and retaining only terms that fall off as $1/r^2$, we obtain

$$s_{\mu\nu} = -\Pi\, k_\mu k_\nu + \frac{d}{du}(\bar{z}^{\mu\nu}\dot{z}_{\mu\nu}) + 4\delta M_0 \ddot{z}_{\mu\nu} + 4\delta M_0 n^\alpha \ddot{z}_{\alpha(\mu}k_{\nu)}, \tag{G.11}$$

where $n^\mu \equiv \frac{1}{2}(1, -n^a)$ is the principal ingoing null vector, and the quantity $\Pi$ is defined as

$$\Pi \equiv \frac{1}{2}\dot{z}^{\mu\nu}\dot{z}_{\mu\nu} - \frac{1}{4}\dot{z}\dot{z}. \tag{G.12}$$

$\Pi$ is related to the gravitational wave luminosity of $h^1_{\mu\nu}$ according to [106]

$$\Pi = 16\pi \left.\frac{d^2 E^{\rm grav}}{du d\Omega}\right|_{h^1}. \tag{G.13}$$

The subscript $h^1$ in (G.13) refers to the fact that $E^{\rm grav}$ is the gravitational energy of the first-order field.

Here we are only interested in the stationary part of Eq. (G.11), since it is the only part we wish to compare to in Sec. 8.4. It is also the only part associated with the infrared divergence described in Chapters 6 and 7. The stationary part resides entirely in the first term. Because it is proportional to $k_\mu k_\nu$, that term is restricted to the $t$-$r$ sector (i.e., $i = 1, 2, 3$). Its $i = 1$ and 2 modes have equal magnitude and opposite sign, and its trace mode ($i = 3$) vanishes. Using the notation $s_{i\ell m}(r)$ to denote the frequency-domain, tensor-harmonic modes of $s_{\mu\nu}$, and $\Pi_{\ell m}$ to denote the scalar harmonic modes of $\Pi$, we may write the only nonvanishing, stationary modes of $s_{\mu\nu}$ as

$$s_{2\ell m,\omega=0} = -s_{1\ell m,\omega=0} = \sqrt{2}\Pi_{\ell m,\omega=0}. \tag{G.14}$$

For quasicircular orbits, the stationary modes are simply the $m = 0$ modes. Hence,

$$s_{2\ell 0} = -s_{1\ell 0} = \sqrt{2}\Pi_{\ell 0}. \tag{G.15}$$

For the monopole mode,

$$s_{200} = -s_{100} = \sqrt{2}\Pi_{00}, \tag{G.16}$$

where, from Eq (G.13), integrating over the unit two-sphere against the $\ell = 0, m = 0$ spherical harmonic, yields

$$\Pi_{00} = 8\sqrt{\pi}\dot{E}_\infty, \tag{G.17}$$

where $\dot{E}_\infty \equiv dE^{\rm grav}/du$ is the flux through infinity.

# References


[1] A. Pound and J. Miller. *"Practical, covariant puncture for second-order self-force calculations"*. *Phys. Rev.*, D **89** (10):104020, 2014.

[2] J. Miller, B. Wardell, and A. Pound. *"Second-order perturbation theory: the problem of infinite mode coupling"*. *Phys. Rev.*, D **94** (10):104018, 2016.

[3] A. Einstein. *"The foundation of the general theory of relativity"*. *Annalen der Physik.*, **49** (7): 769 – 822, 1916.

[4] B. P. Abbott et al. *"Observation of gravitational waves from a binary black hole merger"*. *Phys. Rev. Lett.*, **116** (6):061102, 2016.

[5] B. P. Abbott et al. *"GW151226: Observation of gravitational waves from a 22-solar-mass binary black hole coalescence"*. *Phys. Rev. Lett.*, **116** (24):241103, 2016.

[6] B. P. Abbott et al. *"Tests of general relativity with GW150914"*. *Phys. Rev. Lett.*, **116** (22): 221101, 2016.

[7] H. Poincare. *"Sur la dynamique de l' électron"*. *C.R. Acad. Sci., Paris*, **140** (22): 1504 – 1508, 1905.

[8] J. L. Cervantes-Cota, S. Galindo-Uribarri, and G. F. Smoot. *"A brief history of gravitational waves"*. *Universe*, **2** (3):22, 2016.

[9] D. Kennefick. *"Einstein versus the physical review"*. *Phys. Today*, **58** (9): 43–48, September, 2005.

[10] A. Einstein and N. Rosen. *"On gravitational waves"*. *J. Franklin Inst.*, **223** (1): 43–54, 1937.

[11] C. M. De Witt, editor. *Proceedings: conference on the role of gravitation in physics, Chapel Hill, North Carolina*, Jan 18-23, 1957.

[12] H. Bondi. *"Plane gravitational waves in general relativity"*. *Nature*, **179** :1072–1073, 1957.

[13] R. A. Hulse. *"The discovery of the binary pulsar"*. *Rev. Mod. Phys.*, **66** (3): 699–710, 1994.

[14] T. Hulse and A. Russell. *"Overall measurements of relativistic effects in the binary pulsar PSR 1913 + 16."*. *Nature*, **277** :437440, 1979.

[15] J. Weber. *"Gravitational-wave-detector events"*. *Phys. Rev. Lett.*, **20** (23):1307, 1968.

[16] M. E. Gertsenshtein and V. I. Pustovoit. *"On the detection of low frequency gravitational waves"*. *Sov. Phys. JETP*, **16** :433, 1962.

[17] C. Bradaschia and R. Desalvo. *"A global network listens for ripples in spacetime"*. *CERN Courier.*, **47** (10): 17 – 20, Nov. 20, 2007.

[18] S. Kawamura et al. *"The japanese space gravitational wave antenna: DECIGO"*. *Class. Quant. Grav.*, **28** ( 9): 094011, 2011.

[19] S. Sato et al. *"DECIGO: The japanese space gravitational wave antenna"*. *J. Phys. Conf. Ser.*, **154** :012040, 2009.

[20] L. Blanchet, S. L. Detweiler, A. Le Tiec, and B. F. Whiting. *"High-order post-Newtonian fit of the gravitational self-force for circular orbits in the Schwarzschild geometry"*. *Phys. Rev.*, D **81** (8): 084033, 2010.

[21] M. Favata. *"Conservative self-force correction to the innermost stable circular orbit: comparison with multiple post-Newtonian-based methods"*. *Phys. Rev.*, D **83** (2): 024027, 2011.

[22] A. Le Tiec, A. H. Mroue, L. Barack, A. Buonanno, H. P. Pfeiffer, N. Sago, and A. Taracchini. *"Periastron advance in black hole binaries"*. *Phys. Rev. Lett.*, **107** (14): 141101, 2011.

[23] A. Le Tiec, E. Barausse, and A. Buonanno. *"Gravitational self-force correction to the binding energy of compact binary systems"*. *Phys. Rev. Lett.*, **108** :131103, 2012.

[24] T. Damour. *"Gravitational self force in a Schwarzschild background and the effective one body formalism"*. *Phys. Rev.*, D **81** (2): 024017, 2010.

[25] L. Barack, T. Damour, and N. Sago. *"Precession effect of the gravitational self-force in a Schwarzschild spacetime and the effective one-body formalism"*. *Phys. Rev.*, D **82** (8): 084036, 2010.

[26] E. Barausse, A. Buonanno, and A. Le Tiec. *"The complete non-spinning effective-one-body metric at linear order in the mass ratio"*. *Phys. Rev.*, D **85** :064010, 2012.

[27] S. Akcay, L. Barack, T. Damour, and N. Sago. *"Gravitational self-force and the effective-one-body formalism between the innermost stable circular orbit and the light ring"*. *Phys. Rev.*, D **86** :104041, 2012.

[28] P. Amaro-Seoane, J. R. Gair, A. Pound, S. A. Hughes, and C. S. F. Sopuerta. *"Research update on extreme-mass-ratio inspirals"*. *J. Phys. Conf. Ser.*, **610** (1):012002, 2015.

[29] S. Babak, J. Gair, A. Sesana, E. Barausse, C. S. F. Sopuerta, C. P. L. Berry, E. Berti, P. Amaro-Seoane, A. Petiteau, and A. Klein. *"Science with the space-based interferometer LISA. V: Extreme mass-ratio inspirals"*. *Phys. Rev.*, D **95** (10):103012, 2017.

[30] S. W. Hawking and G. F. R. Ellis. *"The large scale structure of space-time"*. Cambridge Monographs on Mathematical Physics. Cambridge University Press, 2011.

[31] M. Kesden, J. Gair, and M. Kamionkowski. *"Gravitational-wave signature of an inspiral into a supermassive horizonless object"*. *Phys. Rev.*, D **71** :044015, 2005.

[32] B. J. Owen and B. S. Sathyaprakash. *"Matched filtering of gravitational waves from inspiraling compact binaries: Computational cost and template placement"*. *Phys. Rev.*, D **60** :022002, 1999.

[33] J. D. Jackson. *"Classical electrodynamics"*. Wiley, 1998.

[34] P. A. M. Dirac. *"Classical theory of radiating electrons"*. *Proc. Roy. Soc. Lond.*, A **167** :148–169, 1938.

[35] B. S. DeWitt and R. W. Brehme. *"Radiation damping in a gravitational field"*. *Annals Phys.*, **9** :220–259, 1960.

[36] B. S. DeWitt and R. W. Brehme. *"A vierbein formalism of radiation damping"*. *Annals Phys.*, **9** :141–165, 1968.

[37] Y. Mino, M. Sasaki, and T. Tanaka. *"Gravitational radiation reaction to a particle motion"*. *Phys. Rev.*, D **55** (6): 3457–3476, 1997.

[38] T. C. Quinn and R. M. Wald. *"An Axiomatic approach to electromagnetic and gravitational radiation reaction of particles in curved space-time"*. *Phys. Rev.*, D **56** (6): 3381–3394, 1997.

[39] S. E. Gralla and R. M. Wald. *"A rigorous derivation of gravitational self-force"*. *Class. Quant. Grav.*, **25** (20): 205009, 2008. [Erratum: Class. Quant. Grav. **28** (15),159501 (2011)].

[40] A. Pound. *"Singular perturbation techniques in the gravitational self-force problem"*. *Phys. Rev.*, D **81** (12): 124009, 2010.

[41] A. Pound. *"Nonlinear gravitational self-force. I. Field outside a small body"*. *Phys. Rev.*, D **86** (8): 084019, 2012.

[42] A. I. Harte. *"Mechanics of extended masses in general relativity"*. *Class. Quant. Grav.*, **29** (5): 055012, 2012.

[43] S. E. Gralla. *"Second order gravitational self force"*. *Phys. Rev.*, D **85** (12): 124011, 2012.

[44] A. Pound. *"Second-order gravitational self-force"*. *Phys. Rev. Lett.*, **109** (5): 051101, 2012.

[45] E. Rosenthal. *"Second-order gravitational self-force"*. *Phys. Rev.*, D **74** (8): 084018, 2006.

[46] E. Poisson, A. Pound, and I. Vega. *"The motion of point particles in curved spacetime"*. *Living Rev. Rel.*, **14** :7, 2011.

[47] S. E. Gralla, A. I. Harte, and R. M. Wald. *"A Rigorous derivation of electromagnetic self-force"*. *Phys. Rev.*, D**80** (2): 024031, 2009.

[48] R. M. Wald. *"General Relativity"*. Chicago, Usa: Univ. Pr., 1984.

[49] S. L. Detweiler and B. F. Whiting. *"Selfforce via a Green's function decomposition"*. *Phys. Rev.*, D **67** (2): 024025, 2003.

[50] P. D. D'Eath. *"Black holes: Gravitational interactions"*. Oxford mathematical monographs, Oxford, UK. , 1996 .

[51] L. Barack and N. Sago. *"Beyond the geodesic approximation: conservative effects of the gravitational self-force in eccentric orbits around a Schwarzschild black hole"*. *Phys. Rev.*, D **83** (8): 084023, 2011.

[52] M. van de Meent. *"Gravitational self-force on eccentric equatorial orbits around a Kerr black hole"*. *Phys. Rev.*, D **94** (4):044034, 2016.

[53] L. Barack and N. Sago. *"Gravitational self-force correction to the innermost stable circular orbit of a Schwarzschild black hole"*. *Phys. Rev. Lett.*, **102** (19): 191101, 2009.

[54] M. Favata. *"Conservative corrections to the innermost stable circular orbit (ISCO) of a Kerr black hole: A new gauge-invariant post-Newtonian ISCO condition, and the ISCO shift due to test-particle spin and the gravitational self-force"*. *Phys. Rev.*, D **83** (2): 024028, 2011.

[55] S. Isoyama, L. Barack, S. R. Dolan, A. Le Tiec, A. G. Nakano, H.and Shah, T. Tanaka, and N. Warburton. *"Gravitational self-force correction to the innermost stable circular equatorial orbit of a Kerr black hole"*. *Phys. Rev. Lett.*, **113** (16):161101, 2014.

[56] S. L. Detweiler. *"A consequence of the gravitational self-force for circular orbits of the Schwarzschild geometry"*. *Phys. Rev.*, D **77** (12): 124026, 2008.

[57] S. R. Dolan, N. Warburton, A. I. Harte, A. Le Tiec, B. Wardell, and L. Barack. *"Gravitational self-torque and spin precession in compact binaries"*. *Phys. Rev.*, D **89** (6):064011, 2014.

[58] S. R. Dolan, P. Nolan, A. C. Ottewill, N. Warburton, and B. Wardell. *"Tidal invariants for compact binaries on quasicircular orbits"*. *Phys. Rev.*, D **91** (2):023009, 2015.

[59] M. Colleoni, L. Barack, A. G. Shah, and M. van de Meent. *"Self-force as a cosmic censor in the Kerr overspinning problem"*. *Phys. Rev.*, D **92** (8):084044, 2015.

[60] N. Warburton, S. Akcay, L. Barack, J. R. Gair, and N. Sago. *"Evolution of inspiral orbits around a Schwarzschild black hole"*. *Phys. Rev.*, D **85** (6): 061501, 2012.

[61] M. van de Meent and A. G. Shah. *"Metric perturbations produced by eccentric equatorial orbits around a Kerr black hole"*. *Phys. Rev.*, D **92** (6):064025, 2015.

[62] L. Barack and N. Sago. *"Gravitational self force on a particle in circular orbit around a Schwarzschild black hole"*. *Phys. Rev.*, D **75** (2): 064021, 2007.

[63] S. R. Dolan and L. Barack. *"Self-force via m-mode regularization and 2+1D evolution: III. Gravitational field on Schwarzschild spacetime"*. *Phys. Rev.*, D **87** (8): 084066, 2013.

[64] A. G. Shah, J. L. Friedman, and T. S. Keidl. *"EMRI corrections to the angular velocity and redshift factor of a mass in circular orbit about a Kerr black hole"*. *Phys. Rev.*, D **86** (8): 084059, 2012.

[65] S. Akcay, N. Warburton, and L. Barack. *"Frequency-domain algorithm for the Lorenz-gauge gravitational self-force"*. *Phys. Rev.*, D **88** (10):104009, 2013.

[66] T. Osburn, E. Forseth, C. R. Evans, and S. Hopper. *"Lorenz gauge gravitational self-force calculations of eccentric binaries using a frequency domain procedure"*. *Phys. Rev.*, D **90** (10):104031, 2014.

[67] B. Wardell, C. R. Galley, A. Zenginoğlu, M. Casals, S. R. Dolan, and A. C. Ottewill. *"Self-force via Green functions and worldline integration"*. *Phys. Rev.*, D **89** (8):084021, 2014.

[68] L. Barack and A. Ori. *"Mode sum regularization approach for the selfforce in black hole space-time"*. *Phys. Rev.*, D **61** (6): 061502, 2000.

[69] L. Barack, Y. Mino, A. Nakano, H.and Ori, and M. Sasaki. *"Calculating the gravitational selfforce in Schwarzschild space-time"*. *Phys. Rev. Lett.*, **88** (9):091101, 2002.

[70] L. Barack and D. A. Golbourn. *"Scalar-field perturbations from a particle orbiting a black hole using numerical evolution in 2+1 dimensions"*. *Phys. Rev.*, D **76** (4): 044020, 2007.

[71] I. Vega and S. L. Detweiler. *"Regularization of fields for self-force problems in curved spacetime: Foundations and a time-domain application"*. *Phys. Rev.*, D **77** :084008, 2008.

[72] S. Detweiler. *"Gravitational radiation reaction and second order perturbation theory"*. *Phys. Rev.*, D **85** (4): 044048, 2012.

[73] E. Rosenthal. *"Construction of the second-order gravitational perturbations produced by a compact object"*. *Phys. Rev.*, D **73** :044034, 2006.

[74] B. Wardell and N. Warburton. *"Applying the effective-source approach to frequency-domain self-force calculations: Lorenz-gauge gravitational perturbations"*. *Phys. Rev.*, D **92** (8):084019, 2015.

[75] A. Pound. *"Second-order perturbation theory: problems on large scales"*. *Phys. Rev.*, D **92** (10):104047, 2015.

[76] E. Poisson. *"A relativist's toolkit. The mathematics of black-hole mechanics."*. Cambridge University Press, 2004.

[77] A. Pound. *" Nonlinear gravitational self-force: Second-order equations of motion for a monopolar body,"*. *in preparation.*, 2017.

[78] A. Pound. *"Nonlinear gravitational self-force: second-order equation of motion"*. *Phys. Rev.*, D **95** (10):104056, 2017.

[79] E. Poisson. *"Metric of a tidally distorted, nonrotating black hole"*. *Phys. Rev. Lett.*, **94** (16): 161103, 2005.

[80] S. R. Dolan and L. Barack. *"Self force via m-mode regularization and 2+1D evolution: Foundations and a scalar-field implementation on Schwarzschild"*. *Phys. Rev.*, D **83** (2): 024019, 2011.

[81] S. R. Dolan, L. Barack, and B. Wardell. *"Self force via m-mode regularization and 2+1D evolution: II. Scalar-field implementation on Kerr spacetime"*. *Phys. Rev.*, D **84** (8): 084001, 2011.

[82] S. Dolan. *" Time domain schemes for gravitational self force"*. In *Capra Meeting on radiation reaction in general relativity, University of Maryland*, June 11-15, 2012. http://www2.yukawa.kyoto-u.ac.jp/~soichiro.isoyama/CAPRA/CAPRA_2012/Dolan.pdf.

[83] P. Diener, I. Vega, B. Wardell, and S. Detweiler. *"Self-consistent orbital evolution of a particle around a Schwarzschild black hole"*. *Phys. Rev. Lett.*, **108** (19): 191102, 2012.

[84] J. Thornburg and B. Wardell. *"Scalar self-force for highly eccentric equatorial orbits in Kerr spacetime"*. *Phys. Rev.*, D **95** (8):084043, 2017.

[85] N. Warburton and B. Wardell. *"Applying the effective-source approach to frequency-domain self-force calculations"*. *Phys. Rev.*, D **89** (4):044046, 2014.

[86] S. M. Christensen. *"Vacuum expectation value of the stress tensor in an arbitrary curved background: The covariant point separation method"*. *Phys. Rev.*, D **14** (10): 2490–2501, 1976.

[87] R. Haas and E. Poisson. *"Mode-sum regularization of the scalar self-force: Formulation in terms of a tetrad decomposition of the singular field"*. *Phys. Rev.*, D **74** (4): 044009, 2006.

[88] A. Heffernan, A. Ottewill, and B. Wardell. *"High-order expansions of the Detweiler-Whiting singular field in Schwarzschild spacetime"*. *Phys. Rev.*, D **86** (10): 104023, 2012.

[89] L. Barack and C.O. Lousto. *"Perturbations of Schwarzschild black holes in the Lorenz gauge: Formulation and numerical implementation"*. *Phys. Rev.*, D **72** (10): 104026, 2005.

[90] F. J. Zerilli. *"Gravitational field of a particle falling in a Schwarzschild geometry analyzed in tensor harmonics"*. *Phys. Rev.*, D **2** (10): 2141–2160, 1970.

[91] S. Akcay. *"A fast frequency-domain algorithm for gravitational self-force: I. circular orbits in Schwarzschild spacetime"*. *Phys. Rev.*, D **83** (12): 124026, 2011.

[92] GSL Project Contributors. GSL - GNU scientific library - GNU project - free software foundation (FSF). http://www.gnu.org/software/gsl/, 2010.

[93] M. V. Berndtson. *"Harmonic gauge perturbations of the Schwarzschild metric"*. PhD thesis, Colorado U., 2007.

[94] A. Pound. *"Tensor-harmonic decomposition of the second-order einstein equation in Schwarzschild spacetime"*. *in preparation*, 2017.

[95] L. Barack. *"Gravitational self force in extreme mass-ratio inspirals"*. *Class. Quant. Grav.*, **26** :213001, 2009.

[96] J. N. Goldberg, A. J. MacFarlane, E. T. Newman, F. Rohrlich, and E. C. G. Sudarshan. *"Spin s spherical harmonics and edth"*. *J. Math. Phys.*, **8** :2155, 1967.

[97] K.T. Hecht. *"Quantum mechanics"*. Springer-Verlag, Inc., N.Y., 2000.

[98] B. Wardell and A. Gopakumar. *"Self-force: computational strategies"*. *Fund. Theor. Phys.*, **179** :487–522, 2015.

[99] S. A. Orszag. *"Fourier series on spheres"*. *Monthly Weather Review*, **102** (1): 56, January 1974.

[100] G. Lohofer. *"Inequalities for the associated legendre functions"*. *Journal of Approximation Theory*, **95** (2):178 – 193, November 1998.

[101] L. Blanchet and T. Damour. *"Radiative gravitational fields in general relativity I. general structure of the field outside the source"*. *Phil. Trans. Roy. Soc. Lond.*, A **320** :379–430, 1986.

[102] L. Blanchet. *"Radiative gravitational fields in general relativity. 2. Asymptotic behaviour at future null infinity"*. *Proc. Roy. Soc. Lond.*, A **409** :383–399, 1987.

[103] L. Blanchet and T. Damour. *"Tail transported temporal correlations in the dynamics of a gravitating system"*. *Phys. Rev.*, D **37** (6): 1410, 1988.

[104] L. Blanchet and T. Damour. *"Postnewtonian generation of gravitational waves"*. *Ann. Inst. H. Poincare Phys. Theor.*, **50** :377–408, 1989.

[105] T. Damour and B. R. Iyer. *"PostNewtonian generation of gravitational waves. 2. The spin moments"*. *Ann. Inst. H. Poincare Phys. Theor.*, **54** :115–164, 1991.

[106] L. Blanchet and T. Damour. *"Hereditary effects in gravitational radiation"*. *Phys. Rev.*, D **46** :4304–4319, 1992.

[107] T. Hinderer and E. E. Flanagan. *"Two timescale analysis of extreme mass ratio inspirals in Kerr. I. Orbital Motion"*. *Phys. Rev.*, D **78** (6): 064028, 2008.

[108] A. Zenginoğlu. *"A geometric framework for black hole perturbations"*. *Phys. Rev.*, D **83** (12): 127502, 2011.

[109] C. W. Misner, K. S. Thorne, and J. A. Wheeler. *"Gravitation"*. W. H. Freeman, San Francisco, 1973.

[110] K. Ahnert and M. Mulansky. *"odeint. solving ODEs in C++"*. http://www.boost.org/doc/libs/1_61_0/libs/numeric/odeint/doc/html/index.html, 2009.

[111] K. Martel. *"Gravitational wave forms from a point particle orbiting a Schwarzschild black hole"*. *Phys. Rev.*, D **69** (4): 044025, 2004.

[112] L. Barack, A. Ori, and N. Sago. *"Frequency-domain calculation of the self force: The High-frequency problem and its resolution"*. *Phys. Rev.*, D **78** (8): 084021, 2008.

[113] T. S. Keidl, A. G. Shah, J. L. Friedman, D. Kim, and L. R. Price. *"Gravitational Self-force in a radiation gauge"*. *Phys. Rev.*, D **82** (12):124012, 2010. [Erratum: Phys. Rev.D **90**, no.10,109902(2014)].

[114] A. Pound, C. Merlin, and L. Barack. *"Gravitational self-force from radiation-gauge metric perturbations"*. *Phys. Rev.*, D **89** (2):024009, 2014.

[115] L. Barack and A. Ori. *"Regularization parameters for the selfforce in Schwarzschild space-time. 1. Scalar case"*. *Phys. Rev.*, D**66** (8): 084022, 2002.